

Small Molecule Signaling in Nematodes

Dissertation

zur Erlangung des akademischen Grades

doctor rerum naturalium (Dr. rer. nat.)

vorgelegt dem Rat der Chemisch-Geowissenschaftlichen Fakultät

der Friedrich-Schiller-Universität Jena

von Master of Science

Chuanfu Dong

geboren am 13 Juli 1987 in Jiangxi (China)

- | | | |
|----|----------------------|---|
| 1. | Gutachter | <u>Prof. Dr. Stephan H. Von Reuss (Université de Neuchâtel)</u> |
| 2. | Gutachter | <u>Prof. Dr. Georg Pohnert (Friedrich-Schiller-Universität)</u> |
| 3. | Gutachter | <u>Prof. Dr. Frank C. Schroeder (Cornell University)</u> |
| | Tag der Verteidigung | <u>March 29th, 2017</u> |

Dedicated to my parents

Table of Contents

General Introduction.....	1
Chapter 1.....	11
Comparative Analysis of Ascaroside Signals in <i>Caenorhabditis</i> Species.....	11
Chapter 2.....	12
Selective MS Screening Reveals a Sex Pheromone in <i>C. briggsae</i> and Species-Specificity in Indole Ascaroside Signalling	12
Chapter 3.....	26
Comparative Metabolomics Reveals a Panel of Novel Fatty Acid Ascarosides from <i>C. remanei</i> and <i>C. latens</i>	26
Chapter 4.....	39
A Group of <i>Z/E</i> Isomeric Urocanic Acid Ascarosides from <i>C. remanei</i>	39
Chapter 5.....	50
New Phosphoryl Ascarosides from the <i>Caenorhabditis</i> <i>Elegans</i> Group.....	50
Chapter 6.....	57
New Dimeric Ascarosides from <i>Caenorhabditis</i> <i>Elegans</i> Group.....	57
Chapter 7.....	62
(ω)- and (ω -2)-Hydroxylated Ascarosides from <i>Caenorhabditis nigoni</i>	62
Chapter 8.....	66
Amino Benzoic Acid Modified Ascarosides Identified from	66
<i>Caenorhabditis nigoni</i>	66
Chapter 9.....	70
Conclusions and Outlook.....	70
Appendix.....	74
References	137
Curriculum Vitae.....	141
Acknowledgments	143

General Introduction

Ecology of Nematodes: Nematodes such as *Caenorhabditis elegans* is easily to be found because they are globally distributed^[1,2], especially in compost and in rich humus^[3]. *C. elegans* in a diapause stage (called dauer) were originally isolated from compost^[4,5] where the rotting and decomposed materials provide abundant bacterial food source for the reproduction of nematodes. However, we still do not know what types of bacteria nematodes feed on in their natural habitats. Bacteria of *E. coli* is used as the food source for nematodes under laboratory culture condition. When they are well fed, *C. elegans* develops from egg to adult through four stages (L1, L2, L3 and L4) which only takes three days. Alternatively, *C. elegans* enters into the dauer stage under unfavorable environmental conditions including low amount of food, high population density, or high temperature (**Figure G1**).

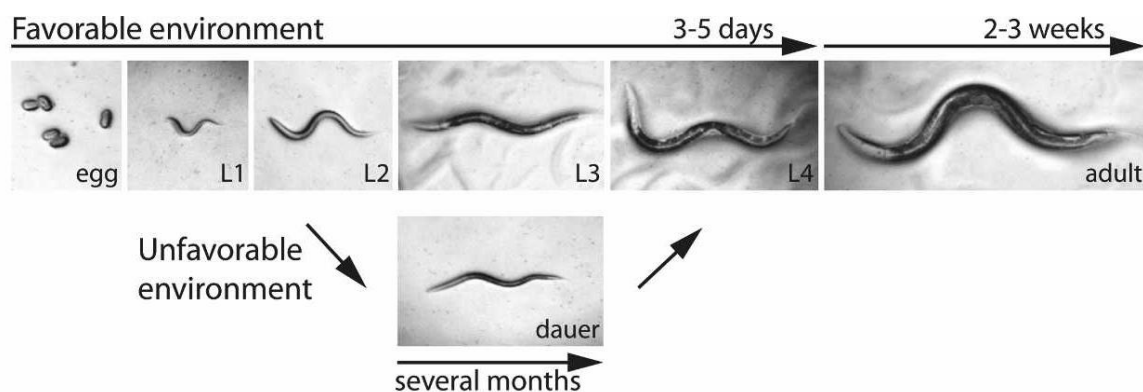


Figure G1: Lifestyle (normal reproductive life cycle and dauer stage) of *C. elegans*.

C. elegans proliferates rapidly and has a short generation time, which makes it very suitable for maintaining on NGM agar plates in laboratory. *C. elegans* can survive again and be reproductive even when they enter into the dauer stage or be stored at -80 °C. Various wild-type strains and many mutants are easily available from the *Caenorhabditis* Genetics Center (CGC). *C. elegans* was the first multicellular organism to be completely sequenced which makes it one of the top model organisms.^[6] Recently, sixteen new *Caenorhabditis* species have been discovered through collaborative worldwide sampling efforts for new *C. elegans* isolates.^[2] *Caenorhabditis* species are well resolved in two

clades called the *Elegans* super group and *Drosophilae* super group. The famous model organism *C. elegans* together with another nine species are aligned as *Elegans* group. Nematodes such as *C. elegans* have been reported to produce a blend of small molecules called ascarosides, which are considered to be widely conserved in the nematodes kingdom.^[7] However, the chemical content of other *Caenorhabditis* species is still unknown to us except for *C. elegans*. In this thesis, the potential for ascaroside-based inter- and intra-species interaction in nematodes (listed in the phylogenetic tree in **Figure G2**) is investigated while taking advantage of these newly discovered *Caenorhabditis* species.

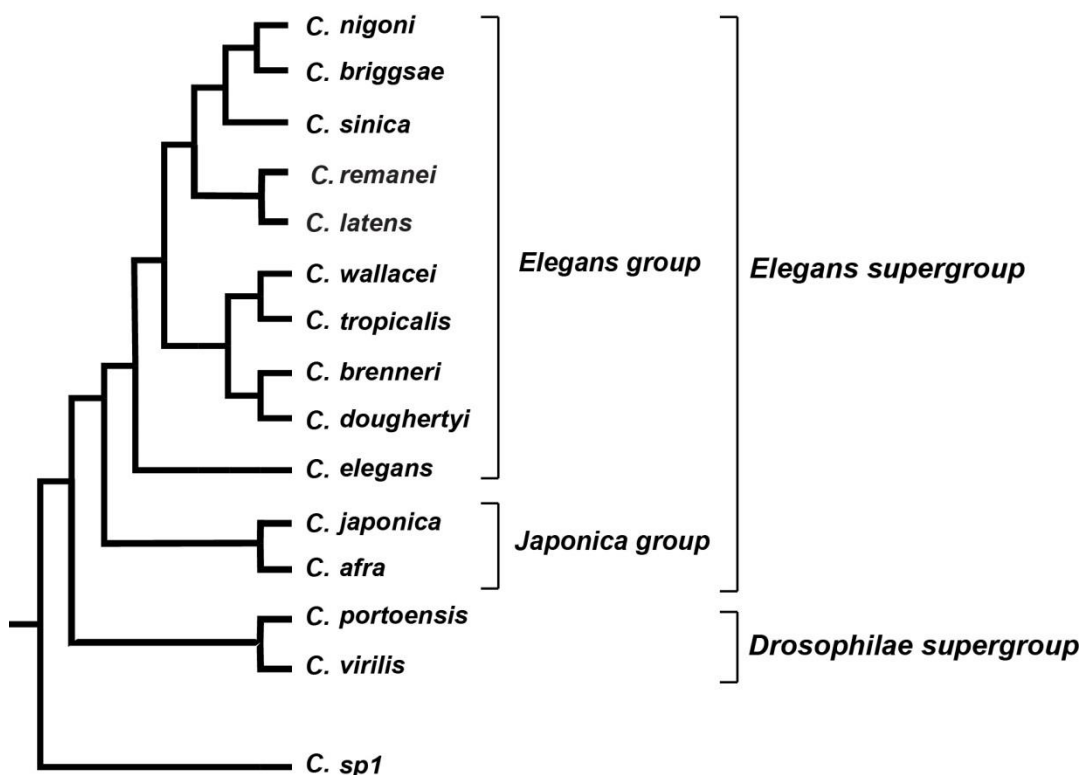


Figure G2: Phylogenetic tree of *Caenorhabditis* genus based on reference 33.

Chemistry of Nematodes: Recent research has shown that nematodes are capable to produce a blend of ascarosides as chemical signals, which consist of glycosides of the 3,6-dideoxysugar ascarylose with different fatty acid derived side chains as well as their derivatives. The ascarosides influence multiple aspects of *C. elegans* biology, including dauer formation (an alternative larval stage evolved by *C. elegans* to endure unfavorable environments), behavior and development.^[8,9] To unravel their chemical structures and

functions actually took a long time since J. W. Golden and D. L. Riddle in 1982 demonstrated that some mysterious nematode produced chemicals induced dauer formation.^[10] In the earlier times similar glycolipids (very long chain ascarosides with around 30 carbons in the fatty acid derived side chain) were isolated from the eggs of the parasitic nematode *Ascaris suum*.^[11] While the function of these compounds has remained unclear, only short chain ascarosides were found to be bioactive.^[8,9] In 2005 the first ascaroside called 'daumone' (also named as ascr#1, **Figure G3**) was isolated from *C. elegans* (N2 strain), chemically synthesized, and shown to be active in dauer formation by the Paik group.^[12] Two years later, Jon Clardy's group reported two significantly more potent ascarosides called ascr#2 and ascr#3 from *C. elegans*, which strongly promote entry into the dauer stage.^[13] Further studies demonstrated that a blend of ascr#2, ascr#3 and ascr#4 synergistically attracts males at extremely low concentration.^[14] Furthermore, even minor changes to the chemical structures of ascarosides might result in completely different biological functions. For example, males of *C. elegans* predominantly produce ascr#10 to attract hermaphrodites, whereas the corresponding dehydro-derivative ascr#3 was abundantly produced by hermaphrodites and attract males.^[15] Another impressive example are the indole ascarosides which were demonstrated to attract hermaphrodites, whereas ascarosides without the indole group are repulsive to hermaphrodites.^[16] To study structure-activity relationships, chemical synthesis efforts were made to create a small library of ascarosides for bioassays, which further confirmed that biological activities are highly dependent on specific chemical structures.^[17]

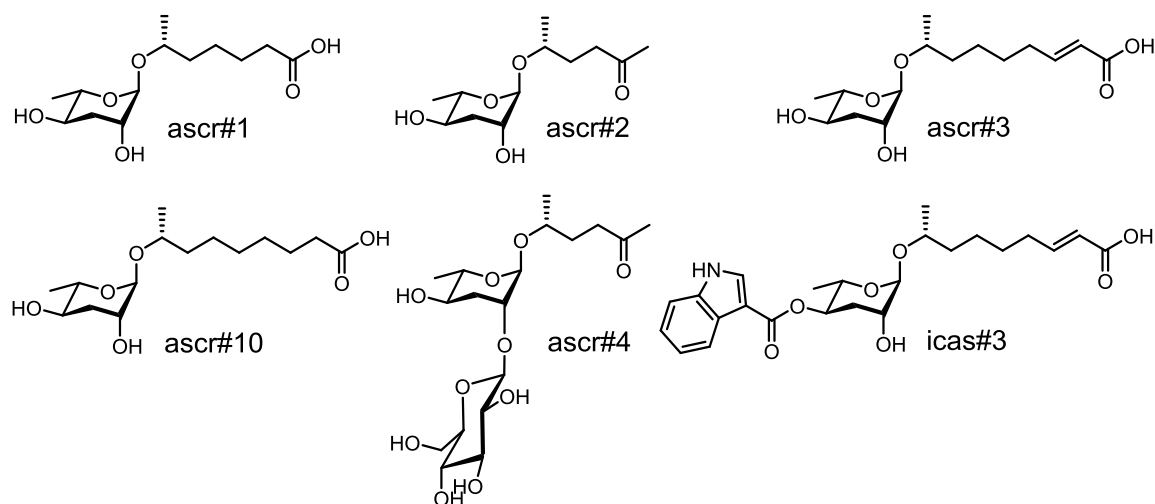


Figure G3: Known ascarosides identified from model organism *C. elegans*.

Since these pioneering discoveries many other ascarosides and their corresponding functions were described. Most of these reports focused on developmental plasticity of nematodes. For example, another potent ascaroside called ascr#5 was discovered from *C. elegans*, which consist of a very short fatty acid side chain with only three carbons that is linked *via* the terminal (ω)-carbon, which acts synergistically with other ascarosides to strongly induce dauer formation.^[18] Another group of ascarosides featuring an indole moiety at the 4-position of the ascarylose unit was also described from *C. elegans* to promote entry into dauer stage.^[19] Recently, the entomopathogenic nematode *Heterorhabditis bacteriophora* was reported to use an ascaroside with 11 carbon side chain that is linked to ethanolamine to form the amide (called ascr-C11-EA, **Figure G4**) to control the development of infective juveniles (IJ, a developmental stage similar to dauer larva in *C. elegans*), preventing IJ recovery to the J4 stage in order to increase nematode survival in their environment until they enter the next insect host.^[20] Ascarosides were also reported to act in cross-kingdom interactions. A recent study of the interaction between soil-dwelling nematodes and nematophagous fungi as their natural predator (which developed adhesive or nonadhesive traps to capture nematodes), revealed that these remarkable microorganisms strongly responded to ascarosides and changed their morphology to make them capable to prey on nematodes. That means fungi have evolved to adapt to the chemical communication between nematodes, and strikingly, fungi was able to interpret the content of communication.^[21]

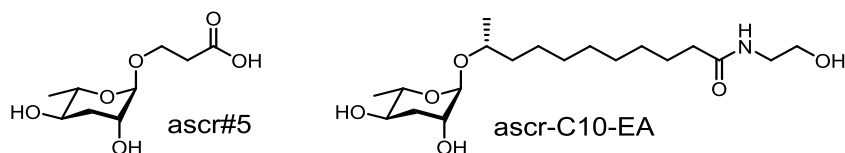


Figure G4: Dauer formation inducing ascarosides identified from *C. elegans* and entomopathogenic nematode *Heterorhabditis bacteriophora*.

Along with the discovery of structures and functions of these ascarosides, their biosynthetic pathway was interrogated and some progress had been achieved. To clarify

the origin of ascarosides, the functions of putative biosynthetic genes were also investigated. Generally, ascarosides are considered to originate from several rounds of peroxisomal β -oxidation cycles, cutting the long fatty acid derived side chain to be shorter. Biochemical studies confirmed that genes of *acox-1* (encoded acyl-SCoA), *maoc-1* (encoded enoyl-SCoA), *dhs-28* (encoded hydroxyacyl-SCoA) and *daf-22* (encoded β -ketoacyl-SCoA) participated in the peroxisomal β -oxidation cycle and finally resulted in the side chain shortening.^[22,23] And very recently, the formation of homo- or heterodimers by three acyl-CoA oxidases (*acox-1*, *acox-2* and *acox-3*) has been linked to different side chain length preferences and the acyl-CoA oxidases were confirmed to directly act on long-chain ($\omega/\omega-1$) ascarosides.^[24] These results essentially excluded other possible biosynthetic pathways. For example, β -oxidation was previously hypothesized to cut long chain hydroxylated fatty acids to short chain hydroxylated fatty acids which were then attached to ascarylose *via* a highly promiscuous ascarylose-transferase; another hypothesis suggested that β -oxidation cut long chain fatty acids to short chain fatty acids which were subsequently hydroxylated and attached to ascarylose. In conclusion, while the later parts of ascaroside biosynthesis such as the chain shortening *via* peroxisomal β -oxidation are well understood, the origin and functions of the very long chain ascarosides as the ultimate biosynthetic precursors which appear to lack any signaling function is unknown.

Another important aspect of chemical communication in nematodes is signal perception by chemoreceptors, which are responsible for sensing ascarosides. In 2008, two types of neurons, the amphid single ciliated sensory neuron type K (ASK) and the male-specific cephalic companion neuron (CEM) in the head of *C. elegans* were reported to be essential for male attraction.^[23] Collaborative work led by Cori Bargmann and Jon Clardy further revealed that RMG inter/motor neuron was the hub of the circuit that is connected by anatomical gap junctions to several sensory neurons, which were essential to promote aggregation in *C. elegans*.^[25] ASK chemosensory neurons were found to respond to dauer pheromone ascarosides, for which two heterotrimeric GTP-binding protein-coupled receptors (GPCRs) were characterized, *SRBC-64* and *SRBC-66*.^[26] *C. elegans* principally develop into dauer worms when cultured at high population density or

low food availability. However, they are resistant to enter into the dauer stage under high density conditions or ascr#5 supplementation, when the two chemoreceptor genes *srg-36* and *srg-37* are deleted.^[27]

Comparative Metabolism with MS and NMR to Reveal Chemical Interaction in Nematodes: To uncover the complicated interplay of chemical signaling in nematodes, advanced analytical tools are highly required. In order to link biological function and molecular structure Frank C. Schroeder developed the Differential Analysis of 2D NMR Spectra (DANS) methodology in order to characterize unknown small molecules in crude extracts, by acquiring double quantum filter correlation spectroscopy (*dqf*-COSY) spectra. This method allowed them to identify several new natural products from crude material by analyzing signal connectivities in double quantum filtered correlation spectroscopy (*dqf*-COSY) spectra of wildtype and mutant metabolomes. In 2007, DNAS was first applied to discover two new indole alkaloids from a small library of fungi extract.^[28] The advantages of using comparative analysis of *dqf*-COSY spectra over the many other available 2D NMR experiments includes: 1) it is able to directly pick out unknown chemicals from the crude extract. This avoids extensive chromatographic separation processes that might destroy the chemical structure and result in the loss of activity, and importantly, repeated discovery of less interesting compounds can also be avoided. 2) High resolution *dqf*-COSY experiments offer excellent sensitivity and dynamic range which facilitates the detection of molecules even with very low abundance.^[29,30] 3) ¹H, ¹H-coupling constants can be extracted by carefully analyzing the *dqf*-COSY spectrum, which provides extremely valuable information for structural characterization. Considering these advantages and the fact that nematodes excrete only low amounts of ascarosides into their environment the *dqf*-COSY technique appears highly suitable to identify unknown ascarosides from nematodes. For example, *dqf*-COSY spectra derived from the *exo*-metabolome extract of the peroxisomal β -oxidation mutant *daf-22* and the wild type N2 were compared to search for *daf-22* dependent ascarosides, leading to the discovery of four previously undescribed components ascr#6.1, ascr#6.2, ascr#7 and ascr#8 (**Figure G5**).^[31] In this study, chemical synthesis and MS experiments further validated the

results and ascr#8 was discovered to specifically attract males. DANS is also widely applied to natural products discovery from bacteria and fungi. And it is particularly useful to study natural products biosynthesis, and to connect chemical structures to biological functions. For example, nine novel biosynthetic intermediates were identified from the *gli* gene cluster in the fungus *Aspergillus fumigatus* by comparative analysis of *dqf*-COSY spectra from wild type and mutant metabolomes, which provided insights into the biosynthesis of gliotoxin.^[32] Using DANS, several new pyrrolizidine alkaloids (PAs) were also identified from entomopathogenic *Xenorhabdus* bacteria.^[33]

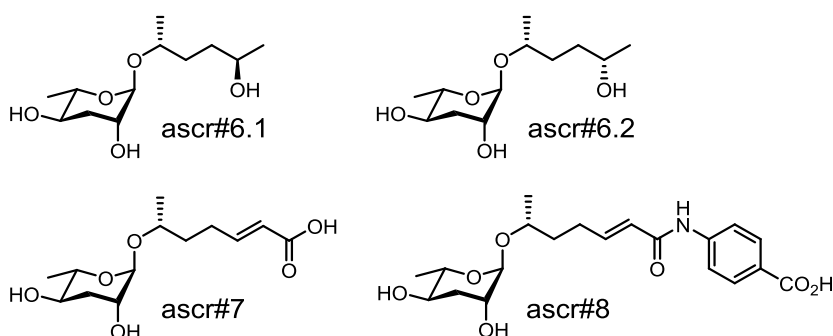


Figure G5: Four known ascarosides revealed by comparative analysis of *dqf*-COSY spectra derived from the *exo*-metabolome extracts of *C. elegans* and mutant *daf-22*.

However, crude *exo*-metabolome extracts derived from nematodes contain tens of hundreds of chemical components, and in many cases the direct detection of ascarosides present only in trace amounts remains a challenge. To address this problem additional analytical tool with dramatically increased sensitivity would be required. In 2012, Stephan H. von Reuss developed a MS/MS precursor ion screen for profiling ascarosides in crude nematode metabolomes, that relies on the detection of a characteristic 3,6-dideoxysugar ascarylose derived fragment ion with a *m/z* value of 73.^[23] Application of this technique led to the discovery of many previously undescribed ascarosides, including those carrying additional 4-hydroxybenzoyl, (*E*)-2-methyl-2-butenoyl (tigloyl) (**Figure G6**) and indole groups. When employed for comparative metabolome analysis of wild type and peroxisomal β -oxidation mutants it also helped to deepen our understanding of the biosynthesis of ascarosides. Based on the application of this particular MS/MS technique, many examples of novel ascarosides and their corresponding functions were reported.

For example, a set of highly complex ascarosides was characterized from the satellite model organism *Pristionchus pacificus*, of which the dimeric ascaroside dasc#1 was found to induce an eury stomatous mouth form that enables predation of other nematodes whereas npar#1 cause dauer formation (Figure G6).^[34] Another study of the sour paste nematode *Panagrellus redivivus* that simultaneously employed activity guided fractionation and MS/MS precursor ion screening revealed sex specific ascaroside production and indicated that males are able to produce a dihydroxylated ascaroside called dhas#18 that acts as sex pheromone to attract females, along with one minor ascaroside called bhas#10.^[35]

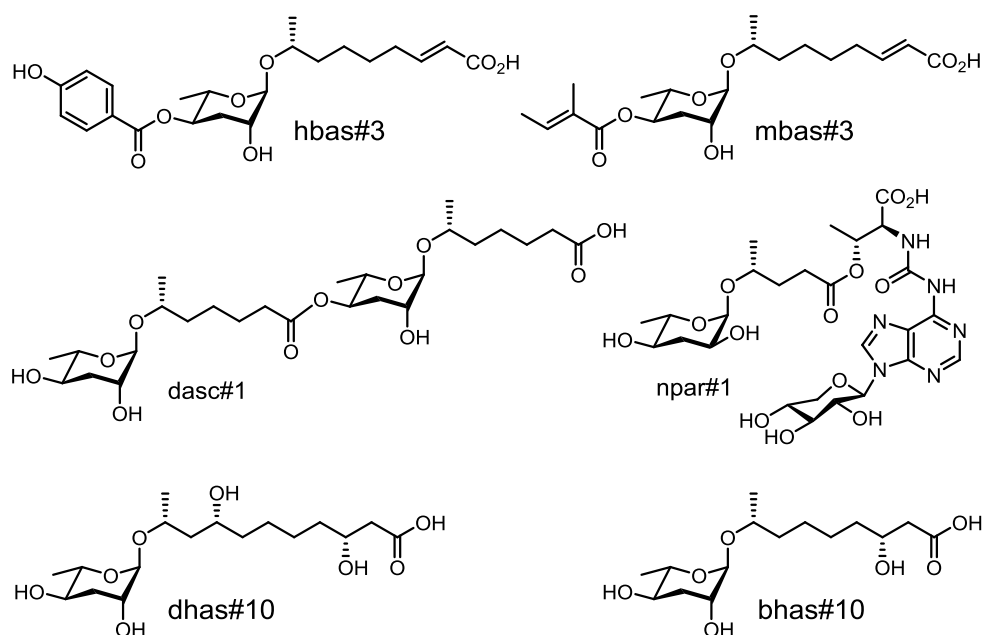


Figure G6: Bioactive ascarosides with high species-specificities were discovered from *Panagrellus redivivus* and the satellite model organism *Pristionchus pacificus*.

Aim of this Dissertation: These pioneering studies provided deep insights into chemical communication in the model organism *C. elegans*. However, it merely represents the tip of an iceberg regarding the chemistry and chemical ecology of nematodes in general. The question remains whether there exist much more complex intra- and inter-species interactions beyond our understanding? Recently, almost all the nematodes are found to be capable to produce ascarosides, which were considered to be important chemical signaling and widely conserved in nematodes.^[7] These studies demonstrate that a large diversity of nematodes can biosynthesize and excrete a blend of ascarosides to communicate with other species, and that ascarosides carried different but overlapping information, which raises a critical question about how specific intra-species communication can be accomplished in sympatric organisms. Detailed investigations of *Pristionchus pacificus* and *Panagrellus redivivus* already revealed highly species-specific ascaroside harboring very unique and specific modification on ascaroside core skeleton, which affect developmental plasticity and act as sex pheromone. This allows us to hypothesize that species-specific modification of ascaroside core skeleton produced dedicated species-specific compounds for intra-species communication. Taking full advantage from the comparative MS/MS analysis, this thesis aims to clarify the widely conserved common ascarosides as well as species-specific components as high interest targets that could in theory be responsible for species-specific functions, and finally to learn about the chemical communication in a set of closely related *Caenorhabditis* species. Nematode producing the most abundant interesting and novel ascarosides will be set up in large liquid culture for further isolation and structural elucidation, which will also support their functional characterization in the following bioassays.

Preview of Chapters: This dissertation describes the detection, isolation and structure elucidation of six classes of novel ascarosides from *Caenorhabditis* nematodes, as well as analysis of their biosynthesis and chemical ecology (**Figure G7**). **Chapter 1** describes the comparative MS-based screening for signaling ascarosides in a set of *Caenorhabditis* species. **Chapter 2** pertaining to indole ascarosides was adapted from a publication^[36] in the scientific journal *Organic & Biomolecular Chemistry*, that is the result of collaborative

efforts in which the author focused on compound isolation and identification, Franziska Dolke subsequently executed the chemical synthesis, and Stephan H. von Reuß performed biological tests. From **Chapter 3** to **Chapter 8**, each chapter describes one class of novel ascarosides, and includes results and discussion, as well as conclusions, which are not published. Franziska Dolke contributed to this research by performing chemical synthesis of novel ascarosides in order to support structural identification and to provide material for bioassays. A final chapter of conclusions and outlook is included to discuss the future of chemical ecology of nematodes and the various open questions. Finally, additional tables and figures are attached as appendix to serve as supporting information.

<i>Caenorhabditis</i> species	Ascarosides							
	Fasc	Icas	Phas	Dasc	Ucas	Hyas	Abas	Ascr
<i>C. nigoni</i>		■		■	■	■	■	■
<i>C. briggsae</i>		■	■	■	■			■
<i>C. sinica</i>		■	■	■				■
<i>C. remanei</i>	■	■	■	■	■			■
<i>C. latens</i>	■	■	■	■				■
<i>C. wallacei</i>		■			■			■
<i>C. tropicalis</i>		■	■	■			■	■
<i>C. brenneri</i>			■	■	■			■
<i>C. doughertyi</i>		■						■
<i>C. elegans</i>		■						■
<i>C. japonica</i>								■
<i>C. afra</i>						■		■
<i>C. portoensis</i>								■
<i>C. virilis</i>								■
<i>C. sp1</i>								■

Figure G7: Novel ascarosides described in this dissertation. Six groups of novel ascarosides were discovered from *Caenorhabditis* species of which some are highly species-specific suggesting important functions in intra-species interactions. (**Fasc**: Fatty acid ascarosides; **Icas**: Indole modified ascarosides; **Phas**: Phosphoryl ascarosides; **Dasc**: Dimeric ascarosides; **Ucas**: Urocanic acid modified ascarosides; **Hyas**: (ω)- and (ω -2)-hydroxylated ascarosides; **Abas**: Amino benzoic acid ascarosides; **Ascr**: Common ascarosides, e.g. ascr#1, ascr#3 and ascr#10, present in all *Caenorhabditis* species).

Chapter 1

Comparative Analysis of Ascaroside Signals in *Caenorhabditis* Species

For comparative analysis of ascaroside signals in *Caenorhabditis* species we selected a variety of species for chemical analysis. Of which cosmopolitan species *C. briggsae* and *C. remanei* are widely distributed in the northern hemisphere, a diversity of various wild-type strains of *C. briggsae* and *C. remanei* were collected to evaluate the strain specificity (listed in **Appendix: Nematodes strains and experimental culture conditions**). To obtain *exo*-metabolome samples nematodes were cultivated in liquid cultures and fed with *E. coli* OP50^[37]. Liquid culture media were separated into worm pellet and supernatant by centrifugation. Supernatant containing the excreted metabolites was lyophilized, extracted by methanol, and analyzed using MS and NMR techniques. Selective MS/MS screening was applied to detect known and putative ascarosides. Species-specificity of those identified ascarosides in *Caenorhabditis* species was analyzed on the basis of comparative analysis, whereas all the nematodes were cultivated under the same experimental conditions. Those species produced large amount of target compounds could hence be cultivated in large scale for isolation and identification. In this thesis large liquid culture media of four species including *C. remanei* (1.8 L), *C. latens* (1.2 L), *C. briggsae* (1.5 L) and *C. nigoni* (1.6 L) were set up for target compounds purification. Detailed experimental procedures and methods were described in the **Experimental Part of Appendix**. Furthermore, solid phase extraction (SPE) and semi-preparative High Pressure Liquid Chromatography (HPLC) were applied to initially fractionate and purify unique compounds with high species-specificity. The biological activity of indole ascarosides was evaluated and described in **Chapter 2** and we are still working on the bioassay of the remaining ascarosides. Comparative analysis of 13 *Caenorhabditis* species finally resulted in the discovery of six groups of novel ascarosides with high species-specificities which might play unique roles in the intra-species interaction. Detailed information of the discovery of these chemical signals was described in the following texts from **Chapter 2 to Chapter 8**.

Chapter 2

Selective MS Screening Reveals a Sex Pheromone in *C. briggsae* and Species-Specificity in Indole Ascaroside Signalling

Detection of *C. briggsae* dependent indole ascarosides (icas#2 and icas#6.2) by selective MS/MS screening: Ascarosides featuring an indole group at the 4-position of the ascarylose, for example icas#9, were previously described to modulate dauer formation in *C. elegans*.^[16] Here, taking advantage of highly sensitive liquid chromatography mass spectrometry, indole ascarosides were selectively screened for in crude *exo*-metabolome extracts. Previously, Stephan H. von Reuß developed a MS/MS precursor ion screen using electrospray ionization in negative ion mode (ESI(-)) to fragment indole ascarosides carrying carboxylic acid aglycone moieties such as icas#9, that resulted in the loss of the indole-3-carbonyl moiety to give side chain-specific fragments. Under these conditions, three additional indole ascarosides icas#9Me, icas#2 and icas#6 were also fragmented in negative ion mode whereas fragment ion signal for $C_{15}H_{14}NO_4^-$ (m/z 272.0928) was detected, suggesting the loss of side chain (**Figure 2.1**).^[16,23] In contrast, when high resolution mass spectrometric (HR-MS) analysis using electrospray ionization in positive ion mode (ESI(+)) and in source collision induced dissociation (ISCID) were applied to fragment icas#9 and its methyl ester icas#9Me, a characteristic and highly intensive fragment ion signal for $C_{15}H_{16}NO_4^+$ (m/z 274.1074) are produced that originates from the loss of fatty acid side chain (**Figure 2.1** and **Figures S1-2**). Analysis of LC-MS/MS fragmentation of other indole ascarosides revealed identical characteristic fragments of $C_{15}H_{16}NO_4$, suggesting ion screening for m/z 274.1074 as a general analytical method for indole ascaroside profiling in nematodes. For example, a blend of indole ascarosides including the prominent known components icas#9, icas#3 and icas#10^[16] were detected in the *exo*-metabolome of *C. elegans* by using the selective ESI(+)-HR-MS screening method (**Figure 2.2A**), indicating that the method facilitates the discovery of known and possibly unknown indole ascarosides from other worms. Hence, the LC-MS screen was employed for targeted comparative analysis of 13 *Caenorhabditis* species, whose chemical content is still unknown.

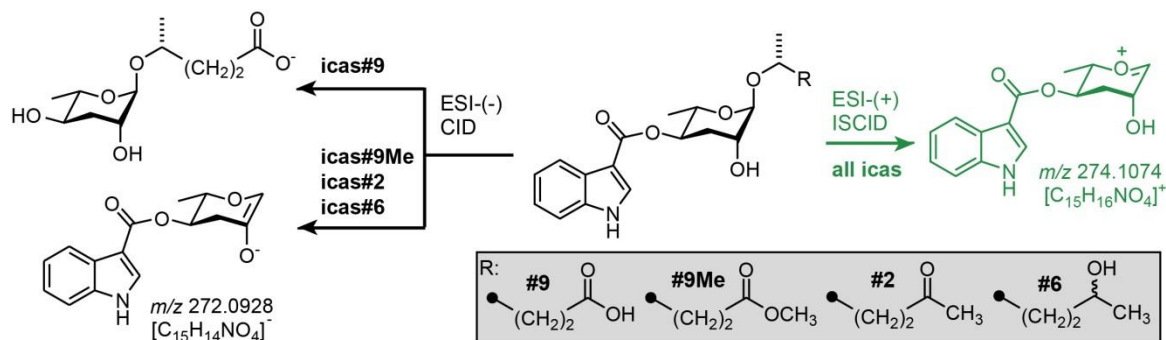


Figure 2.1: MS/MS fragmentation of indole ascarosides in positive and negative ion modes. Fragmentation of indole ascarosides in positive ion mode results in the loss of side chain to give a characteristic $[\text{C}_{15}\text{H}_{16}\text{NO}_4]^+$ fragment (marked in green) which differs from negative ion mode.

Initially we used the ESI(+)-HR-MS screening to analyze the previously unexplored *exo*-metabolome of the closely related hermaphroditic *Caenorhabditis briggsae* strain AF16, which revealed two indole ascarosides peaks of unknown chemical structures, which seems likely to represent novel indole ascarosides (**Figure 2.2B**). Comparative metabolomics study further indicated that both peaks were not corresponding to any of the components known from *C. elegans*, suggesting icas#2 and icas#6.2 to be *C. briggsae*-specific chemical signals.

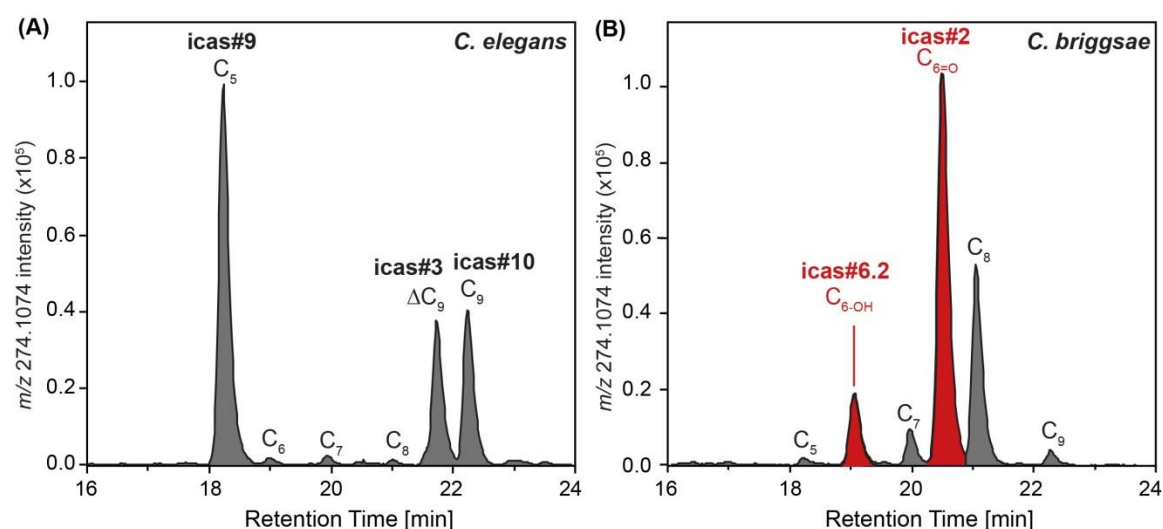


Figure 2.2: Selective MS/MS screening for indole ascarosides reveals *C. briggsae*-dependent components. HPLC-ESI(+)-HR-MS screening for the $[\text{C}_{15}\text{H}_{16}\text{NO}_4]^+$ fragment of (A) *C. elegans* (N2) and (B) *C. briggsae* (AF16) *exo*-metabolome extracts shows signals for indole ascarosides only and reveals two new

indole ascarosides, icas#2 and icas#6.2, in *C. briggsae*.

To test whether other *C. briggsae* strains are able to produce icas#2 and icas#6.2 or not, exo-metabolome extracts derived from 13 wild-type isolates including tropical and temperate strains were prepared for chemical analysis. Targeted LC-MS analysis of these *C. briggsae* strains demonstrated that production of icas#2 and icas#6.2 as dominating indole ascarosides is highly conserved (**Figure 2.3**).

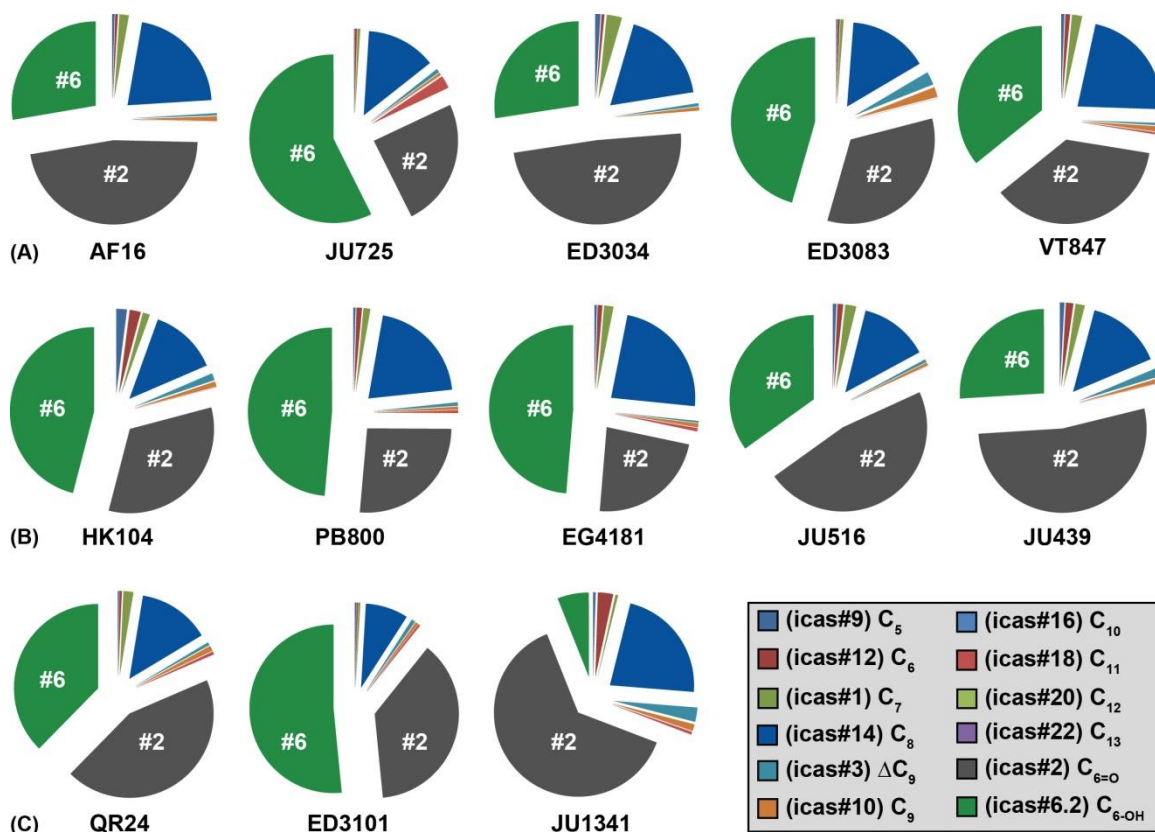


Figure 2.3: Composition of indole ascarosides in 13 wild type isolates of the cosmopolitan *C. briggsae*. (A) Five tropical strains; (B) Five temperate strains; (C) Outgroup strains.

Isolation and structural characterization of indole ascarosides icas#2 and icas#6.2:

High resolution masses of these potential signaling compounds suggested molecular formulas of $C_{21}H_{27}NO_6$ (m/z 388.1775, Δ 2.3 ppm) and $C_{21}H_{29}NO_6$ (m/z 390.1915, Δ 1.8 ppm). MS/MS fragmentation analysis demonstrated that the fragment ion $[C_{15}H_{14}NO_4]^-$ was derived from the loss of the side-chains (**Figure 2.1** and **Figures S3-4**), suggesting that the indole ascaroside structures carried six carbon side-chains with a carbonyl

(icas#2) or hydroxyl group (icas#6), respectively. To unambiguously establish these structural assignments, a chromatographic separation was performed to isolate indole ascarosides icas#2 and icas#6.2 from 1.5 litres of *C. briggsae* liquid culture medium. First, concentrated *C. briggsae* *exo*-metabolome extract was separated into several fractions using reverse phase extraction (RP-SPE) on a C18 column, which were screened by LC-MS. Second, the target fraction containing icas#2 and icas#6.2 (**Figure 2.4**) was further fractionated using high pressure liquid chromatography, which finally resulted in approximately 150 µg icas#2 and 170 µg icas#6. Analysis of one and two dimensional NMR spectra (**Figures S5-12**) suggested a 4-substituted ascarylose unit, an indole-3-carboxylate moiety, and (ω -1)-oxygenated side-chains with a methyl ketone moiety in case of icas#2 or a 2-hydroxyalkyl moiety in case of icas#6.

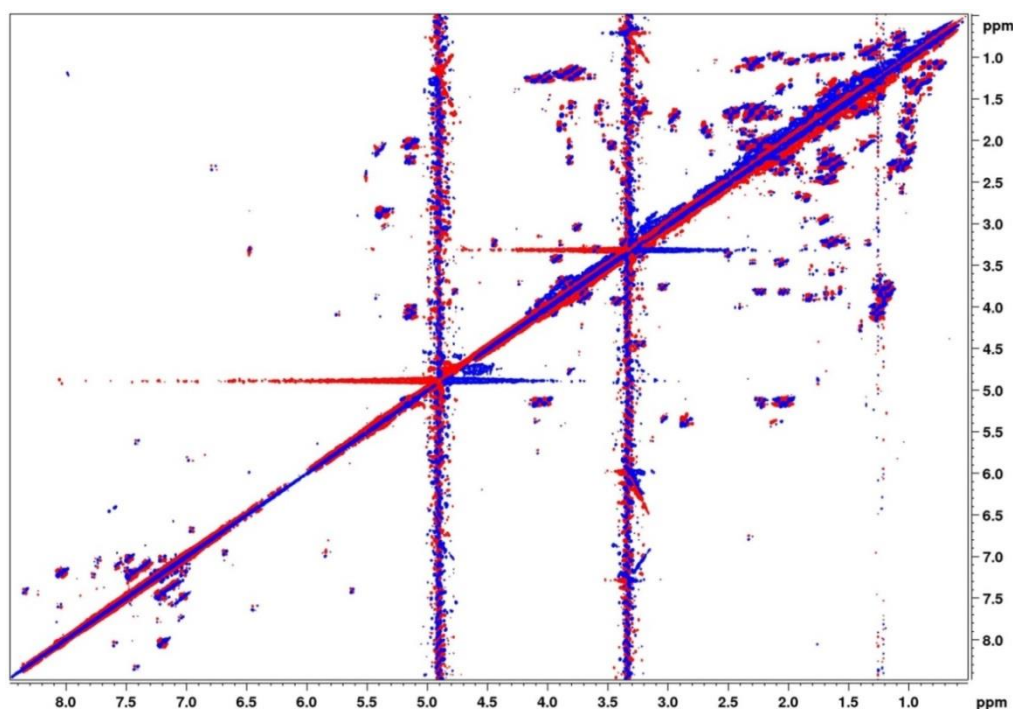


Figure 2.4: *dqf*-COSY spectrum of SPE 70 containing indole ascarosides, which was derived from initial fractionation of the *exo*-metabolome of *C. briggsae*.

The chemical structures of newly discovered indole ascarosides were finally established by total synthesis. Icas#2 has been recently synthesized as an unnatural indole ascaroside, which showed little dauer formation activity in *C. elegans*.^[17] Here, icas#2 and icas#6.1 were synthesized by Franziska Dolke for analytical analysis with the

absolute stereocenter next to the terminal methyl group of icas#6.1 being (*R*). To determine the absolute configuration of icas#6.2, 34 μg icas#2 was further reduced with NaBH_4 to afford a mixture of (*R*)-icas#6.1 and (*S*)-icas#6.2. The acquired ^1H NMR spectrum of this synthetic mixture perfectly agreed with that derived from a 1:1 mixture of 8.5 μg synthetic (*R*)-icas#6.1 and 8.5 μg of the natural icas#6.2 isolated from the *C. briggsae* (AF16) *exo*-metabolome, suggesting a (*S*)-configuration for icas#6.2 (**Figure 2.5**).

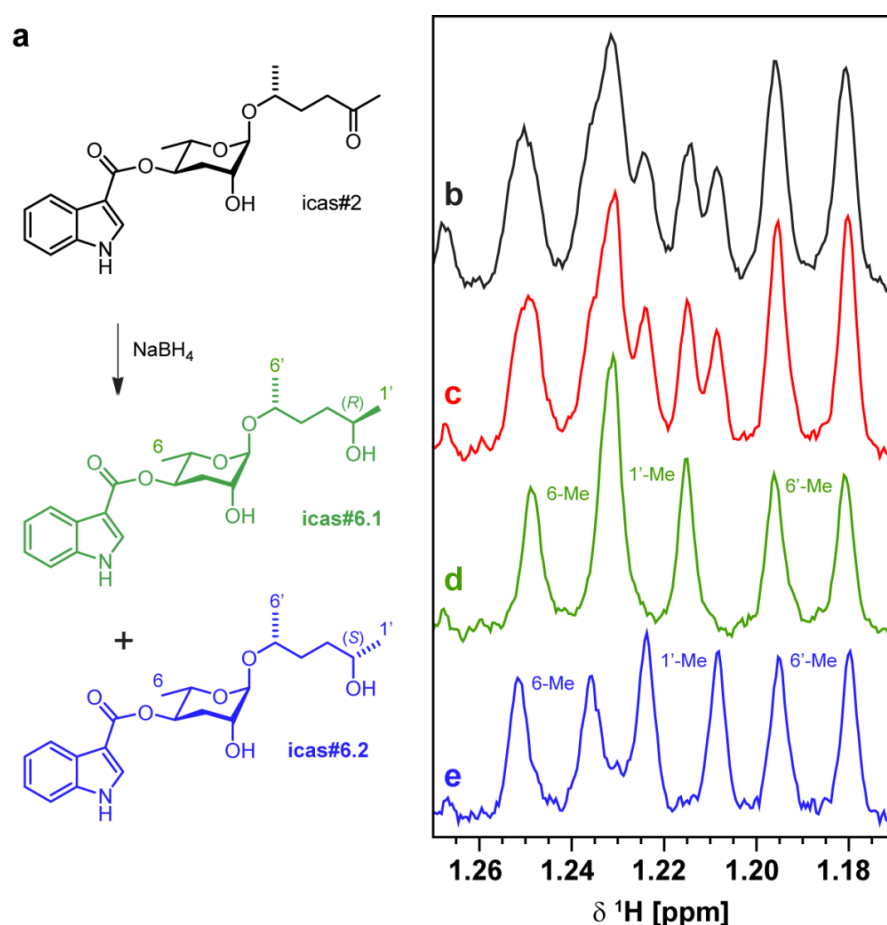


Figure 2.5: Stereochemistry determination of natural (*S*)-icas#6.2 isolated from the *C. briggsae* (AF16) *exo*-metabolome. (a) Sodium borohydride reduction of synthetic icas#2 afforded a 1:1 mixture of diastereoisomeric (*R*)-icas#6.1 and (*S*)-icas#6.2 which could not be separated by HPLC. The same ^1H NMR spectrum section of (b) the diastereoisomeric mixture of synthetic (*R*)-icas#6.1 and (*S*)-icas#6.2, (c) a 1:1 mixture of synthetic (*R*)-icas#6.1 and natural icas#6.2, (d) synthetic (*R*)-icas#6.1 and (e) natural (*S*)-icas#6.2 were compared.

Moreover, the corresponding non-indole derivatives ascr#2 (m/z 269.2922 $[\text{M} + \text{Na}]^+$)

for $C_{12}H_{22}NaO_5$) and ascr#6 (m/z 271.3082 $[M + Na]^+$ for $C_{12}H_{24}NaO_5$) were also detected in the *exo*-metabolome extract of *C. briggsae* (AF16) (**Figure 2.6**). Ascr#2^[13] is known to cause dauer formation in *C. elegans*, whereas ascr#6^[31] with unknown functions was also identified from this model organism.

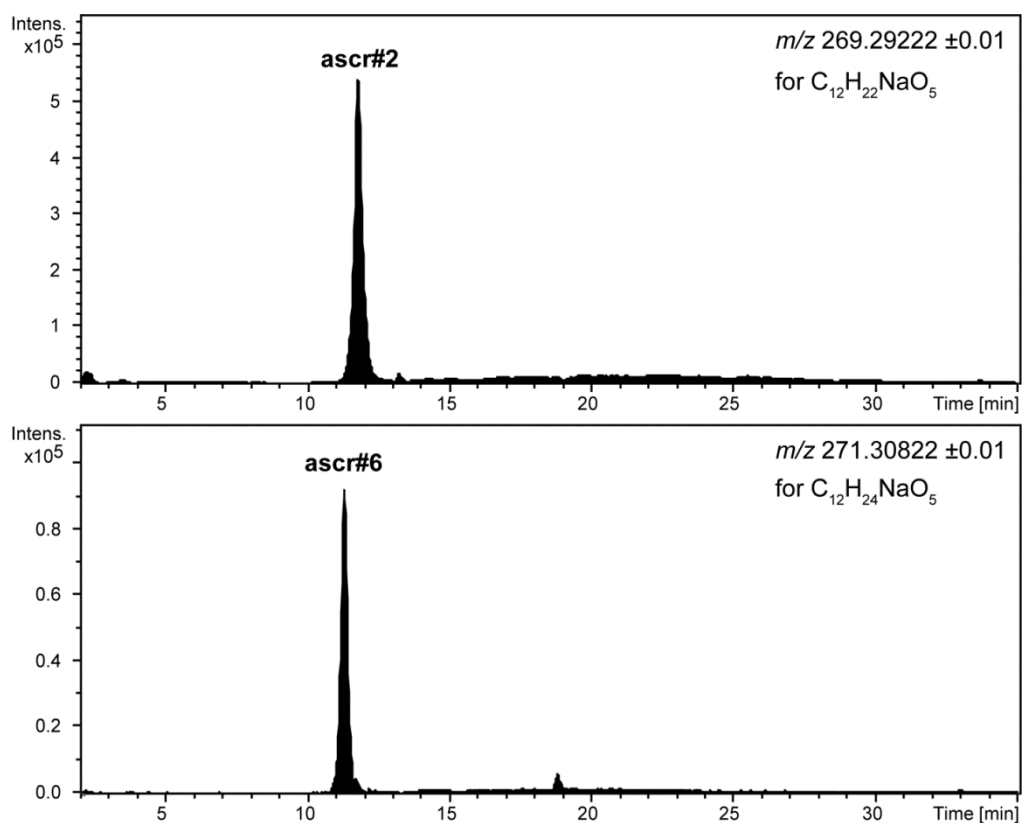


Figure 2.6: Detection of ascr#2 and ascr#6 in *C. briggsae*. HPLC-ESI(+)-HR-MS ion traces corresponding to ascr#2 (m/z 269.29222 $[M+Na]^+$ for $C_{12}H_{22}NaO_5$) and ascr#6 (m/z 271.30822 $[M+Na]^+$ for $C_{12}H_{24}NaO_5$) in the *C. briggsae* (AF16) *exo*-metabolome extract.

Icas#2 and icas#6.2 act synergistically to attract *C. briggsae* males: Biological activities of the two newly characterized indole ascarosides *icas#2* and *icas#6.2* were tested using a holding assay that measures the time nematodes spent within a circular scoring region conditioned with known amounts of indole ascarosides, in comparison with a control region conditioned with methanol. Results in **Figure 2.7A** show that *C. briggsae* males were retained by *icas#2* in amounts as low as 1-25 fmol. The second indole ascaroside *icas#6.2* in amounts as low as 1-2.5 fmol cause retention of *C. briggsae* males in the holding assay (**Figure 2.7B**), whereas hermaphrodites show no response to both

compounds, suggesting that hermaphrodite-produced *icas#2* and *icas#6.2* act as sex pheromone to attract males.

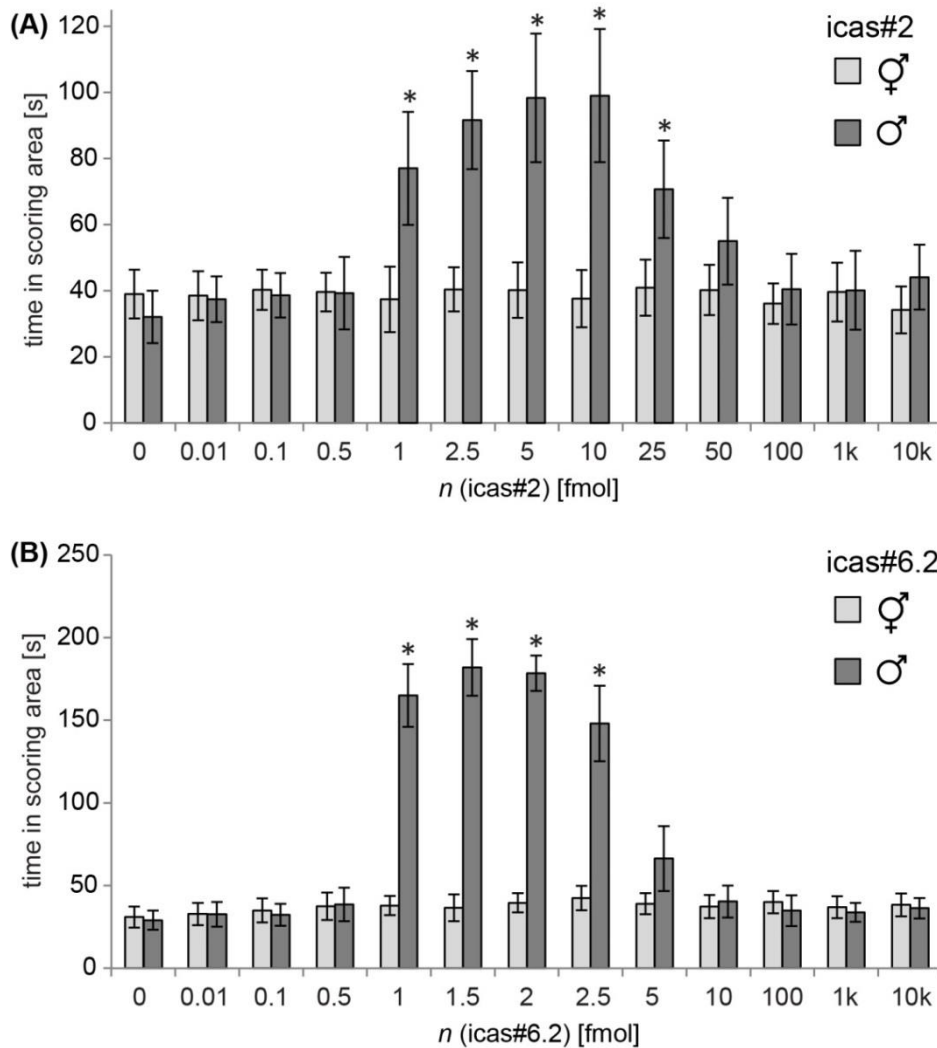


Figure 2.7: Indole ascarosides *icas#2* and *icas#6.2* act as a male-attractant in *C. briggsae*, respectively. (A) *C. briggsae* AF16 males are retained in holding assays with 1-25 fmol *icas#2*; (B) *C. briggsae* AF16 males are retained in holding assays with 1-2.5 fmol *icas#6.2*.

A similar male-specific response to *icas#2* or *icas#6.2* was also recorded for the temperate *C. briggsae* strain HK104 from Japan (**Figure 2.8**).

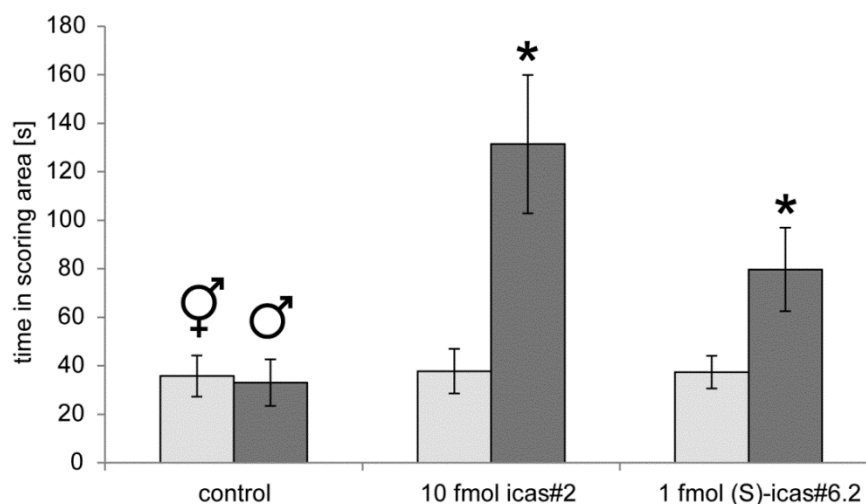


Figure 2.8: Male specific response to icas#2 and icas#6.2 in *C. briggsae* HK104. *C. briggsae* males from the temperate strain HK104 from Japan spent significantly longer times in regions conditioned with 10 fmol icas#2 or 1 fmol (S)-icas#6.2 (± 1 SD, One-way ANOVA with Dunett's posttest, * $p < 0.001$; $n = 10$ worms each).

Most strikingly, the synthesized diastereoisomeric (*R*)-icas#6.1 elicited no response in males (**Figure 2.9**), which highlights the significance of the (*S*)-stereochemistry next to the terminal methyl group on the fatty acid derived side chain.

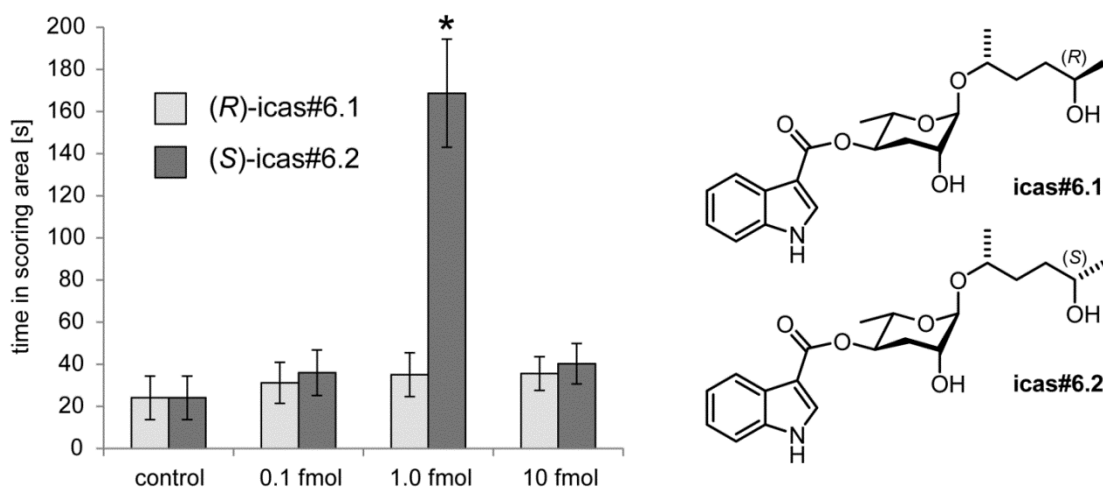


Figure 2.9: Behavioral activity of icas#6.2 depends on the (*S*)-stereochemistry. Holding assay with *C. briggsae* (AF16) males shows significant attraction to 1 fmol of the natural (*S*)-icas#6.2 isolated from the *C. briggsae* *exo*-metabolome whereas the diastereoisomeric (*R*)-icas#6.1 displays no activity at any of the concentrations tested (± 1 SD, One-way ANOVA with Dunett's posttest, * $p < 0.001$; $n = 10$ worms each).

Considering the complex blend of indole ascarosides produced by *C. briggsae*, we asked how combinations of indole ascarosides modulate male attraction. We drastically simplified the complexity of the blend by focusing on the most prominent indole ascarosides icas#2 and icas#6.2 and employed the holding assay to evaluate their activity. Equimolar mixtures of icas#2 and icas#6.2 were used, which showed significant retention by amounts as small as 10 attomol each (**Figure 2.10A**), which do not display any activity if individual components were tested alone (**Figure 2.7A-B**), demonstrating that indole ascarosides exhibit synergistic activities. Moreover, a four-spot attraction bioassay was performed to further test if the observed male retention corresponds to male attraction. Experiments of three groups of indole ascarosides, icas#2, icas#6.2, and a 1:1 mixture, in the four-spot attraction bioassay demonstrated that the mixture shows much more attraction than the single components (**Figure 2.10B**). Taken together, we found that the hermaphrodite-produced species-specific blend of icas#2 and icas#6.2 acts as a synergistically active male attractant, suggesting a function as a sex pheromone in this facultative outcrossing species.

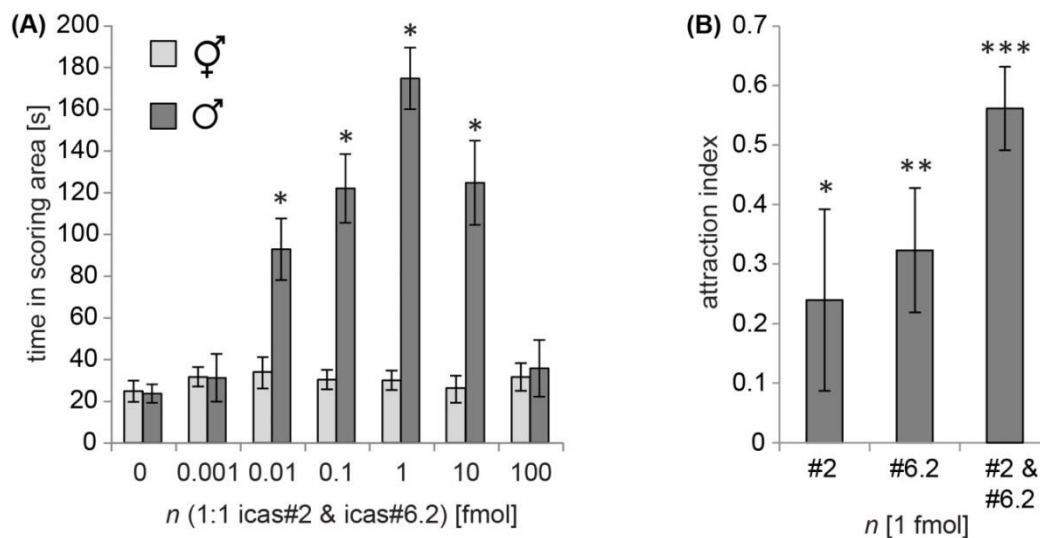


Figure 2.10: Species-specific indole ascarosides icas#2 and icas#6.2 act as a synergistic male-attractant in *C. briggsae*. (C) Equimolar mixtures of atto- to femtomolar amounts of icas#2 and icas#6.2 synergistically retain *C. briggsae* AF16 males in holding assays; (D) femtomolar amounts of icas#2, icas#6.2, and their synergistic blend attract *C. briggsae* AF16 males in the 4-spot attraction assay (A-C: one-way ANOVA with Dunett's posttest, *p<0.001; d: students' t test with Welch's correction, *p<0.05, **p<0.01, ***p<0.001).

Indole ascaroside biosynthesis is widely conserved within the *Elegans* group:

Indole ascarosides were described to be biosynthesized through attachment of indole-3-carboxylic acid, a putative biosynthetic intermediate originating from tryptophan metabolism.^[23] The biosynthesis of indole ascaroside in a collection of 14 representative *Caenorhabditis* species was analyzed using the selective ESI-(+)-HR-MS screening method described above. Of the nine species in the *Elegans* group that were analyzed, eight species are able to produce indole ascarosides, suggesting that their biosynthesis is widely conserved in the *Elegans* group (**Figure 2.11**). However, each species produced a very complex and species-specific blend of indole ascarosides with different side chains harboring 5 to 13 carbons. In contrast indole ascarosides were undetectable in the liquid culture medium derived from *Caenorhabditis* nematodes outside of the *Elegans* group.

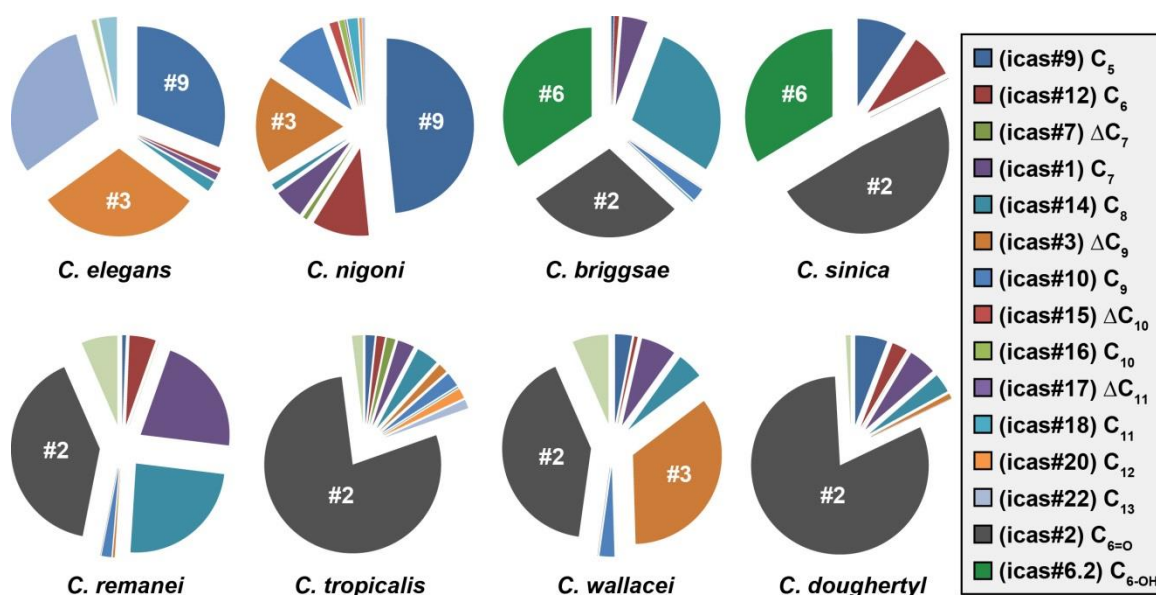


Figure 2.11: Species-specific indole ascaroside biosynthesis is highly conserved in the *Elegans* group. Eight species of nematodes within *Elegans* group produced a complex indole ascaroside blend.

Generally, eight species of nematodes produced icas#2, icas#3, icas#6 and icas#9 as the most prominent indole ascaroside components in their conditioned culture medium. On the other hand, analysis of indole ascaroside composition showed that the biosynthesis of indole ascarosides was highly species-specific (**Figure 2.11**). Indole ascaroside profiles of *C. elegans* and *C. nigoni* are dominated by icas#3 and icas#9,

whereas those of *C. briggsae*, *C. sinica*, *C. remanei*, *C. tropicalis*, and *C. doughertyi* are dominated by icas#2. *C. wallacei* mainly produces a blend of icas#2 and icas#3. The corresponding biosynthetic precursors ascr#2 and ascr#3 were also detected in almost all nematodes in the *Elegans* group (ascr#2 was absent in *C. nigoni* and only traces of ascr#3 were detectable in *C. briggsae*) indicating that attachment of the indole group represents the species-specific step. For quantitative analysis, three replicates of high density nematode culture media grown for 15 days were extracted and analyzed by LC-MS, along with chemically synthesized authentic standards of known concentrations (by Franziska Dolke), which revealed that the physiological concentrations range from nM to pM for most of the prominent indole ascarosides. However, extraordinary high concentrations of 750 nM icas#2 and 1.6 μ M icas#9 were observed in *C. tropicalis* and *C. nigoni*, respectively (Figure 2.12).

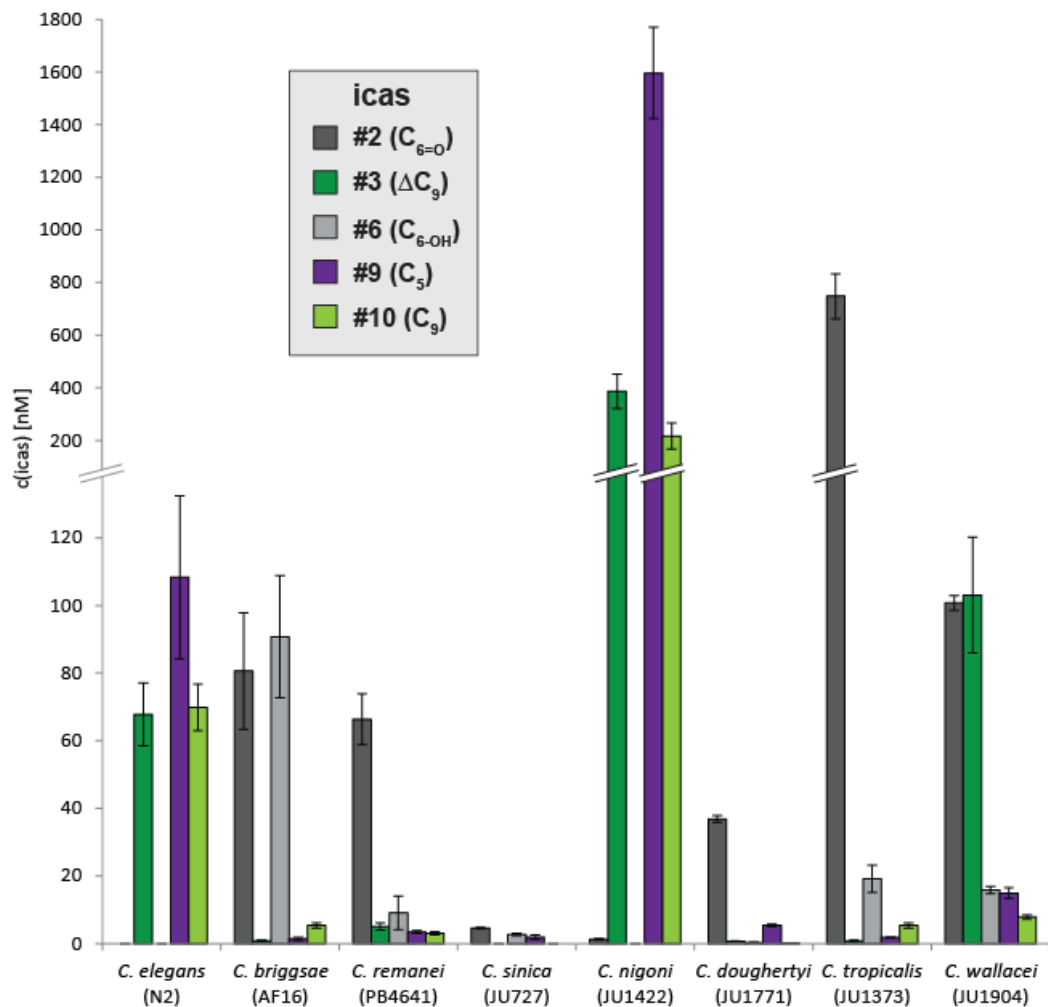


Figure 2.12: Concentrations of dominating indole ascarosides. Quantitative LC-MS analysis of *exo*-metabolome extracts from nematode cultures grown for 15 days under identical conditions using authentic standards indicated that concentrations of the most prominent indole ascaroside components ranges from low nM to pM concentrations ($\pm 1SD$).

Highly species-specific behavioural response in holding assay suggested variant biological functions modulated by indole ascaroside signals: Considering our discovery that the production of species-specific indole ascarosides blends is conserved in the *Elegans* group we aimed to analyze their biological functions in these species focusing on the three dominating components, the newly discovered icas#2, as well as the previously described icas#3 and icas#9 known as dauer inducing^[19] and hermaphrodite attractant and aggregation signal in *C. elegans*^[16]. Aiming to characterize behavioural response, nine species within the *Elegans* group were carefully tested using holding assay (**Figure 2.13**), which demonstrates that the behavioural responses are highly species-specific and exhibit considerable variability with respect to gender specificity, suggesting that indole ascarosides modulate different biological functions within the *Elegans* group. Similar to the attraction response of *C. briggsae* males to icas#2, male-specific activity was also observed in the closely related *C. sinica* as well as distantly related *C. tropicalis*, suggesting that icas#2 might act as a sex pheromone. In contrast to this male-specific response, icas#2 affects males and females in gonochoristic *C. remanei*, *C. doughertyi*, and *C. wallacei*. Similarly, icas#3 and icas#9 affect both genders of *C. elegans* and *C. wallacei* but only males of *C. nigoni*. When the behavioural response was tested over a wide range of concentrations (ranging from 1 to 10000 fmol), bell-shaped dose response curves are observed, which indicated that nematodes exhibit a strong preference for specific pheromone concentrations. In most cases, the behavioural responses shows considerable self-preference for the majority of *Elegans* nematodes, which exhibit no or only very weak responses to the components abundantly produced by other species. For instance, *C. briggsae* and *C. tropicalis* are not attracted by icas#3, which is mainly produced by *C. elegans* and *C. wallacei*. Finally, the behavioural response of *C. brenneri* was also tested, which indicated that males respond

to icas#9 and icas#2, although *C. brenneri* nematodes are not capable to produce indole ascarosides, suggesting the possibility for a cross-species chemical interactions modulated by icas#2 and icas#9.

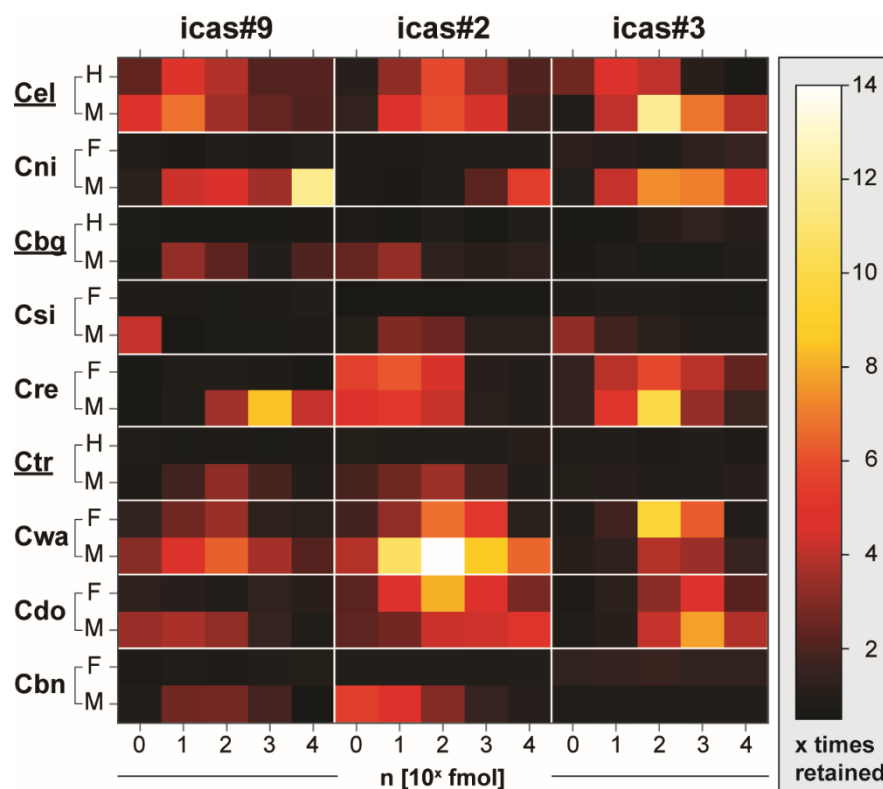


Figure 2.13: species- and gender-specific responses to three indole ascarosides prominent in the *Elegans* group. Heatmap showing nematode retention as an increase of holding times in regions conditioned with 1-10000 fmol of icas#9, icas#2, or icas#3 for both genders of nine *Caenorhabditis* species in comparison to solvent control (H: hermaphrodite; F: female; M: male).

Conclusions: In this study, a highly sensitive MS-based method was established to selectively screen for indole ascarosides in crude nematode *exo*-metabolome extracts, which led to the discovery of two novel species-specific indole ascarosides (icas#2 and icas#6.2) from *C. briggsae*. Both components were isolated, identified by NMR spectroscopy, and their structures were unambiguously confirmed by total synthesis and chemical correlations. Biological tests indicated that icas#2 and icas#6.2 act in synergism to attract males when present in attomolar amounts. Comparative metabolomics further demonstrated that the biosynthesis of indole ascarosides is widely conserved in the *Elegans* group and that the novel icas#2, as well as the previously reported icas#3 and

icas#9 are most abundantly produced. Bioassays with these prominent signaling compounds and nine members of the *Elegans* group demonstrated that the behavioural responses to indole ascarosides are highly species-specific. Taken together our results reveal that species-specific indole ascaroside signaling is widely conserved within the *Elegans* group, suggesting that species-specific modifications of the common ascaroside scaffold might in fact form the basis to facilitate highly species-specific intra-species interactions in co-occurring species.

Chapter 3

Comparative Metabolomics Reveals a Panel of Novel Fatty Acid Ascarosides from *C. remanei* and *C. latens*

Detection and characterization of a prominent and highly species-specific fatty acid ascaroside in the exo-metabolome of *C. remanei*: A prominent peak (Figure 3.1B) was detected in the exo-metabolome of *C. remanei* (PB4641) while analyzing the results of MS/MS precursor screening data derived from comparative metabolomics (described in Chapter 1), which seems likely to be a novel ascaroside with the molecular ion signal at m/z 415. Within the *Elegans* group, only *C. remanei* was found to produce this compound indicating extremely high species-specificity.

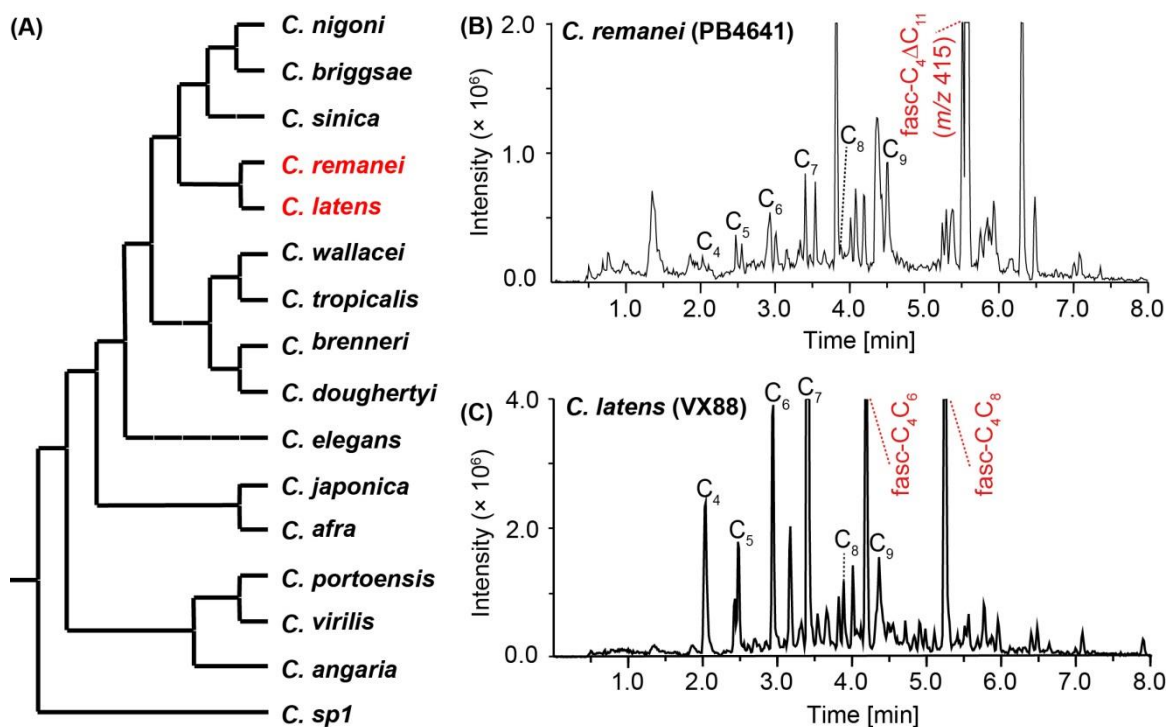
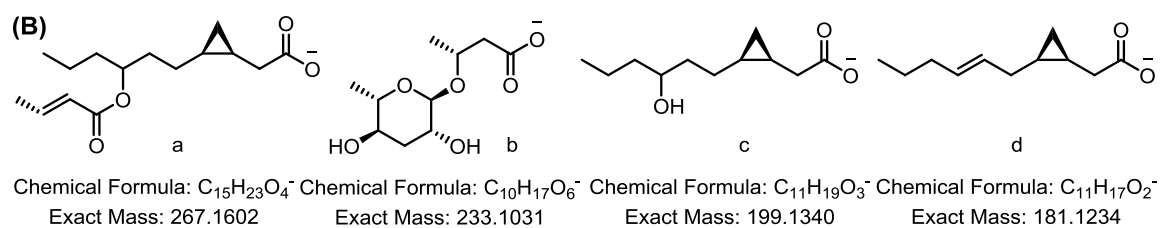
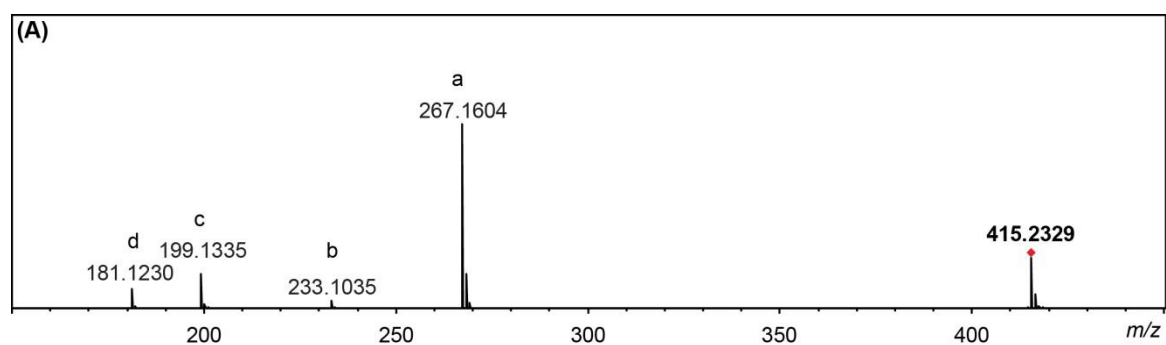


Figure 3.1: Precursor screening of the exo-metabolome extract of *C. remanei* and *C. latens* reveals high species-specific fatty acid ascarosides. (A) Fatty acid ascarosides were exclusively detected in the red color highlighted nematodes. (B) Fatty acid ascarosides signals were detected in PB4641 using the established precursor ion screen. (C) Fatty acid ascaroside signals were detected in VX88.

High resolution mass spectrometry of the target compound suggests a molecular formula of $C_{21}H_{36}O_8$ ($C_{21}H_{35}O_8^-$, obs. m/z 415.2339, calcd. m/z 415.2337). MS^2

fragmentation (**Figures 3.2A-C**) demonstrates two prominent peaks of which one at m/z 267.1604 resulted from the loss of ascarylose moiety, whereas the other at m/z 199.1335 derived from a C11 cyclopropyl fatty acid moiety, as well as one minor peak m/z 146.9 for ascarylose. Further MSⁿ (**Figure 3.2D**) fragmentation of the m/z 267.1 peak shows three daughter ions of m/z 199.1, m/z 181.1 derived from the loss of H₂O from m/z 199.1 along with m/z 84.9. MSⁿ fragmentation of m/z 199.1 finally breaks the C7-C8 bond within the C11 acid and results in two daughter ions of m/z 155.1 and m/z 71.0. All the MS data suggest that the detected prominent peak at m/z 415 was most likely an ascaroside proposed as fasc-C₄ΔC₁₁ in **Figure 3.3B** featuring two units a C4 ascarylose and a C11 cyclopropyl fatty acid. But additional NMR data are required to determine its exact chemical structure, especially to clarify the C11 fatty acid with one unit of unsaturation as suggested by high resolution mass.



(C)

Observed m/z	Calculated m/z	Error (ppm)	Ion Formula	Ion assignment
415.2329	415.2337	1.9	C ₂₁ H ₃₅ O ₈ ⁻	[M-H] ⁻
267.1604	267.1602	-0.6	C ₁₅ H ₂₃ O ₄ ⁻	a
233.1035	233.1031	-1.8	C ₁₀ H ₁₇ O ₆ ⁻	b
199.1335	199.1340	2.5	C ₁₁ H ₁₉ O ₃ ⁻	c
181.1230	181.1234	2.4	C ₁₁ H ₁₇ O ₂ ⁻	d

(D)

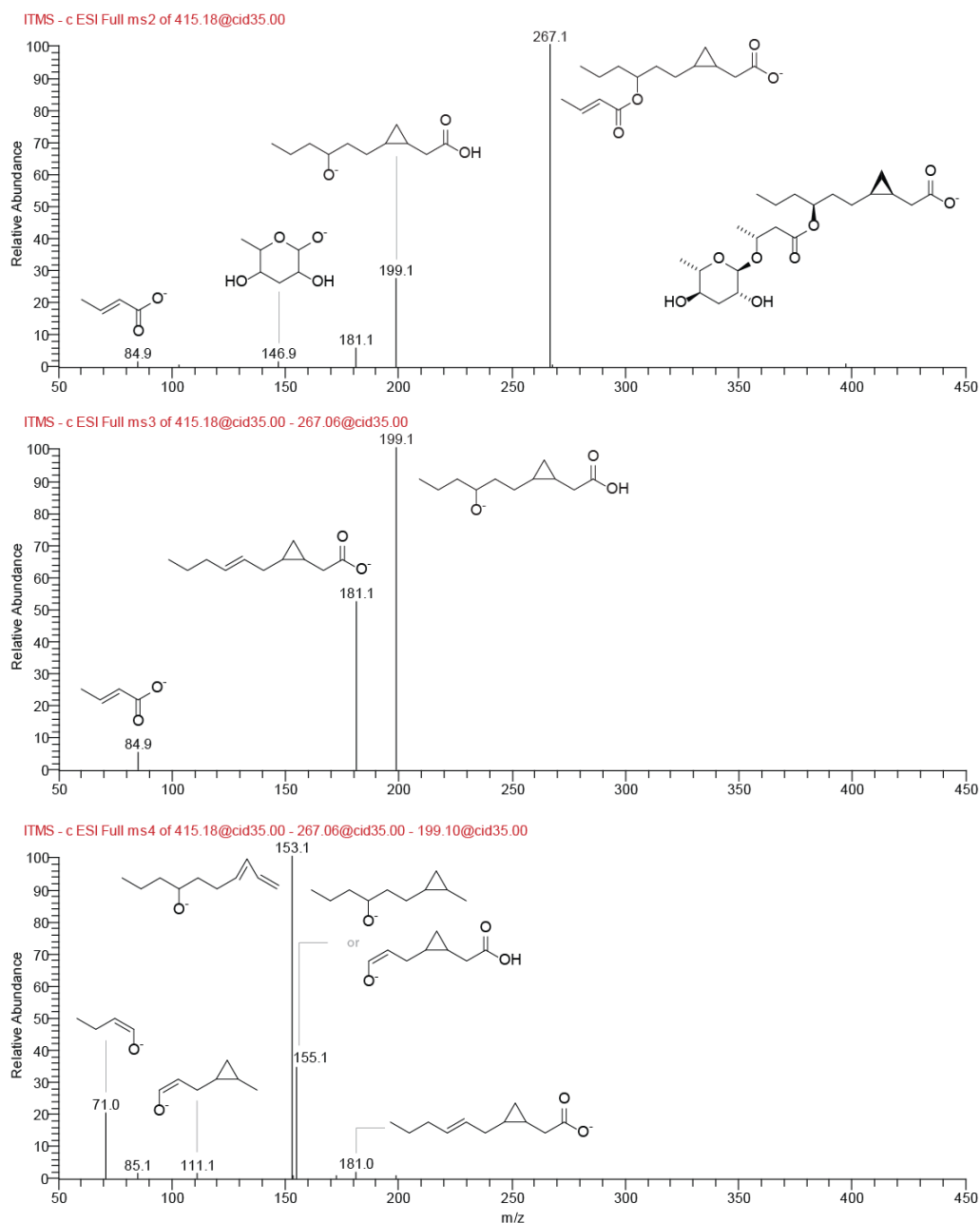


Figure 3.2: LC-MS/MS data analysis of fasc-C₄ΔC₁₁. (A) MS/MS spectrum of fasc-C₄ΔC₁₁. (B) Putative ion structures. (C) Table of MS/MS ion peak assignments. (D) MSⁿ fragmentation spectrum of fasc-C₄ΔC₁₁.

For further structural characterization of fasc-C₄ΔC₁₁, 1.2 L culture medium of *C. remanei* strain PB4641 was fractionated *via* solid phase chromatography (SPE) and HPLC followed by *dqf*-COSY analysis of the target-containing fractions (described in **Chapter 1**). A total amount ca. 100 μg of fasc-C₄ΔC₁₁ was isolated and purified from PB4641. Despite the low abundance of fasc-C₄ΔC₁₁, derived proton and 2D spectra (**Figures S13-17**) were successfully acquired, which confirmed the assignment of a C₄

ascaroside, and indicated that the unsaturated C11 fatty acid is a (ω -3)-hydroxycascarillic acid moiety carrying a cyclopropyl ring. NOESY correlations between H-4'' and H-2'' as well as H-6'' (**Figure 3.3B**) indicated the relative configuration of the *cis*-fused cyclopropyl ring in the C11 fatty acid of *fasc*-C₄ Δ C₁₁. Finally Mosher's method^[38] was applied to determine the absolute configuration. The definition of the absolute stereochemistry of *fasc*-C₄ Δ C₁₁ required derivatization reaction and spectroscopic analysis of its products. Using hydrolysis with a strong base, *fasc*-C₄ Δ C₁₁ was chemically degraded in the NMR tube to free the secondary hydroxyl group at C-8'' of the cyclopropyl fatty acid and the C4-ascaroside, which were both converted to their methyl esters using TMS-diazomethane and subsequently isolated. Next, (*R*)-(-)- and (*S*)-(+)- α -methoxy- α -trifluoromethyl-phenylacetic acid (MTPA) chlorides efficiently reacted with the free secondary hydroxyl group to give the diastereoisomeric MTPA esters (*R*- and *S*-MTPA) (**Figure 3.3A**). A consistent distribution of positive and negative $\Delta\delta$ ($= \delta_S - \delta_R$) values allowed the stereochemistry to be assigned as *S* configurations for C8''. Furthermore, the fact that the $\Delta\delta$ values within the methylene bridge of the cyclopropyl unit were rather large suggested that it was located on the same side as the MTPA group, thus suggesting a *S, S* configuration for C3'' and C5'' (**Figure 3.3C**). Subsequently, the chemical structure of *fasc*-C₄ Δ C₁₁ was clarified and shown in **Figure 3.3B**, featuring an additional cyclopropyl fatty acid attached to the C4 side chain. Ascarosides bearing two layers of fatty acids have not yet been observed in nematodes, which is reminiscent of rhamnolipids discovered from *Pseudomonas aeruginosa*.^[39] Meanwhile, multiple steps of chemical synthesis were established by Franziska Dolke to confirm the molecular structure of *fasc*-C₄ Δ C₁₁ and to obtain pure samples for bioassays. Spectroscopic data and HPLC retention time of the synthetic compound perfectly agree with those of the isolated material, which unambiguously determined the proposed structure of *fasc*-C₄ Δ C₁₁.

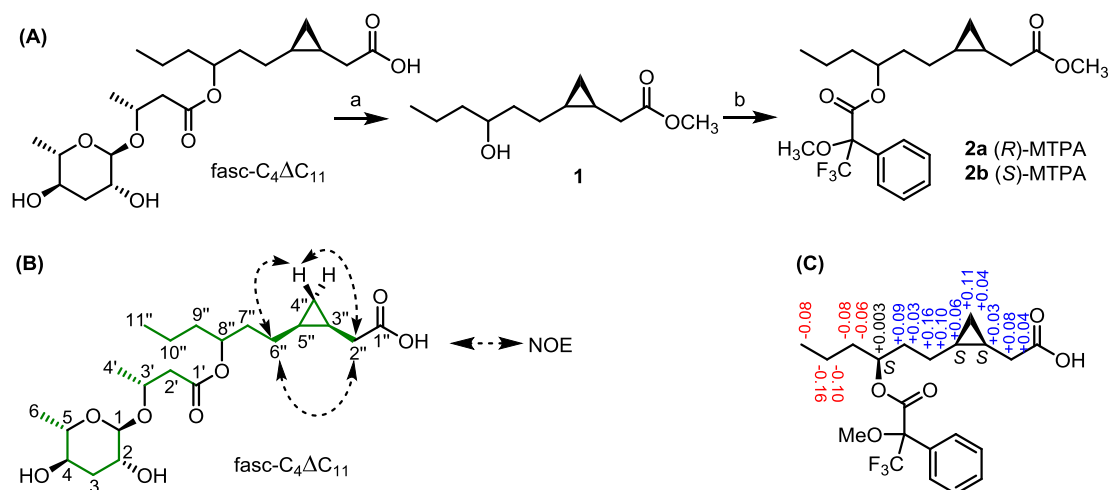


Figure 3.3: Absolute stereochemistry characterization of fasc-C₄ΔC₁₁. (A) Synthesis of (R)-MTPA and (S)-MTPA esters. a: 1. NaOD/D₂O, CD₃OD; 2. TMS-diazomethane, MeOH/toluene; b: (R)-MTPA-Cl or (S)-MTPA-Cl, pyridine-*d*₆. (B) Selective NOESY correlations of fasc-C₄ΔC₁₁. Green color indicated selective ¹H, ¹H-COSY correlations. HMBC correlations are listed in **Table S5**. (C) Δδ (δ_S - δ_R) values calculated for the MTPA esters of C11 cyclopropyl fatty acid.

Biochemical diversity of fatty acid ascarosides in *C. remanei*: The precursor ion screening of *C. remanei* also showed four minor peaks sharing very similar MS² fragmentation patterns to the characterized fasc-C₄ΔC₁₁. MS² fragmentation of these molecules revealed that one common fragment *m/z* 233.1035 (**Figures 3.2 and 3.4**) is cleaved off, suggesting that detected components might also be fatty acid ascarosides that share identical unit of a C4 ascaroside. Based on their high resolution masses along with MSⁿ analysis and microscale chemical derivatization (performed by Stephan H. von Reuß), we proposed the chemical structures of these ascarosides as shown in **Figure 3.6**. Finally, the fatty acid ascarosides can be categorized into three types according to the remaining moieties of a cyclopropyl fatty acid, a saturated or an unsaturated fatty acid. Thus, one MS method of selectively screening for the characteristic fragment of *m/z* 233.1035 (C₁₀H₁₇O₆⁻; calcd. *m/z* 233.1031) was established for detecting fatty acid ascarosides, which resulted in the discovery of a series of homologues (**Tables S3-4**). Ascarosides of fasc-C₄C₆ and fasc-C₄C₈ were detected to be most abundant in the *exo*-metabolome of the newly isolated species *C. latens*, a sister species to *C. remanei*. Next, we also set up large liquid culture of *C. latens* (VX88) for isolation and chemical

characterization of fasc-C₄C₆ and fasc-C₄C₈. Both components were isolated from VX88 metabolome extracts, which enabled their structure identification. Analysis of proton and *dqf*-COSY spectra (**Figures S18-19**), MS/MS fragmentation (**Figure 3.4**) and chemical synthesis subsequently helped to determine the full structures of fasc-C₄C₆ and fasc-C₄C₈ and revealed that they carry an (ω -5)-linked fatty acid in contrast with the (ω -3)-linked cyclopropyl acid observed in *C. remanei*.

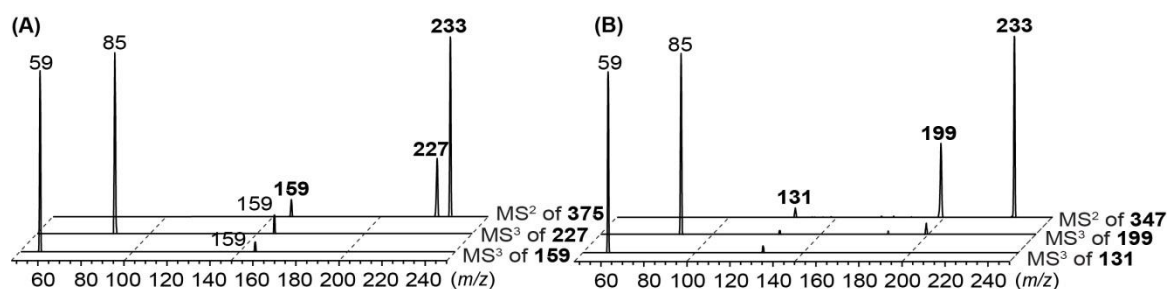


Figure 3.4: MSⁿ (ESI) fragmentation analysis of fasc-C₄C₈ and fasc-C₄C₆. (A) MS² and MS³ spectra of fasc-C₄C₈. (B) MS² and MS³ spectra of fasc-C₄C₆.

It is still challenging to clarify the unsaturated and cyclopropyl fatty acids encoded in fatty acid ascarosides. Firstly, resistance to Pd/C catalyzed hydrogenation and MS² fragmentation of cyclopropyl ascarosides fasc-C₄ΔC₁₁ and fasc-C₄ΔC₁₃ suggests that C13 cyclopropyl fatty acid in fasc-C₄ΔC₁₃ owns two CH₂ units more than that of fasc-C₄ΔC₁₁ and these are located in a terminal pentyl chain (instead of the propyl chain of fasc-C₄ΔC₁₁). As described above, when the C7-C8 bond in the cyclopropyl moiety was broken upon MSⁿ fragmentation the terminal gives rise to a fragment ion peak at *m/z* 99, which suggests two more CH₂ units than that of fasc-C₄ΔC₁₁ which allows the clarification of the position of connectivity of the two fatty acids. Similarly, MSⁿ fragmentation also helps to characterize the (ω -5)-position of the connectivity in fasc-C₄ΔC₁₂ a representative of the series of unsaturated fatty acid ascarosides observed in *C. remanei* (**Figure 3.5**).

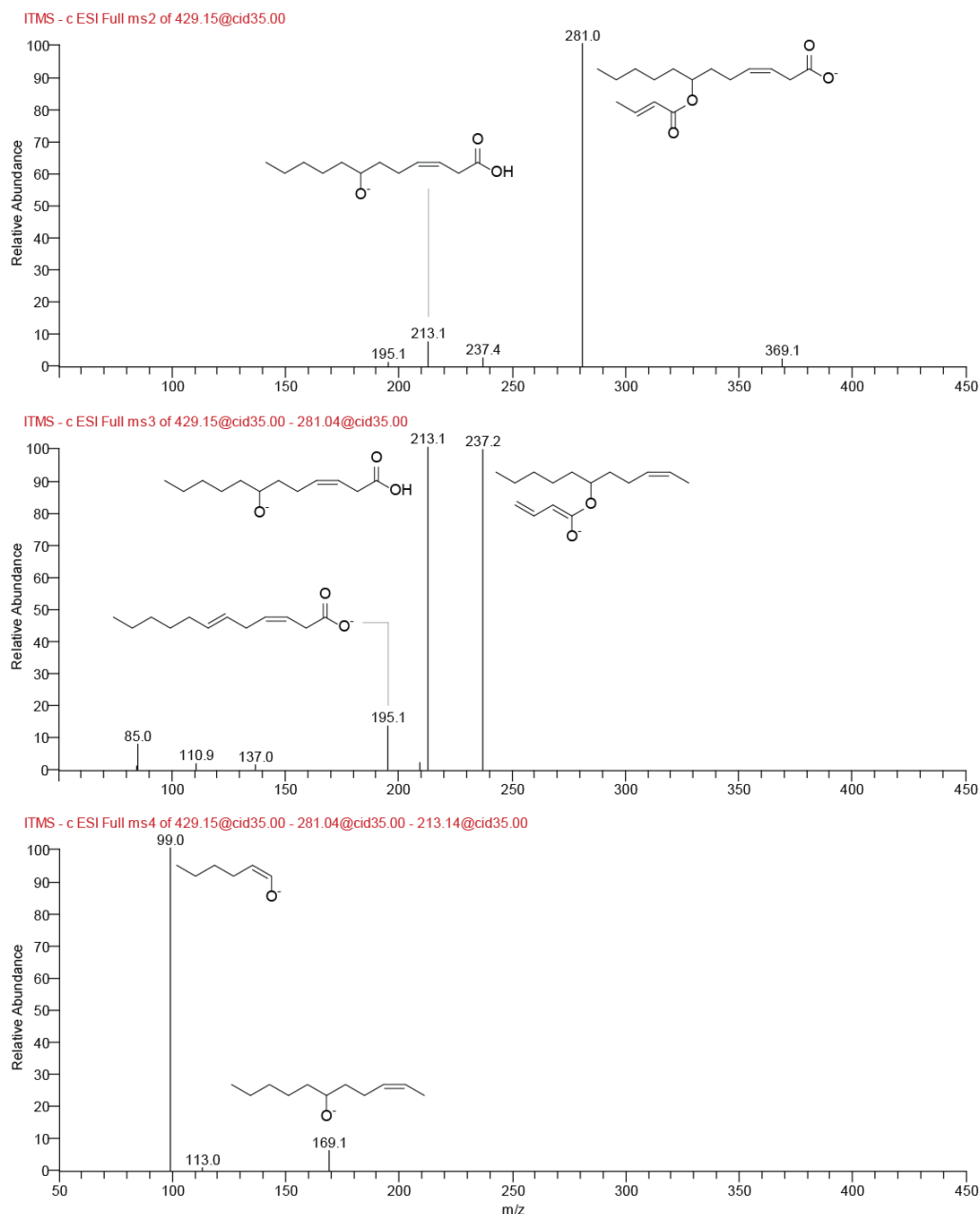


Figure 3.5: MS² and MSⁿ (ESI) fragmentation analysis of unsaturated fasc-C₄ΔC₁₂. Upper is the MS/MS spectrum of fasc-C₄ΔC₁₂. Middle is the MS³ spectrum of fragment at *m/z* 281.0. Lower is the MS³ spectrum of fragment at *m/z* 213.1.

In addition osmium tetroxide (OsO₄) induced *cis*-dihydroxylation was employed using enriched SPE fraction containing unsaturated fatty acid ascarosides, which allows alkene fatty acids in unsaturated fatty acid ascarosides to be converted to *cis*-diols, which are subsequently fragmented between the hydroxyl groups upon MSⁿ. With these MSⁿ experiments of dihydroxylated samples after OsO₄ treatment, we were able to assign the

exact position of the double bond in unsaturated fatty acid ascarosides. In conclusion, one novel class of fatty acid ascarosides (fasc) were characterized from *C. remanei* and *C. latens* (**Figure 3.6**), demonstrating a great biochemical diversity and high species-specificity.

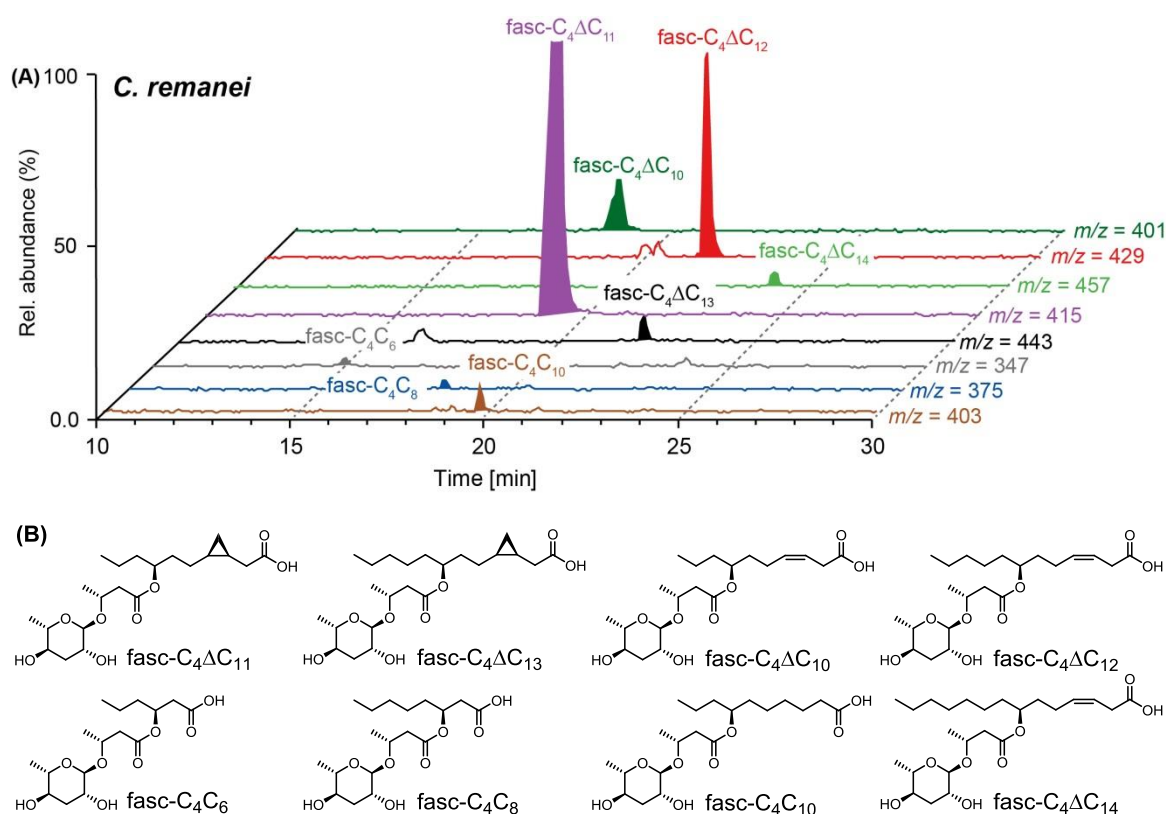


Figure 3.6: Fatty acid ascarosides identified from *C. remanei* and *C. latens*. (A) Fatty acid ascarosides were profiled from *C. remanei* by LC-MS. (B) Chemical structures of novel fatty acid ascarosides.

Metabolic variation of *C. remanei* and *C. latens* dependent fatty acid ascarosides:

Comparative analysis of 13 *Caenorhabditis* species showed that fasc are exclusively produced by the closely related *C. remanei* and *C. latens*, suggesting that fasc are highly specific to *C. remanei* and *C. latens*. Next, metabolic variation of fasc was investigated. To quantify fasc production, *exo*-metabolome extracts of six *C. remanei* and two *C. latens* wild-type isolates were analyzed using LC-MS. *C. remanei* nematodes included two strains from New York (PB4641) and Ohio (PB228), United States, one strain from Japan (JU1082) as well as three strains from Freiburg (SB146) and Tübingen (MY2231 and

MY726), Germany. Two *C. latens* strains were isolated from Jiangsu (JU724) and Hubei (VX88), China. Our results demonstrate that all eight strains are capable of producing fasc. Considerable qualitative and quantitative differences between the various strains were also observed whereas *C. remanei* abundantly produces cyclopropyl and unsaturated fatty acid ascarosides, in contrary, *C. latens* mainly produced saturated fatty acid ascarosides (**Figure 3.7**). For example, ascarosides fasc-C₄ΔC₁₁ and fasc-C₄ΔC₁₂ are found to be two major compounds in the *C. remanei* strains, and whereas fasc-C₄C₈ is the main constitute in *C. latens* strains. Moreover, metabolic variation appears to be independently regulated because of their genetic divergence and worldwide biogeographic distribution. For example, nematodes (PB4641 and PB228) from US produce much higher amount of fasc-C₄ΔC₁₁ than the other strains, Furthermore, all three strains (SB146, MY2231 and MY726) from Germany are quite different from each other SB146 and MY2231 share almost the same composition with the unsaturated fasc-C₄ΔC₁₂ to be more prominent than cyclopropyl containing fasc-C₄ΔC₁₁, although they were isolated from distinct locations of Germany. In contrast, MY726 (which was isolated in close proximity to MY2231) is able to abundantly produce fasc-C₄ΔC₁₁, similar to the American strains (PB4641, PB228).

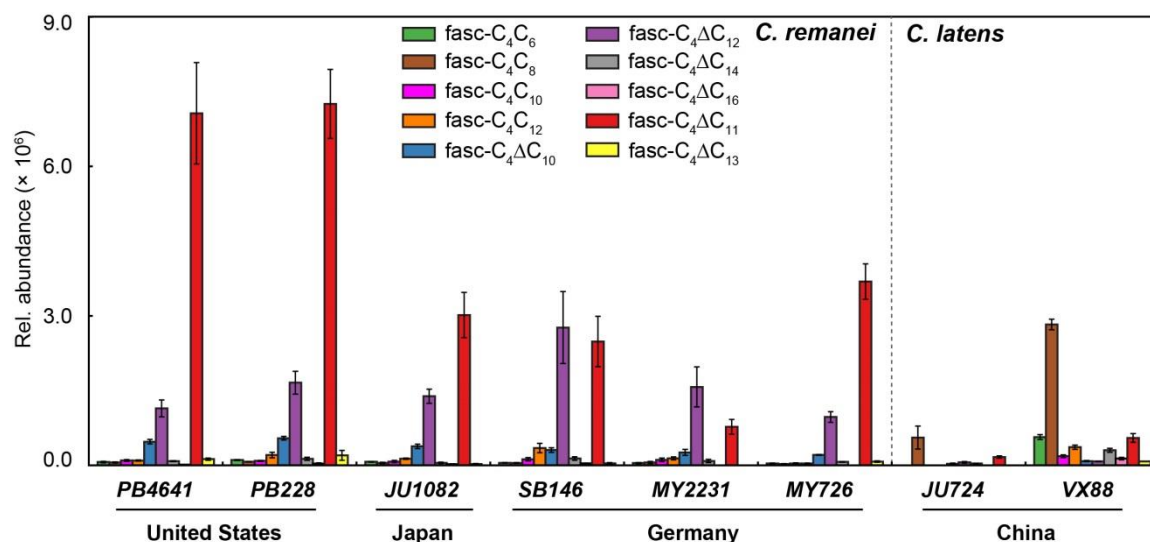


Figure 3.7: Relative abundance of fatty acid ascarosides detected in *C. remanei* strains by using HR-QTOF-LCMS with negative ion mode (ESI). Each strain was cultivated with three biological replicates. Error bar represents \pm SD.

Most notably, the recently described *C. latens* strains JU724 and VX88 secrete only trace amount of fasc-C₄ΔC₁₁ and fasc-C₄ΔC₁₂. However, the shorter chain ascarosides such as fasc-C₄C₈ is found to be mainly produced by *C. latens*, which is characterized by analyzing four dominating fatty acid ascarosides (fasc-C₄C₆, fasc-C₄C₈, fasc-C₄ΔC₁₁ and fasc-C₄ΔC₁₂) and minor components in each strain. VX88 was recently reported to be able to form F1 hybrids with *C. remanei* nematodes, but caused high mortality of hybrid progeny in the second generation.^[40] Our results confirm that, according to their ascaroside composition, *C. latens* is also chemically a close relative to *C. remanei*.

Biosynthesis of fasc-C₄ΔC₁₁: Nematodes enter into dauer stage when they sense ascarosides pheromone, and low food source availability also drives them into this special developmental stage. In contrast, dauer larvae recover from diapause to continue their normal production and life cycle, which is thought to be stimulated by chemical signals from the food source.^[10] Bacteria constitute the main fatty acid source provider, which is the typical food source in the standard laboratory maintenance of nematodes.^[41,42,43] In exponential growth phase, bacteria mainly produce saturated or monounsaturated fatty acids as integral components of their membrane. However, upon the stationary phase bacteria produce the enzyme cyclopropane fatty acyl phospholipid synthase (CFA) which catalyzes the formation of cyclopropyl fatty acids from monounsaturated fatty acids using SAM (*S*-adenosyl methionine) (**Figure 3.8A**).^[44,45] The cyclo-C17 acid was isolated and structurally characterized from *E. coli* B-ATCC 1103.^[46] The metabolism of cyclopropyl fatty acids and their biological activities are still elusive. After dissecting the exact chemical structure of fasc-C₄ΔC₁₁, we hypothesize that bacteria derived cyclo-C17 acid might be a starting substrate in the biosynthesis of fasc-C₄ΔC₁₁. To test the hypothesis and investigate the biosynthesis of fasc-C₄ΔC₁₁, three groups of *C. remanei* (PB4641) samples were prepared for comparative analysis, which differed in being fed with different *E. coli* food sources, *E. coli* OP50, an uracil auxotroph considered wildtype in fatty acid biosynthesis, a mutant *E. coli* ΔCFA that lacks the cyclopropane fatty acyl phospholipid synthase and thus is unable to produce cyclo-C17 fatty acid, as well as the mutant *E. coli* ΔCFA supplemented with chemically synthesized cyclo-C17 acid

(Figure 3.8B). Excretion levels of three fasc (fasc-C₄ΔC₁₁, fasc-C₄ΔC₁₀, fasc-C₄ΔC₁₂) in media supernatants were quantified using LC-MS. For the first group, PB4641 excretes large amount of fasc-C₄ΔC₁₁ when the worms were fed on *E. coli* OP50. The amount of fasc-C₄ΔC₁₁ was sharply decreased in the second group when mutant *E. coli* ΔCFA was fed as the food source. Comparing to the second group, increased amounts of fasc-C₄ΔC₁₁ was observed in the third group when cyclo-C17 acid was additionally added. These results indicate that *C. remanei* is able to integrate a bacteria derived cyclopropyl fatty acid moiety into their chemical signaling.

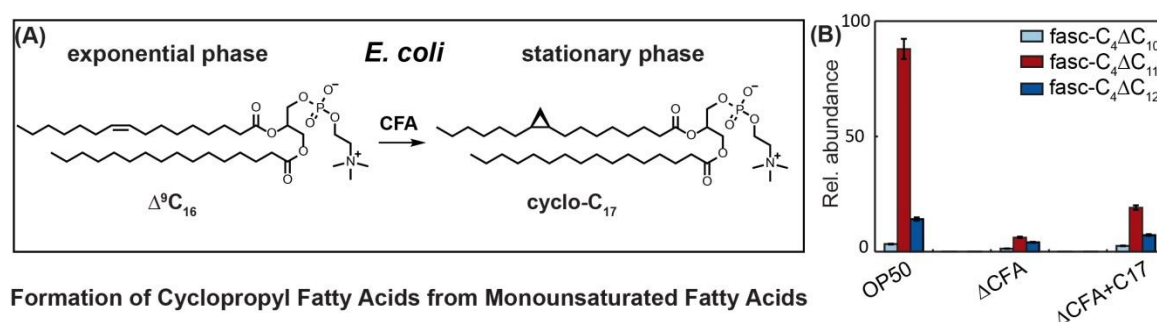


Figure 3.8: Biosynthetic investigation of fasc-C₄ΔC₁₁. (A) cyclo-C17 acid biosynthesis in the membrane of the bacterial *E. coli* food source. (B) Three groups of *C. remanei* (PB4641) samples were fed on *E. coli* OP50, *E. coli* ΔCFA, or *E. coli* ΔCFA supplemented with chemically synthesized cyclo-C17 acid, respectively. Each experiment was performed with three biological replicates. Error bar represent ±SD.

Furthermore, we also isolated a series of cyclopropyl fatty acids from *Caenorhabditis* metabolomes including the important precursor 8-hydroxy-*cis*-cascairillic acid, which could be biosynthetically derived from cyclo-C17 acid upon chain shortening *via* β-oxidation and CYP-450 dependent (ω-3) hydroxylation. Based on this hypothesis we propose a biosynthetic pathway as shown in **Figure 3.9**. NMR data of 8-hydroxy-*cis*-cascairillic acid were acquired for structural characterization (**Figures S22-23**). Hydrolysis of a small aliquot of fasc-C₄ΔC₁₁ also resulted in pure 8-hydroxy-*cis*-cascairillic acid whose structure was unambiguously assigned by analyzing its spectral data (retention time, MS and NMR). Additionally, the biogenic fatty acids *cis*-cascairillic acid, 10-hydroxy-*cis*-cascairillic acid, 11-carboxy-*cis*-cascairillic acid, 9-carboxy-*cis*-cascairillic acid and 7-carboxy-*cis*-cascairillic acid were also chemically

characterized based on their NMR data (**Figures S20-22** and **S25-32**). Discovery of these intermediates indicates that cyclo-C17 acid derived from *E. coli* is metabolized by nematodes through a series of biochemical transformations including β -oxidation and hydroxylation, resulting in a subset of shorter cyclopropyl fatty acids. Furthermore, *C. remanei* and *C. latens* are able to integrate the precursor 8-hydroxy-*cis*-cascairillic acid and a C4-ascaroside to biosynthesize fasc-C₄ Δ C₁₁ as a putative chemical signal. However, further experimental evidence is required to fully clarify the biosynthesis of fasc-C₄ Δ C₁₁. In the future, it is important to characterize those enzymes that function in producing fasc-C₄ Δ C₁₁ in order to interrogate its biosynthetic pathway on a molecular biology level.

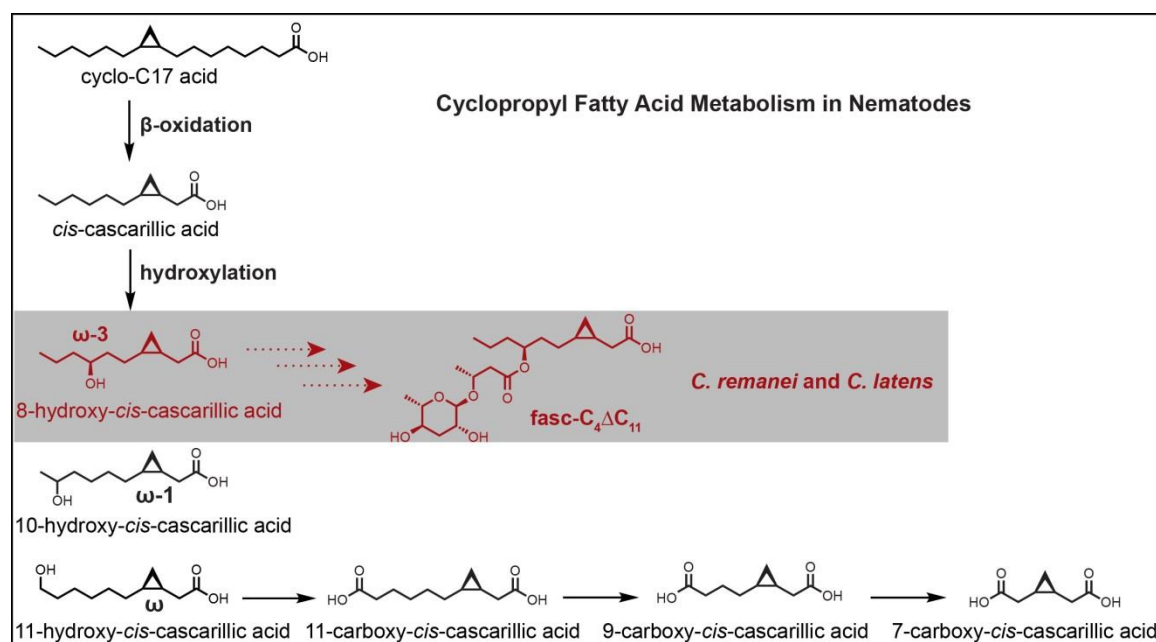


Figure 3.9: Proposed biosynthetic pathway of fasc-C₄ Δ C₁₁ in *C. remanei*. Red color highlighted 8-hydroxy-*cis*-cascarillic acid was proposed to be the precursor of fasc-C₄ Δ C₁₁; its biosynthesis was specifically conserved in *C. remanei* and *C. latens*.

Conclusions: Comparative MS analysis revealed a group of novel fatty acid ascarosides (fasc) from *C. remanei* and *C. latens*. Based on their MS² fragmentation pattern, selective MS screening of a characteristic fragment at *m/z* 233.1035 was specifically established for detecting fasc, of which three prominent components, fasc-C₄ Δ C₁₁, fasc-C₄C₆ and fasc-C₄C₈ were purified and enriched. Mosher's method and chemical synthesis (by

Franziska Dolke) were employed to determine the absolute configuration of fasc-C₄ΔC₁₁. Our results show that fasc is highly specific to *C. remanei* and *C. latens* and great metabolic variation was observed in eight strains of *C. remanei* and *C. latens*. Further investigation of the biosynthesis of fasc-C₄ΔC₁₁ suggested that cyclo-C17 acid underwent β-oxidation and hydroxylation to yield a series of cyclopropyl fatty acids in nematodes, which were isolated and structurally characterized. Taken together our results suggested that *C. remanei* and *C. latens* are able to integrate a bacteria derived cyclopropyl fatty acid moiety and thereby encode information of bacteria's growth phase into a nematode derived putative signal. Initially isolated fasc-C₄ΔC₁₁ was consumed in the Mosher's method experiment. To obtain pure material for bioassay, the *exo*-metabolome of six strains of *C. remanei* were combined for further isolation of fasc-C₄ΔC₁₁, which might constitute a chemical signal modulated inter-species interactions in *C. remanei* nematodes.

Chapter 4

A Group of *Z/E* Isomeric Urocanic Acid Ascarosides from *C. remanei*

Detection and characterization of a prominent urocanic acid modified ascaroside in the *exo-metabolome* of *C. remanei*: Comparative analysis of 13 *Caenorhabditis* species revealed, in addition to many previously described ascarosides, one prominent peak with m/z 421 in the *exo-metabolome* of *C. remanei* (PB4641), which seemed likely to be a novel ascaroside. High resolution mass spectrometry revealed a molecular formula of $C_{21}H_{30}N_2O_7$ ($C_{21}H_{29}N_2O_7^-$, obs. m/z 421.1982, calcd. m/z 421.1980) (**Figure 4.1**).

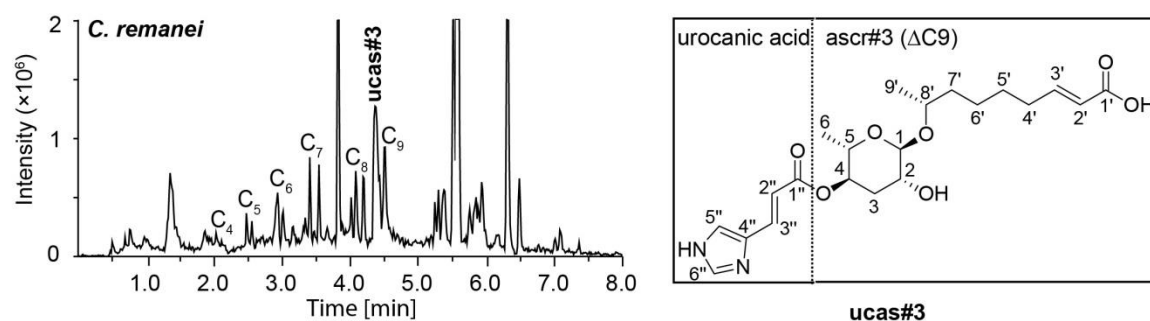


Figure 4.1: Discovery of ucas#3 in the *exo-metabolome* extract of *C. remanei* using ascaroside selective MS/MS precursor ion screening.

MS/MS fragmentation of the target compound using HPLC-(ESI⁺)-HRMS reveals one prominent fragment with molecular ion at m/z 251.1031 ($C_{12}H_{15}N_2O_4^+$, obs. m/z 251.1031, calcd. m/z 251.1026), resulting from the loss of C9 fatty acid derived side chain which harbors one unit of unsaturation (**Figure 4.2**). Analysis of urocanic acid derived ion peak with molecular formula of $C_6H_6N_2O_2$ ($C_6H_7N_2O_2^+$, obs. m/z 139.0502, calcd. m/z 139.0502) which was resulted from the loss of ascarylose on the basis of m/z 251.1031, indicated that target compound might be an ascaroside featuring additional urocanic acid group connected to ascr#3.

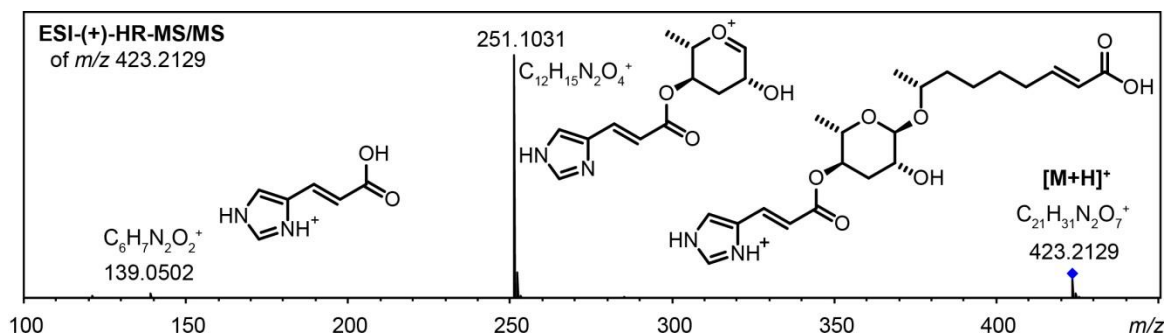


Figure 4.2: MS/MS fragmentation analysis of ucas#3. MS/MS fragmentation of ucas#3 by high resolution LC-MS in positive ion mode revealed a characteristic fragment ion of m/z 251.1 through releasing the fatty acid side chain.

To clarify the chemical structure, solid phase extraction (SPE) and semi-preparative HPLC were employed to isolate and purify the target compound from 1.5 liters of liquid culture derived from *C. remanei*. Proton and *dqf*-COSY spectra of the purified compound were acquired for structural characterization (**Figures S33-34**). Two doublet peaks corresponding to methyl groups were observed in proton and *dqf*-COSY spectra, suggesting ω -1 style of the fatty acid derived side chain. Comparison of acquired proton and *dqf*-COSY spectra with those of *ascr#3* showing additional chemical shifts at low field (four sets of chemical signals at 6.43, 7.60, 7.79 and 7.44 ppm) confirmed the presence of one unit of urocanic acid with *E* configuration ($J_{2'', 3''} = 15.9$ Hz). Additional substitution of an (*E*)-urocanic acid caused the chemical shift of H-4 shifting to the relatively low field at 4.95 ppm, suggesting that urocanic acid linked at the 4-position of ascarose. Another set of proton signals at (H-2') 5.84 ppm and (H-3') 6.82 ppm ($J_{2', 3'} = 15.5$ Hz) demonstrated one double bond in the C9 fatty acid derived side chain. NMR data subsequently confirmed the proposed chemical structure, and the novel ascaroside was named as ucas#3 depending on one additional urocanic acid group. Furthermore, chemical synthesis of ucas#3 was established by Stephan H. von Reuß to clarify the exact chemical structure. Co-injection of both synthetic standard and natural material into HPLC-MS demonstrated identical retention time and MS/MS fragmentation pattern, which unambiguously confirmed the proposed structure of ucas#3. Until now, ucas#1 and ucas#6.1 has also been synthesized as the standard compounds. Subsequently, detected target compound was assigned as an ascaroside ucas#3 (**Figure 4.1**) that

harbors an (*E*)-urocanic acid connected to the 4-position of ascr#3, which presents as one novel chemical signaling in nematodes.

Additional minor urocanic acid ascarosides were detected and characterized: Along with ucas#3, another closely related ascaroside with molecular weight at m/z 423 was also isolated from *C. remanei*. High resolution mass spectrometry revealed a molecular formula of $C_{21}H_{32}N_2O_7$ ($C_{21}H_{31}N_2O_7^-$, obs. m/z 423.2138, calcd. m/z 423.2137). MS/MS fragmentation of this ascaroside also revealed one prominent fragment with molecular ion at m/z 251.1028 ($C_{12}H_{15}N_2O_4^+$; calcd. m/z 251.1026), using HPLC-(ESI⁺)-HRMS (**Figure 4.3A**). MS data indicated that this ascaroside harbors a saturated fatty acid derived side chain, which was confirmed by acquired NMR data (**Figures S35-36**). In conclusion, MS² fragmentation of ucas#3 and ucas#10 by high resolution LC-MS with positive ionization mode produced one common fragment of m/z 251.10 (**Figure 4.3A**) derived from the loss of fatty acid side chain, which permitted identification of the length of side chains. Thus, by selectively searching for characteristic m/z 251.10, a number of ucas (with different fatty acid derived side chains) ion peaks were extracted from the *exo*-metabolome of *C. remanei* (**Figure 4.3B**).

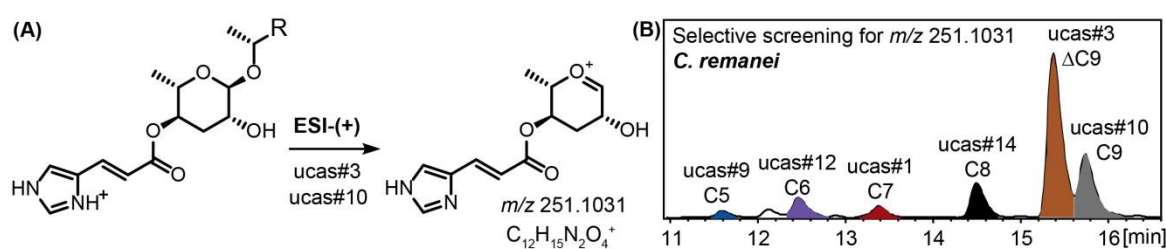


Figure 4.3: Identification of minor urocanic acid ascarosides. (A) MS/MS fragmentation pattern of ucas in positive ion mode shared one characteristic fragment (m/z 251.1031, $C_{12}H_{15}N_2O_4^+$) derived from the loss of side chain. (B) Extracted ion traces of a number of ucas by searching for characteristic m/z 251.1031 in the *exo*-metabolome of *C. remanei*.

Utilizing the established MS/MS screening method to examine ucas in all the *Caenorhabditis* species, which demonstrated that ucas were widely conserved amongst five strains including *C. briggsae* (AF16), *C. remanei* (PB4641), *C. brenneri* (PB2801), *C.*

nigoni (sp 9) and *C. wallacei* (sp16) (Figure 4.4).

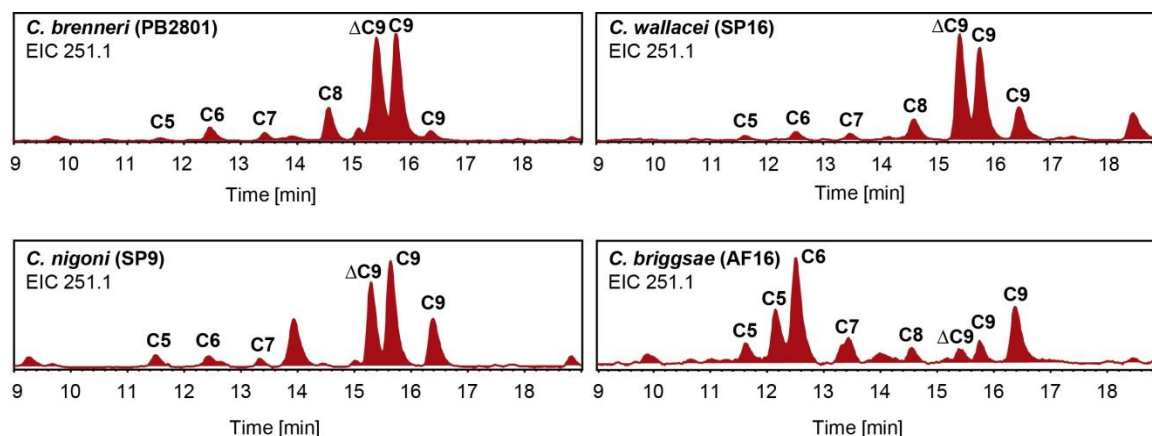


Figure 4.4: HPLC-MS screen for urocanic acid ascarosides (ucas) using electrospray ionization in positive mode (ESI-+) by screening for the fragment ion of m/z 251.1. Ion traces of a series of ucas were extracted from LC-MS chromatograms of the *exo*-metabolomes produced by *C. brenneri*, *C. wallacei*, *C. nigoni* and *C. briggsae*, by searching for the characteristic ion peak of m/z 251.1.

One pair of ion peaks was extracted in the high resolution LC-MS examination of ucas, which share identical molecular weight but are eluted with different retention time at 15.28 min and 15.55 min (e.g. one pair of ion peaks were extracted while profiling ucas#3 with molecular weight of m/z 421). Initially, we thought they were one pair of ascarosides with ω and $\omega-1$ styles fatty acid derived side chains. However, protons at 2nd, 3rd position become two sets of signals with another one harboring much small coupling constant than *E* configuration coupling constant of $J_{2'',3''} = 15.9$ Hz, suggesting that purified ucas#3 might be converted into one pair of isomeric (*E*)-ucas#3 and (*Z*)-ucas#3. Thus, we hypothesize that ucas might be vulnerable to UV light or even visible light, which resulted in two isomeric compounds in the NMR tube. In comparison of the retention times of crude extract and isomeric (*E/Z*)-ucas#3 by co-injecting into HPLC indicated that extracted ion peaks in **Figure 4.5A** are actually one pair of isomeric ascarosides with *E* and *Z* configurations. Finally, a number of urocanic acid modified ascarosides were profiled from the *exo*-metabolome of *C. remanei* (**Tables S6-7**), their chemical structures were proposed on the basis of high resolution masses and MS/MS fragmentation pattern as well as retention times in **Figure 4.5B**.

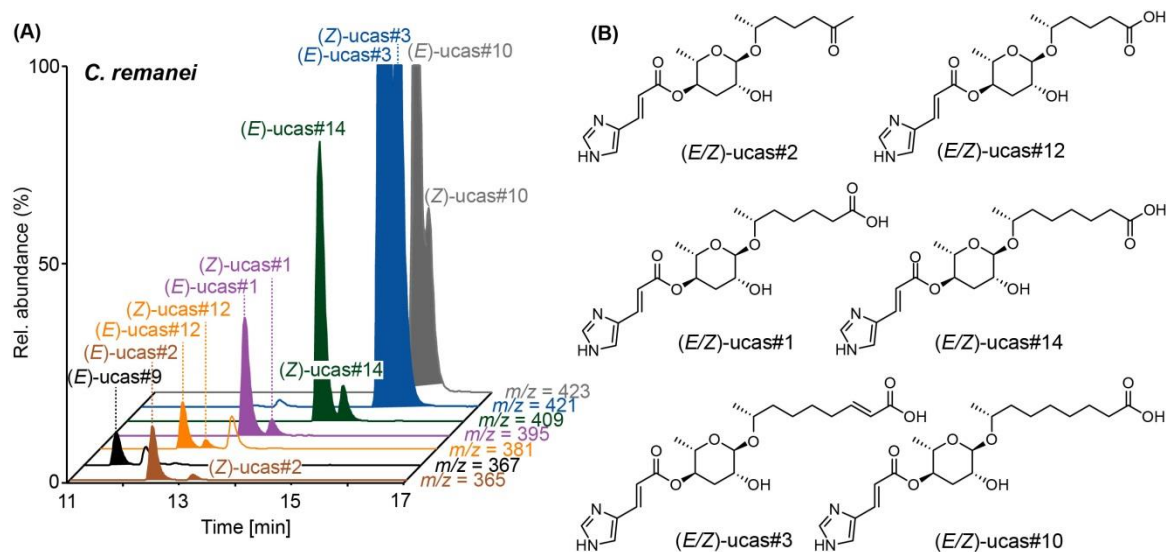


Figure 4.5: Identification of urocanic acid modified ascarosides in *C. remanei* nematode. (A) HRLC-MS analysis revealed a set of ucas with different side chain length in *C. remanei* (PB4641). (B) Chemical structures of urocanic acid ascarosides (ucas).

Biosynthesis of ucas#3: Having clarified the chemical signaling of ucas in nematodes, biosynthesis of the most prominent ucas#3 was readily investigated. Origin of urocanic acid is of particular interest, which might be derived from histidine metabolism. This is common for ascarosides assembly building blocks to be derived from primary metabolism pathway, for example, tryptophan metabolism intermediate of indole was described in **Chapter 2** to participate in the assembly of sex pheromone icas#6.1. Thus it was reasonable to propose that urocanic acid group might be derived from histidine metabolism pathway (**Figure 4.6A**), whereas urocanic acids (*E/Z* configuration) were produced by catalysis of *haly-1* encoded enzyme histidase on histidine. Moreover, urocanic acids can be degraded into other end products by *Y51H4A.7* encoded enzyme urocanase.

To examine this hypothesis, three wild-type isolates of *C. elegans* (N2, AB1 and CB4865) together with two mutants with defects in histidine metabolism, the two ammonia lyase (histidase) mutants *haly-1* (am130) strain WU970 and *haly-1* (am132) strain WU971, as well as the previously uncharacterized urocanase mutant *Y51H4A.7* (gk324463) strain VC20403 were cultivated for analysis of ucas#3 production.

Mutations of *C. elegans*, *am130* and *am132* were reported to show significant

resistance to metal toxicity including zinc and nickel.^[47,48,49] am132 mutation changes a tryptophan to a stop codon at position of codon 296 (transition of C to T), which affects the gene F47B10.2 (also named the gene *haly-1*) that is widely conserved in vertebrates and encodes a protein histidine ammonia lyase (HAL) to catalyze the deamination of histidine to urocanic acid.^[47,50] Histidine was considered to chelate zinc and nickel to modulate the metal tolerance. am130 mutation changes amino acid 536 that is conserved in histidine ammonia lyase in vertebrates from the negatively charged aspartic acid to the polar uncharged asparagine, resulting from the G to A transition at the position close to the gene *haly-1*.^[47] The gene *Y51H4A.7* is an ortholog of human OROC1 (urocanate hydratase 1) that metabolizes urocanic acid. The *Y51H4A.7* (gk324463) mutation of strain VC20403 from the million mutants project contains a substitution that converts the codon for tryptophan at position 396 into a stop codon. In addition this strain features another 3 mutations resulting in truncated proteins (*egl-27*, *fbxa-67*, *acr-18*), plus 69 attritional mutations resulting in exchange of amino acids in a variety of proteins. Using standard nematode culture protocol, exo-metabolome extracts of all the strains were prepared as described in **Chapter 1**. Relative abundance of ion peak of ucas#3 was quantified for comparative analysis (**Figure 4.6B**). Only (*E*)-ucas#3 was quantified in this study because of extremely low amount of the (*Z*) isomer.

LC-MS was employed to search for ucas#3, which showed all strains produced ucas#3 but with distinguishable quantitative difference. Of three wild isolates, N2 and AB1 produced similar amount of ucas#3 but strain CB4865 produced much less ucas#3 with unknown reasons. *Haly-1* mutation strains am130 and am132 decreases the amount of ucas#3 by approximately fourfold or fivefold relative to wide type isolate N2. This might be explained that gene *haly-1* responsible for converting histidine into urocanic acid was defective in am130 and am132, which led to the sharply decreased production of ucas#3. In contrary, *Y51H4A.7* mutation gk324463 increased the amount of ucas#3 by approximately twenty percent relative to N2, taking advantage of partly dysfunctional urocanase on catalyzing urocanic acids. Taken together, nematodes are capable of integrating building block urocanic acid from histidine metabolism pathway and further producing novel chemical signaling ucas based on known ascarosides. To gain insights

into biosynthesis of ucas, additional studies will be needed to clarify the mechanism of urocanic acid incorporation.

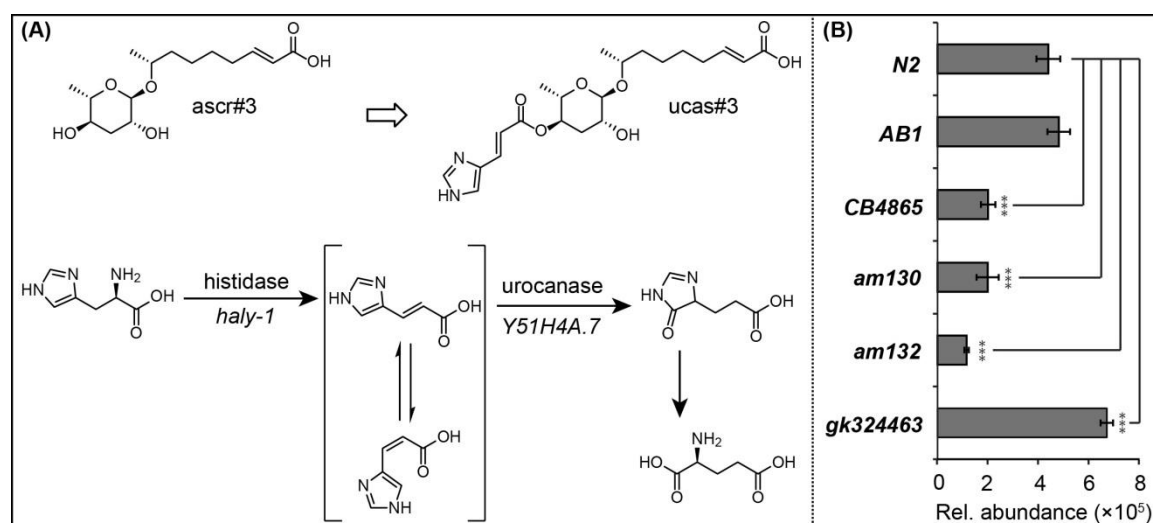


Figure 4.6: Biosynthesis of ucas#3. (A) Urocanic acid group in ucas#3 was proposed to be derived from histidine metabolism. *Haly-1* encoded histidase upregulated and *Y51H4A.7* encoded urocanase downregulated the production of urocanic acid, respectively. (B) Production of ucas#3 was comparatively analyzed in the *exo*-metabolome extracts of three wild-type isolates of *C. elegans* (N2, AB1 and CB4865) and three mutants (am130, am132 and gk324463).

Ecological significance of urocanic acid ascarosides: Comparative analysis showed that five strains [*C. briggsae* (AF16), *C. remanei* (PB4641), *C. brenneri* (PB2801), *C. nigoni* (sp 9) and *C. wallacei* (sp 16)] were able to produce ucas. And significant qualitative and quantitative differences were observed in ucas production, of which most prominent ucas#3 and ucas#10 were assessed in **Figure 4.7A**, suggesting that ucas#3 and ucas#10 with (*E*) configuration are much more abundant than their (*Z*) isomers. Other minor ucas (ucas with *Z* configuration are not included because of their extremely low abundance) were also quantified in **Figure 4.7B**, which showed that nematodes produced a complex blend of ucas. In addition, purified ucas#3 and ucas#10 notably existed as a pair of isomers with *E/Z* configuration, suggesting instability of ucas#3 and ucas#10 under the condition of UV light or visible light. Further experiment to irradiate pure ucas#3 with UV light showed that *E*-ucas#3 can be easily converted to *Z*-ucas#3 (**Figure 4.7C**). These findings suggested that nematodes might produce ucas not only as chemical

signals but also as sunscreen. But more evidence are needed to support this hypothesis. Thus in the near future, it is very important to explore the biological activity of ucas#3, which can help to understand the chemistry and biology of ucas.

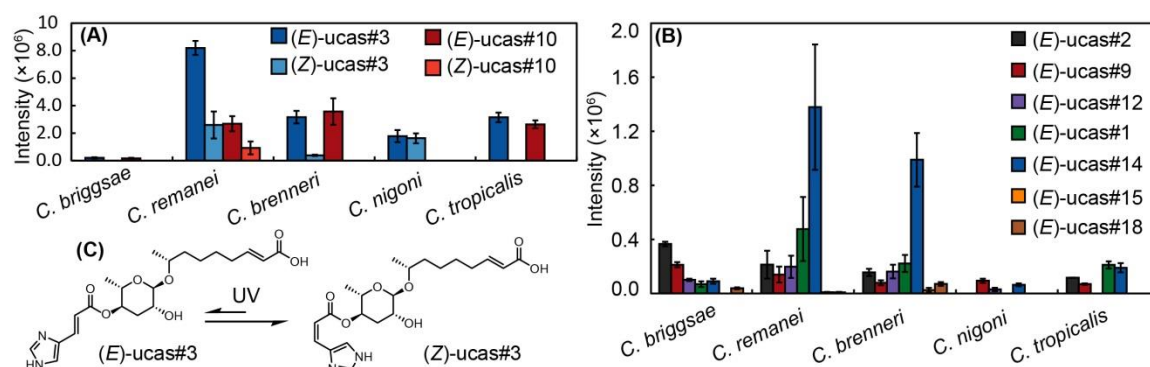


Figure 4.7: Ecological significance of ucas in *Caenorhabditis* species. Relative abundances of the dominating ucas#3 and ucas#10 (A) and minor ucas with *E* configuration (minor *Z*-ucas with trace amounts were excluded) (B) were assessed in metabolomes derived from five *Caenorhabditis* species including *C. briggsae* (AF16), *C. remanei* (PB4641), *C. brenneri* (PB2801), *C. nigoni* (sp9) and *C. wallacei* (sp16). Experiments were performed with three biological replicates. Error bars represent \pm SD. (C) Isomerization transformation of (*Z*)-ucas#3 to (*E*)-ucas#3 with the radiation of UV or visible light.

As described in **Chapter 3**, fatty acid ascarosides were found to be present in eight strains of *C. remanei* nematodes. Here, the major representatives ucas#3 and ucas#10 were also profiled in *C. remanei* strains, revealing that all strains produce *E*-ucas#3 as the most prominent compound whose biological function is still unknown (**Figure 4.8**). Further examination of minor ucas in the *exo*-metabolome of *C. remanei* strains showed that (*E*)-ucas is much more abundant than *Z* isomers (**Figure 4.9**).

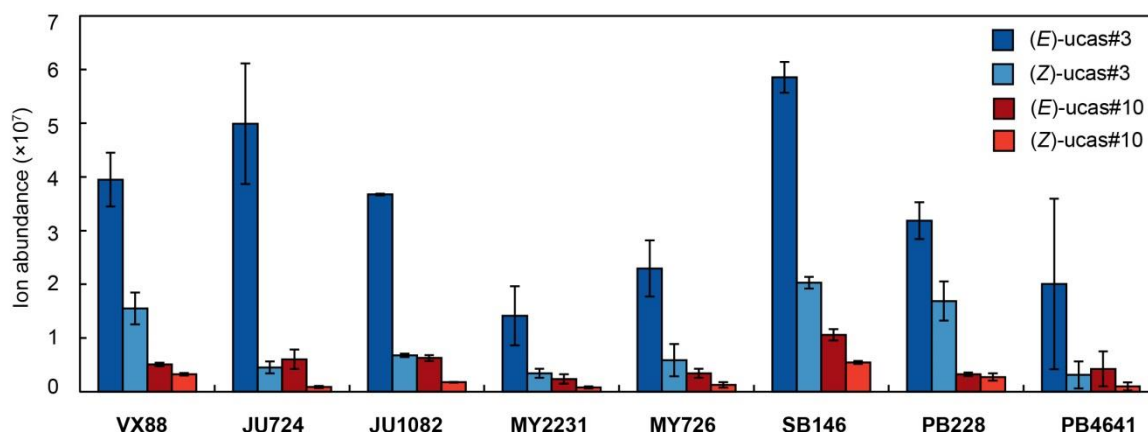


Figure 4.8: Relative abundances of ucas#3 and ucas#10 in *C. remanei* and *C. latens* strains. Major components ucas#3 and ucas#10 with both *E* and *Z* configurations were profiled in eight strains of *C. remanei* and *C. latens*. Experiments were performed with three biological replicates. Error bars represent \pm SD.

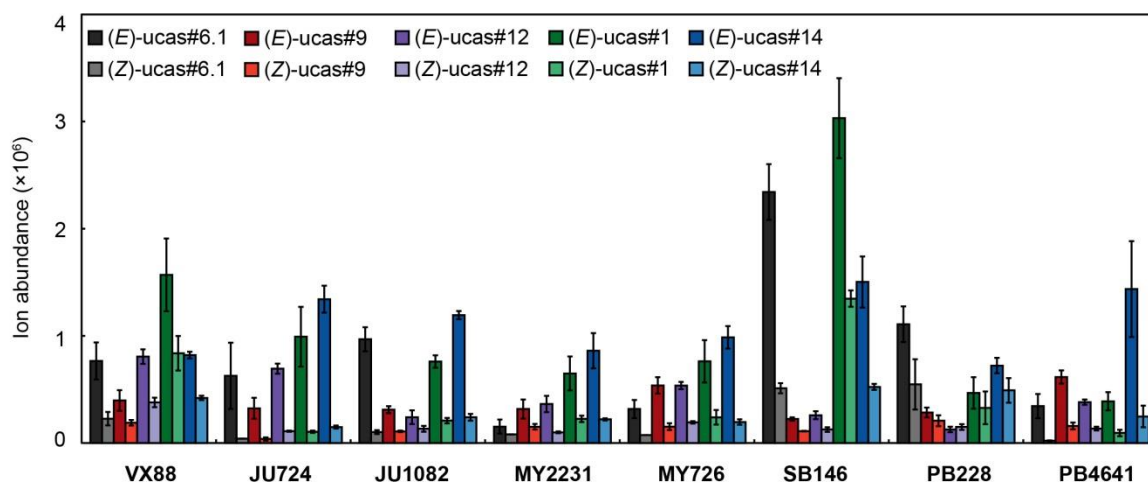


Figure 4.9: Relative abundances of minor ucas in *C. remanei* and *C. latens* strains. Minor ucas with both *E* and *Z* configurations were profiled by analyzing metabolomes produced by *C. remanei* and *C. latens* strains. Experiments were performed with three biological replicates. Error bars represent \pm SD.

C. elegans, *C. remanei* and *C. briggsae* nematodes were found to share the same ecological niche in nature. Analysis of chemical signal excreted by these three species are of interest considering their chemical communication. Thus it is intended to examine whether other *C. briggsae* strains produce ucas or not. *Exo*-metabolomes of twelve *C. briggsae* strains were prepared as described in **Chapter 1** and relative ucas abundances were assessed (**Figures 4.10-4.11**). All the analyzed strains were found to be able to

produce ucas, and particularly strain JU516 produced much more *E*-ucas#3 than other strains. Chemical signaling ucas, especially ucas#3, might play a critical role in the interaction of *C. elegans*, *C. remanei* and *C. riggsae* nematodes, which was might be overlooked in previous studies.

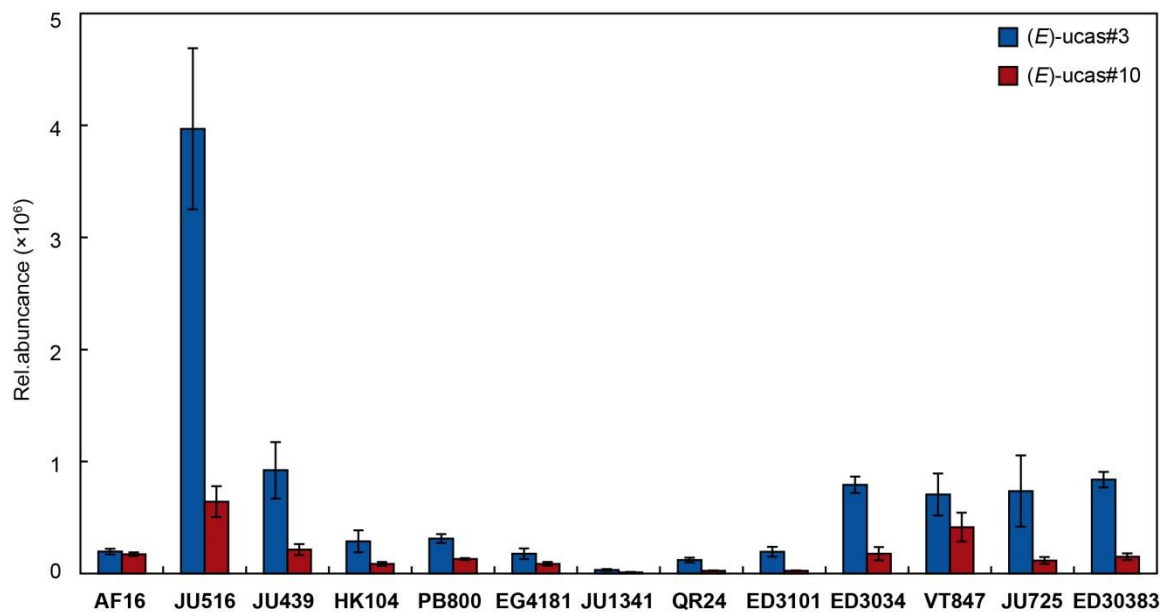


Figure 4.10: Relative abundances of ucas#3 and ucas#10 in *C. briggsae* strains. Ucas#3 and ucas#10 with both *E* and *Z* configurations were profiled in twelve *C. briggsae* strains. Experiments were performed with three biological replicates. Error bars represent \pm SE.

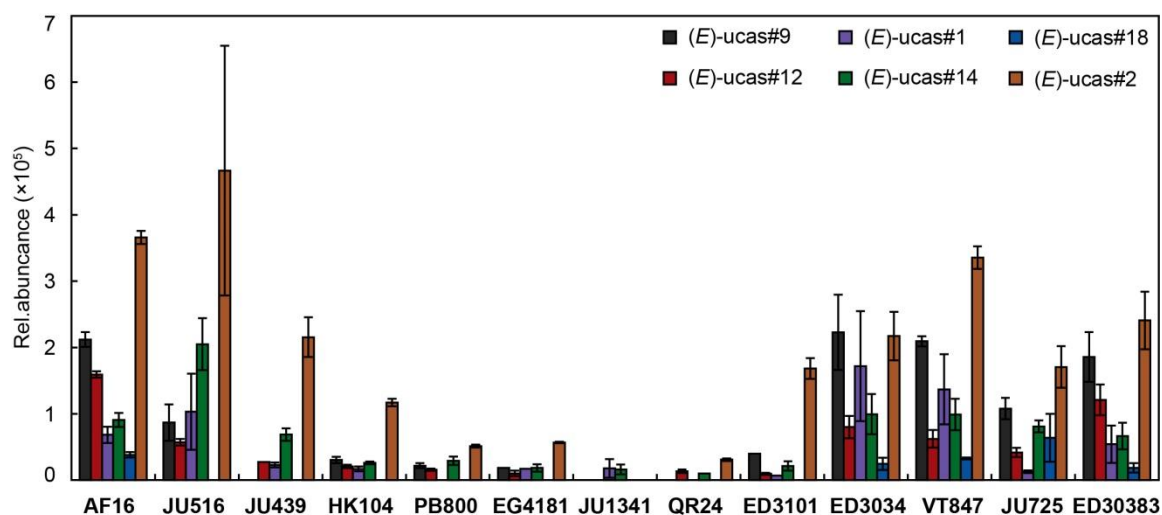


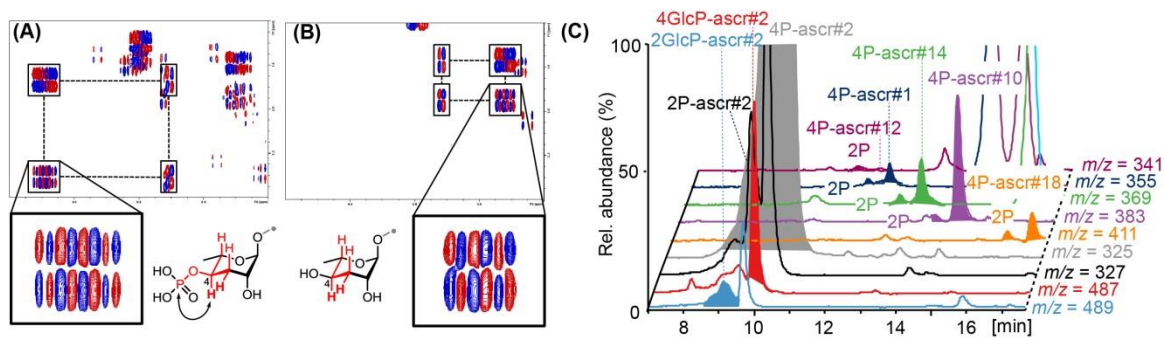
Figure 4.11: Relative abundances of minor ucas in *C. briggsae* strains. Minor components of ucas were profiled in twelve *C. briggsae* strains. Experiments were performed with three biological replicates. Error bars represent \pm SE.

Conclusions: Comparative metabolomics analyses of 13 *Caenorhabditis* species revealed one prominent ascaroside ucas#3 in *C. remanei* with the 4-position of ascarylose connected to one additional urocanic acid group. Chemical structure of ucas#3 was determined by analyzing acquired high resolution mass, MS/MS fragmentation and NMR data derived from purified material. Another dominating ascaroside ucas#10 was also isolated and structurally characterized. Based on their MS² fragmentation pattern, one selective screening method was established for detecting ucas by searching for fragment *m/z* 251.10, which revealed one group of ucas that present a series of novel ascarosides. In our study, ucas were found to be widely conserved in five *Caenorhabditis* species including *C. briggsae*, *C. remanei*, *C. brenneri*, *C. nigoni* and *C. wallacei*. Moreover, Biosynthetic investigation reveals that urocanic acid group might be derived from histidine metabolism pathway. Most interestingly, light can induce isomerization of ucas, which results in a mixture of *E* and *Z* configuration in pure material. Taken together, all these findings suggest that it is very important and urgent to explore the biological activity of ucas#3 and ucas#10 in the future.

Chapter 5

New Phosphoryl Ascarosides from the *Caenorhabditis Elegans* Group

Discovery and structural characterization of 4P-ascr#2 and 4GlcP-ascr#2: While many of the novel classes of ascarosides discovered during the course of this research were initially detected using the ascaroside-selective MS/MS precursor ion screen^[23], there might exist certain ascaroside derivatives that escape their detection because they either do not ionize using electrospray ionization in negative ion mode (ESI(-)) or do not produce the characteristic fragment at $m/z = 73$. One such example is represented by the phosphoryl-ascarosides (phas), an abundant group of ascaroside derivatives present in various *Caenorhabditis* species in large quantities. These components were first detected in a highly polar SPE fraction of the *C. remanei* *exo*-metabolome extract upon careful analysis of the *dqf*-COSY spectrum (**Figure S37**), which revealed an ascarylose dependent spin system, suggesting an uncommon highly polar ascaroside derivative. For further structural characterization, the corresponding SPE fraction was subjected to semi-preparative HPLC which led to the isolation of two major compounds called 4P-ascr#2 and 4GlcP-ascr#2 (**Figure 5.1D**). In addition to an (ω -1)-linked C6 methylketone side chain previously known from ascr#2, an additional moiety attached to the 4-position of the ascarylose was proposed to be a phosphate group, due to the high resolution mass m/z 325.1070 ($C_{12}H_{22}O_8P^-$, calcd. m/z 325.1058) as well as careful analysis of the *dqf*-COSY spectrum that exhibits an additional 3J (1H , ^{31}P) coupling of ca. 8.0 Hz (**Figure 5.1A**) which is absent in the *dqf*-COSY spectrum of structurally related ascr#2 (**Figure 5.1B**).



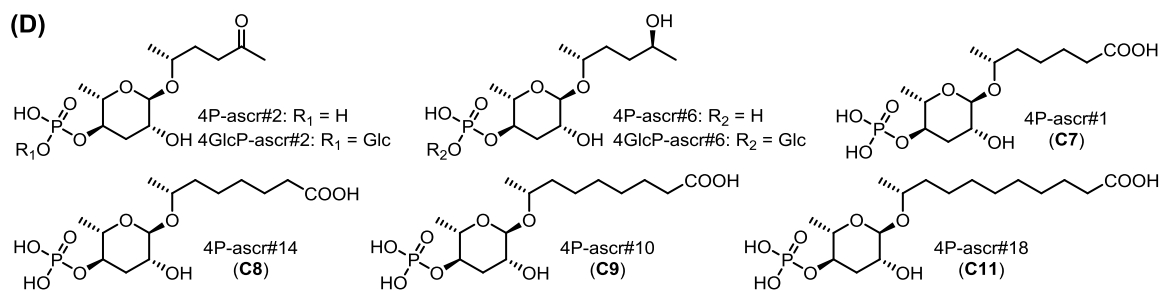


Figure 5.1: 4-phosphoryl ascarosides identified from *C. briggsae* and *C. remanei*. *dqf*-COSY spectrum of 4P-ascr#2 (A) demonstrated $^3J(^1\text{H}, ^{31}\text{P})$ coupling which was absent in asc#2 (B). (C) Extracted ion traces of phosphoryl ascarosides from *C. briggsae* (AF16). (D) Chemical structures of prominent 4P-ascr#2 and other phosphoryl ascarosides.

Fragment signals derived from 4P-ascr#2 were not detected while LC-MS/MS fragmentation with negative ion mode was applied. And identification of the (ω -1)-oxygenated side chain by NMR was hampered by fast H/D-exchange in CD₃OD to afford the [D₅]-isotopomer as shown by MS (**Figure S38A**). Thus, purified samples were exchanged back from deuterated protons to normal protons, and its dimeric and trimeric ions were further fragmented by ESI⁺-HR-LC-MS/MS (**Figures 5.2A-C**). Analysis of ESI⁺-HR-MS/MS spectra (**Figure S38**) indicated loss of a C₆H₁₂O₂ side chain moiety which resulted in the assignment of the novel 4P-ascr#2 structure shown in **Figure 5.1D**. Established MS method greatly supported the structural characterization of phosphorylated ascarosides. For example, 4GlcP-ascr#2 was identified to harbor additional glucose group based on such a MS method (**Figures S39-40**). Acquired proton and *dqf*-COSY spectra in **Figures S43-44** indicated signals derived from glucose moiety which further confirmed the chemical structure of 4GlcP-ascr#2. To further confirm the proposed chemical structures, 4P-ascr#2 (**Figure 5.2D**) was chemically synthesized by Franziska Dolke as the standard compound. Naturally isolated 4P-ascr#2 shared identical retention time, MS/MS fragmentation pattern and NMR data (**Figures 5.2E-F**) with synthetic compound, which helped to finally clarify the whole structure of 4P-ascr#2. To our knowledge, it was the first time to identify phosphorylated ascarosides which were present with micromole concentrations in media supernatants of *C. briggsae* and *C. remanei*. In nature, only few examples of phosphorylated compounds were reported from

marine microorganism^[51].

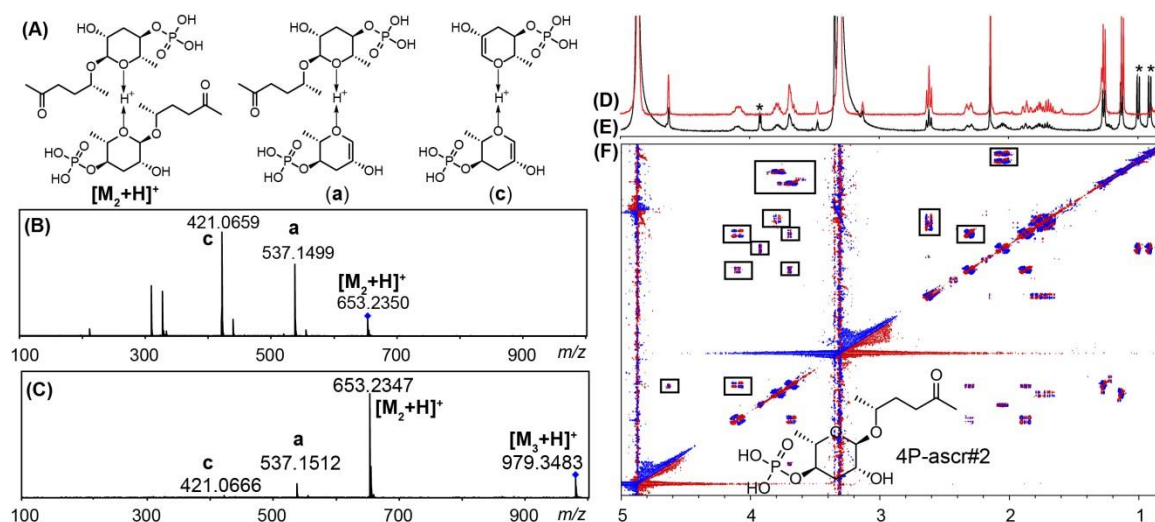


Figure 5.2: Structural characterization of 4P-ascr#2. (A) Structural assignments of ion peaks derived from MS/MS fragmentation of dimeric and trimeric ions of 4P-ascr#2. (B) MS/MS fragmentation of dimeric ion of 4P-ascr#2. (C) MS/MS fragmentation of trimeric ion of 4P-ascr#2. (D) Proton spectrum of synthetic 4P-ascr#2. (E) Proton spectrum of natural 4P-ascr#2. Asterisks marked signals are derived from impurity of valine. (F) *dqf*-COSY spectrum of natural 4P-ascr#2.

Identification of 2- and 4-phosphoryl ascarosides derivatives: In addition to the largely dominating 4P-ascr#2 targeted MS screening revealed a diversity of related components with fatty acid derived side chains ranging from C6 to C11. Interestingly, in contrast to 4P-ascr#2, pairs of peaks corresponding to phosphoryl ascarosides were observed for the corresponding minor components, which suggested two types of phosphorylation at the 2- and 4-position or the phosphorylation of a single site in two series of (ω)- and (ω -1)-oxygenated ascarosides. To clarify the exact chemical identity of each pair of ion peaks, 4P-ascr#1 and 2P-ascr#1 were synthesized by Franziska Dolke as standard compounds. Based on targeted high resolution MS analysis, both of the synthetic ascarosides profiles were co-injected into LC-MS and side chain length versus corresponding retention time were plotted in **Figure 5.3E**, which revealed two additional homologous series of phosphorylated ascarosides present in trace quantities (**Figures 5.3A-B**) that were identified as 2P- and 4P-derivatives. Comparison of their relative abundance with those of the unmodified precursors (**Figures 5.3C-D**) indicated that

phosphorylation appears to be specific for the 4-position of C9 (and C8) ascarosides. These results also revealed two corresponding homologous series of glycosylated phosphoryl ascarosides corresponding to 2P- and 4P-ascarosides. Subsequently, a list of phosphorylated ascarosides were identified from *C. briggsae* and *C. remanei* (**Figure 5.1C & Table S10**). Phosphorylated ascarosides would be another group of novel ascarosides, featuring rare phosphate group at the 2- or 4-position of ascarylose, which further showed primary metabolism derived functional group participated in the assembly of chemical signals.

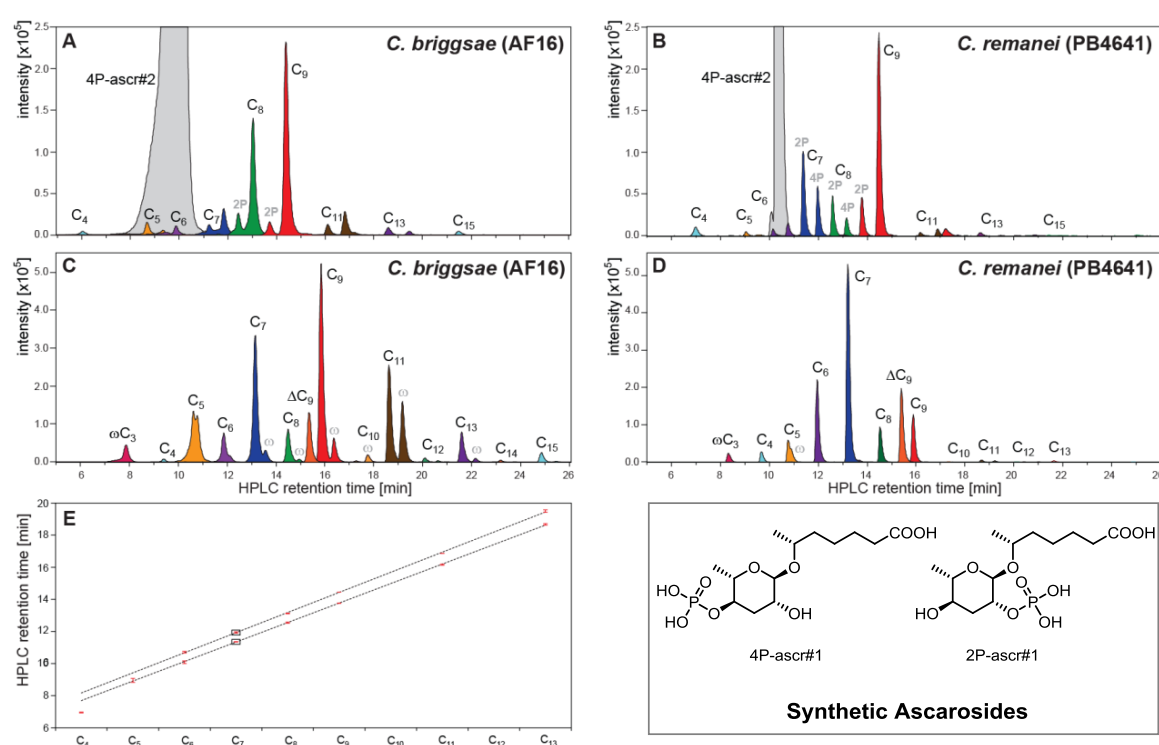


Figure 5.3: HR-MS ion traces for phosphoryl ascarosides (A & B) and their unmodified ascaroside precursors (C & D) detected in metabolome extracts of *C. briggsae* and *C. remanei*. Plotting of HPLC-retention times versus ascaroside sidechain length reveals two homologous series corresponding to 2P-ascarosides and 4P-ascarosides (E) as shown by co-injection with synthetic standards of 2P-ascr#1 and 4P-ascr#1 (error bars represent $\pm 1SD$, $n = 3$; $R^2 > 0.999$ for linear fit, P-ascr-C₄ not included).

Ecological significance of phosphoryl ascarosides: Comparative analysis of 13 *Caenorhabditis* species revealed that phosphorylation of ascr#2 is prominent in *Elegans* group (**Figure 5.4**). Of the nine analyzed species all but one (*C. nigoni*) released ascr#2

and five of those were capable of converting it into 4P-ascr#2 and 4GlcP-ascr#2. Particularly, *C. briggsae* abundantly produced larger amount of 4P-ascr#2 than any other nematodes (**Figure 5.5B**). Five species of nematodes produced a very complex blend of phosphoryl ascarosides, of which 4P-ascr#2 and 4GlcP-ascr#2 are the most abundant phosphorylated and glycosylated phosphoryl ascarosides, excluding *C. wallacei* nematodes that released 4P-ascr#3 as the major component and did not produce glycosylated phosphoryl ascarosides (**Figure 5.4**). Phosphoryl ascarosides composition derived from eight strains of *C. remanei* and *C. latens* nematodes were also carefully analyzed, revealing that 4P-ascr#2 and 4GlcP-ascr#2 were most abundant compounds. Thirteen species of *C. briggsae* nematodes in our study were also found to be capable of producing a complex mixture of phosphoryl ascarosides and particularly large amount of 4P-ascr#2.

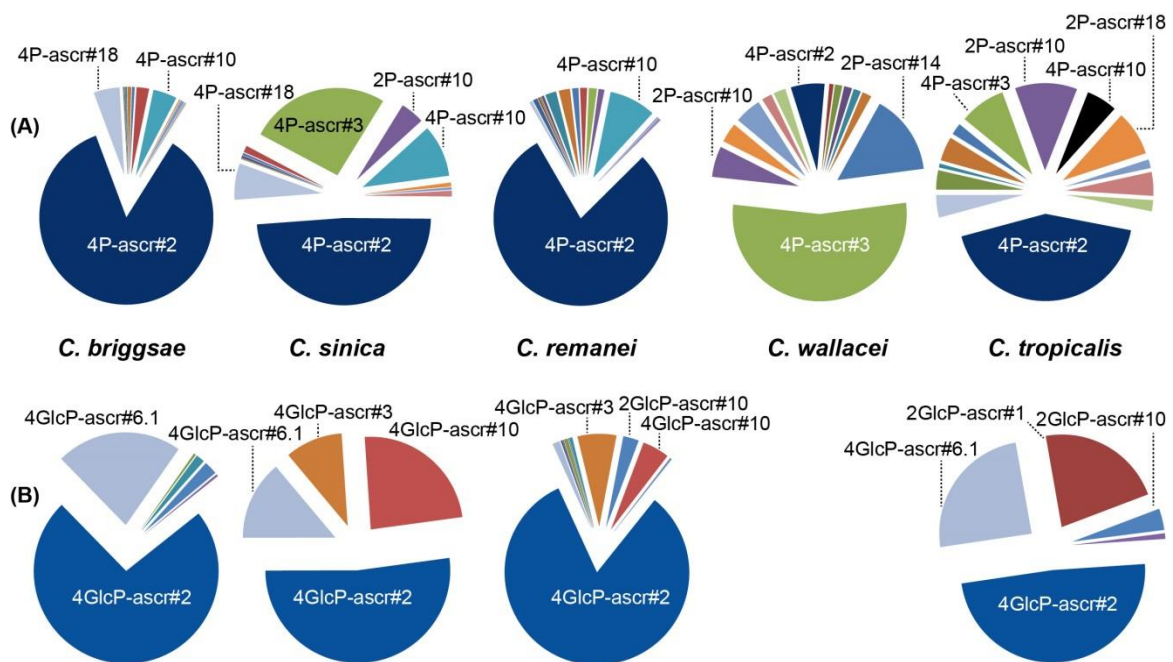


Figure 5.4: Ion abundances of phosphoryl ascarosides in *Elegans* group. Phosphoryl ascarosides were detected in five species of nematodes within the *Elegans* group (*C. briggsae*, *C. sinica*, *C. remanei*, *C. wallacei* and *C. tropicalis*). (A) 2P- and 4P-ascarosides were profiled in *C. briggsae* (AF16), *C. sinica* (sp5), *C. remanei* (PB4641), *C. wallacei* (sp16) and *C. tropicalis* (sp11). (B) Glycosylated phosphoryl ascarosides including 2GlcP- and 4GlcP-ascarosides were profiled in these nematodes. Quantification results showed that 4GlcP-ascr#2 was the most abundant compound in all nematodes except *C. wallacei* (sp16).

Generally, *C. briggsae*, *C. remanei* and *C. elegans* nematodes were isolated in the same natural ecological niche. Thus here, concentrations of ascarosides including normal ascarosides and newly discovered 4P-ascr#2 were comparatively studied (**Figure 5.5C**). All of them produced a series of normal ascarosides (e.g. ascr#1, ascr#2 and ascr#3) which were extensively studied before. However, *C. briggsae* and *C. remanei* but not *C. elegans* abundantly produced 4P-ascr#2 with micromole concentrations. According to previous studies,^[52] we hypothesized that *C. elegans* released ascr#2 to cause dauer formation of *C. briggsae* and *C. remanei* in order to compete for food source and space, in contrast, *C. briggsae* and *C. remanei* established one survival strategy of producing 4P-ascr#2 to 'detoxify' ascr#2. To test these hypotheses, more experiments are needed to further clarify the biological activity of phosphoryl ascarosides, which is still going on in our laboratory.

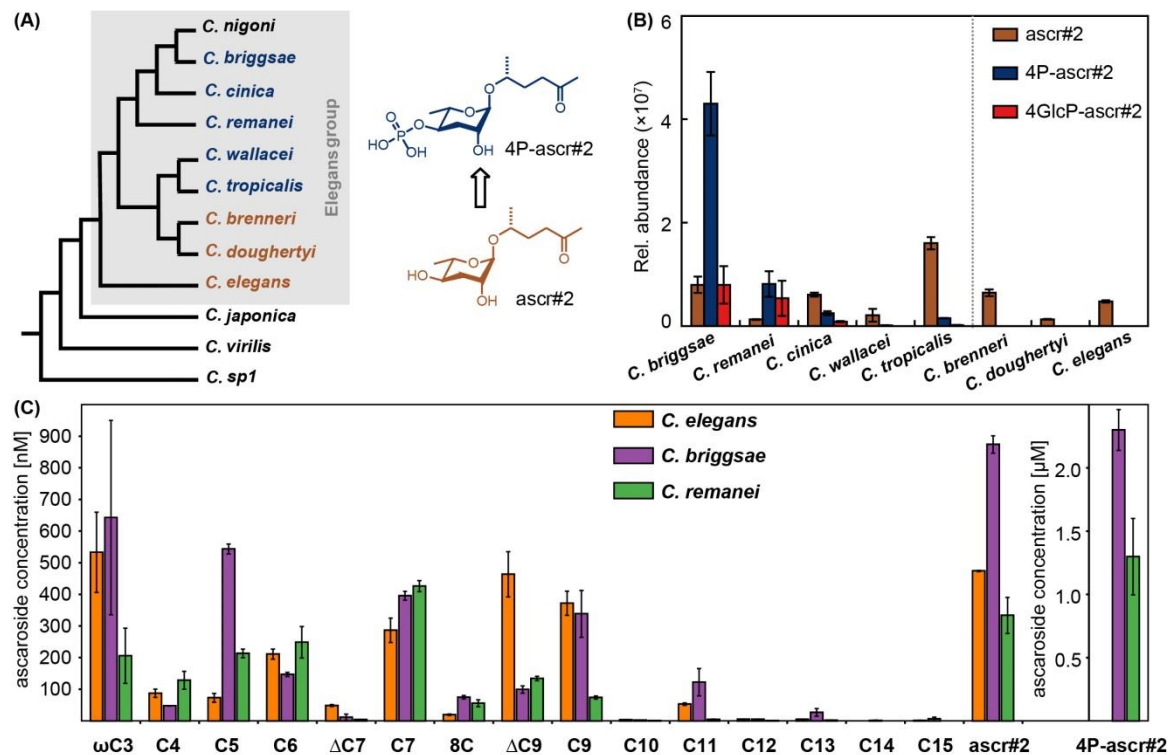


Figure 5.5: 4P-ascr#2 relating ecological significance. (A) Conversion of ascr#2 into 4P-ascr#2 and its distribution within the *Elegans* group. (Error bars represent \pm SE, n=3). (B) Quantification of ion abundance of ascr#2, 4P-ascr#2 and 4GlcP-ascr#2. (C) Comparative quantification of 4P-ascr#2 produced by *C. remanei*, *C. briggsae* and *C. elegans*. (Error bars represent \pm SD, n=3).

Conclusions: Using comparative HR-MS and NMR techniques as well as chemical synthesis we have identified a rare series of phosphorylated ascarosides that are prominent in the *Elegans* group but absent in *C. elegans*. 4P-ascr#2, a derivative of the potent *C. elegans* dauer inducing ascr#2, constitutes the most abundant component present in micromolar concentrations. The most dominating compounds 4P-ascr#2 and 4GlcP-ascr#2 were isolated and purified for structural characterization. With the support of chemical synthesis, we identified two homologous series of phosphorylated ascarosides from nematodes that particularly preferred to biosynthesize 4P-derivatives. In our study, unique MS method was established for phosphorylated ascarosides identification. This overlooked group of ascarosides produced by nematodes provided us a great chemical diversity of the ascarosides library. Bioassays with the synthetic compounds to unravel their significance in nematode communication are in progress.

Chapter 6

New Dimeric Ascarosides from *Caenorhabditis Elegans* Group

Detection and structural characterization of a prominent dimeric ascaroside: Using a triple quadrupole LC-MS/MS system for ascaroside selective precursor ion screening, comparative analysis of *exo*-metabolome extracts of 13 *Caenorhabditis* species, revealed a dimeric ascaroside in the *exo*-metabolome produced by *C. remanei* (**Figure 6.1**). HR-MS analysis indicated the molecular formula of $C_{21}H_{36}O_{11}$ (obs. m/z 463.2176, calcd. m/z 463.2185).

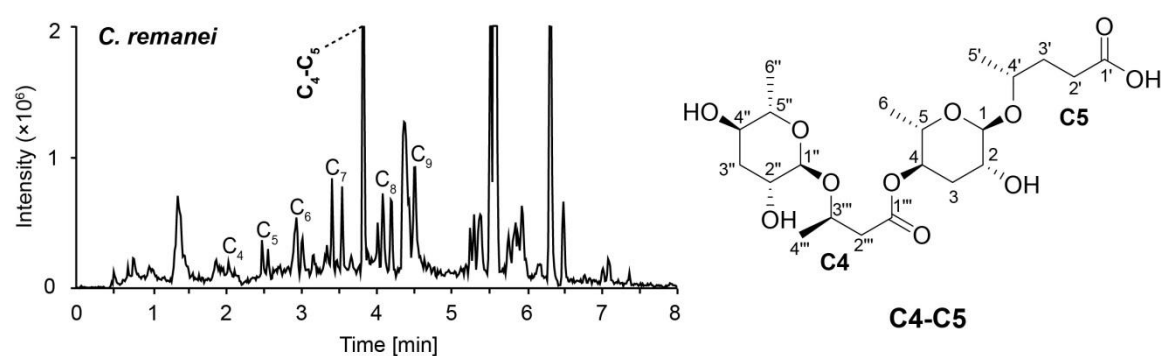


Figure 6.1: Discovery of dimeric ascaroside C4-C5 from the *exo*-metabolome extract derived from *C. remanei* by using liquid chromatography triple quadrupole mass spectrometry. Heterodimeric ascaroside C4-C5 was detected by selectively screening precursor ion of m/z 73. Chemical structure of C4-C5 was proposed on the right.

Analysis of the CID-MS/MS fragmentation spectra upon electrospray ionization in negative ion mode (ESI⁻) indicated a fragment ion for $C_{15}H_{23}O_7^-$ (obs. m/z 315.1449, calcd. m/z 315.1449) and $C_{11}H_{19}O_6^-$ (obs. m/z 247.1195, calcd. m/z 247.1187) that resulted in the proposal of a heterodimeric structure formed by the combination of ascarosides featuring a C4 unit and C5 unit. However, it was unavailable to determine the length and position of both fatty acid side chains based on limited MS information because there are might be two types of dimeric ascarosides (C4-C5 or C5-C4). To clarify the exact chemical structure, target compound was isolated from 1.2 L liquid culture of *C. remanei* via solid phase extraction (SPE) and semi-preparative HPLC. 1D and 2D NMR datasets (**Table S13, Figures S45-48**) were acquired to characterize the chemical structure as a

heterodimeric ascaroside with C4 ascaroside connected to the 4-position of another C5 ascaroside, whereas hydrogen at the 4-position of ascarylose readily shifted to the low field (4-H, 4.87 ppm) and two sets of characteristic spin system derived from ascarylose were observed (**Figure S47**).

Identification of additional minor dimeric ascarosides: To characterize chemical structures of heterodimeric ascarosides, MS/MS fragmentation method was established to support the clarification of the length and connection of each fatty acid side chain. Take the MS/MS fragmentation of prominent dimeric ascarosides C4-C5 for example, C4-C5 was fragmented into two major precursor ions with m/z values of 315.1438 and 247.1176 using high resolution LC-MS/MS in negative ion mode (**Figure 6.2C**). Fragment of m/z 315.1438 was derived from the loss of one ascarylose, and another fragment of m/z 247.1176 was produced *via* releasing C4 fatty acid side chain of m/z 315.1438, which supported to fix the length of C4 side chain that attached to the ascarylose of C5 ascaroside. On the other hand, C4-C5 was further fragmented to yield two major precursor ions with m/z values of 347.1429 and 217.1084 in positive ion mode (**Figure 6.2D**). Fragment ion of m/z 347.1429 was produced by losing C5 fatty acid derived side chain, which was further fragmented into m/z 217.1084 with the loss of ascarylose, suggesting that the free fatty acid side chain harbors five carbons. Based on the MS/MS fragmentation method applied to C4-C5 with a combination of negative and positive ion modes along with their high resolution masses, a series of dimeric ascarosides were identified from nematodes (**Table S12**). For instance, a number of dimeric ascarosides ions were identified from the *exo*-metabolome extract of *C. remanei* (**Figure 6.2A**), with chemical structures of major compounds listed in **Figure 6.2B**. Meanwhile, chemical synthesis of dimeric ascaroside C4-C5 was also established by Franziska Dolke to finally confirm the proposed chemical structure.

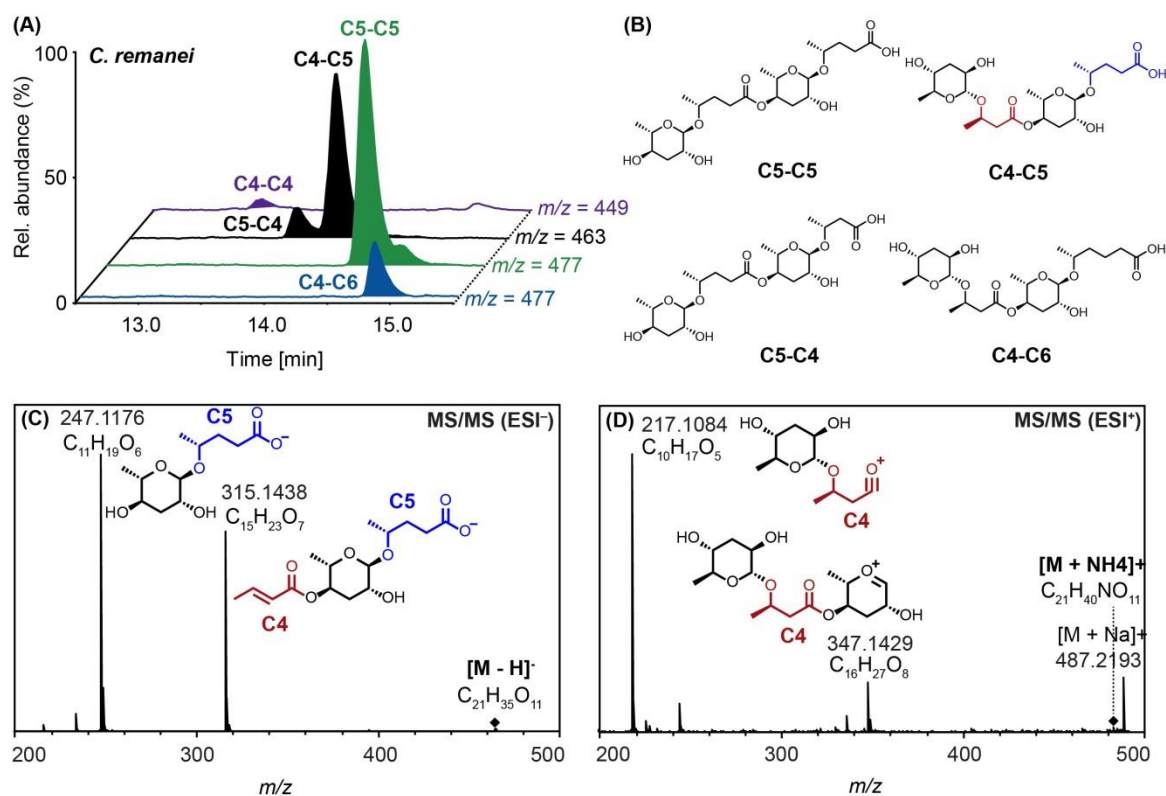


Figure 6.2: Identification of novel dimeric ascarosides. Extracted ion traces (A) and proposed chemical structures (B) of dimeric ascarosides identified from the *exo*-metabolome extract of *C. remanei*. (C) MS/MS fragmentation of C4-C5 by using high resolution LC-MS/MS in negative ion mode. (D) MS/MS fragmentation of C4-C5 by using high resolution LC-MS/MS in positive ion mode.

Identification of 2-substituted dimeric ascarosides from the *exo*-metabolome of *C.*

***nigoni*:** Three dimeric ascarosides derived ion peaks with m/z values of 477.2343, 491.2495 and 505.2649 (**Table S12**) were detected in the *exo*-metabolome of *C. nigoni*. Compounds m/z 491.2495 and m/z 505.2649 shared identical MS/MS fragmentation pattern but different HPLC retention times with C6-C6 and C6-C7 which were identified from *C. briggsae* to be 4-substituted dimeric ascarosides on the basis of newly established MS method. Thus, we hypothesized that they were elusively modified with different substitution whereas one unit of ascaroside connected to the 2-position of another ascaroside. To test our hypothesis, three target compounds were isolated and purified (enriched) from the target SPE fraction using semi-preparative HPLC. Acquired 2D NMR (*dqf*-COSY) data (**Figures S51, S54 and S57**) clearly demonstrated that one ascaroside connected to the 2-position of another ascaroside because chemical shift of

H-2 shifted into low field, which showed a different substitution style of dimeric ascarosides (**Figure 6.3**). Chemical synthesis is on progress in the laboratory.

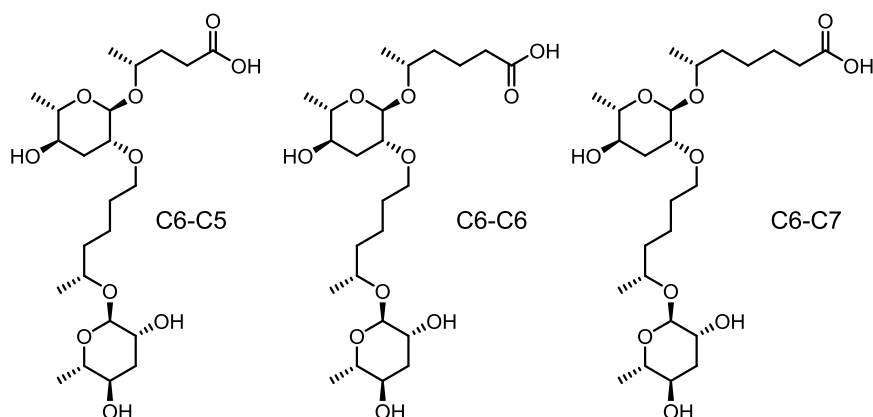


Figure 6.3: Chemical structures of 2-substituted dimeric ascarosides (C6-C5, C6-C6 and C6-C7) identified from the *exo*-metabolome extract of *C. nigoni*.

Ecological significance of dimeric ascarosides: On the basis of high resolution masses and NMR data, a series of dimeric ascarosides were proposed in **Table S12**. In our study, chemical composition of dimeric ascarosides in 13 *Caenorhabditis* species was carefully analyzed, which revealed that five species (*C. remanei*, *C. briggsae*, *C. tropicalis*, *C. sinica* and *C. nigoni*) were capable of producing a blend of dimeric ascarosides (**Figure 6.4**). Particularly, *C. briggsae* and *C. nigoni* produced a very complex blend of dimeric ascarosides. However, only few dimeric ascarosides were detected in the *exo*-metabolome extracts of *C. sinica* and *C. tropicalis*. And some dimeric ascarosides are highly specific to their producer. For example, major components of C7-C7, C5-C9 and C7-C9 as well as minor dimeric ascarosides C7-C8 and C7-C11 are specific to *C. briggsae*; C4-C6 and C4-C7 were specific to *C. remanei*; C6-C8, C6-C10, C6-C11 and C6-C12 were specifically produced by *C. nigoni*. At this stage, we do not know the biological activity of these dimeric ascarosides (biological tests are being planned). Up to now, no dimeric ascarosides has been reported from nematodes excepting *dasc#1* which was described to regulate mouth-form dimorphism, a particular phenotypic plasticity evolved for predatory behavior by the satellite model organism nematode *Pristionchus pacificus*.^[34] It was absolutely necessary to investigate the biological activities of these

novel dimeric ascarosides, especially for the dominating components, which will provide us deeper understanding of chemical communication in *Caenorhabditis* species.

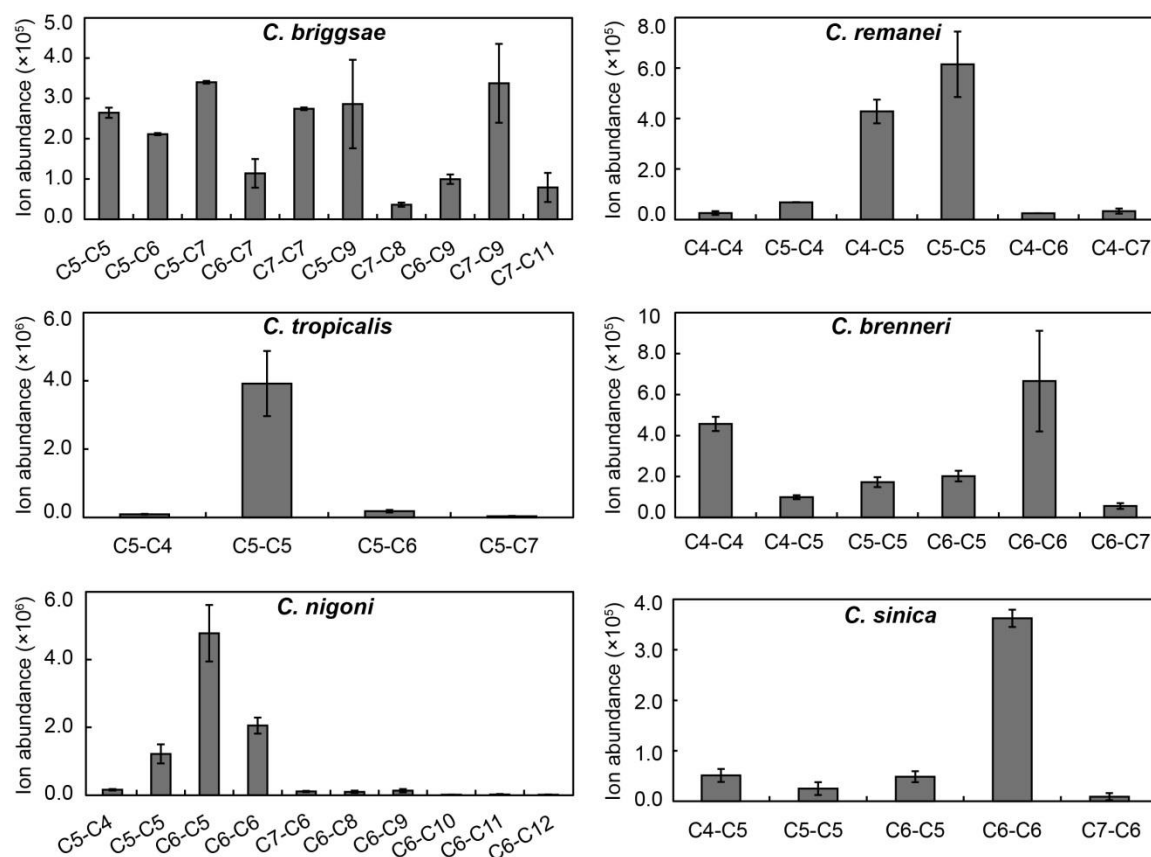


Figure 6.4: Qualitative and quantitative differences of dimeric ascarosides in five *Caenorhabditis* species. Relative abundances of dimeric ascarosides were quantified in the *exo*-metabolome extracts derived from five *Caenorhabditis* species including *C. remanei*, *C. briggsae*, *C. tropicalis*, *C. sinica* and *C. nigoni*. (n = 3; Error bars represent \pm SE)

Conclusions: A prominent ascaroside was detected using MS/MS precursor ion screen. High resolution mass and MS/MS fragmentation indicated that the target compound was a heterodimeric ascaroside C4-C5. Acquired NMR data of the isolated compound finally clarified its chemical structure. Chemical syntheses of dimeric ascarosides are going on in our lab. And three dimeric ascarosides with 2-substitution were also identified from the *exo*-metabolome of *C. nigoni*. Five *Caenorhabditis* species including *C. remanei*, *C. briggsae*, *C. tropicalis*, *C. sinica* and *C. nigoni* were detected to produce a mixture of dimeric ascarosides.

Chapter 7

(ω)- and (ω -2)-Hydroxylated Ascarosides from *Caenorhabditis nigoni*

Comparative metabolomics reveals (ω)- and (ω -2)-hydroxylated ascarosides: Using MS-based comparative metabolomics with selective precursor ion screening of exo-metabolomes of 13 *Caenorhabditis* species revealed three signals that were highly specific to *Caenorhabditis nigoni* (Figure 7.1A). High resolution masses suggested molecular formulas of $C_{15}H_{26}O_7$ ($C_{15}H_{25}O_7^-$, obs. m/z 317.1631, calcd. m/z 317.1606), $C_{15}H_{28}O_7$ ($C_{15}H_{27}O_7^-$, obs. m/z 319.1755, calcd. m/z 319.1762) and $C_{15}H_{26}O_7$ ($C_{15}H_{25}O_7^-$, obs. m/z 317.1601, calcd. m/z 317.1606) for these target components, which also suggested that they are likely to be three ascarosides that were each decorated with one additional hydroxyl group on the fatty acid derived side chain. Two of these compounds feature three unsaturation units respectively. Fragments of $C_9H_{15}O_4^-$ (obs. m/z 187.0961, calcd. m/z 187.0976), $C_9H_{17}O_4^-$ (obs. m/z 189.1129, calcd. m/z 189.1132) and $C_9H_{17}O_4^-$ (obs. m/z 189.1120, calcd. m/z 189.1132) derived from the MS/MS fragmentation (Figures S63, S66 and S70) further demonstrated that three target compounds were derived from known ascarosides ascr#3 and ascr#10 which were modified with hydroxyl group on the fatty acid derived side chain.

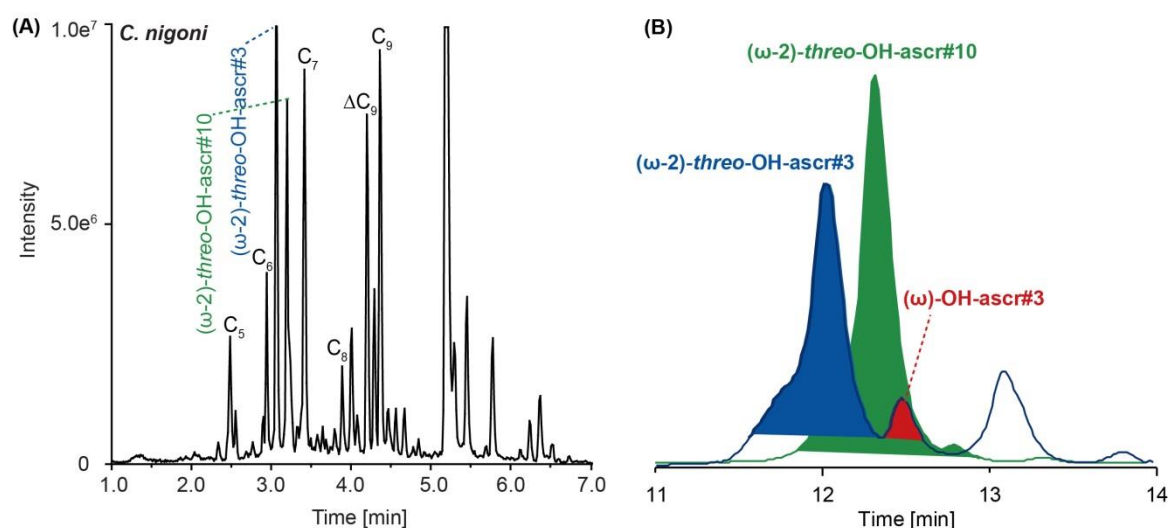


Figure 7.1: Discovery of hydroxylated ascarosides from *C. nigoni*. (A) Hydroxylated ascarosides were detected using triple quadrupole mass spectrometer. These novel ascarosides were also detected by GC-MS, which was recently established and

described in **Chapter 7**. (B) Extracted ion traces of hydroxylated ascarosides using high resolution LC-MS mass spectrometer.

Structural characterization of (ω)- and (ω -2)-hydroxylated ascarosides: For further characterization of these target metabolites, 1.6 L *exo*-metabolome of *C. nigoni* was prepared, which was separated by solid phase extraction (SPE) and hydroxylated ascarosides were enriched in SPE40 *via* analyzing the *dqf*-COSY spectrum (**Figure S59**). Semi-preparative HPLC was further applied for isolation, which finally resulted in three purified (or partly enriched) compounds in separated sub-fractions (described in **Chapter 1**). Analysis of 1D and 2D NMR spectra acquired for one of the purified hydroxylated ascarosides showed the characteristic spin system corresponding to ascarylose, two methyl groups which suggested a (ω -1)-style of fatty acid derived side chain, as well as one double bond with *E*-configuration as indicated by proton signals at 5.83 ppm and 6.86 ppm harboring coupling constant of 15.7 Hz. The *dqf*-COSY spectrum showed ^1H , ^1H correlations from H-6' and H-8' to H-7' which is located at 3.53 ppm indicating the presence of a hydroxyl group at the C-7' position (ω -2) of the fatty acid side chain. We hypothesized that the absolute stereochemistry at the (ω -1) position is *R* because all the (ω -1) style ascarosides were identified with *R* configuration at this position. Furthermore, the small coupling constant between H-8' and H-7' suggested a *threo* configuration between C-8' and C-7', which implied a *R* configuration for the (ω -2) C-7' position and the molecular structure was proposed as shown in **Figure 7.2A** as (ω -2)-*threo*-OH-ascr#3. Another purified compound shared a similar molecular composition and NMR data but lacks the unsaturation in comparison to the chemical structure of (ω -2)-*threo*-OH-ascr#3, which was finally proposed to be (ω -2)-*threo*-OH-ascr#10. The third compound featuring ascarylose and a fatty acid derived side chain with one unsaturation (*E* configuration). However, NMR data clearly showed that the methyl group of the side chain disappeared and instead one hydroxymethylene signal was observed, which suggested that hydroxylation happened at ω position and the chemical structure was proposed as (ω)-OH-ascr#3 (**Figure 7.2A**). Chemical synthesis of (ω -2)-*threo*-OH-ascr#3, (ω -2)-*threo*-OH-ascr#10 and (ω)-OH-ascr#3 (by Stephan H. von Reuß) was established

to clarify the molecular structures of hydroxylated ascarosides. Comparison of the ^1H NMR data of the isolated natural material with those of the synthetic compounds showed perfect agreement with (ω -2)-*threo*-OH-ascr#3 (**Figure 7.2B**), which finally confirmed the proposed chemical structures shown in **Figure 7.2A**.

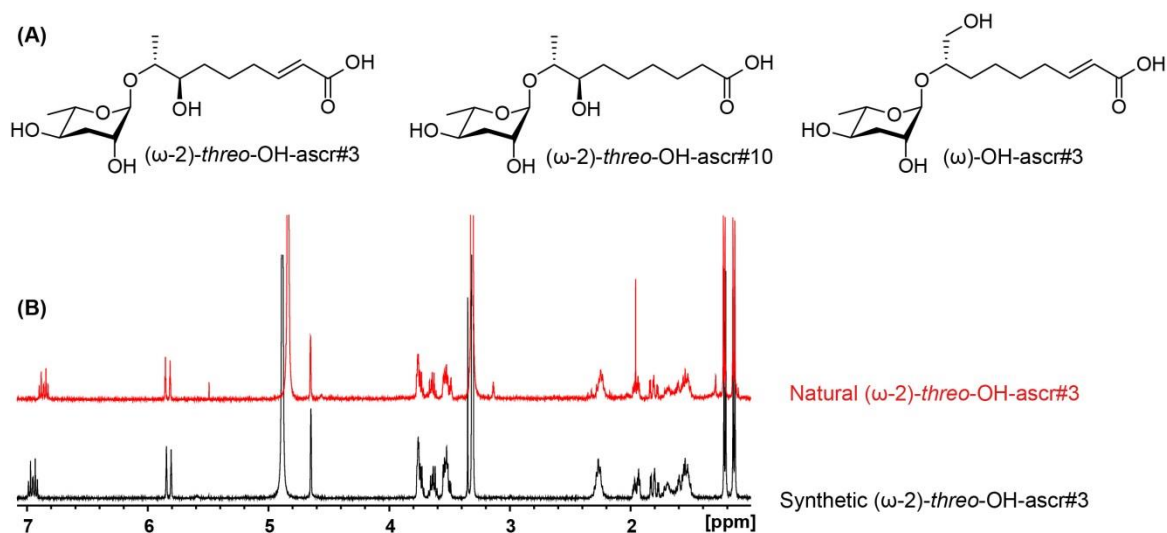


Figure 7.2: Identification of (ω)- and (ω -2)-hydroxylated ascarosides from *C. nigoni*. (A) Chemical structures of (ω)- and (ω -2)-hydroxylated ascarosides including (ω -2)-*threo*-OH-ascr#3, (ω -2)-*threo*-OH-ascr#10 and (ω)-OH-ascr#3 identified from *C. nigoni*. (B) Comparison of proton spectra of naturally isolated and synthetic (ω -2)-*threo*-OH-ascr#3.

Ecological significance of (ω)- and (ω -2)-hydroxylated ascarosides: In this thesis, 13 *Caenorhabditis* species were screened for ascarosides, from which two species (*C. nigoni* and *C. afra*) were found to specifically produce (ω)- and (ω -2)-hydroxylated ascarosides. Previously males of the sour paste nematode, *Panagrellus redivivus* was reported to produce hydroxylated ascarosides (**Figure 7.3**) of which the sex pheromone dhas#18 was identified to be specifically released by males to attract females.^[35] The unique dihydroxylated ascaroside dhas#18 features a (3*R*)-hydroxy moiety thought to be introduced during chain shortening upon peroxisomal β -oxidation along with a (ω -3)-hydroxyl group of unknown origin. The discovery of hydroxylated ascarosides in *C. nigoni* and *C. afra* now further demonstrates that nematodes employ side chain hydroxylations at the (ω)-, (ω -2)-, or (ω -3)-positions to generate highly species-specific ascarosides from commonly produced components. Given the high degree of species

specificity of (ω)-, (ω -2)-hydroxylated ascaroside it will be important to clarify their biological activities and biosynthetic pathways in *C. nigoni* and *C. afra*.

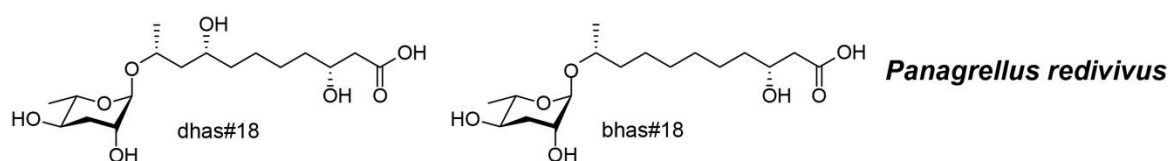


Figure 7.3: Known (ω -3)-hydroxylated ascarosides identified from *Panagrellus redivivus*.

Conclusions: Using targeted metabolomics as well as chemical synthesis, (ω)- and (ω -2)-hydroxylated ascarosides were identified from *C. nigoni*. Three hydroxylated ascarosides, highly specific to *C. nigoni* and *C. afra*, were isolated and purified for structural characterization. More efforts are currently taken to investigate their biological activity and biosynthetic pathway.

Chapter 8

Amino Benzoic Acid Modified Ascarosides Identified from *Caenorhabditis nigoni*

Comparative metabolomics reveals amino benzoic acid modified ascarosides:

Detailed analysis of *dqf*-COSY spectra acquired for each SPE fraction of the *exo*-metabolome of *C. nigoni* led to the discovery of one additional class of novel ascarosides that was not detectable *via* LC-MS/MS precursor ion screening. Characteristic signals derived from ascaroside modified with additional functional group at the 4-position of ascarylose were detected in the *dqf*-COSY spectrum of SPE 70 fraction (**Figure 8.1**). High resolution mass of the target compound suggested a molecular formula of $C_{19}H_{27}NO_7$ ($C_{19}H_{26}NO_7^-$, obs. m/z 380.1708, calcd. m/z 380.1715) and seven units of unsaturation, which indicated that one amino benzoic acid group might be connected to the 4-position of a common ascaroside ascr#12. MS/MS fragmentation data also supported the proposed chemical structure. Generally, there are two types of amino benzoic acids (*ortho*- and *para*-substitution) that are prominent in secondary metabolites. *p*-aminobenzoic acid (PABA) is formed from chorismate catabolism and integrated into the highly potent male attractant ascr#8.^[31] In contrast, *o*-aminobenzoic acid (anthranilic acid) originates from tryptophan metabolism and has previously been described as a modular unit of pasa#9, a complex ascaroside involved in the dauer formation of *Pristionchus pacificus*.^[53]

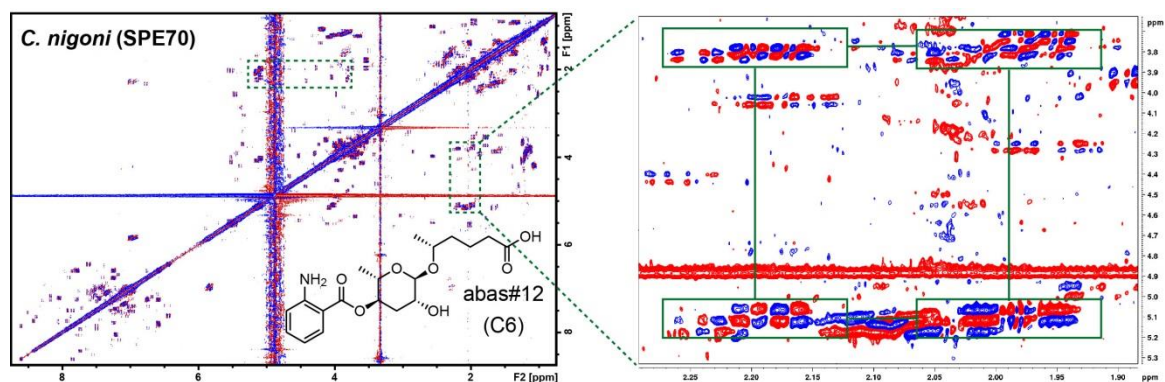


Figure 8.1: Abas#12 was detected by analysis of the *dqf*-COSY spectrum of SPE 70 fraction. Enlarged section demonstrates that ascaroside is substituted at the 4-position of

ascarylose.

To determine the substitution pattern of the amino benzoic acid and to confirm our structure assignment, three dominating compounds (abas#1, abas#9 and abas#12) were isolated using semi-preparative HPLC. High resolution masses of abas#1 (obs. m/z 394.1893, calcd. m/z 394.1871, $C_{20}H_{28}NO_7^-$), abas#9 (obs. m/z 366.1581, calcd. m/z 366.1558, $C_{18}H_{24}NO_7^-$) suggested very similar molecular structures to abas#12. Proton spectra (Figures 8.2B-D) were acquired for three isolated compounds including abas#1, abas#9 and abas#12, aromatic area of which clearly demonstrated one set of signal (7.76, 6.58, 7.23 and 6.73 ppm) derived from amino benzoic acid group. Further analysis of dqf -COSY (Figures 8.2E-F) spectra acquired for ascaroside abas#12 revealed the presence of *ortho*-amino benzoic acid incorporated at the 4-position of the ascarylose. The chemical shift of H-4 was shifted to 5.06 ppm, which indicated that the amino benzoic acid was connected to the 4-position of ascarylose.

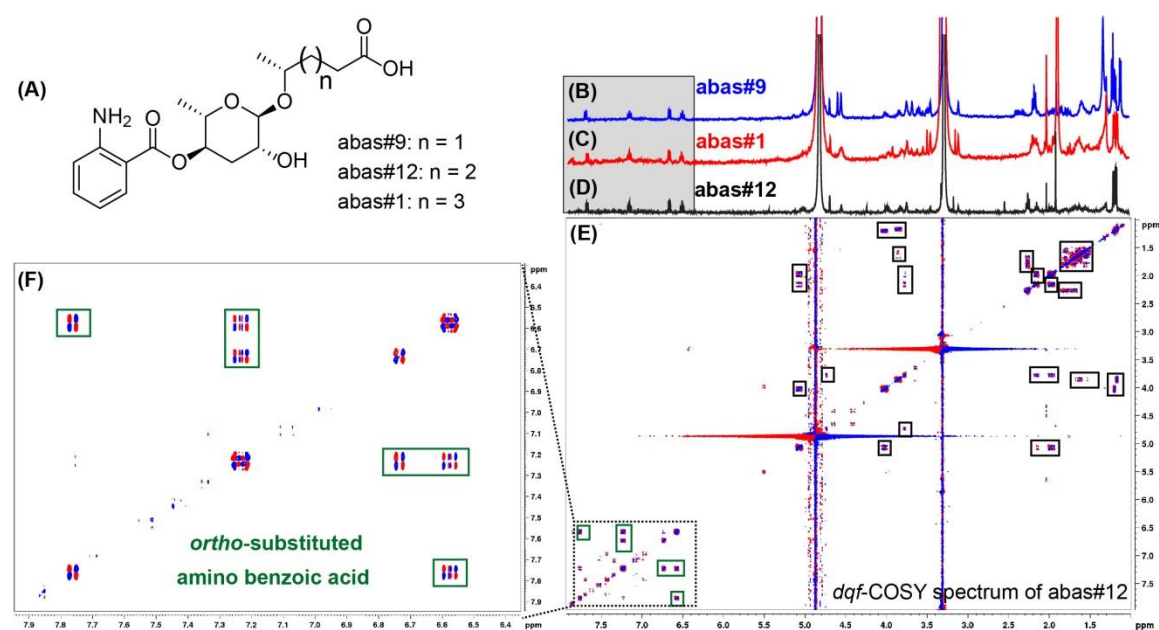


Figure 8.2: Structural characterization of amino benzoic acid modified ascarosides.

(A) Chemical structures of abas#1, abas#9 and abas#12. (B) Proton spectrum of abas#9. (C) Proton spectrum of abas#1. (D) Proton spectrum of abas#12. (E) dqf -COSY spectrum of abas#12. A set of signals in gray rectangle area indicated *ortho*-substitution at aromatic ring which was also confirmed by part of dqf -COSY spectrum enlarged in (F).

Identification of additional amino benzoic acid modified ascarosides: MS/MS fragmentation of abas#9 resulted in a prominent daughter ion with the molecular formula

of $C_{13}H_{16}NO_4$ (obs. m/z 250.1136, calcd. m/z 250.1074) which is derived from the loss of C5 fatty acid side chain (**Figure 8.3A**). Similarly, MS/MS fragmentation of major components abas#1 and abas#12 in positive ion mode also produced a fragment of m/z 250.1136 *via* release of the relative fatty acid side chains. Based on their characteristic MS/MS fragmentation pattern upon electrospray ionization in positive ion mode (ESI-+), a series of amino benzoic acid modified ascarosides with side chains ranging from 5 to 9 carbons were discovered in the crude *exo*-metabolome extract of *C. nigoni* (**Table S15**, **Figure 8.3B**). Their chemical structures were proposed as shown in **Figure 8.3C**.

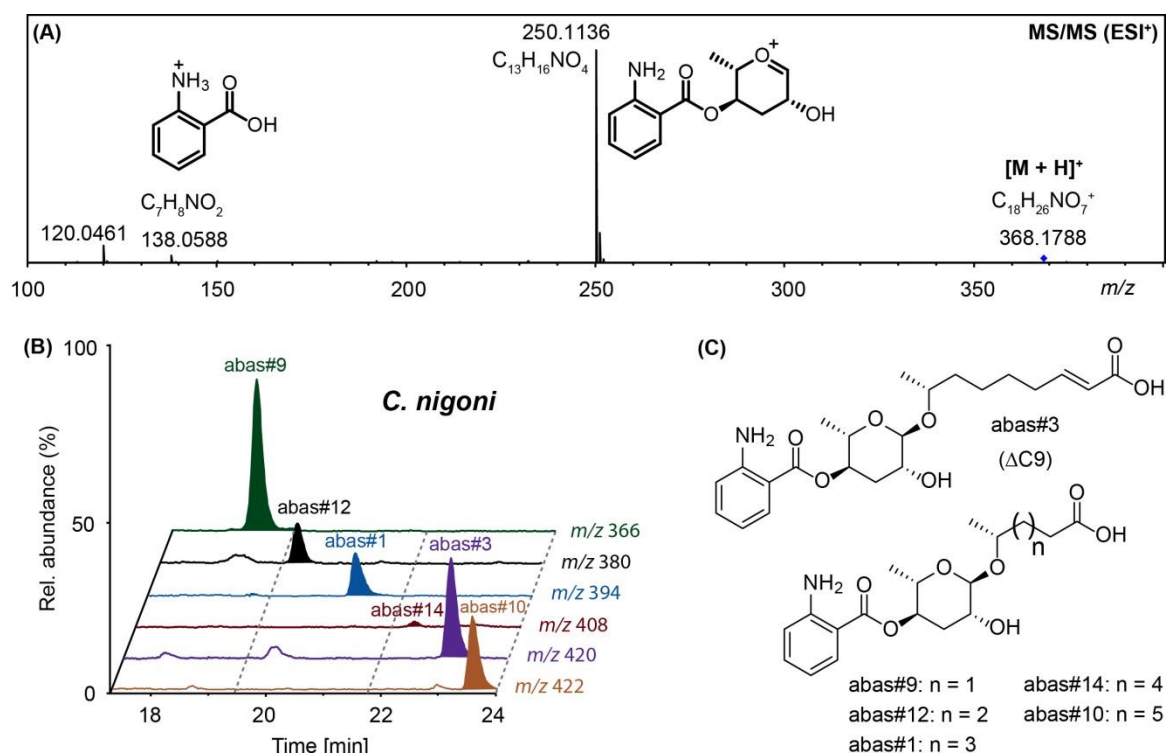


Figure 8.3: Identification of diverse amino benzoic modified ascarosides from *C. nigoni*. (A) MS/MS fragmentation analysis of abas#9. (B) Ion traces of a series of amino benzoic acid modified ascarosides identified from *C. nigoni*. (C) Chemical structures of amino benzoic acid ascarosides.

Ecological significance of amino benzoic acid modified ascarosides: Amino benzoic acid modified ascarosides were detected in the *exo*-metabolomes produced by two species, *C. nigoni* and *C. tropicalis*. Quantification of their relative ion abundances (**Figure 8.4**) showed that *C. nigoni* produced a broad range of amino benzoic acid modified ascarosides with side chain ranging from C5 to C11. In contrast, *C. tropicalis*

excretes much larger amounts of amino benzoic acid ascarosides (abas) in comparison to *C. nigoni* with short chain components such as abas#9, abas#12 and abas#1 being most abundant.

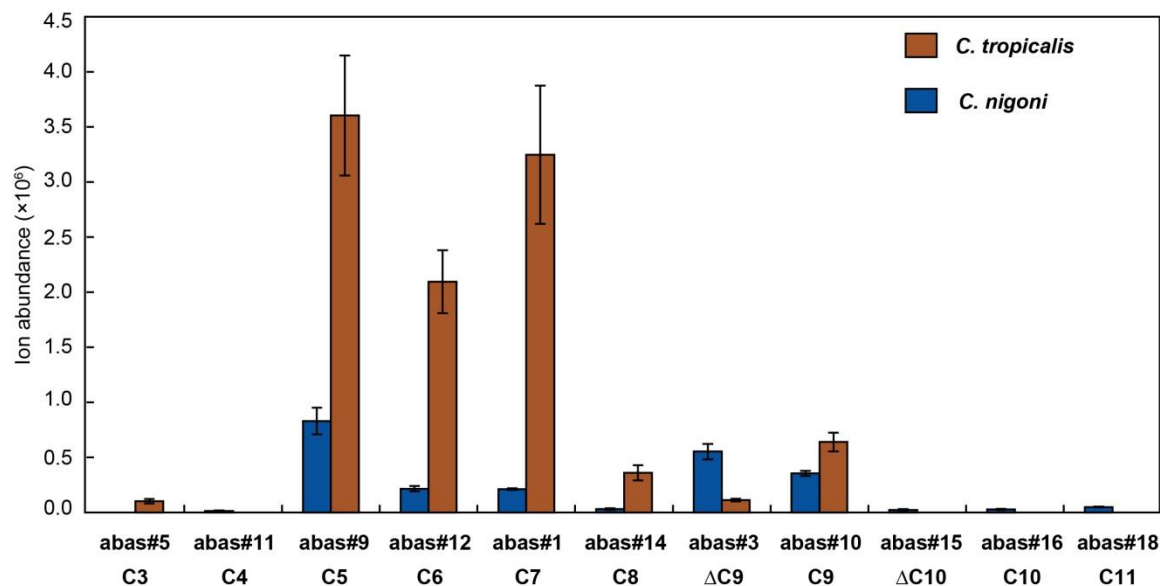


Figure 8.4: Amino benzoic acid modified ascarosides in *C. nigoni* and *C. tropicalis*. A panel of amino benzoic acid modified ascarosides was detected in *C. nigoni* and *C. tropicalis*. Relative abundances of abas were quantified (n = 3; ±SE).

Conclusions: Using analysis of *dqf*-COSY spectra, one group of amino benzoic acid modified ascarosides, featuring one additional amino benzoic acid at the 4-position of ascarylose, was identified from *C. nigoni*, which present another group of novel chemical signals in nematodes. Currently, we are still working on the biological tests for amino benzoic acid modified ascarosides.

Chapter 9

Conclusions and Outlook

Based on the previous fascinating research on ascarsodies, this dissertation aims to work on chemical communication between *Caenorhabditis* species. In particular the identification of ascarosides is the holy grail of this topic. Using comparative metabolomics and sophisticated analytical tools, seven groups of unanticipated ascarosides featuring rare chemical motifs were discovered for the first time from nematodes. In particular, selective MS screening facilitated detection of minor or even trace ascarosides missed by conventional analysis. Here, structural characterization, biosynthesis and chemical ecology related to the newly discovered ascarosides were described in chapters, which added great biochemical diversity and novelty to our understanding of chemical signaling in nematodes (**Figure C1**). These findings suggest that ascaroside diversity in *Caenorhabditis* is far more complex than previously anticipated. Examples as fasc, ucas and phas ascarosides are characterized which display unprecedented architectures. For the synthetic chemists, it is challenging and exciting to perform their total synthesis, and in the case of fasc-C₄ΔC₁₁ more than twenty steps were established by Franziska Dolke to finally synthesize it. Comparative analysis results suggests that chemical signaling is much more complex than we imagined, providing great potential to study chemical communication between nematodes. For instance, the *C. remanei* nematode, an important species used in ecological and genetic studies, is capable of producing several types of ascarosides including fasc, icas, phas, dasc and ucas. This complex chemical content makes it challenging to clarify their potential functions in inter- and intra-species interactions. In addition, characterization of these novel chemical structures further confirmed that they were assembled by building blocks derived from primary metabolism. For example, abas harbor additional amino benzoic acid at 4-position of ascarylose which is derived from tryptophan metabolism. Thus, ascarosides share distinguishable origins with traditional defined secondary metabolites, which transcend both primary and secondary metabolites. Finally, despite of the complex content and low abundance of ascarosides, a total of seven classes of

ascariosides were identified from nematodes, suggesting that the targeted MS screening method can significantly accelerate the discovery of new ascariosides. Nevertheless, our data and others also indicate that there are other ascariosides that are yet to be identified in the future. However, it remains a challenge to know the actual chemical content produced by nematodes while they live under non-laboratory conditions in their natural habitat or original ecological niche, because nematodes are generally cultivated in laboratory with standard condition with 23 °C temperature and food source of *E. coli*. It is still a big question to know whether nematodes eat other species of bacteria as their real food in nature.^[54]

Prevalence of ascariosides throughout different nematode population suggests that ascariosides has long been an evolutionary driver in development and behavior. Distinct ascarioside content might result from genetic divergence and in part from the adaptation to the specific ecological niche. For example, *C. remanei* and *C. latens* are capable of producing fatty acid ascariosides, but no trace of these ascariosides were detected in any other species. For those ascariosides described in **Chapter 7**, htas are exclusively detected in *C. nigoni* and *C. afra*, while abas are specifically produced by *C. nigoni* and *C. tropicalis*. In addition, *C. nigoni* and *C. briggsae* nematodes share the smallest genetic divergence but distinct chemical content. From a global perspective of evolution, nematodes located in the *Elegans* group evolved to produce many different types of ascariosides which were transduced into their chemical language. For many species of those nematodes located outside of *Elegans* group, standard cultivation condition in laboratory are not suitable for their growth. Thus, unfortunately, chemical signaling of these nematodes could not be considered in the comparative analysis. All in all, we can envisage that these results will largely expand our knowledge about chemical ecology of nematodes and create huge space to study chemical communication in nematodes. However, there are two critical questions still waiting to be answered.

1: How do nematodes produce ascariosides?

Most notably, ascariosides are assembled in a modular fashion with building blocks of ascarylose, fatty acid side chain and some cases of additional tailoring groups. Until now, we have very limited knowledge about genes and encoded enzymes that participated in

the biosynthesis of ascarosides.^[22,24,55] Particularly, for the newly discovered ascarosides in this dissertation, much more efforts are strongly required to understand how they are biosynthesized. In the future, it will be another challenge ahead because of their complex structures. In 2014, putative PKS genes were reported from *C. elegans* and they were hypothesized to be involved in the biosynthesis of ascarosides,^[56] suggesting that one machinery line similar to PKS biosynthesis might conserved in nematodes. With evidence of gene alignment with bacterial PKS domains and fatty acid synthase gene, authors hypothesized that a fatty acid synthase gene was duplicated and diverged to form PKSs in nematodes. That would be a breakthrough and we can envisage that it is available to analyze, predict and manipulate the biosynthesis of ascarosides, if this hypothesis is confirmed by experimental evidence. Very recently, two polyketide-nonribosomal peptides were reported to promote larval survival in *C. elegans* for the first time.^[58] It will be very important to explore the biosynthetic mechanism and original precursor, and identification of intermediates will also be highlighted in the future.

2: Why do nematodes excrete ascarosides?

As a next step, it is important to clarify the functions of these newly discovered ascarosides. Many ascarosides are demonstrated to be bioactive to induce dauer formation and influence development as well as behavior of nematodes. Comparing new ascarosides in this dissertation with those previously described, highlights key differences in chemical structures that may encode distinct biological meanings. Notably, two species-specific indole ascarosides, icas#2 and icas#6.2 described in **Chapter 2**, are produced by *C. briggsae* hermaphrodites and can synergistically attract conspecific males. Reflecting on the potential biological roles of remaining ascarosides, their biological assays are being planned. At this stage, we still do not know what kind of activities they possess. Further investigations of the roles of ascarosides in nematodes might benefit from the expanded knowledge of chemical structures and help clarify the biological activities of newly discovered ascarosides. And finally, investigation on the mechanism how nematodes perceive ascarosides is seemingly also important. For example, ascr#18 produced by parasitic nematode was reported to cause immunity response in plants that set up defense.^[58] More details of chemical interaction between

parasitic nematodes and plant are highly required, which can improve economy and agricultural production, because nematodes caused worldwide damage to agriculture.^[59]

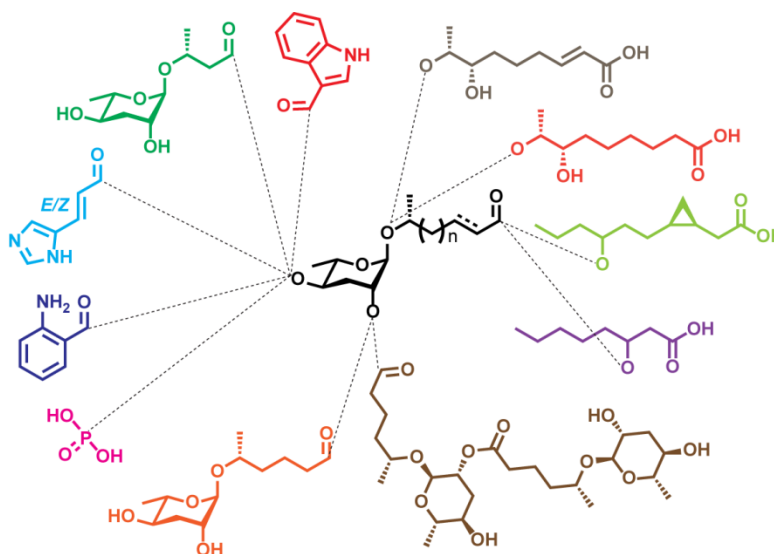


Figure C1: Diversity and novelty of ascarosides discovered in this thesis. All the chemical entities shared one common structural group with the black color in the middle. Diverse building blocks from primary metabolism biosynthetic pathway, including indole group, amino benzoic acid group, urocanic acid group and phosphate group played as another combinatorial part of these novel ascarosides.

Appendix

Experimental Part

Nematodes strains and experimental culture conditions: (A) Nematodes strains used in this thesis. Eight wild-type isolates of *Caenorhabditis remanei*: PB4641 (New York, US), PB288 (Ohio, US), JU1082 (Japan), SB146 (Freiburg, US), MY2231 (Tübingen, Germany), MY726 (Tübingen, Germany). Two wild-type isolates of *Caenorhabditis latens*: JU724 (Jiangsu, China) and VX88 (Hubei, China). Thirteen wild-type isolates of *Caenorhabditis briggsae* including the five tropical strains: AF16 (India), JU725 (China), ED3034 (Taiwan), ED3083 (South Africa), VT847 (Hawaii), the five temperate strains: HK104 (Japan), PB800 (Ohio, US), EG4181 (Utah, US), JU516 (France), JU439 (Iceland), and three outgroup strains: QR24 (Canada), ED3101 (Kenya), JU1341 (India). Thirteen wild-type isolates of other *Caenorhabditis* species: *C. elegans* N2 (Bristol), *C. remanei* PB4641 (USA), *C. wallacei* (sp.16) JU1904 (Indonesia), *C. sinica* (sp.5) JU727 (China), *C. brenneri* (sp.4) PB2801 (Costa Rica), *C. nigoni* (sp.9) JU1422 (India), *C. doughertyi* (sp.10) JU1771 (India), *C. tropicalis* (sp.11) JU1373 (La Reunion), *C. japonica* DF5081 (Japan), *C. afra* (sp.7) JU1286 (Ghana), *C. portoensis* (sp.6) EG4788 (Portugal), *C. virilis* (sp.13) JU1968 (France) and *C. sp 1* JU1667 (Germany). Two wild-type isolates of *Caenorhabditis elegans* strains: AB1 and CB4865. Three mutants of *Caenorhabditis elegans* strains: am130, am132 and gk324463. **(B) Experimental culture conditions.** All the nematodes were kept on solidified nematode growth medium (NGM agar) seeded with *E. coli* OP50. For comparative analysis of metabolomes, worms were washed into the autoclaved 250 ml flasks using 15 ml M9 solution. 100 ml S-Basal solution and pellet of *E. coli* as well as additional chemicals (5 ml Citrate, 5 ml TMS, 1.5 ml CaCl₂, 1.5 ml MgSO₄ and 0.5 ml Cholesterol) were added into flask. Increased amount of *E. coli* OP50 pellet was added into flasks during the culture process of 15 days. Nematodes were cultivated at 23-25 °C. Androdioecious populations of hermaphroditic *C. briggsae* (AF16, HK104), *C. elegans* (N2), *C. tropicalis* (JU1373) were generated by heat shock of late L4 hermaphrodites at 30 °C for 6 h and subsequently maintained by mating.

Analytical methods and instruments: (A) NMR spectroscopy. NMR spectra were recorded in CD₃OD or CDCl₃ at 400 (or 500 or 700) MHz for ¹H and 100 (or 125 or 175) MHz for ¹³C using a Bruker AMX400 (or 500 or 700) instrument. Residual solvent signals were used as internal standard with ¹H at 3.31 ppm and ¹³C at 49.05 ppm for CD₃OD, or ¹H at 7.26 ppm and ¹³C at 77.16 ppm for CDCl₃. Two-dimensional homonuclear double quantum filtered (*dqf*)-COSY spectra were recorded using phase cycling for coherence selection. A total of 32 scans were acquired using a time domain of 8k in F2 (acquisition time of 1.2 s) and 512 scans in F1. For two dimensional heteronuclear HSQC spectra 96 scans were acquired using a time domain of 1k in F2 and 256 increments in F1. Spectra were zero-filled to 8k × 4k (COSY) or 4k × 2k (HSQC) prior to Fourier transformation and phasing using the Bruker Topspin software. **(B) MS spectrometry.** HPLC-ESI-HR-MS/MS analysis was performed using a Dionex UltiMate 3000 HPLC instrument coupled to a Bruker Maxis ultrahigh resolution (UHR) qTOF mass spectrometer equipped with a electrospray ionization (ESI) unit operated in positive or negative mode. Chromatographic separations were achieved using an Agilent ZORBAX Eclipse XDB-C18 column (250 × 3 mm, 5 μm) with a flow rate of 400 μl/min gradient elution with 3% aqueous acetonitrile for 5 minutes and a linear gradient to 100% acetonitrile within 35 minutes using 0.5% acetic acid as an additive. Quantification of ascarosides was performed by comparison with authentic standards of known concentration using three independent replicates. **(C) Chromatography.** Solid phase extraction (SPE) fractionation was performed with Chromabond SPE cartridges of C18 ec (6 mL/500 mg), SiOH (3 mL/500 mg) or C18 (40 mL/5000 mg).

Preparation of exo-metabolome extracts for comparative analysis: Cultures were established using mixed stage nematodes from five 10 cm plates collected in M9 buffer as inoculums and grown in 100 ml S complete medium at 23 °C and 150 rpm. Concentrated *E. coli* OP50 bacteria pellet from an overnight culture in LB medium at 37 °C and 170 rpm was provided as food on day 1 (3 ml), day 2 (3 ml), day 3 (3 ml), day 4 (5 ml), and day 5 (10 ml). After 15 days nematodes were separated by centrifugation (5 min at 2000 rpm).

The filtered supernatant representing the *exo*-metabolome was frozen at -80 °C, lyophilized, and extracted with 3 x 100 ml methanol for 12 h each. The combined extract was filtered and concentrated to dryness at 40 °C under reduced pressure. The metabolome extract was further concentrated by subsequent extraction of the residues with decreasing amounts of methanol and concentration of the supernatants at 40 °C under reduced pressure. The resulting material was dissolved in 1 ml methanol for HPLC-MS analysis. All experiments were performed in triplicate.

Preparation of *exo*-metabolome extracts for initial fractionation: Large liquid culture of four species of *C. remanei* (1.8 L), *C. latens* (1.2 L), *C. briggsae* (1.5 L) and *C. nigoni* (1.6 L) were set up for solid phase extraction (SPE) fractionation. Nematodes cultured on every five NGM agar plates (10 cm) inoculated with *E. coli* OP50 were washed into a flask that contained 100 ml S-Basal solution and 3 ml concentrated *E. coli* OP50 bacteria pellet. After two days, another 3 ml concentrated *E. coli* OP50 bacteria pellet was added into the flask. Food source was increasingly supplemented every two days with the amount of 3 ml, 5 ml and 10 ml concentrated *E. coli* OP50 bacteria pellet. Worms were cultured in the liquid solution at 23-25 °C and 130 rpm and they were harvested after 15 days. For example, 1.6 L (16 flasks × 100 ml) *C. nigoni* culture medium was separated by centrifugation into worm pellets and supernatant (*exo*-metabolome) which were stored in -80 °C refrigerator and lyophilized. Freeze dried materials were extracted with 3 x 100 ml methanol for 12 h each. Combined extract was concentrated to dryness at 40 °C under reduced pressure.

Preparation of crude extract and solid phase extraction (SPE) fractionation: Methanol dissolved metabolome extract mixed with 2.0 g Celite was concentrated to dryness at 40 °C under reduced pressure. Fully mixed samples were subjected to the reversed phase extract (C18, 40 mL/5000 mg) column which was washed by water and then increased methanol from 10 % to 100%, resulting in the flash through fraction and other 10 fractions.

Purification or enrichment of novel ascarosides and fatty acids: Agilent HP-1100 HPLC instrument equipped with Gilson 206 Abimed fraction collector was used to separate target SPE fractions, which finally resulted in 44 sub-fractions (F1-F44). A Grom-Sil 120 ODS-4 HE (C18, 5 μ m, 250 \times 8 mm) column was used with solvent system of Acetonitrile (ACN) and water containing 0.5% acetic acid at 2 ml/min: 0-3 min, 3% ACN; 3-30 min, 3-100% ACN; 33-40 min, 100% ACN; 40-45 min, 100-3% ACN; 45-55 min, 3% ACN. Fractions were monitored by HPLC-MS equipped with Bruker ultrahigh resolution qTOF mass spectrometer and target fractions containing the desired mass were concentrated for NMR analysis. For example, SPE70-F18 refers to ascaroside of icas#2 was isolated and purified from SPE70 using semi-preparative HPLC and finally collected in the sub-fraction 18. In this thesis, seven types of new ascarosides (**Table 1**) as well as cyclopropyl fatty acids (**Table 2**) were isolated from the *exo*-metabolome extracts of *C. remanei*, *C. latens*, mixture of *C. remanei* strains, *C. briggsae* and *C. nigoni*.

Table 1. Ascarosides derived from metabolome extracts of *C. remanei*, *C. latens*, mixture of *C. remanei* strains, *C. briggsae* and *C. nigoni*.

	<i>C. remanei</i>	<i>C. latens</i>	§Mixture	<i>C. briggsae</i>	<i>C. nigoni</i>
icas#2				SPE70-F18	
icas#6.2				SPE70-F18	
fasc-C4 Δ C11	SPE70-F23		SPE70-F25		
fasc-C4C6		SPE50-F18			
fasc-C4C8		SPE60-F28			
ucas#3	SPE60-F12				
ucas#10	SPE60-F13				
4P-ascr#2	SPE10-F32				
4GlcP-ascr#2	SPE10-F33				
(ω -2)-threo-OH-ascr#3					SPE40-F12
(ω -2)-threo-OH-ascr#10					SPE40-F13
(ω)-OH-ascr#3					SPE40-F14
abas#1					SPE70-F23
abas#9					SPE70-F12
abas#12					SPE70-F17
C4-C5	SPE50-F23				
C6-C5					SPE50-F25
C6-C6					SPE60-F30

C6-C7					SPE60-F34
-------	--	--	--	--	-----------

§Mixture refers to the mixed *exo*-metabolome extracts of six *C. remanei* strains.

Table 2. Fatty acids derived from metabolome extracts of mixture of *C. remanei* strains and *C. briggsae*.

	§Mixture	<i>C. briggsae</i>
<i>cis</i> -cascairillic acid	SPE80-F10	
8-hydroxy- <i>cis</i> -cascairillic acid	SPE70-F22	
10-hydroxy- <i>cis</i> -cascairillic acid	SPE70-F20	
11-carboxy- <i>cis</i> -cascairillic acid		SPE60-SPE60
9-carboxy- <i>cis</i> -cascairillic acid		SPE40-SPE40
7-carboxy- <i>cis</i> -cascairillic acid		SPE10-F33

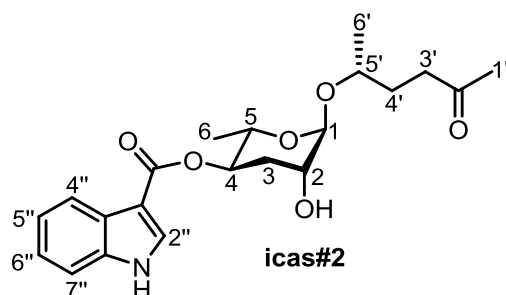
§Mixture refers to the mixed *exo*-metabolome extracts of six *C. remanei* strains.

Biological activity tests of icas#2 and icas#6.2: (A) Retention assay to evaluate nematode behavioural response. Nematode preference for environments conditioned with known amounts of indole ascarosides was measured using a retention assay. On a 6 cm petri dish filled with 6 ml peptone free NGM agar circular scoring regions of 9 mm diameter were marked. Next, 1 µl of 10% aqueous methanol (as negative control) or indole ascaroside solutions, e.g. icas#2, (*R*)-icas#6.1, (*S*)-icas#6.2, icas#3, icas#9, or their mixtures in 10% aqueous methanol were placed in the centre of the scoring areas onto the agar and left to dry for 5 minutes. Young adult nematodes from non-starved and non-crowded 6 cm NGM plates seeded with *E. coli* OP50 were transferred to peptone-free NGM agar without any food for ca. 15 min before being used for the assay to minimize the amount of concomitant bacteria. Individual worms were placed into the centre of the conditioned scoring region and the time required for the nematode to leave the scoring region was measured. Nematodes were defined to have left the scoring area when no part of the nematode was still within the circular boundary. A total number of 10 worms per condition were analyzed. A one-way between subjects ANOVA with Dunnett's posttest was performed using the SPSS software to evaluate the effect of indole ascarosides on mean times nematode spent in scoring regions. **(B) Four spot attraction assay.** To evaluate nematode behavioural response, nematode attraction to known amounts of indole ascarosides was measured using a 4 spot attraction assay. On a 6 cm

petri dish filled with 6 ml peptone free NGM agar four circular scoring regions of 9 mm diameter were marked in a square of 3 x 3 cm. Next, 2 µl of 1 M sodium azide solution was placed in the centre of all four scoring areas and left to dry for 5 minutes. Next, 1 µl of 10% aqueous methanol (as negative control) or indole ascaroside test solutions (1 nM icas#2, 1 nM (S)-icas#6.2, or a blend of 1 nM icas#2 and 1 nM (S)-icas#6.2) in 10% aqueous methanol were placed in the centre of the two opposing scoring areas onto the agar and left to dry for 5 minutes. Young adult male nematodes of *C. briggsae* strain AF16 from non-starved and non-crowded 6 cm NGM plates seeded with *E. coli* OP50 were transferred to peptone-free NGM agar without any food for ca. 15 min before being used for the assay to minimize the amount of concomitant bacteria. A total number of 50 worms were placed into the centre of the plate between the 4 scoring regions. After 30 minutes immobilized nematodes in the scoring regions were scored and the attraction index was calculated according to: $CI = (n[icas] - n[control]) / (n[icas] + n[control])$. A total number of 4 x 50 worms per condition were analyzed and the experiments were performed in duplicate on two separate days. Student's t test with Welch's correction was performed using the SPSS software to evaluate attraction of nematodes to indole ascarosides in the 4 spot attraction assays.

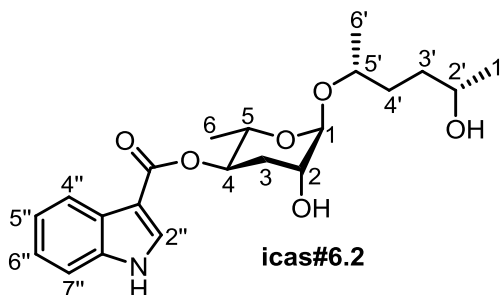
Tables and Figures

Table S1: ^1H and ^{13}C NMR spectroscopic data for icas#2 in CD_3OD . Chemical shifts were referenced to $\delta(\text{CHD}_2\text{OD}) = 3.31$ ppm and $\delta(^{13}\text{CHD}_2\text{OD}) = 49.00$ ppm. ^1H - ^1H coupling constants were determined from proton spectrum or *dqf*-COSY spectrum. Carbon shifts were determined from HSQC spectrum. Coupling multiplicities are annotated as: *s*, singlet; *s.br*, broad singlet; *d*, doublet; *dd*, doublet of doublet; *dq*, doublet of quartet; *ddd*, doublet of doublet of doublet; *m*, multiplet.



Position	δ_{C} (ppm)	δ_{H} (mult., <i>J</i> in Hz, intensity)
1	97.7	4.74 (<i>s</i> , 1H)
2	69.3	3.79 (<i>s.br</i> , 1H)
3ax	33.1	2.01 (<i>ddd</i> , $J_{2,3\text{ax}} = 3.1$, $J_{3\text{ax},3\text{eq}} = 13.8$, 1H)
3eq	33.1	2.21 (<i>ddd</i> , $J_{2,3\text{eq}} = 4.0$, 1H)
4	70.5	5.12 (<i>ddd</i> , $J_{3\text{ax},4} = 10.7$, $J_{3\text{eq},4} = 4.7$, 1H)
5	68.8	4.00 (<i>dq</i> , $J_{4,5} = 9.4$, 1H)
6	17.9	1.24 (<i>d</i> , $J_{5,6} = 6.2$, 3H)
1'	29.6	2.22 (<i>s</i> , 3H)
3'	40.3	2.69 (<i>m</i> , 2H)
4'	31.9	1.83 (<i>m</i> , 2H)
5'	71.9	3.87 (<i>m</i> , 1H)
6'	18.9	1.18 (<i>d</i> , $J_{5',6'} = 6.1$, 3H)
2''	133.1	7.98 (<i>s</i> , 1H)
4''	121.7	8.04 (<i>d</i> , $J_{4'',5''} = 6.9$, 1H)
5''	122.3	7.20 (<i>m</i> , 1H)
6''	123.5	7.23 (<i>m</i> , 1H)
7''	112.7	7.45 (<i>d</i> , $J_{6'',7''} = 7.4$, 1H)

Table S2: ^1H and ^{13}C NMR spectroscopic data for icas#6.2 in CD_3OD . Chemical shifts were referenced to $\delta(\text{CHD}_2\text{OD}) = 3.31$ ppm and $\delta(^{13}\text{CHD}_2\text{OD}) = 49.00$ ppm. ^1H - ^1H coupling constants were determined from proton spectrum or *dqf*-COSY spectrum. Carbon shifts were determined from HSQC spectrum. Coupling multiplicities are annotated as: *s*, singlet; *s.br*, broad singlet; *d*, doublet; *dd*, doublet of doublet; *dq*, doublet of quartet; *ddd*, doublet of doublet of doublet; *m*, multiplet.



Position	δ_{C} (ppm)	δ_{H} (mult., <i>J</i> in Hz, intensity)
1	97.8	4.76 (<i>s</i> , 1H)
2	69.5	3.80 (<i>s.br</i> , 1H)
3ax	33.3	2.02 (<i>ddd</i> , $J_{2,3\text{ax}} = 3.2$, $J_{3\text{ax},3\text{eq}} = 13.2$, 1H)
3eq	33.3	2.22 (<i>ddd</i> , $J_{2,3\text{eq}} = 4.1$, 1H)
4	70.5	5.13 (<i>ddd</i> , $J_{3\text{ax},4} = 10.7$, $J_{3\text{eq},4} = 4.7$, 1H)
5	68.7	4.08 (<i>dq</i> , $J_{4,5} = 9.6$, 1H)
6	18.0	1.24 (<i>d</i> , $J_{5,6} = 6.3$, 3H)
1'	23.3	1.22 (<i>d</i> , $J_{1',2'} = 6.2$, 3H)
2'	68.5	3.78 (<i>m</i> , 1H)
3'a	36.3	1.55 (<i>m</i> , 1H)
3'b	36.4	1.68 (<i>m</i> , 1H)
4'a	34.4	1.62 (<i>m</i> , 1H)
4'b	34.4	1.68 (<i>m</i> , 1H)
5'	73.3	3.85 (<i>m</i> , 1H)
6'	19.1	1.19 (<i>d</i> , $J_{5',6'} = 6.1$, 3H)
2''	133.2	7.96 (<i>s</i> , 1H)
4''	121.7	8.02 (<i>d</i> , $J_{4'',5''} = 6.9$, 1H)
5''	122.4	7.18 (<i>m</i> , 1H)
6''	123.6	7.21 (<i>m</i> , 1H)
7''	112.9	7.45 (<i>d</i> , $J_{6'',7''} = 7.4$, 1H)

Table S3: High resolution masses of fatty acid ascarosides were detected using HR-QTOF-LC-MS in positive ion mode.

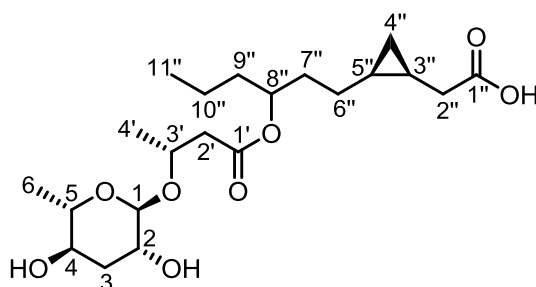
Observed (<i>m/z</i>)	Calculated (<i>m/z</i>)	Error (ppm)	Ion Formula	RT (min)	Name	Type of fatty acid
366.2124	366.2122	-0.4	C ₁₆ H ₃₂ NO ₈ ⁺	15.28	fasc-C ₄ C ₆	Saturated
394.2448	394.2435	-3.2	C ₁₈ H ₃₆ NO ₈ ⁺	18.37	fasc-C ₄ C ₈	
422.2756	422.2748	-1.9	C ₂₀ H ₄₀ NO ₈ ⁺	19.92	fasc-C ₄ C ₁₀	
450.3051	450.3061	2.3	C ₂₂ H ₄₄ NO ₈ ⁺	22.21	fasc-C ₄ C ₁₂	
478.3364	478.3374	2.2	C ₂₃ H ₄₈ NO ₈ ⁺	23.77	fasc-C ₄ C ₁₄	
434.2756	434.2748	-1.8	C ₂₁ H ₄₀ NO ₈ ⁺	19.25	fasc-C ₄ ΔC ₁₁	Cyclopropyl
462.3048	462.3061	2.9	C ₂₃ H ₄₄ NO ₈ ⁺	22.21	fasc-C ₄ ΔC ₁₃	
490.3359	490.3374	3.3	C ₂₅ H ₄₈ NO ₈ ⁺	24.18	fasc-C ₄ ΔC ₁₅	
420.2586	420.2592	1.4	C ₂₀ H ₃₈ NO ₈ ⁺	18.79	fasc-C ₄ ΔC ₁₀	Unsaturated
448.2924	448.2905	-4.2	C ₂₂ H ₄₂ NO ₈ ⁺	21.67	fasc-C ₄ ΔC ₁₂	
476.3323	476.3218	-1.1	C ₂₄ H ₄₆ NO ₈ ⁺	24.16	fasc-C ₄ ΔC ₁₄	
504.3513	504.3531	3.6	C ₂₆ H ₅₀ NO ₈ ⁺	26.85	fasc-C ₄ ΔC ₁₆	

Table S4: High resolution masses of fatty acid ascarosides were detected using HR-QTOF-LC-MS in negative ion mode.

Observed (<i>m/z</i>)	Calculated (<i>m/z</i>)	Error (ppm)	Ion Formula	RT (min)	Name	Type of fatty acid
319.1410 [‡]	319.1398	-3.6	C ₁₄ H ₂₃ O ₈ ⁻	12.50	fasc-C ₄ C ₄	Saturated
347.1719	347.1711	-2.0	C ₁₆ H ₂₇ O ₈ ⁻	15.28	fasc-C ₄ C ₆	
375.2026	375.2024	-0.4	C ₁₈ H ₃₁ O ₈ ⁻	18.38	fasc-C ₄ C ₈	
403.2336	403.2337	-0.4	C ₂₀ H ₃₅ O ₈ ⁻	19.92	fasc-C ₄ C ₁₀	
431.2653	431.2650	-0.5	C ₂₂ H ₃₉ O ₈ ⁻	22.21	fasc-C ₄ C ₁₂	
445.2790 [†]	445.2807	3.8	C ₂₃ H ₄₁ O ₈ ⁻	23.89	fasc-C ₄ C ₁₃	Cyclopropyl
415.2339	415.2337	-0.5	C ₂₁ H ₃₅ O ₈ ⁻	19.25	fasc-C ₄ ΔC ₁₁	
443.2644	443.2650	1.4	C ₂₃ H ₃₉ O ₈ ⁻	22.45	fasc-C ₄ ΔC ₁₃	
471.2957	471.2963	1.3	C ₂₅ H ₄₃ O ₈ ⁻	25.51	fasc-C ₄ ΔC ₁₅	Unsaturated
401.2184	401.2181	-0.7	C ₂₀ H ₃₃ O ₈ ⁻	18.78	fasc-C ₄ ΔC ₁₀	
429.2488	429.2494	1.3	C ₂₂ H ₃₇ O ₈ ⁻	21.74	fasc-C ₄ ΔC ₁₂	
457.2818	457.2807	-2.5	C ₂₄ H ₄₁ O ₈ ⁻	24.23	fasc-C ₄ ΔC ₁₄	
485.3104	485.3120	3.3	C ₂₆ H ₄₅ O ₈ ⁻	26.92	fasc-C ₄ ΔC ₁₆	

[‡] Only detected in PB228 and VX88. [†] Only detected in VX88.

Table S5: ^1H and ^{13}C NMR spectroscopic data for fasc- $\text{C}_4\Delta\text{C}_{11}$ was recorded with 700 MHz NMR in CD_3OD . Chemical shifts were referenced to $\delta(\text{CHD}_2\text{OD}) = 3.31$ ppm and $\delta(^{13}\text{CHD}_2\text{OD}) = 49.00$ ppm. Carbon shifts were determined from HSQC and HMBC spectra. ^1H - ^1H coupling constants were determined from proton spectrum or *dqf*-COSY spectrum. Coupling multiplicities are annotated as: *s*, singlet; *s.br*, broad singlet; *d*, doublet; *dd*, doublet of doublet; *dq*, doublet of quartet; *ddd*, doublet of doublet of doublet; *dddd*, doublet of doublet of doublet of doublet; *m*, multiplet. HMBC correlations are from the indicated proton or protons to relating carbons.



No.	δ_{C} (ppm)	δ_{H} (mult., <i>J</i> in Hz, intensity)	HMBC
1	96.8	4.63 (<i>s</i> , 1H)	2, 3, 5, 3'
2	69.0	3.71 (<i>s.br</i> , $J_{1,2} = 2.5$, 1H)	1, 3, 4
3ax	34.8	1.69 (<i>ddd</i> , $J_{2,3\text{ax}} = 3.3$, $J_{2\text{ax},3\text{eq}} = 12.4$, 1H)	2, 4, 5
3eq	34.8	1.89 (<i>ddd</i> , $J_{2,3\text{eq}} = 2.9$, 1H)	1, 2, 4, 5
4	67.5	3.48 (<i>ddd</i> , $J_{3\text{ax},4} = 11.5$, $J_{3\text{eq},4} = 4.8$, 1H)	2, 3, 5, 6
5	70.4	3.59 (<i>dq</i> , $J_{4,5} = 9.4$, 1H)	1, 3, 4, 6
6	17.2	1.22 (<i>d</i> , $J_{5,6} = 6.2$, 3H)	4, 5
1'	173.0		
2'a	42.6	2.44 (<i>dd</i> , $J_{2'\text{a},2'\text{b}} = 15.2$, 1H)	1', 3', 4'
2'b	42.6	2.54 (<i>dd</i> , $J_{2'\text{a},3'} = 5.7$, $J_{2'\text{b},3'} = 7.2$, 1H)	1', 3', 4'
3'	68.8	4.19 (<i>m</i> , 1H)	1, 1', 2', 4'
4'	18.2	1.21 (<i>d</i> , $J_{3',4'} = 6.3$, 3H)	2', 3'
1''	181.6		
2''a	36.6	2.07 (<i>dd</i> , $J_{2''\text{a},2''\text{b}} = 15.4$, $J_{2''\text{a},3''} = 7.8$, 1H)	1'', 3'', 4'', 5''
2''b	36.6	2.20 (<i>dd</i> , $J_{2''\text{b},3''} = 7.0$, 1H)	1'', 3'', 4'', 5''
3''	12.7	1.07 (<i>m</i> , $J_{3'',4''\text{a}} = 7.4$, $J_{3'',4''\text{b}} = 6.8$, 1H)	1'', 2'', 4'', 5'', 6''
4''a	10.6	-0.20 (<i>dddd</i> , $J_{4''\text{a},4''\text{b}} = 11.9$, 1H)	2'', 3'', 5'', 6''
4''b	10.6	0.63 (<i>dddd</i> , $J_{4''\text{b},5''} = 7.1$, 1H)	2'', 3'', 5'', 6''
5''	15.4	0.72 (<i>m</i> , $J_{4''\text{a},5''} = 6.8$, 1H)	2'', 3'', 4'', 7''
6''a	24.9	1.21 (<i>m</i> , 1H)	3'', 4'', 5'', 7'', 8''
6''b	24.9	1.36 (<i>m</i> , 1H)	3'', 4'', 5'', 7'', 8''
7''	34.6	1.63 (<i>m</i> , $J_{7'',8''} = 6.0$, 2H)	5'', 6'', 8'', 9''
8''	74.9	4.88 (<i>m</i> , $J_{8'',9''} = 7.2$, 1H)	1', 6'', 7'', 9'', 10''
9''	36.4	1.51 (<i>m</i> , 2H)	7'', 8'', 10'', 11''
10''a	18.8	1.28 (<i>m</i> , 1H)	8'', 9'', 11''
10''b	18.8	1.33 (<i>m</i> , 1H)	8'', 9'', 11''
11''	13.4	0.93 (<i>t</i> , $J_{10''\text{a},11''} = 7.3$, $J_{10''\text{b},11''} = 7.3$, 3H)	9'', 10''

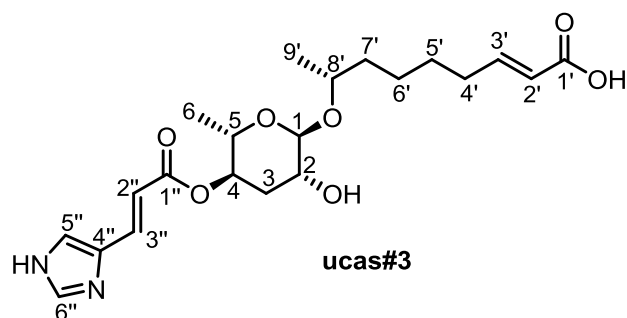
Table S6: High resolution masses of urocanic acid modified ascarosides were detected using (ESI⁻) HR-qTOF-LC/MS.

Observed (<i>m/z</i>)	Calculated (<i>m/z</i>)	Error (ppm)	Ion Formula [M-H] ⁻	RT (min)	Ion assignment
367.1514	367.1511	-0.9	C ₁₇ H ₂₃ N ₂ O ₇ ⁻	11.61	(<i>E</i>)-ucas#9 (C5)
381.1671	381.1667	-0.9	C ₁₈ H ₂₅ N ₂ O ₇ ⁻	12.47	(<i>E</i>)-ucas#12 (C6)
381.1670	381.1667	-0.6	C ₁₈ H ₂₅ N ₂ O ₇ ⁻	12.89	(<i>Z</i>)-ucas#12 (C6)
393.1661	393.1667	1.7	C ₁₉ H ₂₅ N ₂ O ₇ ⁻	13.14	(<i>E</i>)-ucas#7 (ΔC7)
393.1657	393.1667	2.6	C ₁₉ H ₂₅ N ₂ O ₇ ⁻	13.65	(<i>Z</i>)-ucas#7 (ΔC7)
395.1825	395.1824	-0.3	C ₁₉ H ₂₇ N ₂ O ₇ ⁻	13.34	(<i>E</i>)-ucas#1 (C7)
395.1826	395.1824	-0.7	C ₁₉ H ₂₇ N ₂ O ₇ ⁻	13.83	(<i>Z</i>)-ucas#1 (C7)
407.1821	407.1824	0.6	C ₂₀ H ₂₇ N ₂ O ₇ ⁻	14.25	(<i>E</i>)-ucas#13 (ΔC8)
409.1981	409.1980	-0.2	C ₂₀ H ₂₉ N ₂ O ₇ ⁻	14.42	(<i>E</i>)-ucas#14 (C8)
409.1982	409.1980	-0.5	C ₂₀ H ₂₉ N ₂ O ₇ ⁻	14.84	(<i>Z</i>)-ucas#14 (C8)
421.1982	421.1980	-0.5	C ₂₁ H ₂₉ N ₂ O ₇ ⁻	15.28	(<i>E</i>)-ucas#3 (ΔC9)
421.1982	421.1980	-0.5	C ₂₁ H ₂₉ N ₂ O ₇ ⁻	15.55	(<i>Z</i>)-ucas#3 (ΔC9)
423.2138	423.2137	-0.3	C ₂₁ H ₃₁ N ₂ O ₇ ⁻	15.65	(<i>E</i>)-ucas#10 (C9)
423.2137	423.2137	-0.1	C ₂₁ H ₃₁ N ₂ O ₇ ⁻	15.87	(<i>Z</i>)-ucas#10 (C9)
435.2141	435.2137	-1.0	C ₂₂ H ₃₁ N ₂ O ₇ ⁻	16.10	(<i>E</i>)-ucas#15 (ΔC10)
451.2444	451.2450	1.2	C ₂₃ H ₃₅ N ₂ O ₇ ⁻	17.83	(<i>E</i>)-ucas#18 (C11)
365.1720	365.1718	-0.4	C ₁₈ H ₂₅ N ₂ O ₆ ⁻	12.47	(<i>E</i>)-ucas#2 (C6=o)
365.1723	365.1718	-1.5	C ₁₈ H ₂₅ N ₂ O ₇ ⁻	13.18	(<i>Z</i>)-ucas#2 (C6=o)

Table S7: High resolution masses of urocanic acid modified ascarosides were detected using (ESI⁺) HR-qTOF-LC/MS.

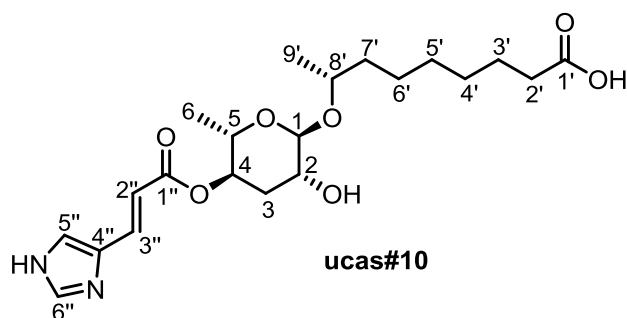
Observed (<i>m/z</i>)	Calculated (<i>m/z</i>)	Error (ppm)	Ion Formula [M+H] ⁺	RT (min)	Ion assignment
369.1650	369.1656	1.8	C ₁₇ H ₂₅ N ₂ O ₇ ⁺	11.71	(<i>E</i>)-ucas#9 (C5)
383.1796	383.1813	1.7	C ₁₈ H ₂₇ N ₂ O ₇ ⁺	12.65	(<i>E</i>)-ucas#12 (C6)
397.1968	397.1969	0.4	C ₁₉ H ₂₉ N ₂ O ₇ ⁺	13.59	(<i>E</i>)-ucas#1 (C7)
397.1955	397.1969	3.5	C ₁₉ H ₂₉ N ₂ O ₇ ⁺	13.84	(<i>Z</i>)-ucas#1 (C7)
409.1958	409.1969	2.7	C ₂₀ H ₂₉ N ₂ O ₇ ⁺	14.50	(<i>E</i>)-ucas#13 (ΔC8)
411.2126	411.2126	0.0	C ₂₀ H ₃₁ N ₂ O ₇ ⁺	14.74	(<i>E</i>)-ucas#14 (C8)
411.2113	411.2126	3.1	C ₂₀ H ₃₁ N ₂ O ₇ ⁺	15.21	(<i>Z</i>)-ucas#14 (C8)
423.2133	423.2126	-1.6	C ₂₁ H ₃₁ N ₂ O ₇ ⁺	15.54	(<i>E</i>)-ucas#3 (ΔC9)
423.2128	423.2126	3.0	C ₂₁ H ₃₁ N ₂ O ₇ ⁺	16.35	(<i>Z</i>)-ucas#3 (ΔC9)
425.2285	425.2282	-0.7	C ₂₁ H ₃₃ N ₂ O ₇ ⁺	15.95	(<i>E</i>)-ucas#10 (C9)
425.2269	425.2282	3.0	C ₂₁ H ₃₃ N ₂ O ₇ ⁺	16.35	(<i>Z</i>)-ucas#10 (C9)
367.1853	367.1864	2.9	C ₁₈ H ₂₇ N ₂ O ₆ ⁺	12.65	(<i>E</i>)-ucas#2 (C6=o)

Table S8: ^1H NMR spectroscopic data for **ucas#3** in CD_3OD . Chemical shifts were referenced to $\delta(\text{CHD}_2\text{OD}) = 3.31$ ppm. ^1H - ^1H coupling constants were determined from proton spectrum or *dqf*-COSY spectrum. Coupling multiplicities are annotated as: *s*, singlet; *s.br*, broad singlet; *d*, doublet; *dd*, doublet of doublet; *dq*, doublet of quartet; *ddd*, doublet of doublet of doublet; *m*, multiplet.



Position	δ_{H} (mult., <i>J</i> in Hz, intensity)
1	4.71 (<i>s</i> , 1H)
2	3.74 (<i>s.br</i> , $J_{1,2} = 2.2$, 1H)
3 _{ax}	1.89 (<i>ddd</i> , $J_{2,3_{ax}} = 6.9$, $J_{3_{ax},3_{eq}} = 12.9$, 1H)
3 _{eq}	2.10 (<i>ddd</i> , $J_{2,3_{eq}} = 6.8$, 1H)
4	4.95 (<i>ddd</i> , $J_{3_{ax},4} = 11.6$, $J_{3_{eq},4} = 4.8$, 1H)
5	3.91 (<i>dq</i> , $J_{4,5} = 9.4$, 1H)
6	1.16 (<i>d</i> , $J_{5,6} = 6.3$, 3H)
2'	5.84 (<i>d</i> , $J_{2',3'} = 15.5$, 1H)
3'	6.82 (<i>ddd</i> , $J_{3',4'a} = 6.8$, $J_{3',4'b} = 7.0$, 1H)
4'a	2.22 (<i>m</i> , $J_{4'a,5'} = 6.9$, 1H)
4'b	2.25 (<i>m</i> , $J_{4'b,5'} = 6.7$, 1H)
5'	1.52 (<i>m</i> , 2H)
6'	1.53 (<i>m</i> , 2H)
7'	1.58 (<i>m</i> , 2H)
8'	3.82 (<i>m</i> , 1H)
9'	1.15 (<i>d</i> , $J_{8',9'} = 6.1$, 3H)
2''	6.43 (<i>d</i> , $J_{2'',3''} = 15.9$, 1H)
3''	7.60 (<i>d</i> , $J_{3'',5''} = 1.6$, 1H)
5''	7.79 (<i>d</i> , $J_{5'',6''} = 1.9$, 1H)
6''	7.44 (<i>s</i> , 1H)

Table S9: ^1H NMR spectroscopic data for ucas#10 in CD_3OD . Chemical shifts were referenced to $\delta(\text{CHD}_2\text{OD}) = 3.31$ ppm. ^1H - ^1H coupling constants were determined from proton spectrum or *dqf*-COSY spectrum. Coupling multiplicities are annotated as: *s*, singlet; *s.br*, broad singlet; *d*, doublet; *dd*, doublet of doublet; *dq*, doublet of quartet; *ddd*, doublet of doublet of doublet; *m*, multiplet.

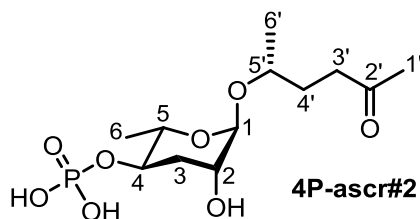


Position	δ_{H} (mult., <i>J</i> in Hz, intensity)
1	4.71 (<i>s</i> , 1H)
2	3.74 (<i>s.br</i> , 1H)
3ax	1.89 (<i>ddd</i> , $J_{2,3\text{ax}} = 3.4$, $J_{3\text{ax},3\text{eq}} = 13.9$, 1H)
3eq	2.10 (<i>ddd</i> , $J_{2,3\text{eq}} = 3.3$, 1H)
4	4.95 (<i>ddd</i> , $J_{3\text{ax},4} = 11.2$, $J_{3\text{eq},4} = 4.8$, 1H)
5	3.91 (<i>dq</i> , $J_{4,5} = 9.6$, 1H)
6	1.16 (<i>d</i> , $J_{5,6} = 6.4$, 3H)
2'a	2.20 (<i>m</i> , 1H)
2'b	2.17 (<i>m</i> , 1H)
3'a	1.63 (<i>m</i> , 1H)
3'b	1.50 (<i>m</i> , 1H)
4'	2.24 (<i>m</i> , 2H)
5'	1.49 (<i>m</i> , 2H)
6'	1.53 (<i>m</i> , 2H)
7'	1.58 (<i>m</i> , 2H)
8'	3.82 (<i>m</i> , 1H)
9'	1.15 (<i>d</i> , $J_{8',9'} = 6.0$, 3H)
2''	6.43 (<i>d</i> , $J_{2'',3''} = 16.0$, 1H)
3''	7.60 (<i>d</i> , 1H)
5''	7.79 (<i>s</i> , 1H)
6''	7.43 (<i>s</i> , 1H)

Table S10: High resolution masses of phosphoryl and glycosylated phosphoryl ascarosides were detected using HR-QTOF-LC-MS/MS with negative ion mode. Prominent phosphoryl ascarosides were determined by co-injecting natural and synthetic standards. Chemical identities of minor components were confirmed by analyzing their MS/MS fragmentation pattern as well as retention time.

Observed (m/z)	Calculated (m/z)	Error (ppm)	Ion Formula	RT (min)	Ion assignment
313.0690	313.0694	1.2	C ₁₀ H ₁₈ O ₉ P ⁻	6.09	4P-C4 (4P-ascr#11)
327.0853	327.0850	-0.8	C ₁₁ H ₂₀ O ₉ P ⁻	8.80	4P-C5 (4P-ascr#9)
341.0995	341.1007	3.6	C ₁₂ H ₂₂ O ₉ P ⁻	9.99	2P-C6 (2P-ascr#12)
341.0991	341.1007	4.7	C ₁₂ H ₂₂ O ₉ P ⁻	10.67	4P-C6 (4P-ascr#12)
355.1160	355.1163	1.0	C ₁₃ H ₂₄ O ₉ P ⁻	11.34	2P-C7 (2P-ascr#1)
355.1161	355.1163	0.7	C ₁₃ H ₂₄ O ₉ P ⁻	11.86	4P-C7 (4P-ascr#1)
369.1313	369.1320	1.9	C ₁₄ H ₂₆ O ₉ P ⁻	12.43	2P-C8 (2P-ascr#14)
369.1313	369.1320	1.9	C ₁₄ H ₂₆ O ₉ P ⁻	13.06	4P-C8 (4P-ascr#14)
381.1327	381.1320	-1.8	C ₁₅ H ₂₆ O ₉ P ⁻	13.28	4P-ΔC9 (4P-ascr#3)
383.1472	383.1476	1.2	C ₁₅ H ₂₈ O ₉ P ⁻	13.75	2P-C9 (2P-ascr#10)
383.1472	383.1476	1.2	C ₁₅ H ₂₈ O ₉ P ⁻	14.39	4P-C9 (4P-ascr#10)
411.1785	411.1789	1.1	C ₁₇ H ₃₂ O ₉ P ⁻	16.12	2P-C11 (2P-ascr#18)
411.1785	411.1789	1.1	C ₁₇ H ₃₂ O ₉ P ⁻	16.79	4P-C11 (4P-ascr#18)
439.2106	439.2102	-0.9	C ₁₉ H ₃₆ O ₉ P ⁻	18.56	2P-C13 (2P-ascr#22)
439.2020	439.2102	-4.1	C ₁₉ H ₃₆ O ₉ P ⁻	18.88	4P-C13 (4P-ascr#22)
451.2100	451.2102	0.5	C ₂₀ H ₃₆ O ₉ P ⁻	19.38	4P-ΔC14 (4P-ascr#23)
467.2438	467.2415	-4.8	C ₂₁ H ₄₀ O ₉ P ⁻	21.47	4P-C15 (4P-ascr#26)
325.1070	325.1058	-3.8	C ₁₂ H ₂₂ O ₈ P ⁻	10.03	4P-ascr#2
327.1204	327.1214	3.0	C ₁₂ H ₂₄ O ₈ P ⁻	9.92	4P-ascr#6.1
503.1541	503.1535	-1.2	C ₁₈ H ₃₂ O ₁₄ P ⁻	10.36	2GlcP-C6 (2GlcP-ascr#12)
517.1704	517.1692	-2.4	C ₁₉ H ₃₄ O ₁₄ P ⁻	10.91	2GlcP-C7 (2GlcP-ascr#1)
517.1678	517.1692	2.6	C ₁₉ H ₃₄ O ₁₄ P ⁻	11.48	4GlcP-C7 (4GlcP-ascr#1)
531.1850	531.1848	-0.4	C ₂₀ H ₃₆ O ₁₄ P ⁻	12.00	2GlcP-C8 (2GlcP-ascr#14)
531.1840	531.1848	1.5	C ₂₀ H ₃₆ O ₁₄ P ⁻	12.53	4GlcP-C8 (4GlcP-ascr#14)
543.1837	543.1848	-0.4	C ₂₁ H ₃₆ O ₁₄ P ⁻	12.27	4GlcP-ΔC9 (4GlcP-ascr#3)
545.1997	545.2005	1.4	C ₂₁ H ₃₈ O ₁₄ P ⁻	13.80	2GlcP-C9 (2GlcP-ascr#10)
545.1994	545.2005	1.9	C ₂₁ H ₃₈ O ₁₄ P ⁻	16.24	4GlcP-C9 (4GlcP-ascr#10)
573.2314	573.2318	0.7	C ₂₃ H ₄₂ O ₁₄ P ⁻	15.97	2GlcP-C11 (2GlcP-ascr#18)
601.2637	601.2631	-1.0	C ₂₅ H ₄₆ O ₁₄ P ⁻	18.15	4GlcP-C13 (4GlcP-ascr#22)
487.1592	487.1586	-1.2	C ₁₈ H ₃₂ O ₁₃ P ⁻	9.78	4GlcP-ascr#2
489.1724	489.1743	3.7	C ₁₈ H ₃₄ O ₁₃ P ⁻	9.74	4GlcP-ascr#6.1

Table S11: ^1H NMR spectroscopic data for 4P-ascr#2 in CD_3OD . Chemical shifts were referenced to $\delta(\text{CHD}_2\text{OD}) = 3.31$ ppm. ^1H - ^1H coupling constants were determined from proton spectrum or *dqf*-COSY spectrum. Coupling constant between H-4 and phosphate group ($^3J_{4,\text{P}} = 8.0$ Hz) was determined from *dqf*-COSY spectrum. Coupling multiplicities are annotated as: *s*, singlet; *s.br*, broad singlet; *d*, doublet; *dd*, doublet of doublet; *dq*, doublet of quartet; *ddd*, doublet of doublet of doublet; *dddd*, doublet of doublet of doublet of doublet; *m*, multiplet.



Position	δ_{H} (mult., J in Hz, intensity)
1	4.63 (<i>s</i> , 1H)
2	3.70 (<i>s.br</i> , $J_{1,2} = 2.8$, 1H)
3ax	1.87 (<i>ddd</i> , $J_{2,3\text{ax}} = 6.1$, $J_{3\text{ax},3\text{eq}} = 13.4$, 1H)
3eq	2.31 (<i>ddd</i> , $J_{2,3\text{eq}} = 6.1$, 1H)
4	4.10 (<i>dddd</i> , $J_{3\text{ax},4} = 12.0$, $J_{3\text{eq},4} = 4.2$, $^3J_{4,\text{P}} = 8.0$, 1H)
5	3.68 (<i>dq</i> , $J_{4,5} = 10.4$, 1H)
6	1.27 (<i>d</i> , $J_{5,6} = 6.6$, 3H)
1'	2.15 (<i>s</i> , 3H)
3'	2.62 (<i>m</i> , 2H)
4'a	1.70 (<i>m</i> , 1H)
4'b	1.77 (<i>m</i> , 1H)
5'	3.79 (<i>m</i> , 1H)
6'	1.13 (<i>d</i> , $J_{5',6'} = 6.0$, 3H)

Table S12: High resolution masses of dimeric ascarosides were detected by using high resolution LC-MS system in negative ion mode.

Observed (<i>m/z</i>)	Calculated (<i>m/z</i>)	Error (ppm)	Ion Formula	RT (min)	Ion assignments
477.2327	477.2341	3.0	C ₂₂ H ₃₇ O ₁₁ ⁻	14.55	§C5-C5
491.2490	491.2498	1.7	C ₂₃ H ₃₉ O ₁₁ ⁻	16.02	§C6-C5
505.2637	505.2654	3.4	C ₂₄ H ₄₁ O ₁₁ ⁻	16.22	§C6-C6
519.2805	519.2811	1.2	C ₂₅ H ₄₃ O ₁₁ ⁻	16.96	§C6-C7
533.2961	533.2967	1.2	C ₂₆ H ₄₅ O ₁₁ ⁻	17.87	§C7-C7
533.2970	533.2967	-0.5	C ₂₆ H ₄₅ O ₁₁ ⁻	18.04	§C5-C9
547.3102	547.3124	4.1	C ₂₇ H ₄₇ O ₁₁ ⁻	18.71	§C7-C8
561.3255	561.3280	4.5	C ₂₈ H ₄₉ O ₁₁ ⁻	20.00	§C7-C9
505.2637	505.2654	3.4	C ₂₄ H ₄₁ O ₁₁ ⁻	16.22	§C7-C5
589.3596	589.3593	-0.4	C ₃₀ H ₅₃ O ₁₁ ⁻	23.83	§C7-C11
449.2026	449.2028	0.4	C ₂₀ H ₃₃ O ₁₁ ⁻	13.30	†C4-C4
463.2178	463.2185	1.5	C ₂₁ H ₃₅ O ₁₁ ⁻	13.83	†C5-C4
463.2176	463.2185	1.8	C ₂₁ H ₃₅ O ₁₁ ⁻	14.13	†C4-C5
477.2339	477.2341	0.4	C ₂₂ H ₃₇ O ₁₁ ⁻	14.86	†C4-C6
491.2501	491.2498	-0.7	C ₂₃ H ₃₉ O ₁₁ ⁻	15.83	†C4-C7
505.2653	505.2654	0.2	C ₂₄ H ₄₁ O ₁₁ ⁻	16.42	‡C5-C7
519.2809	519.2811	0.3	C ₂₅ H ₄₃ O ₁₁ ⁻	16.95	#C7-C6
533.2989	533.2967	-4.0	C ₂₆ H ₄₅ O ₁₁ ⁻	18.09	*C6-C8
561.3277	561.3280	0.7	C ₂₈ H ₄₉ O ₁₁ ⁻	20.48	*C6-C10
575.3459	575.3437	-3.8	C ₂₉ H ₅₁ O ₁₁ ⁻	21.72	*C6-C11
477.2343	477.2341	-0.3	C ₂₂ H ₃₇ O ₁₁ ⁻	14.60	*C6-C5
491.2495	491.2498	0.6	C ₂₃ H ₃₉ O ₁₁ ⁻	15.40	*C6-C6
505.2649	505.2654	1.1	C ₂₄ H ₄₁ O ₁₁ ⁻	16.00	*C6-C7

† Identified in *C. remanei* (PB4641)

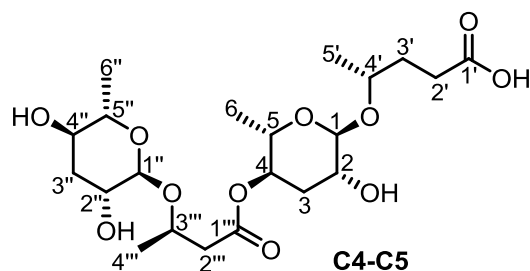
‡ Identified in *C. tropicalis* (sp11)

Identified in *C. sinica* (sp5)

* 2-substituted dimers were identified in *C. nigoni* (sp9)

§ Identified in *C. briggsae* (AF16)

Table S13: NMR spectroscopic data for C4-C5 was recorded with 700 MHz NMR in CD₃OD. Chemical shifts were referenced to $\delta(\text{CHD}_2\text{OD}) = 3.31$ ppm and $\delta(^{13}\text{CCHD}_2\text{OD}) = 49.00$ ppm. Carbon shifts were determined from HSQC and HMBC spectra. Coupling multiplicities are annotated as: *s*, singlet; *s.br*, broad singlet; *d*, doublet; *dd*, doublet of doublet; *dq*, doublet of quartet; *ddd*, doublet of doublet of doublet; *m*, multiplet. HMBC correlations are from the indicated proton or protons to relating carbons.



Position	δ_c (ppm)	δ_H (mult., <i>J</i> in Hz, intensity)	HMBC
1	96.9	4.69 (<i>s</i> , 1H)	2, 3, 5, 4'
2	69.2	3.72 (<i>s.br</i> , $J_{1,2} = 3.5$, 1H)	4
3 _{ax}	32.7	1.90 (<i>ddd</i> , $J_{2,3_{ax}} = 6.8$, $J_{3_{ax},3_{eq}} = 13.6$, 1H)	1, 5
3 _{eq}	32.7	2.08 (<i>ddd</i> , $J_{2,3_{eq}} = 6.8$, 1H)	1, 5
4	71.4	4.87 (<i>ddd</i> , $J_{3_{ax},4} = 10.4$, $J_{3_{eq},4} = 6.5$, 1H)	1''
5	67.9	3.90 (<i>dq</i> , $J_{4,5} = 10.4$, 1H)	3, 4, 6
6	17.9	1.17 (<i>d</i> , $J_{5,6} = 6.9$, 3H)	4, 5
1'	181.0		
2' _a	35.2	2.22 (<i>m</i> , $J_{2'_a,2'_b} = 20.4$, 1H)	1', 3', 4'
2' _b	35.2	2.35 (<i>m</i> , 1H)	1', 3', 4'
3'	35.0	1.82 (<i>m</i> , 2H)	1', 2', 4', 5'
4'	72.2	3.82 (<i>m</i> , 1H)	3', 1
5'	18.7	1.15 (<i>d</i> , $J_{4',5'} = 6.9$, 3H)	3', 4'
1''	97.2	4.67 (<i>s</i> , 1H)	3''', 2'', 3'', 5''
2''	69.5	3.71 (<i>s.br</i> , $J_{1'',2''} = 3.5$, 1H)	4''
3'' _{ax}	35.5	1.73 (<i>ddd</i> , $J_{2'',3''_{ax}} = 6.8$, $J_{3''_{ax},3''_{eq}} = 13.5$, 1H)	2'', 4'', 5''
3'' _{eq}	35.5	1.91 (<i>ddd</i> , $J_{2'',3''_{eq}} = 6.8$, 1H)	2'', 4'', 5''
4''	67.9	3.50 (<i>ddd</i> , $J_{3''_{ax},4''} = 10.2$, $J_{3''_{eq},4''} = 3.4$, 1H)	5''
5''	70.9	3.62 (<i>dq</i> , $J_{4'',5''} = 7.1$, 1H)	4''
6''	17.7	1.22 (<i>d</i> , $J_{5'',6''} = 6.9$, 3H)	4'', 5''
1'''	170.6		
2''' _a	43.0	2.51 (<i>dd</i> , $J_{2'''_a,2'''_b} = 14.5$, $J_{2'''_a,3'''} = 7.9$, 1H)	1''', 3''', 4'''
2''' _b	43.0	2.55 (<i>dd</i> , $J_{2'''_b,3'''} = 5.3$, 1H)	1''', 3''', 4'''
3'''	69.2	4.23 (<i>m</i> , 1H)	2''', 1''', 1''
4'''	18.8	1.21 (<i>d</i> , $J_{3''',4'''} = 6.9$, 3H)	2''', 3'''

Table S14: High resolution masses of (ω)- and (ω -2)-hydroxylated ascarosides were profiled in *C. nigoni* by using high resolution LC-MS/MS in negative ion mode.

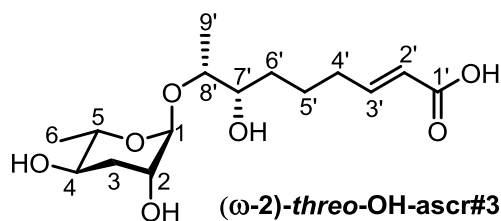
Observed (<i>m/z</i>)	Calculated (<i>m/z</i>)	Error (ppm)	Ion Formula	RT (min)	Ion assignments
317.1596	317.1606	3.2	C ₁₅ H ₂₅ O ₇ ⁻	11.96	(ω -2)- <i>threo</i> -OH-ascr#3
319.1755	319.1762	2.3	C ₁₅ H ₂₇ O ₇ ⁻	12.32	(ω -2)- <i>threo</i> -OH-ascr#10
317.1601	317.1606	1.6	C ₁₅ H ₂₅ O ₇ ⁻	12.42	(ω)-OH-ascr#3

Table S15: High resolution masses of amino benzoic acid modified ascarosides were profiled in *C. nigoni* and *C. tropicalis* by using high resolution LC-MS/MS in negative ion mode.

Observed (<i>m/z</i>)	Calculated (<i>m/z</i>)	Error (ppm)	Ion Formula	RT (min)	Ion assignments
338.1252	338.1245	-1.9	C ₁₆ H ₂₀ NO ₇ ⁻	17.58	[§] abas#5 (C3)
352.1407	352.1402	-1.3	C ₁₇ H ₂₂ NO ₇ ⁻	18.00	abas#11 (C4)
366.1557	366.1558	0.3	C ₁₈ H ₂₄ NO ₇ ⁻	18.73	abas#9 (C5)
380.1708	380.1715	1.9	C ₁₉ H ₂₆ NO ₇ ⁻	19.67	abas#12 (C6)
392.1720	392.1715	-1.3	C ₂₀ H ₂₆ NO ₇ ⁻	20.53	abas#7 (Δ C7)
394.1866	394.1871	1.4	C ₂₀ H ₂₈ NO ₇ ⁻	20.81	abas#1 (C7)
408.2033	408.2028	-1.2	C ₂₁ H ₃₀ NO ₇ ⁻	22.14	abas#14 (C8)
420.2025	420.2028	0.7	C ₂₂ H ₃₀ NO ₇ ⁻	22.90	abas#3 (Δ C9)
422.2180	422.2184	1.1	C ₂₂ H ₃₂ NO ₇ ⁻	23.50	abas#10 (C9)
434.2193	434.2184	-2.0	C ₂₃ H ₃₂ NO ₇ ⁻	24.29	abas#15 (Δ C10)
436.2334	436.2341	1.4	C ₂₃ H ₃₄ NO ₇ ⁻	24.98	abas#16 (C10)
448.2351	448.2341	-2.4	C ₂₄ H ₃₄ NO ₇ ⁻	25.79	abas#17 (Δ C11)
450.2493	450.2497	1.0	C ₂₄ H ₃₆ NO ₇ ⁻	26.53	abas#18 (C11)

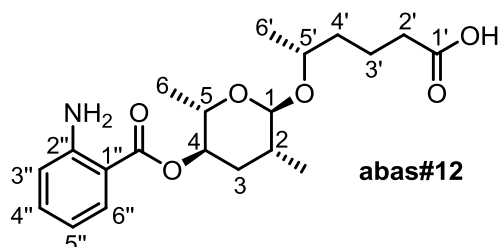
[§] Only detected in *C. tropicalis*.

Table S16: ^1H NMR spectroscopic data for (ω -2)-threo-OH-ascr#3 in CD_3OD . Chemical shifts were referenced to $\delta(\text{CHD}_2\text{OD}) = 3.31$ ppm. ^1H - ^1H coupling constants were determined from proton spectrum or *dqf*-COSY spectrum. Coupling multiplicities are annotated as: *s*, singlet; *s.br*, broad singlet; *d*, doublet; *dd*, doublet of doublet; *dq*, doublet of quartet; *ddd*, doublet of doublet of doublet; *m*, multiplet.



Position	δ_{H} (mult., J in Hz, intensity)
1	4.65 (<i>s</i> , 1H)
2	3.76 (<i>s.br</i> , $J_{1,2} = 2.7$, 1H)
3ax	1.81 (<i>ddd</i> , $J_{2,3\text{ax}} = 3.1$, $J_{3\text{ax},3\text{eq}} = 13.6$, 1H)
3eq	1.95 (<i>ddd</i> , $J_{2,3\text{eq}} = 3.4$, 1H)
4	3.50 (<i>ddd</i> , $J_{3\text{ax},4} = 10.0$, $J_{3\text{eq},4} = 5.5$, 1H)
5	3.64 (<i>dq</i> , $J_{4,5} = 10.4$, 1H)
6	1.22 (<i>d</i> , $J_{5,6} = 6.2$, 3H)
2'	5.83 (<i>d</i> , $J_{2',3'} = 15.7$, 1H)
3'	6.86 (<i>ddd</i> , $J_{3',4'\text{a}} = 7.2$, $J_{3',4'\text{b}} = 7.2$, 1H)
4'a	2.24 (<i>m</i> , 1H)
4'b	2.25 (<i>m</i> , 1H)
5'a	1.53 (<i>m</i> , 1H)
5'b	1.68 (<i>m</i> , 1H)
6'a	1.53 (<i>m</i> , 1H)
6'b	1.61 (<i>m</i> , 1H)
7'	3.53 (<i>m</i> , 2H)
8'	3.74 (<i>m</i> , 1H)
9'	1.14 (<i>d</i> , $J_{8',9'} = 6.4$, 3H)

Table S17: ^1H NMR spectroscopic data for abas#12 in CD_3OD . Chemical shifts were referenced to $\delta(\text{CHD}_2\text{OD}) = 3.31$ ppm. ^1H - ^1H coupling constants were determined from proton spectrum or *dqf*-COSY spectrum. Coupling multiplicities are annotated as: *s*, singlet; *s.br*, broad singlet; *d*, doublet; *t*, triplet; *dd*, doublet of doublet; *dq*, doublet of quartet; *ddd*, doublet of doublet of doublet; *m*, multiplet.



Position	δ_{H} (mult., J in Hz, intensity)
1	4.74 (<i>s</i> , 1H)
2	3.78 (<i>s.br</i> , $J_{1,2} = 2.2$, 1H)
3 _{ax}	1.97 (<i>ddd</i> , $J_{2,3\text{ax}} = 3.0$, $J_{3\text{ax},3\text{eq}} = 13.0$, 1H)
3 _{eq}	2.16 (<i>ddd</i> , $J_{2,3\text{eq}} = 3.3$, 1H)
4	5.06 (<i>ddd</i> , $J_{3\text{ax},4} = 11.1$, $J_{3\text{eq},4} = 5.4$, 1H)
5	4.03 (<i>dq</i> , $J_{4,5} = 9.6$, 1H)
6	1.20 (<i>d</i> , $J_{5,6} = 6.5$, 3H)
2'	2.27 (<i>t</i> , $J_{2',3'} = 6.5$, 2H)
3'	1.80 (<i>m</i> , 2H)
4'a	1.55 (<i>m</i> , 1H)
4'b	1.63 (<i>m</i> , 1H)
5'	3.86 (<i>m</i> , 1H)
6'	1.17 (<i>d</i> , $J_{5',6'} = 6.5$, 1H)
3''	7.76 (<i>dd</i> , $J_{3'',4''} = 8.1$, $J_{3'',5''} = 1.5$, 1H)
4''	6.58 (<i>ddd</i> , $J_{4'',5''} = 7.1$, $J_{4'',6''} = 1.0$, 1H)
5''	7.23 (<i>ddd</i> , $J_{5'',6''} = 8.4$, 1H)
6''	6.73 (<i>dd</i> , 1H)

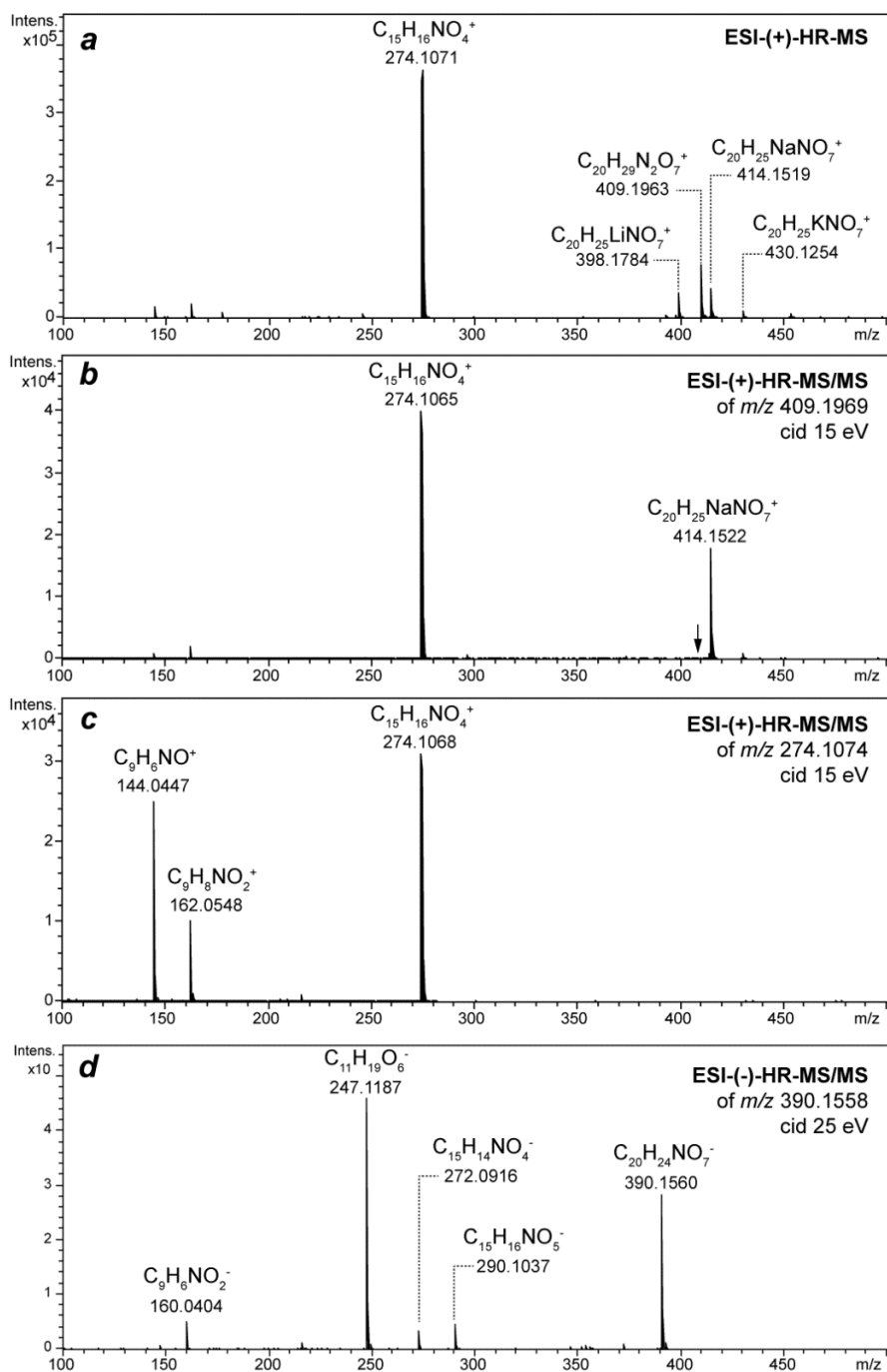


Figure S1: ESI-HR-MS/MS analysis of synthetic icas#9. a) ESI-(+)-HR-MS fragmentation of icas#9 in source collision induced dissociation (ISCID) shows a cluster of quasi molecular ion adducts; b) intensive $C_{15}H_{16}NO_4$ fragment originates from icas#9 via ESI-(+)-HR-MS/MS fragmentation of $[M+NH_4]^+$ adduct in collision induced fragmentation (CID); c) icas-specific $C_{15}H_{16}NO_4$ ion was further fragmented to afford indole-3-carboxylic acid dependent $[C_9H_8NO_2]^+$ and $[C_9H_6NO]^+$; d) ESI-(-)-HR-MS/MS fragmentation shows loss of the indole carbonyl moiety to afford the ascr#9 ion $C_{11}H_{19}O_6$ as previously reported.

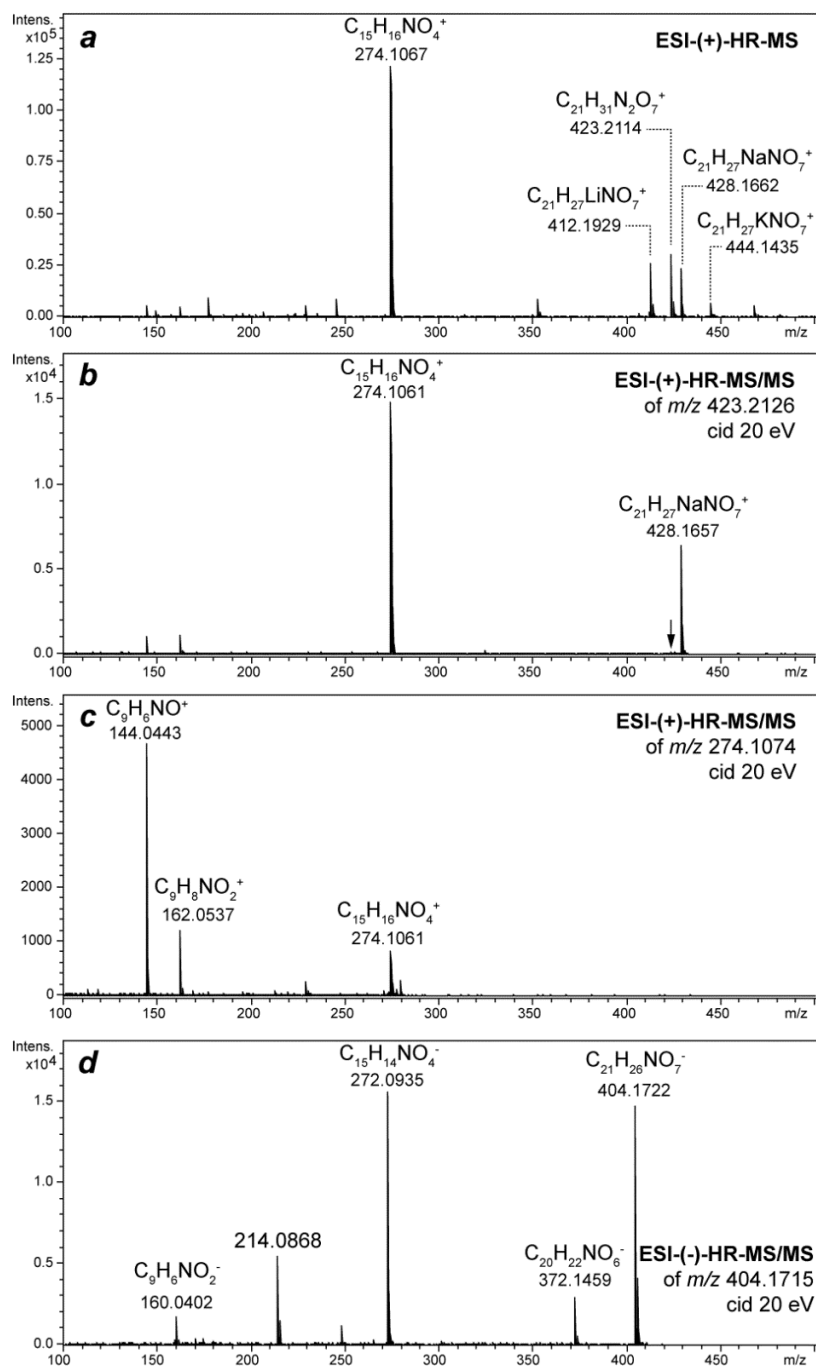


Figure S2: ESI-HR-MS/MS analysis of synthetic icas#9 methyl ester. a) ESI-(+)-HR-MS fragmentation of icas#9Me in source collision induced dissociation (ISCID) shows a cluster of quasi molecular ion adducts; b) intensive $C_{15}H_{16}NO_4$ fragment originates from icas#9Me via ESI-(+)-HR-MS/MS fragmentation of $[M+NH_4]^+$ adduct in collision induced fragmentation (CID); c) icas-specific $C_{15}H_{16}NO_4$ ion was further fragmented to afford indole-3-carboxylic acid dependent $[C_9H_8NO_2]^+$ and $[C_9H_6NO]^+$; d) ESI-(-)-HR-MS/MS fragmentation of $[M-H]^-$ ion affords a fragment ion for $C_{15}H_{14}NO_4$.

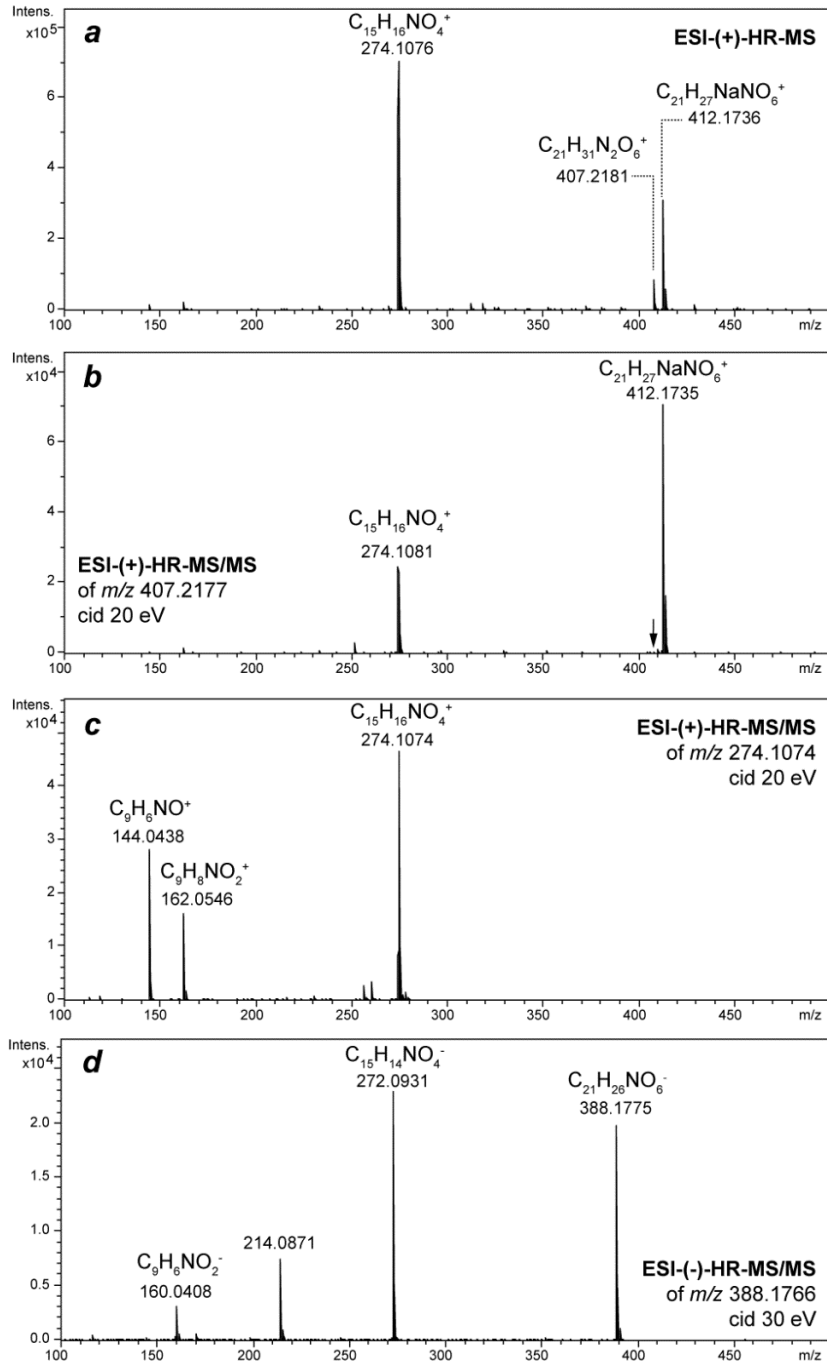


Figure S3: ESI-HR-MS/MS analysis of icas#2 from *C. briggsae*. a) ESI(+)-HR-MS fragmentation of icas#2 in source collision induced dissociation (ISCID) shows a cluster of quasi molecular ion adducts; b) intensive $C_{15}H_{16}NO_4$ fragment originates from icas#2 via ESI(+)-HR-MS/MS fragmentation of $[M+NH_4]^+$ adduct in collision induced fragmentation (CID); c) icas-specific $C_{15}H_{16}NO_4$ ion was further fragmented to afford indole-3-carboxylic acid dependent $[C_9H_8NO_2]^+$ and $[C_9H_6NO]^+$; d) ESI(-)-HR-MS/MS fragmentation of $[M-H]^-$ ion affords a fragment ion for $C_{15}H_{14}NO_4$.

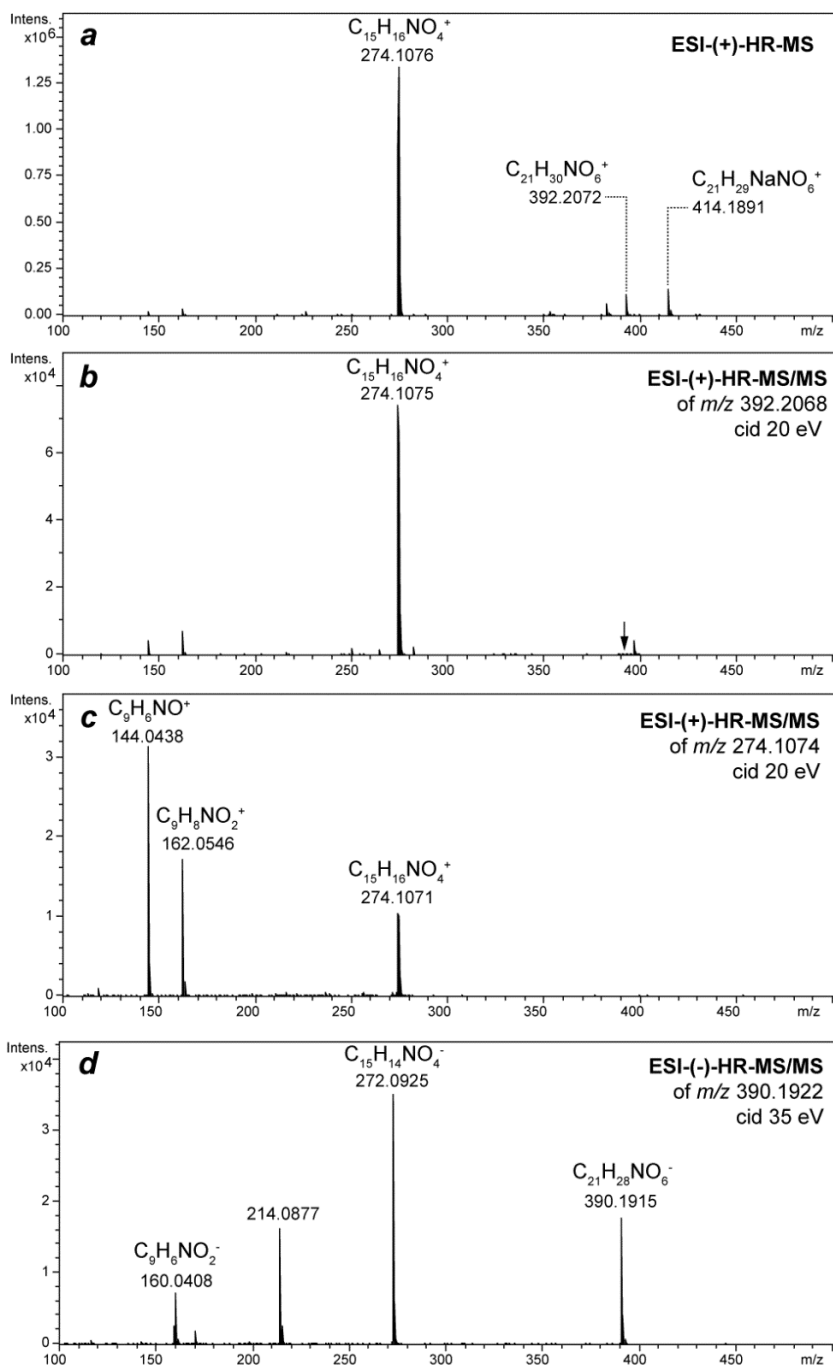


Figure S4: ESI-HR-MS/MS analysis of icas#6.2 from *C. briggsae*. a) ESI(+)-HR-MS fragmentation of icas#6.2 in source collision induced dissociation (ISCID) shows a cluster of quasi molecular ion adducts; b) intensive $C_{15}H_{16}NO_4$ fragment originates from icas#6.2 via ESI(+)-HR-MS/MS fragmentation of $[M+NH_4]^+$ adduct in collision induced fragmentation (CID); c) icas-specific $C_{15}H_{16}NO_4$ ion was further fragmented to afford indole-3-carboxylic acid dependent $[C_9H_8NO_2]^+$ and $[C_9H_6NO]^+$; d) ESI(-)-HR-MS/MS fragmentation of $[M-H]^-$ ion affords a fragment ion for $C_{15}H_{14}NO_4$.

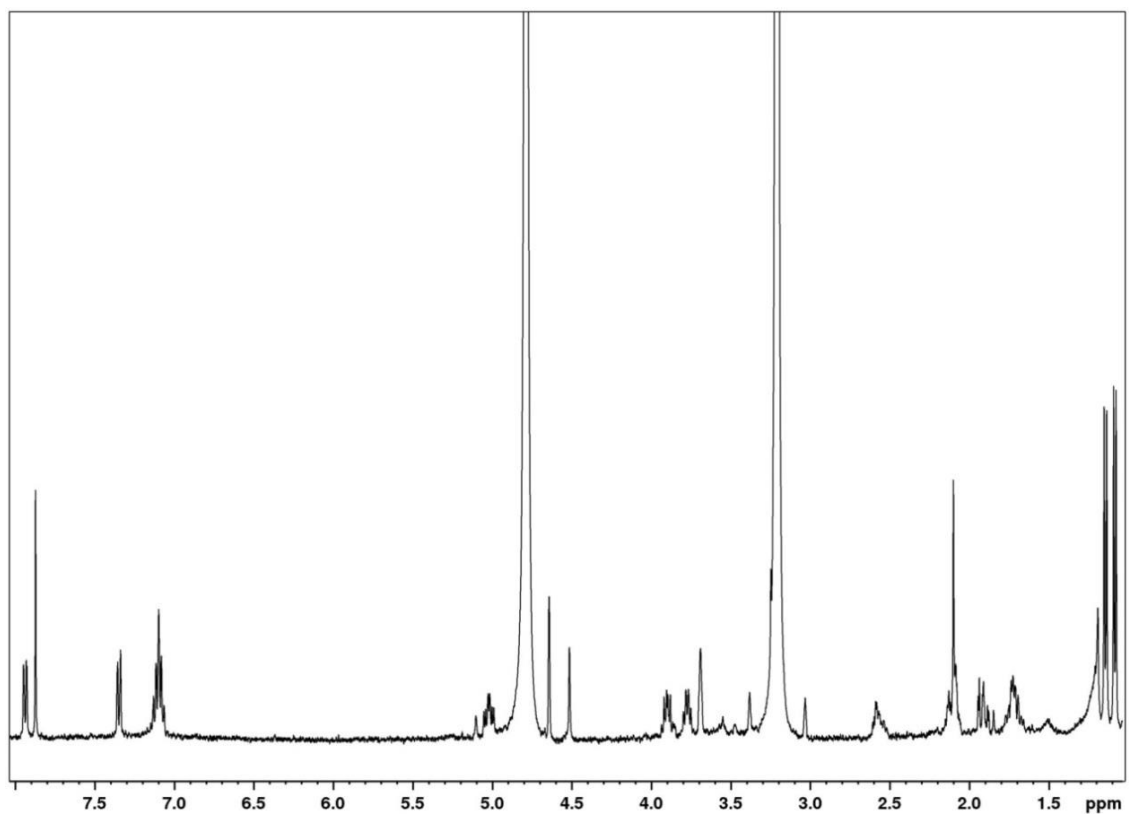


Figure S5: ^1H NMR spectrum of isolated icas#2.

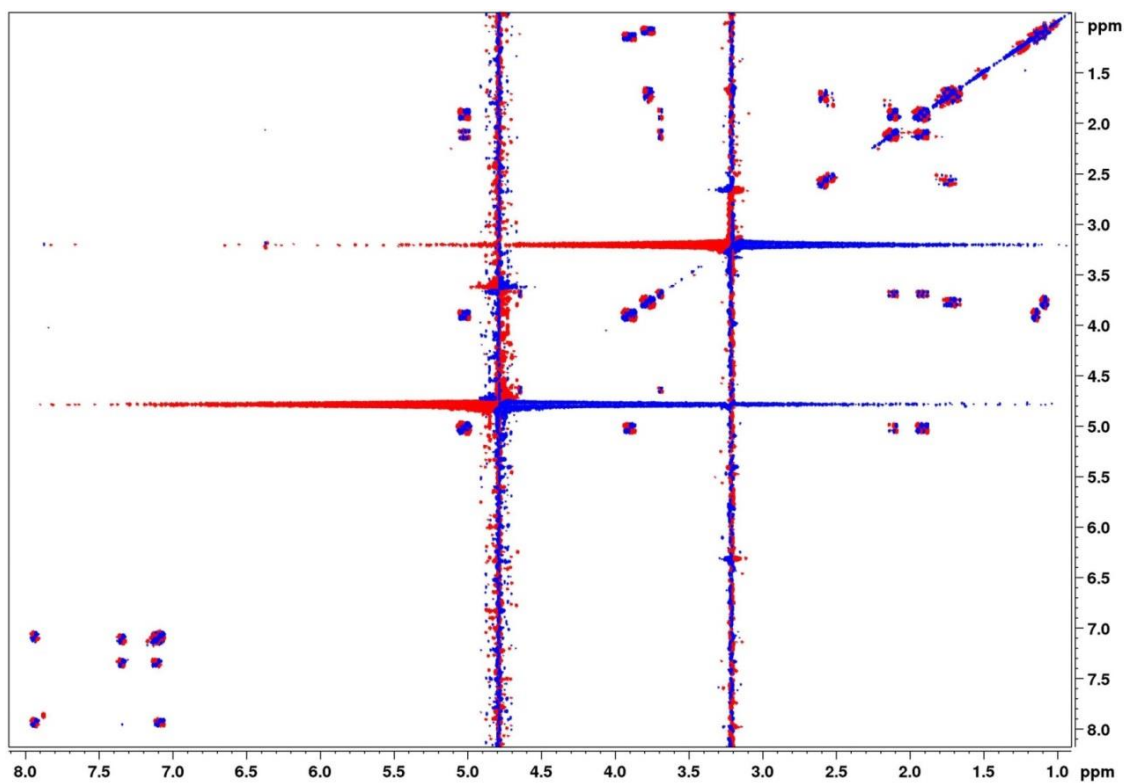


Figure S6: *dqf*-COSY spectrum of isolated icas#2.

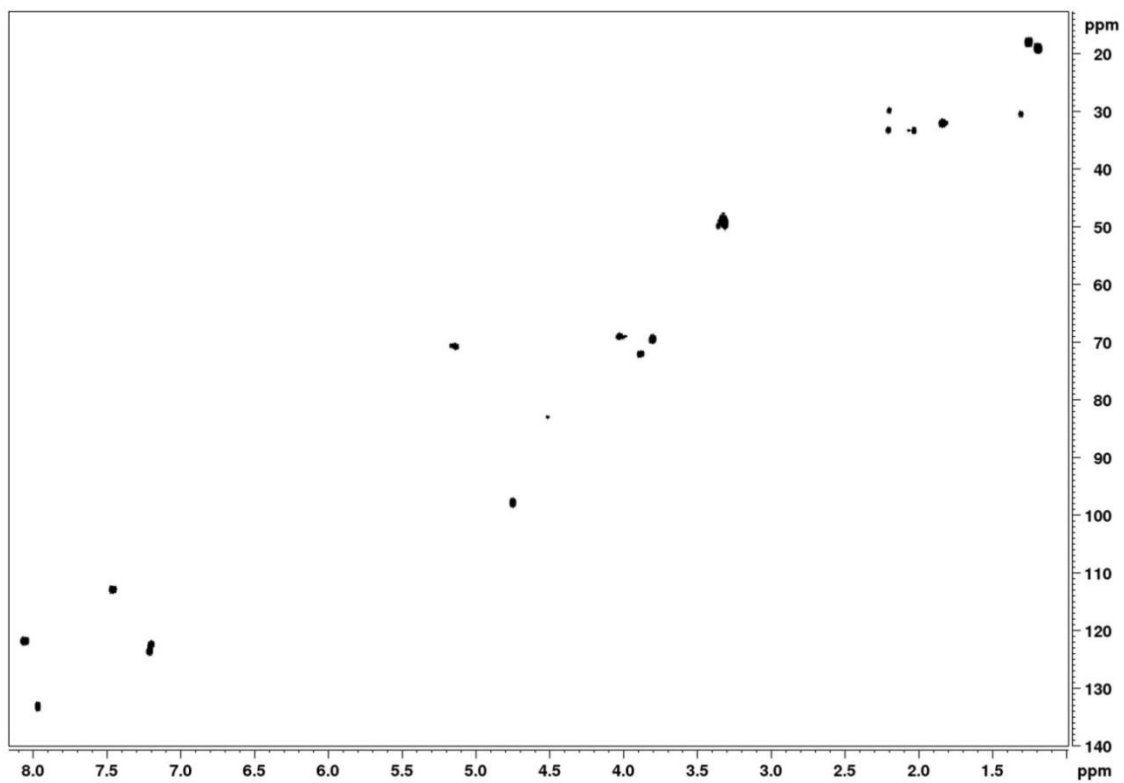


Figure S7: HSQC spectrum of isolated icas#2.

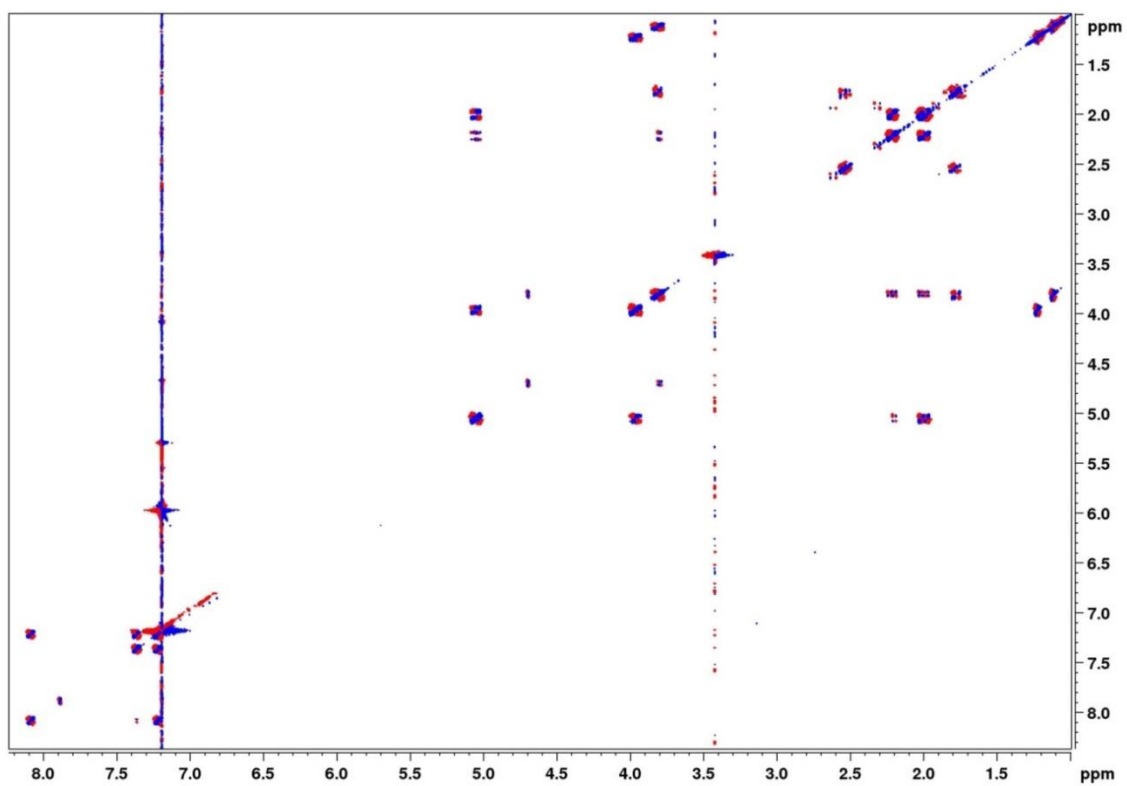


Figure S8: *dqf*-COSY spectrum of isolated icas#2

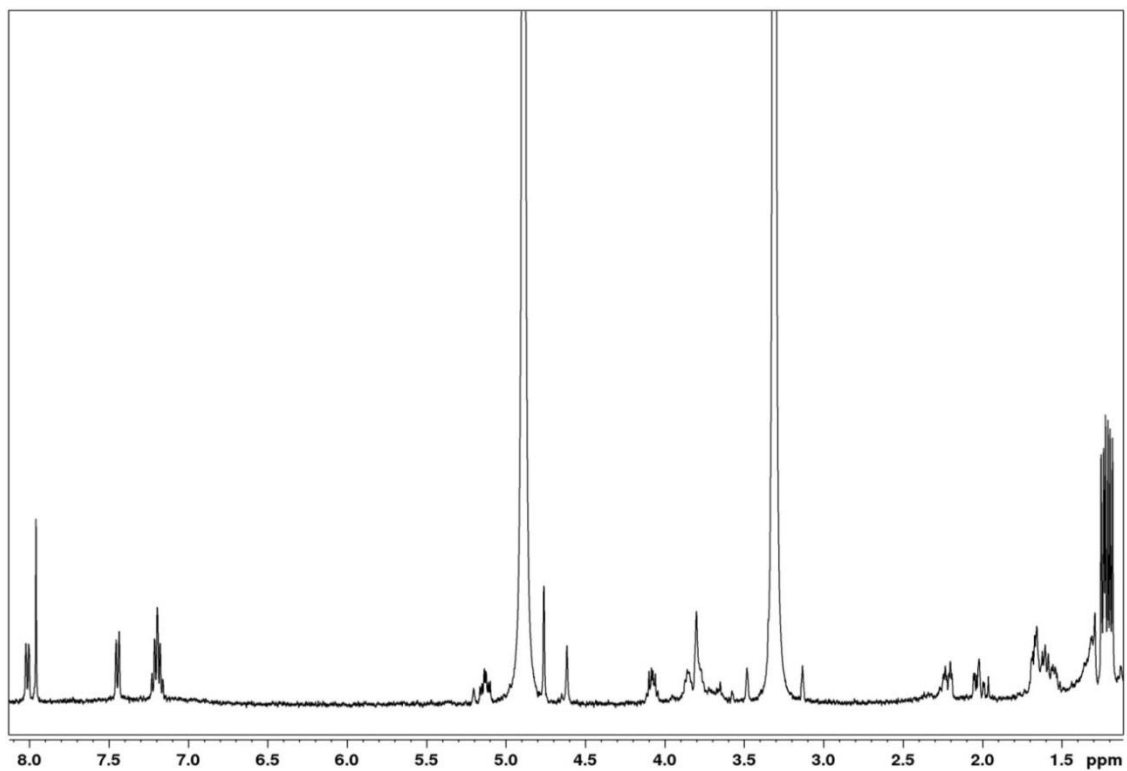


Figure S9: ^1H NMR spectrum of isolated (S)-icas#6.2.

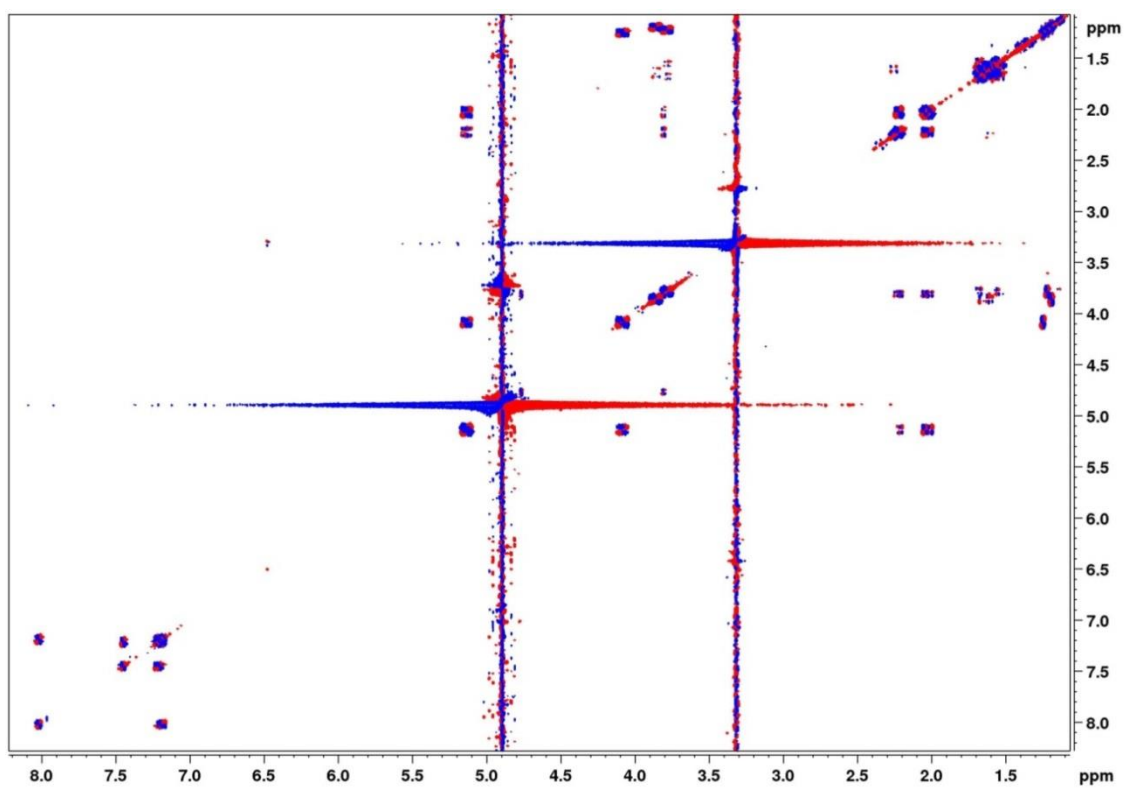


Figure S10: *dqf*-COSY spectrum of isolated (S)-icas#6.2.

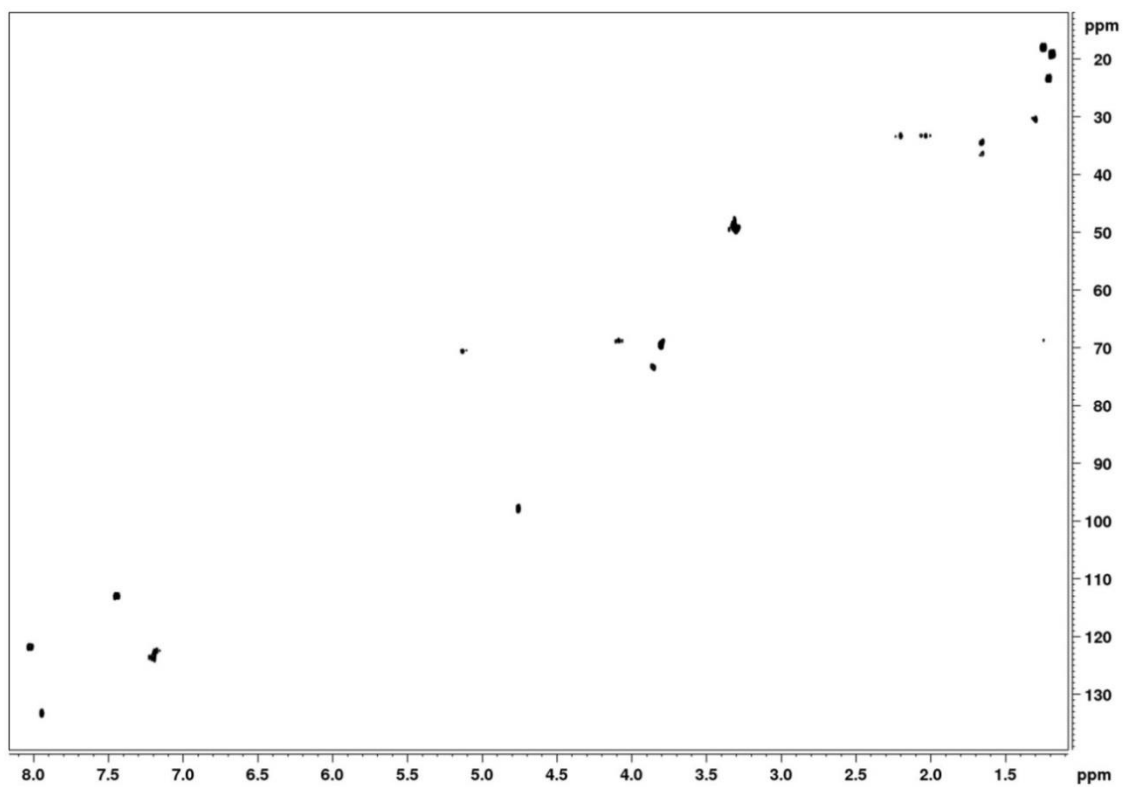


Figure S11: HSQC spectrum of isolated (S)-icas#6.2.

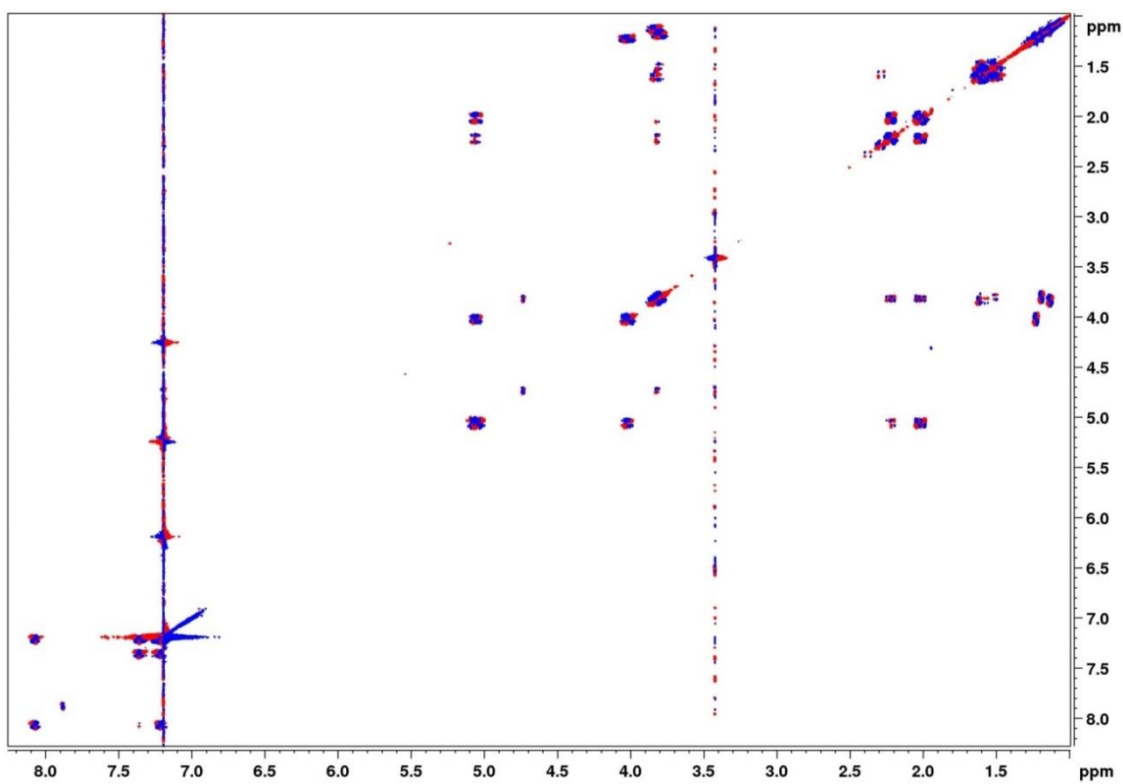


Figure S12: dqf-COSY spectrum of isolated (S)-icas#6.2.

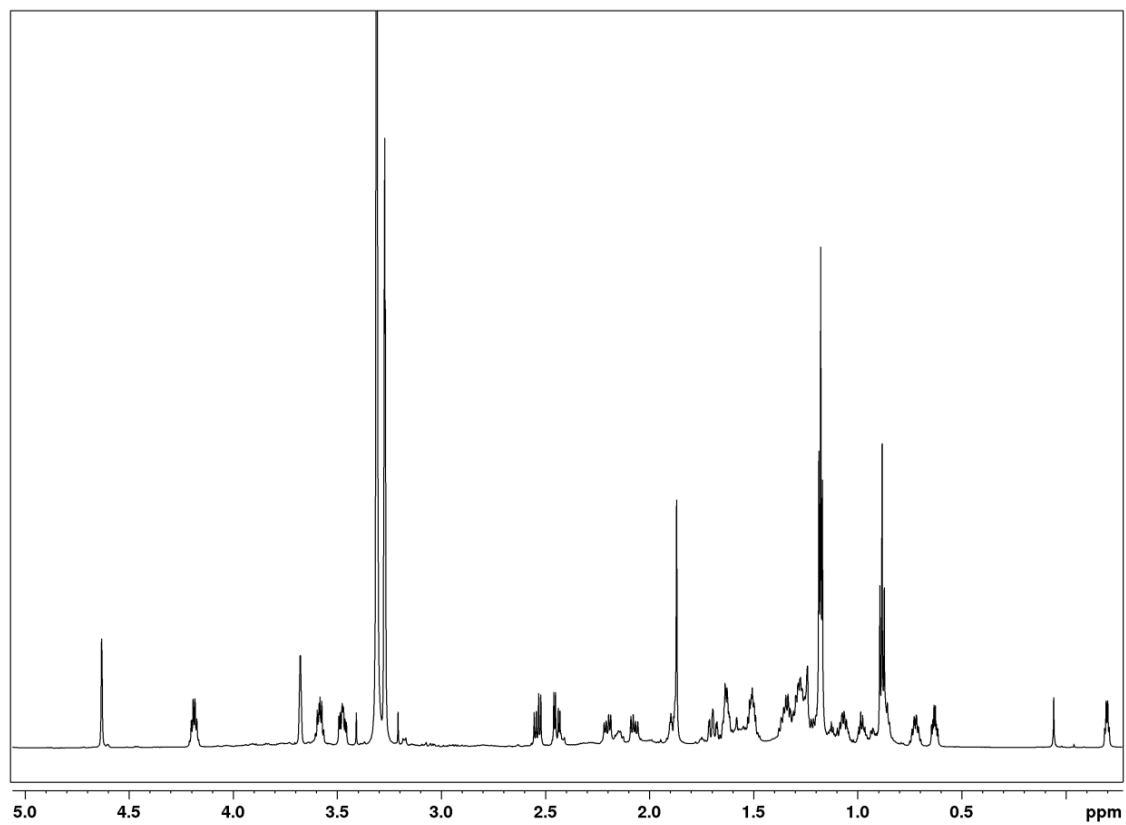


Figure S13: ¹H NMR spectrum of isolated fasc-C₄ΔC₁₁.

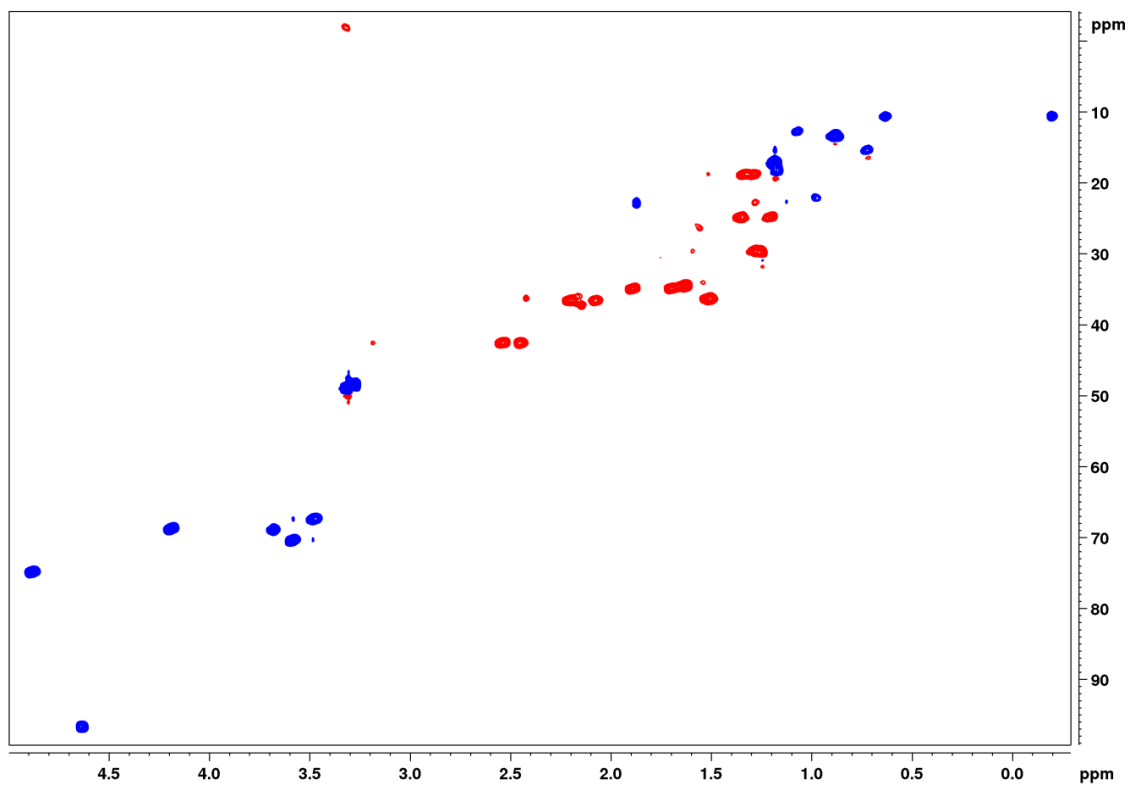


Figure S14: HSQC spectrum of isolated fasc-C₄ΔC₁₁.

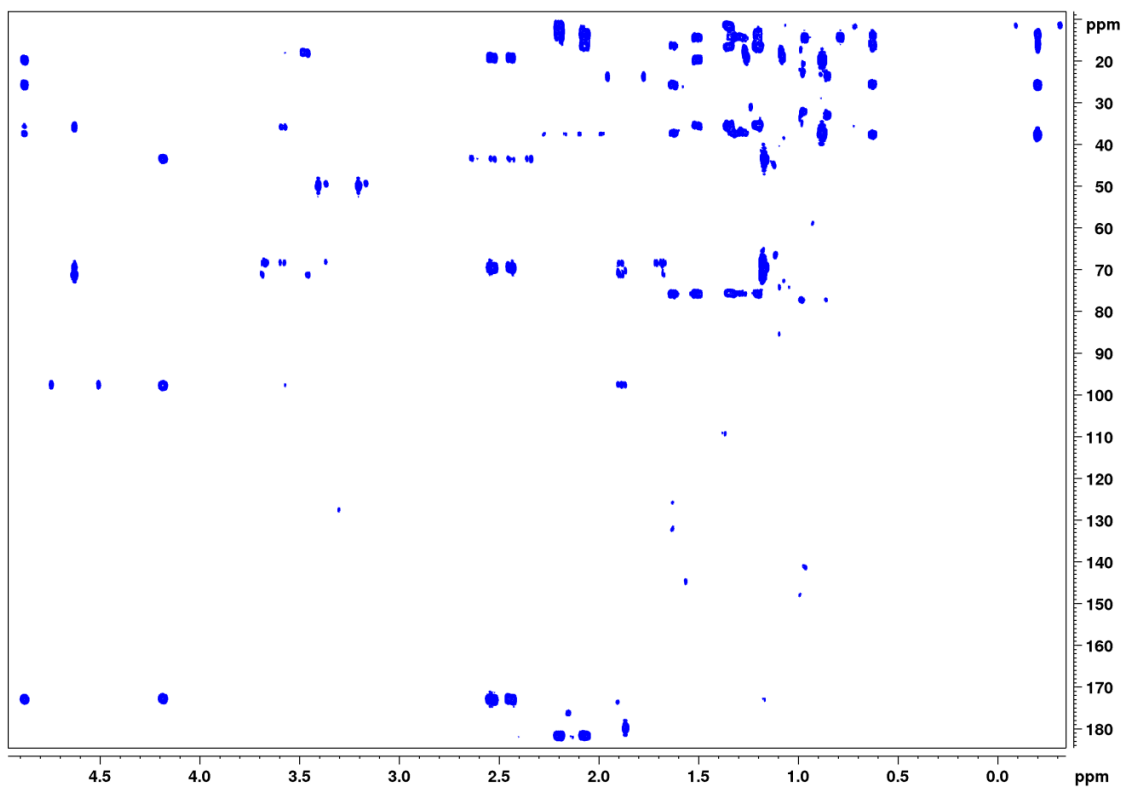


Figure S15: HMBC spectrum of isolated fasc-C₄ΔC₁₁.

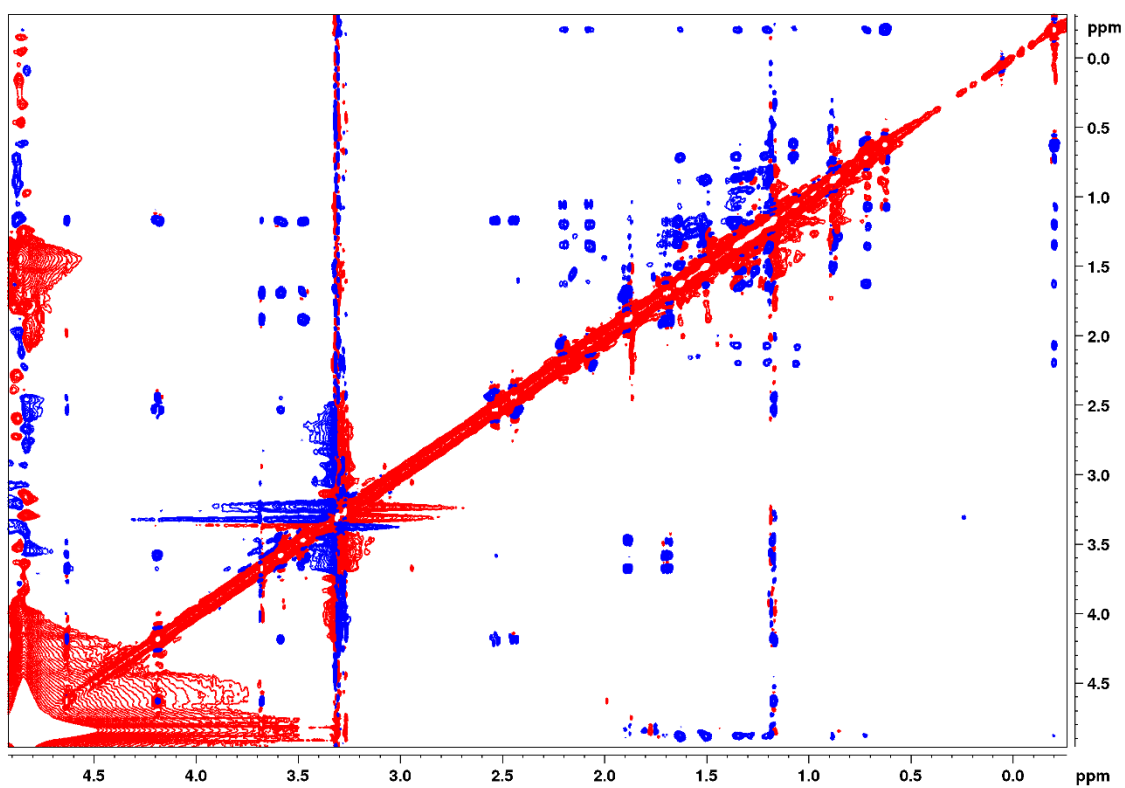


Figure S16: NOESY spectrum of isolated fasc-C₄ΔC₁₁.

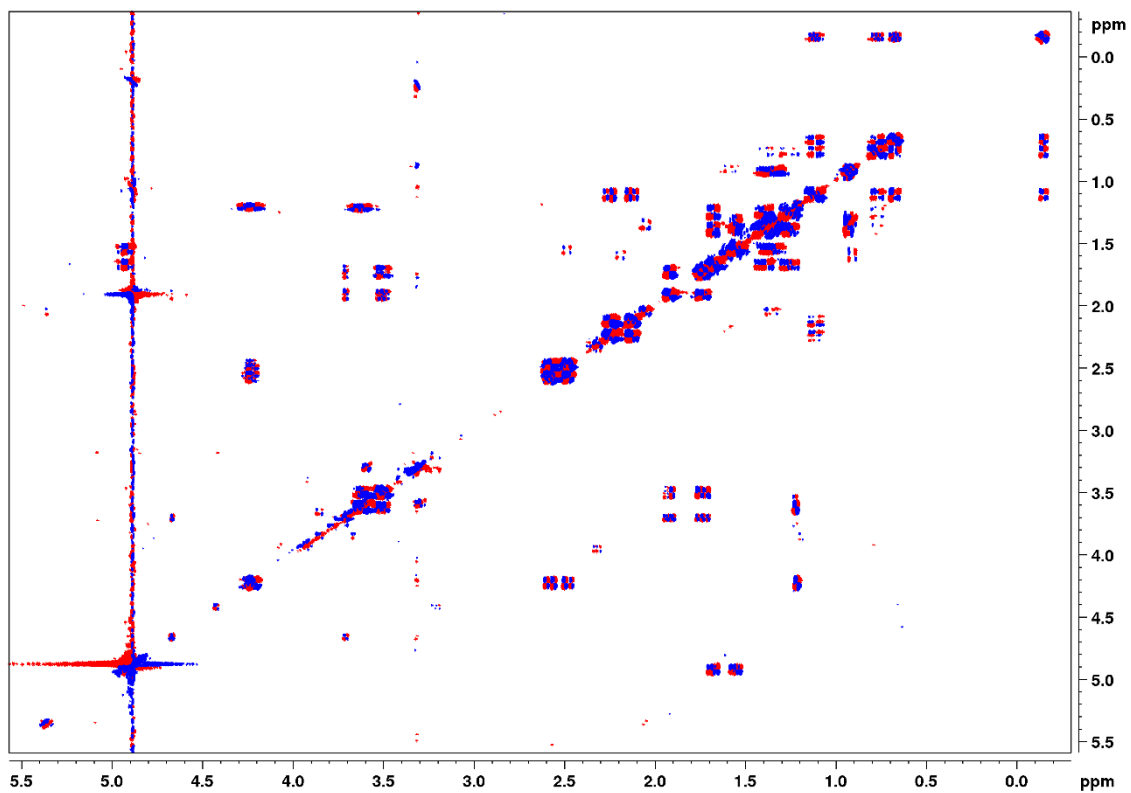


Figure S17: *dqf*-COSY spectrum of isolated fasc-C₄ΔC₁₁.

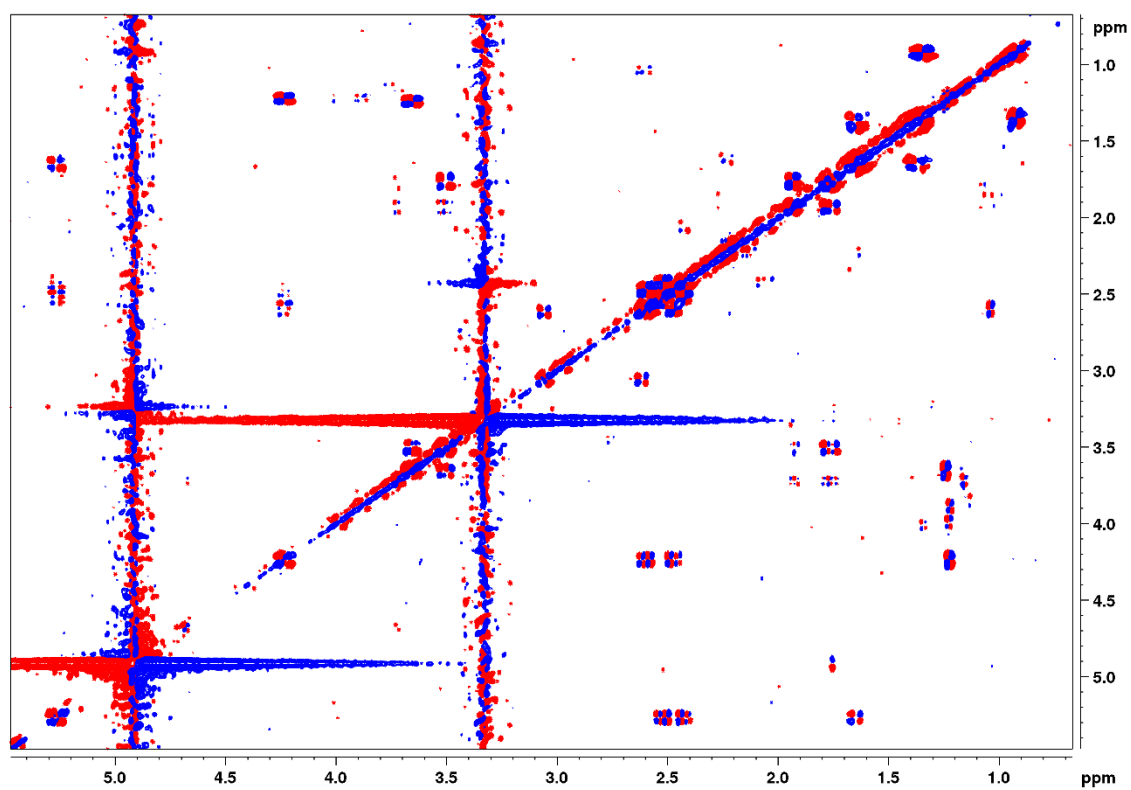


Figure S18: *dqf*-COSY spectrum of isolated fasc-C₄C₈.

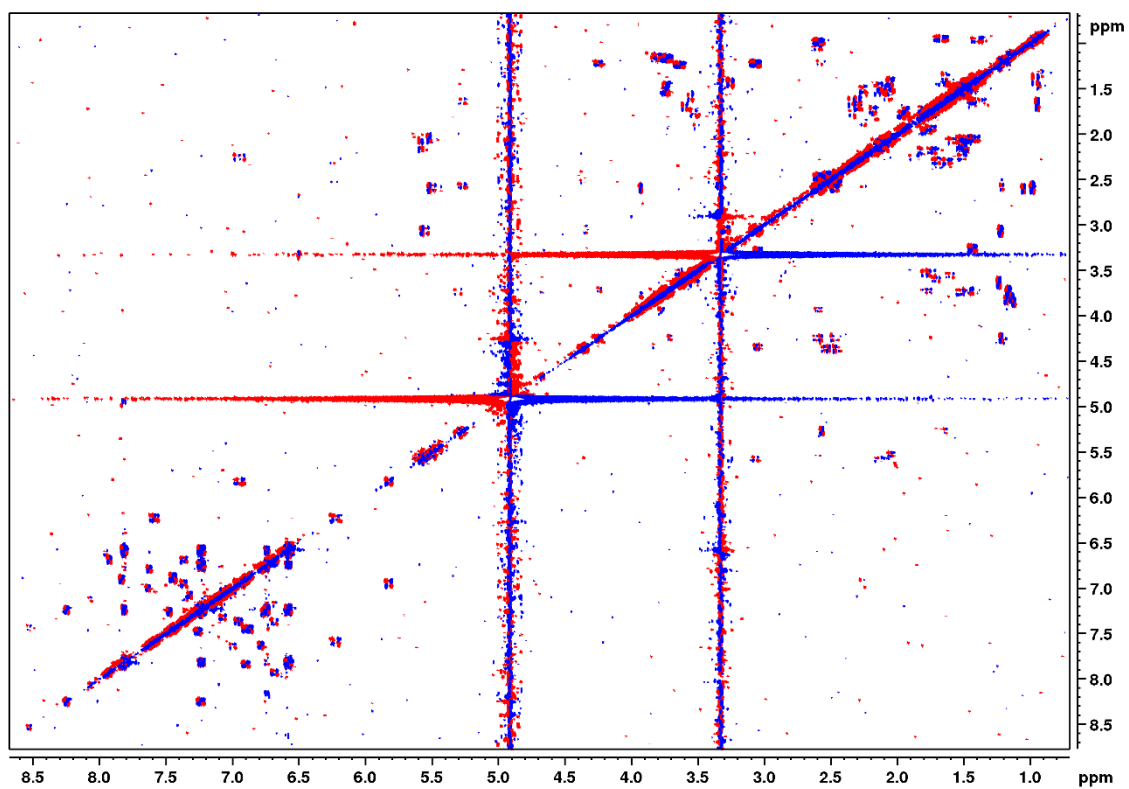


Figure S19: *dqf*-COSY spectrum of isolated *fasc*-C₄C₆.

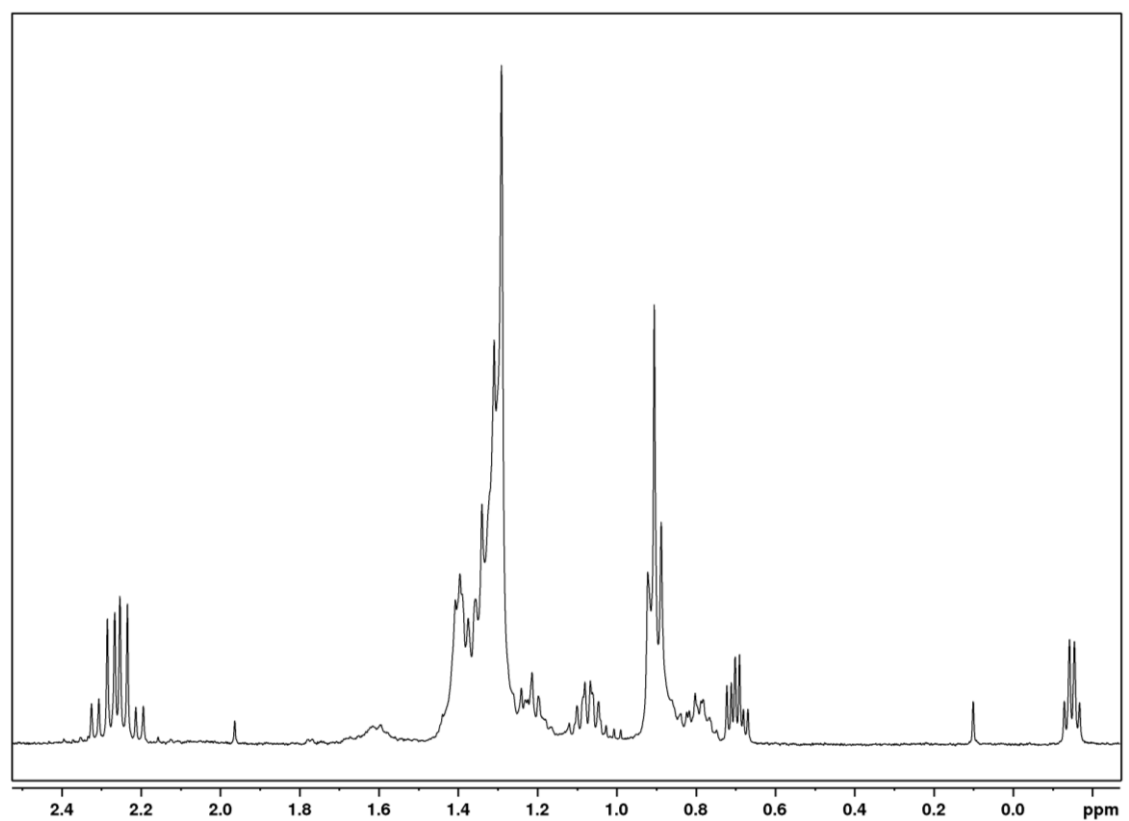


Figure S20: ¹H NMR spectrum of isolated *cis*-cascarillic acid.

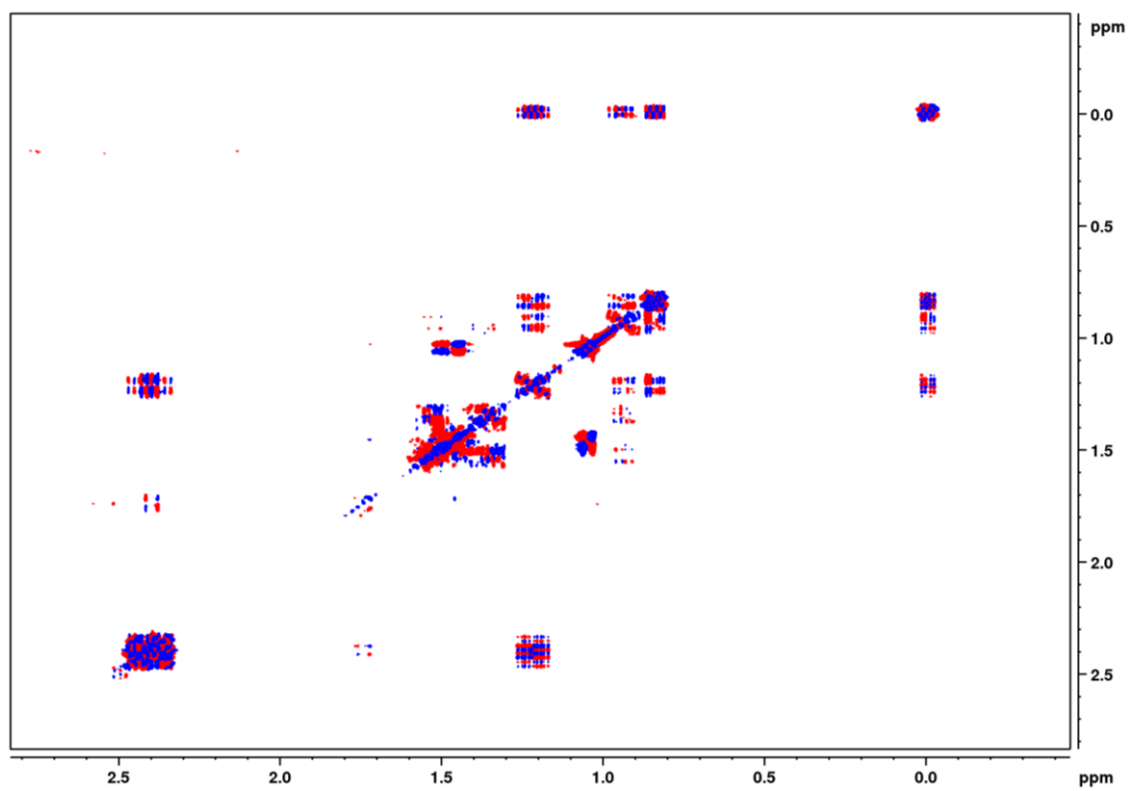


Figure S21: *dqf*-COSY spectrum of isolated *cis*-cascarillic acid.

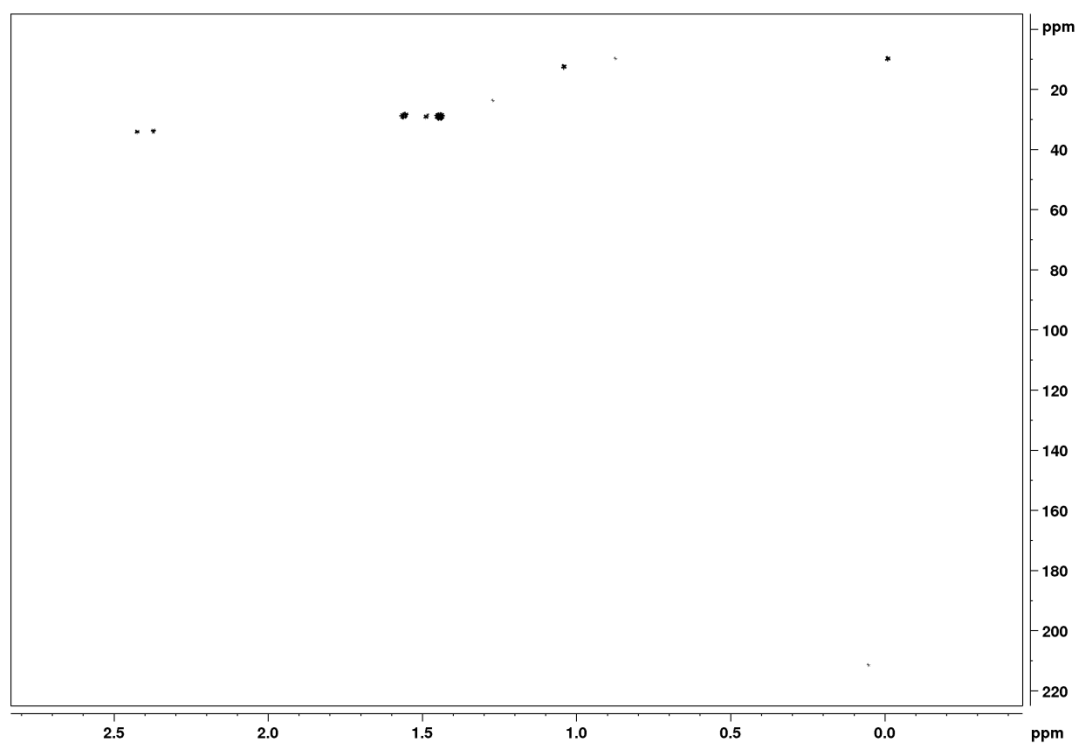


Figure S22: HSQC spectrum of isolated *cis*-cascarillic acid.

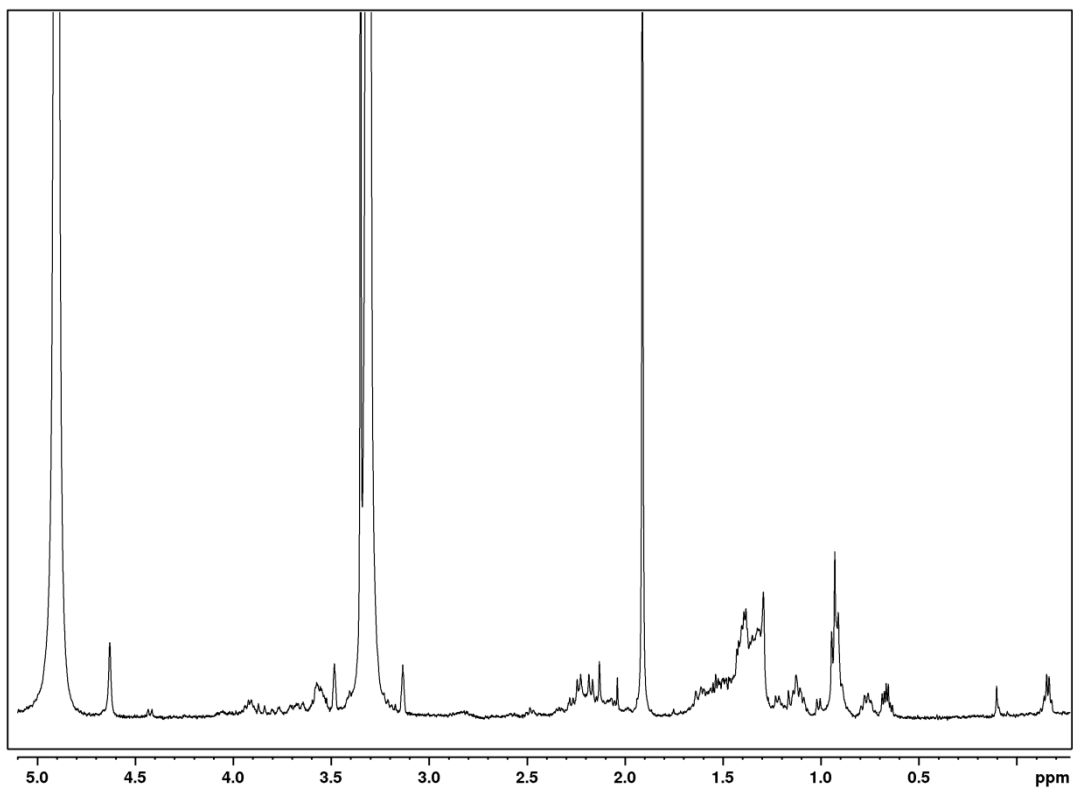


Figure S23: ^1H NMR spectrum of isolated 8-hydroxy-*cis*-cascarillic acid.

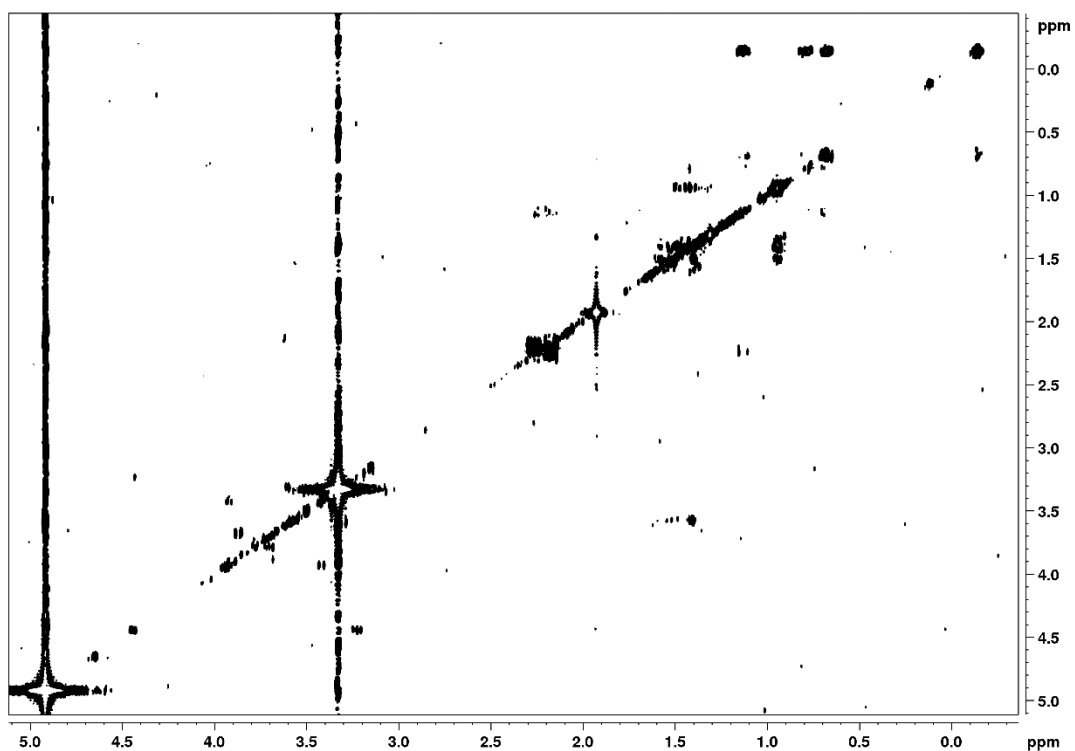


Figure S24: COSY spectrum of isolated 8-hydroxy-*cis*-cascarillic acid.

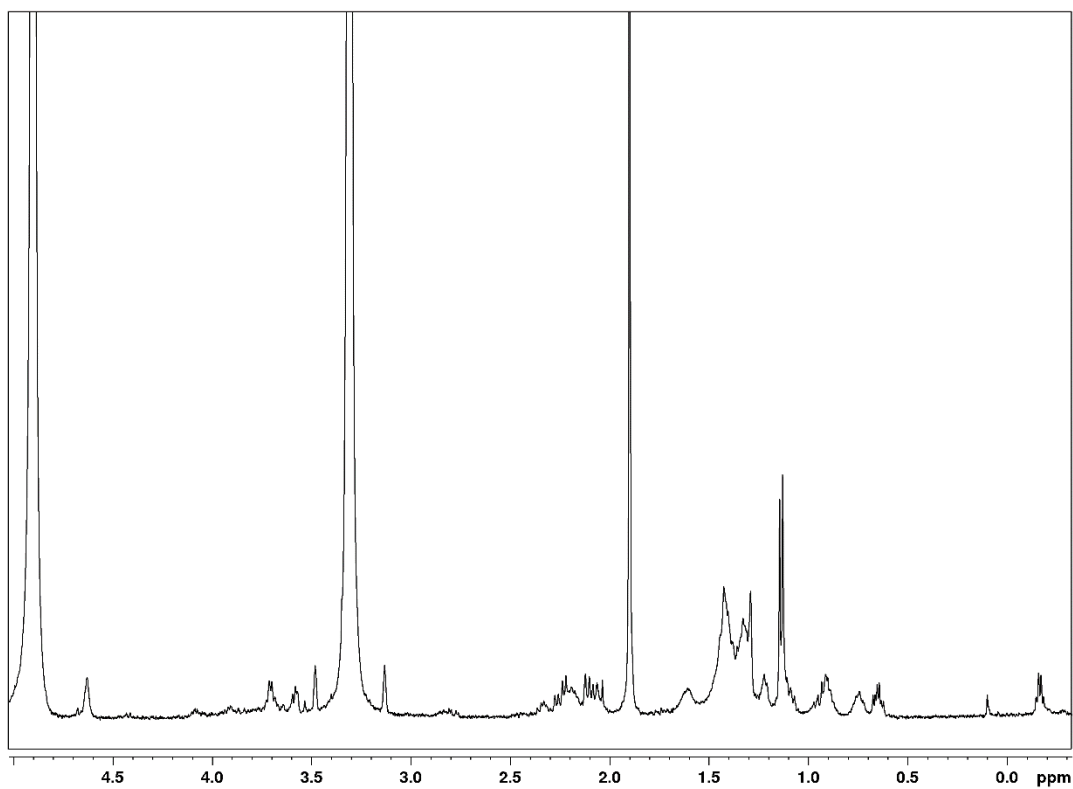


Figure S25: ^1H NMR spectrum of isolated 10-hydroxy-*cis*-cascarillic acid.

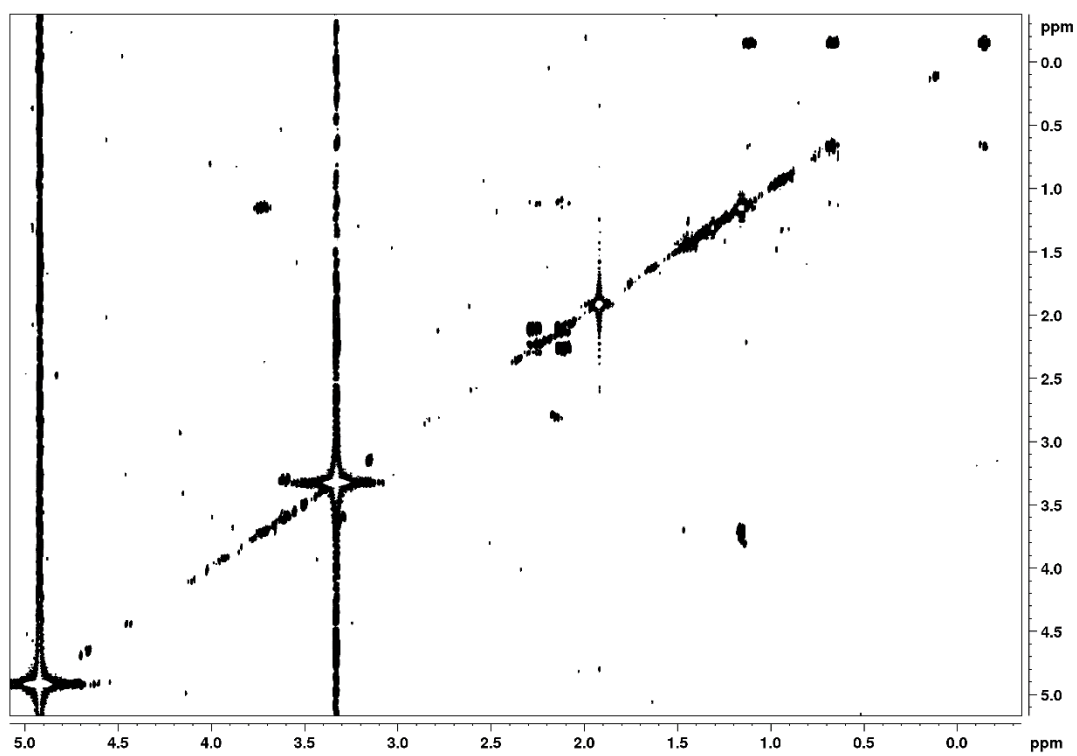


Figure S26: ^1H , ^1H -COSY spectrum of isolated 10-hydroxy-*cis*-cascarillic acid.

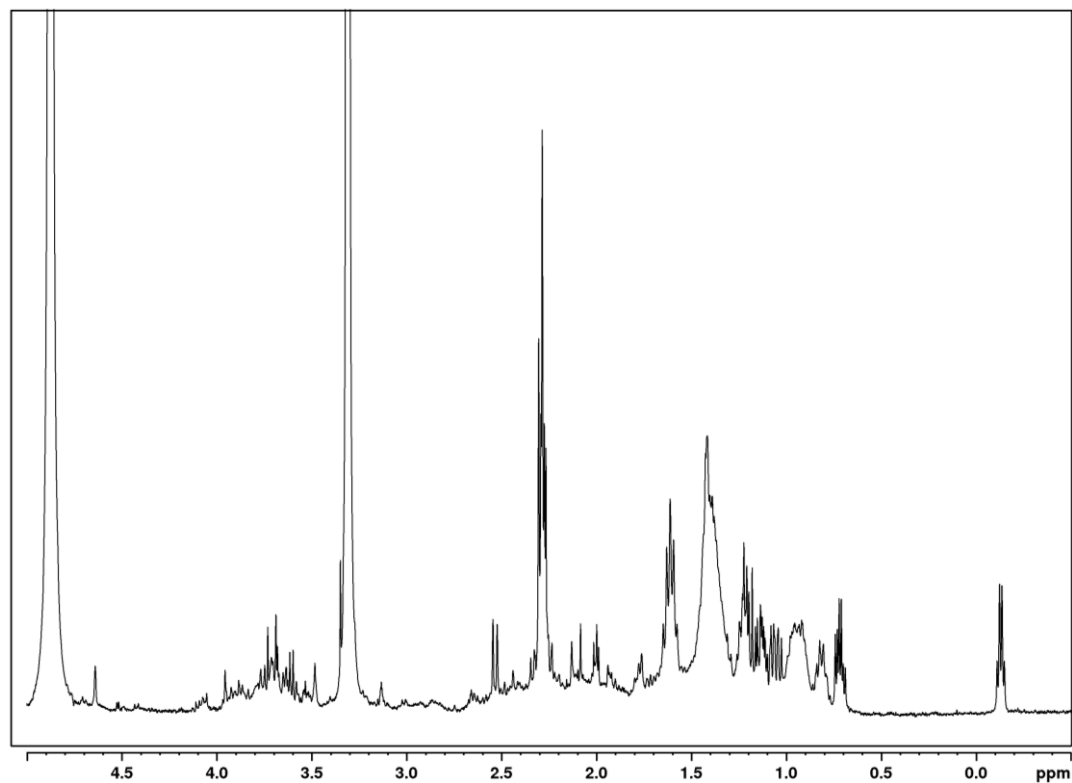


Figure S27: ^1H NMR spectrum of isolated 11-carboxy-*cis*-cascarillic acid.

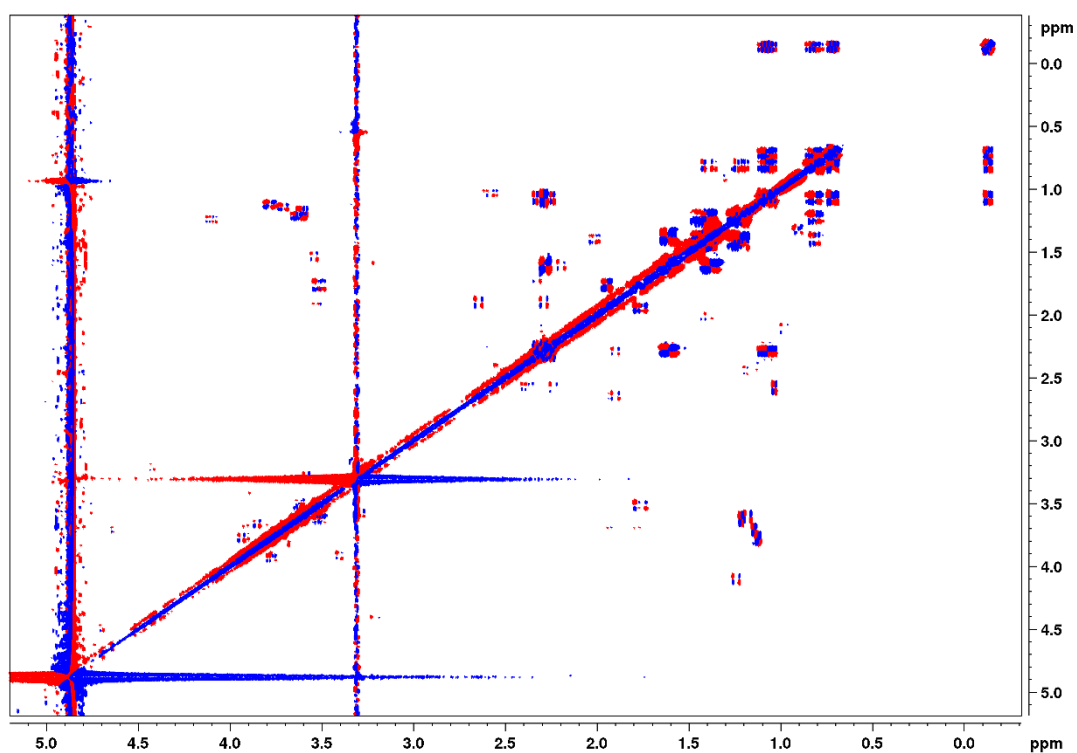


Figure S28: *dqf*-COSY spectrum of isolated 11-carboxy-*cis*-cascarillic acid.

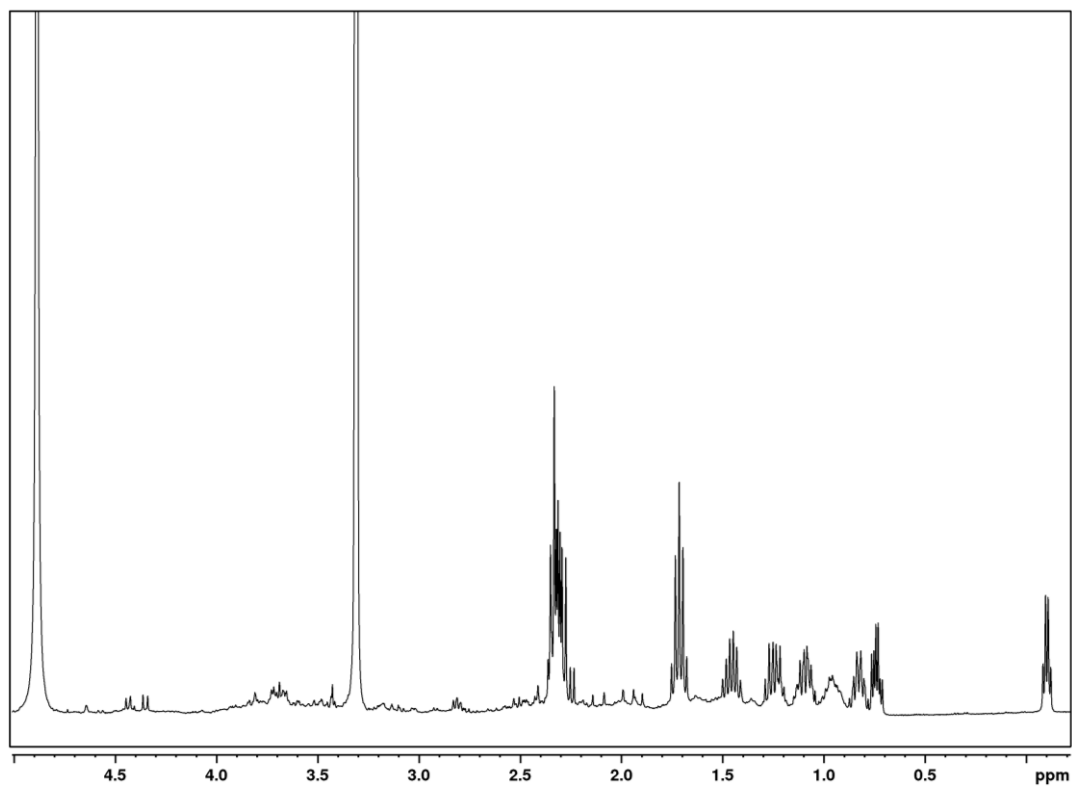


Figure S29: ^1H NMR spectrum of isolated 9-carboxy-*cis*-cascarillic acid.

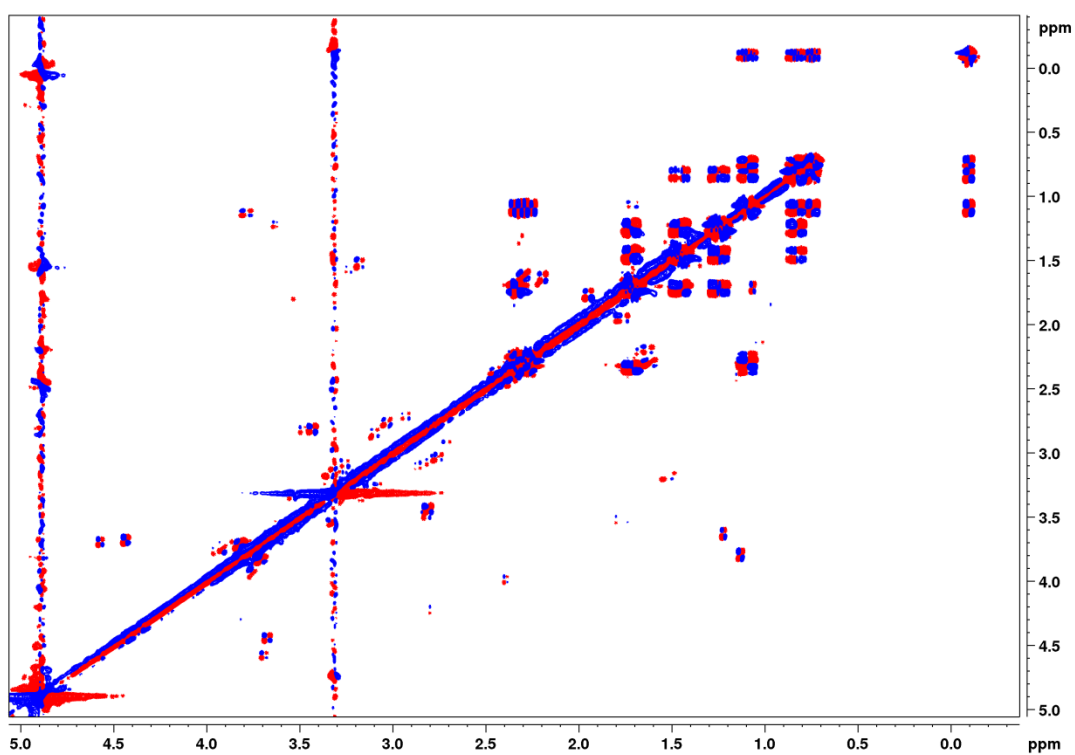


Figure S30: *dqf*-COSY spectrum of isolated 9-carboxy-*cis*-cascarillic acid.

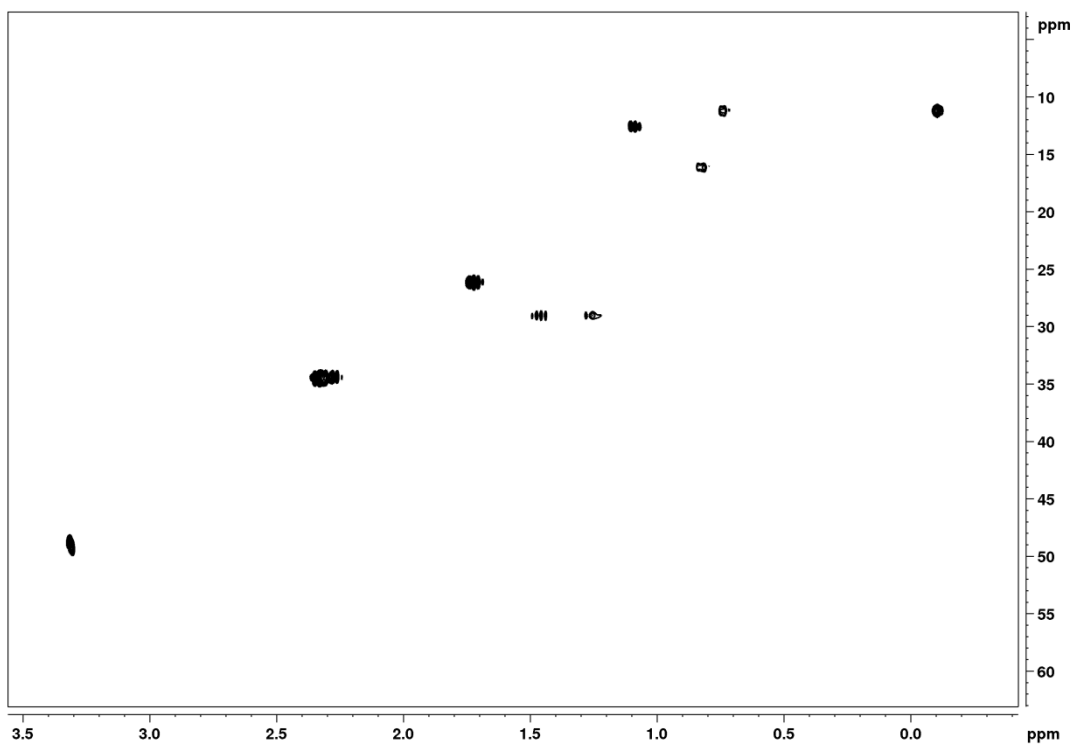


Figure S31: HSQC spectrum of isolated 9-carboxy-*cis*-cascarillic acid.

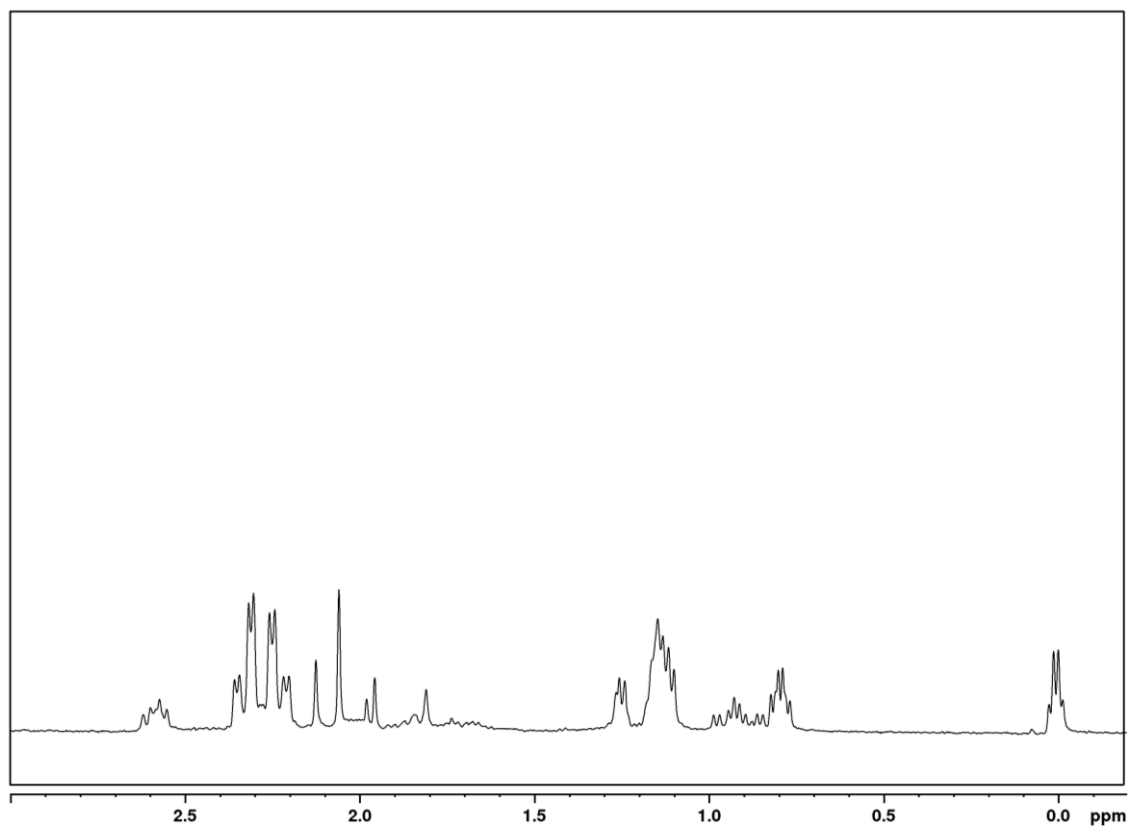


Figure S32: ¹H NMR spectrum of isolated 7-carboxy-*cis*-cascarillic acid.

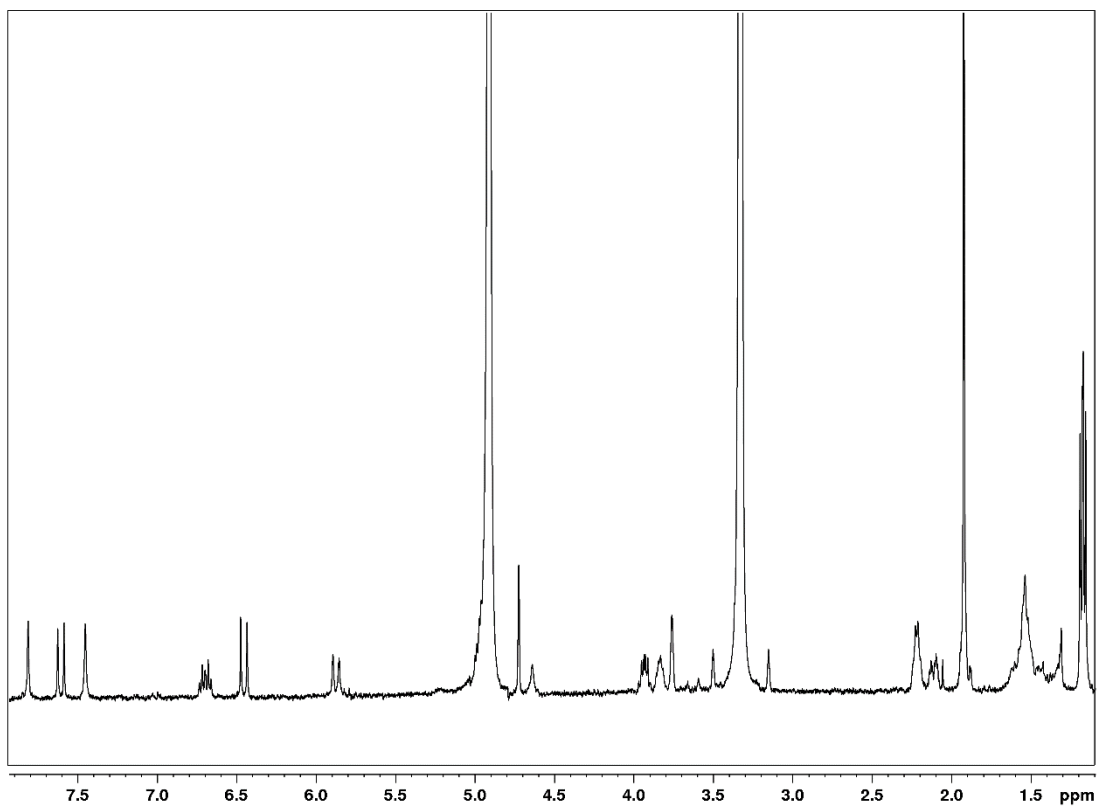


Figure S33: ^1H NMR spectrum of isolated ucas#3.

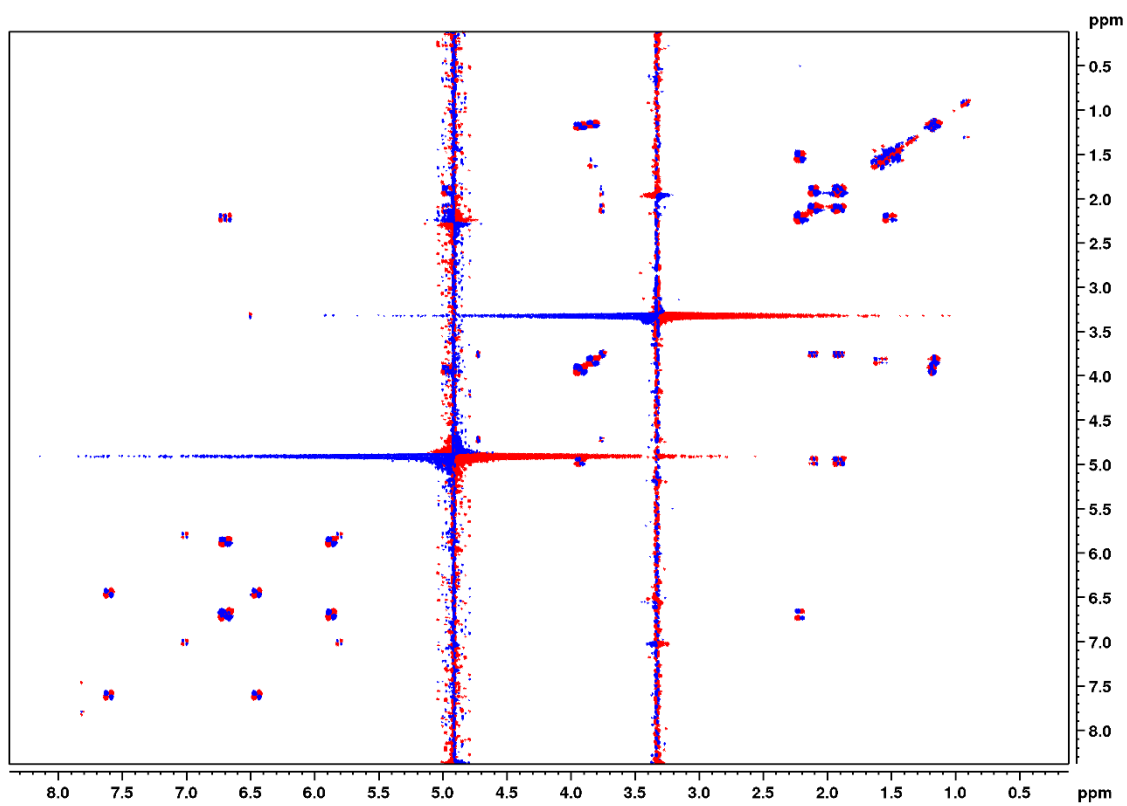


Figure S34: *dqf*-COSY spectrum of isolated ucas#3.

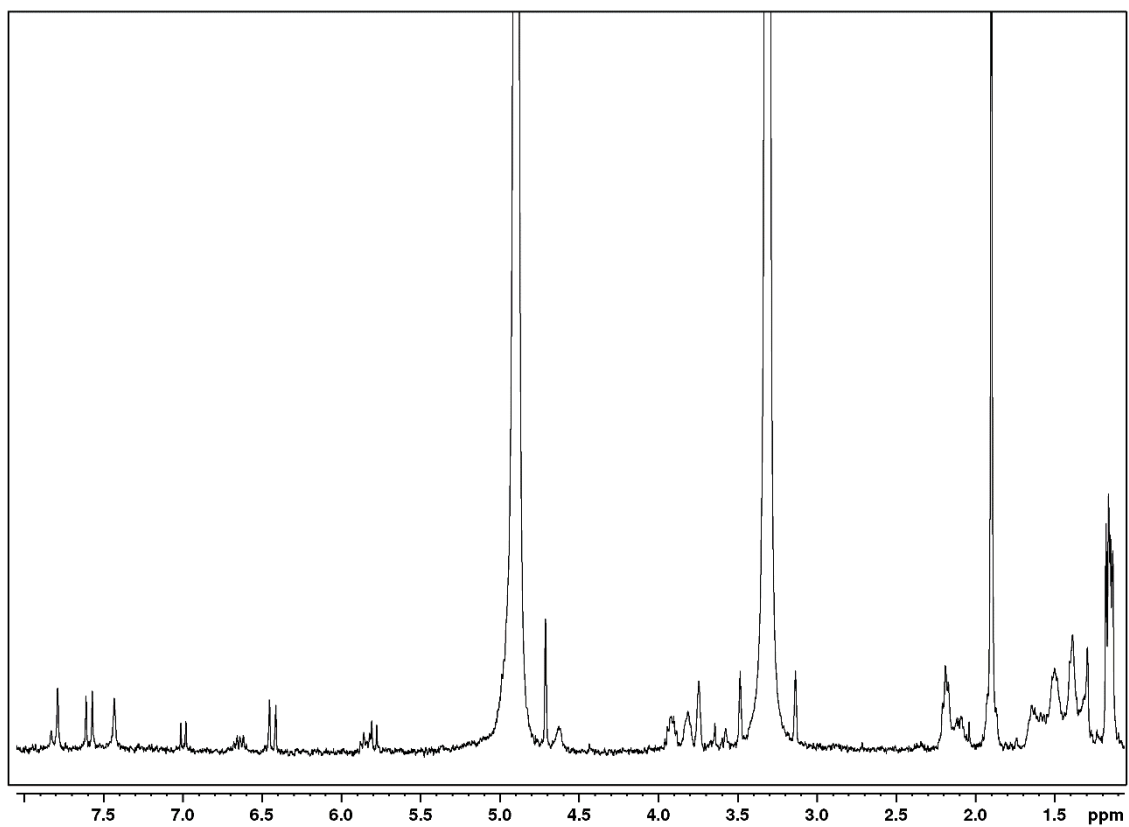


Figure S35: ^1H NMR spectrum of isolated ucas#10.

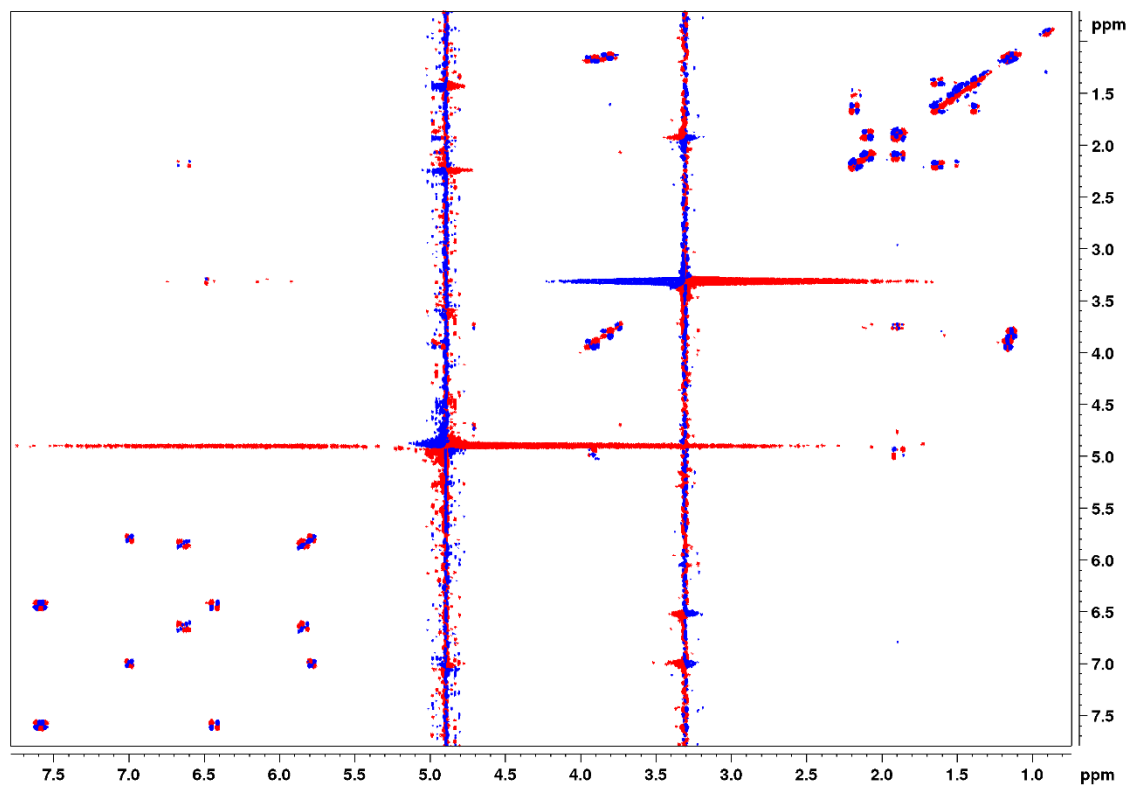


Figure S36: *dqf*-COSY spectrum of isolated ucas#10.

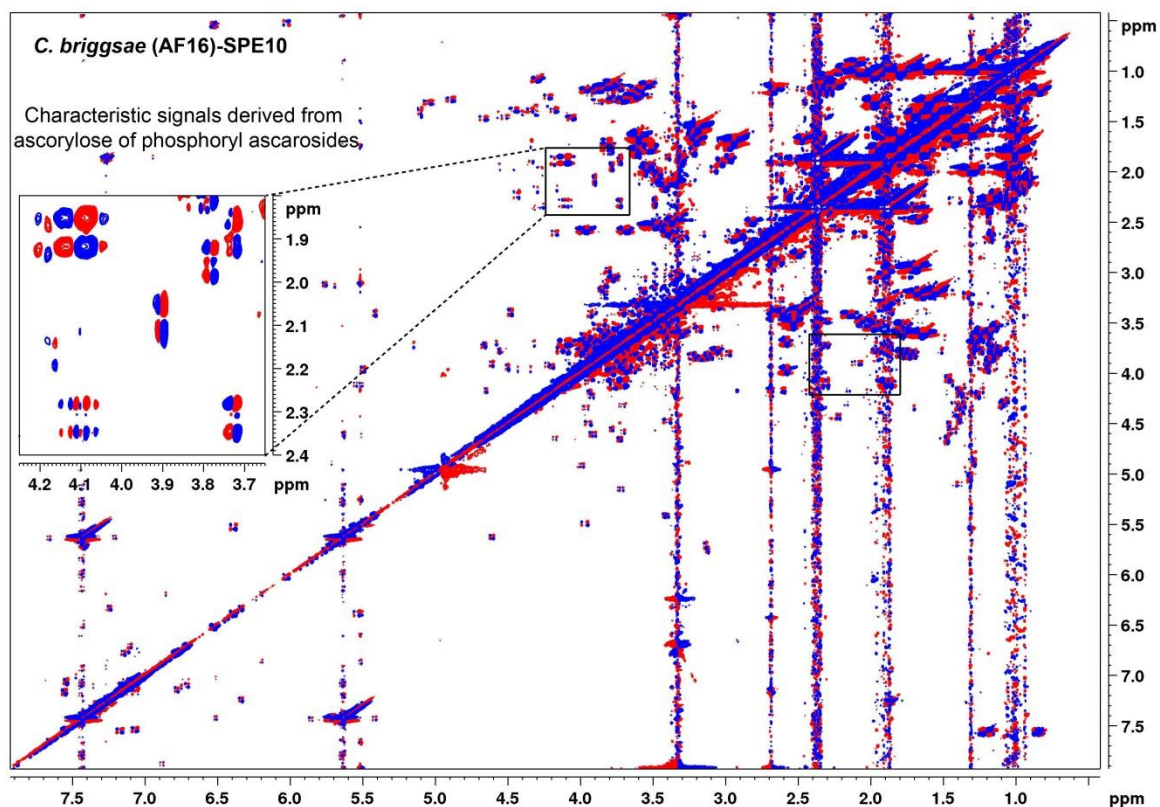
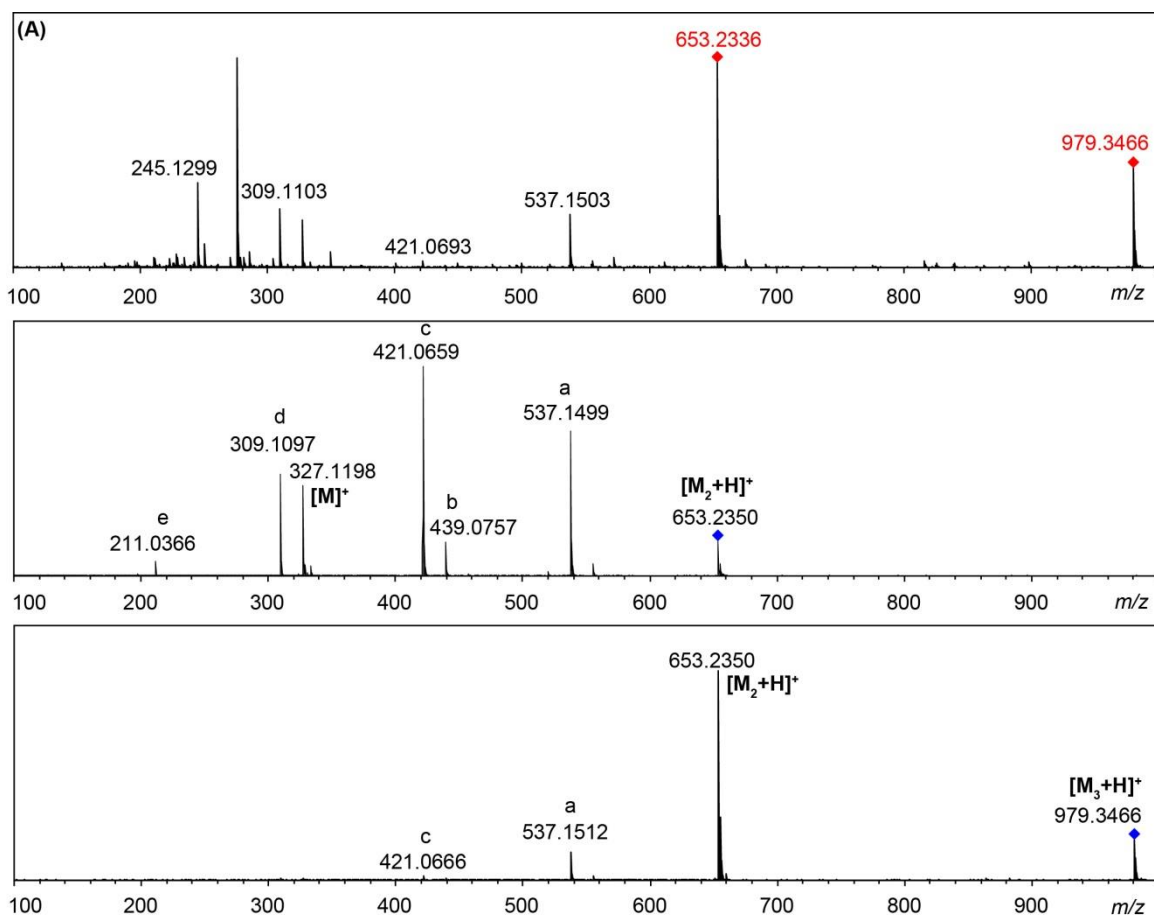


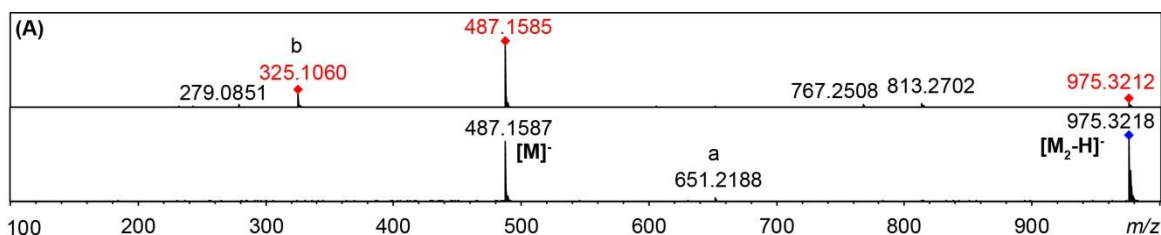
Figure S37: dqf-COSY spectrum of fraction SPE10 derived from *exo*-metabolome of *C. briggsae* (AF16). dqf-COSY spectrum of fraction SPE10 that was eluted using a mixture solvent of 10% MeOH and 90% H₂O was recorded with 400 MHz NMR in CD₃OD. Enlarged section showed ¹H-¹H COSY correlation derived from ascrylose, which strongly suggested the presence of ascarosides.



(B)

Observed m/z	Calculated m/z	Error (ppm)	Ion Formula	Ion assignment
653.2336	653.2334	-0.3	$C_{24}H_{47}O_{16}P_2^+$	$[M_2+H]^+$
979.3466	979.3464	-0.1	$C_{36}H_{70}O_{24}P_3^+$	$[M_3+H]^+$
537.1499	537.1497	-0.5	$C_{18}H_{35}O_{14}P_2^+$	a
439.0757	439.0765	1.9	$C_{12}H_{22}O_{13}P_2^+$	b
421.0659	421.0659	0.1	$C_{12}H_{23}O_{12}P_2^+$	c
327.1198	327.1203	1.6	$C_{12}H_{24}O_8P^+$	$[M]^+$
309.1097	309.1098	0.2	$C_{12}H_{22}O_7P^+$	d
211.0366	211.0366	0.1	$C_6H_{12}O_6P^+$	e

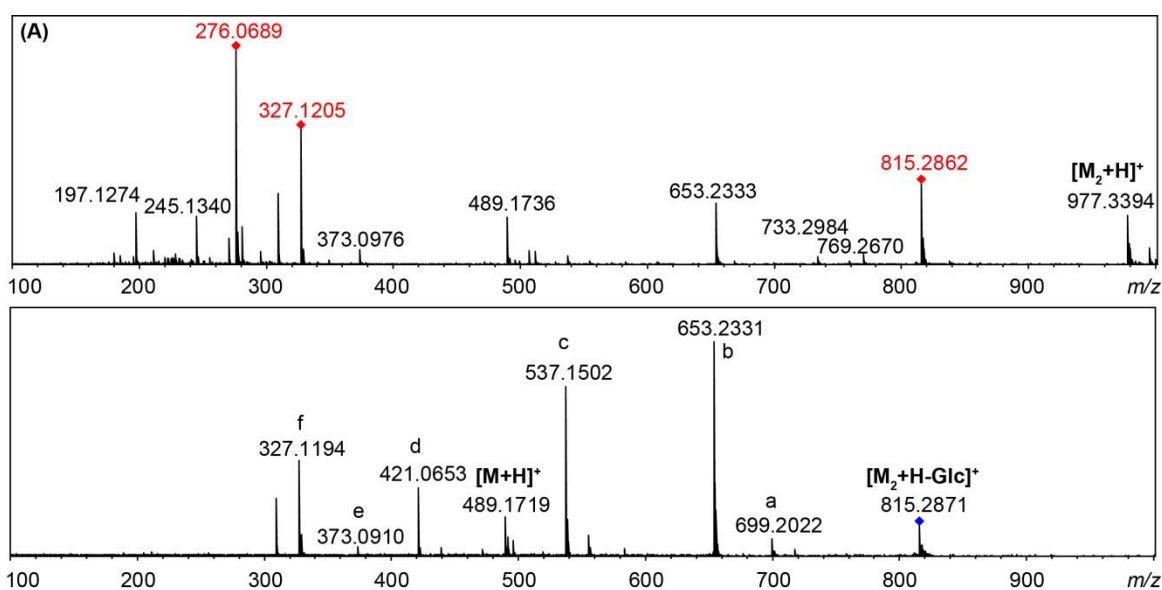
Figure S38: MS/MS fragmentation analysis of 4P-ascr#2. (A) MS² fragmentation of dimeric and trimeric ions of 4P-ascr#2 by using HR-QTOF-LC/MS in positive ion mode. (B) High resolution masses of fragments and ion assignment.



(B)

Observed m/z	Calculated m/z	Error (ppm)	Ion Formula	Ion assignment
975.3212	975.3245	3.4	$C_{36}H_{65}O_{26}P_2^-$	$[M_2-H]^-$
651.2188	651.2271	12.6	$C_{24}H_{44}O_{18}P^-$	a
487.1587	487.1586	-0.2	$C_{18}H_{32}O_{13}P^-$	$[M-H]^-$
325.1066	325.1058	-2.6	$C_{12}H_{22}O_8P^-$	b

Figure S39: MS/MS fragmentation for dimeric ion of 4GlcP-ascr#2. (A) MS² fragmentation of dimeric ion derived from 4GlcP-ascr#2 by using HR-QTOF-LC/MS in negative ion mode. (B) High resolution masses of fragments and ion assignment.



(B)

Observed m/z	Calculated m/z	Error (ppm)	Ion Formula	Ion assignment
977.3394	977.3390	-0.4	$C_{36}H_{67}O_{26}P_2^+$	$[M_2+H]^+$
815.2862	815.2862	0.0	$C_{30}H_{57}O_{21}P_2^+$	$[M_2+H-Glc]^+$
699.2022	699.2025	0.4	$C_{24}H_{45}O_{19}P_2^+$	a
653.2331	653.2334	0.4	$C_{24}H_{47}O_{16}P_2^+$	b
537.1502	537.1497	-1.0	$C_{18}H_{35}O_{14}P_2^+$	c
489.1736	489.1732	-0.9	$C_{18}H_{34}O_{13}P^+$	$[M+H]^+$
421.0653	421.0659	1.5	$C_{12}H_{23}O_{12}P_2^+$	d
373.0910	373.0894	-4.3	$C_{12}H_{22}O_{11}P^+$	e
327.1205	327.1203	-0.4	$C_{12}H_{24}O_8P^+$	f

Figure S40: MS/MS fragmentation for dimeric ion of 4GlcP-ascr#2. (A) MS² fragmentation of dimeric ion derived from 4GlcP-ascr#2 by using HR-QTOF-LC/MS in positive ion mode. (B) High resolution masses of fragments and ion assignment.

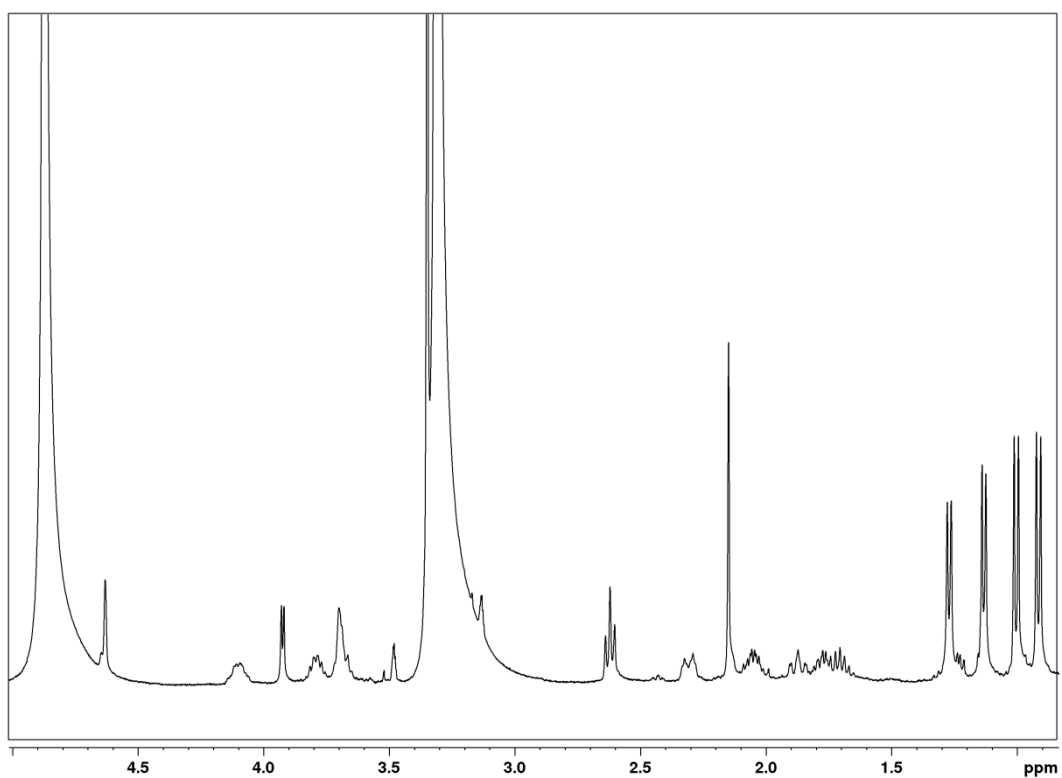


Figure S41: ^1H NMR spectrum of isolated 4P-ascr#2.

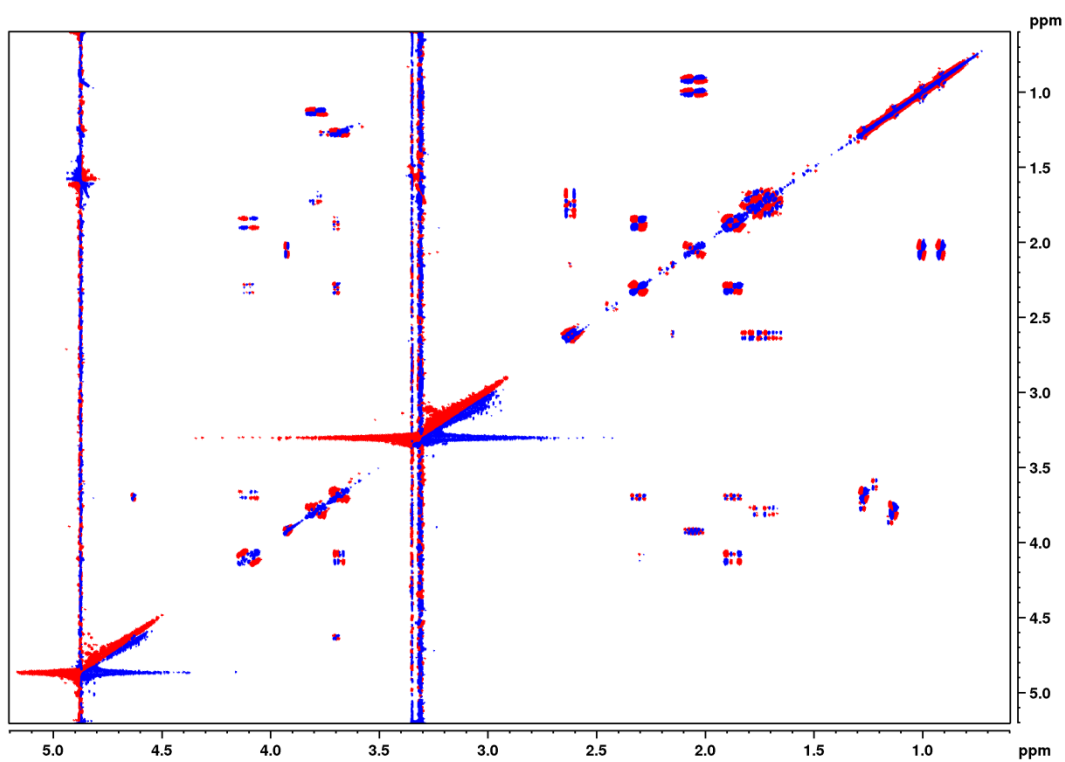


Figure S42: *dqf*-COSY spectrum of isolated 4P-ascr#2.

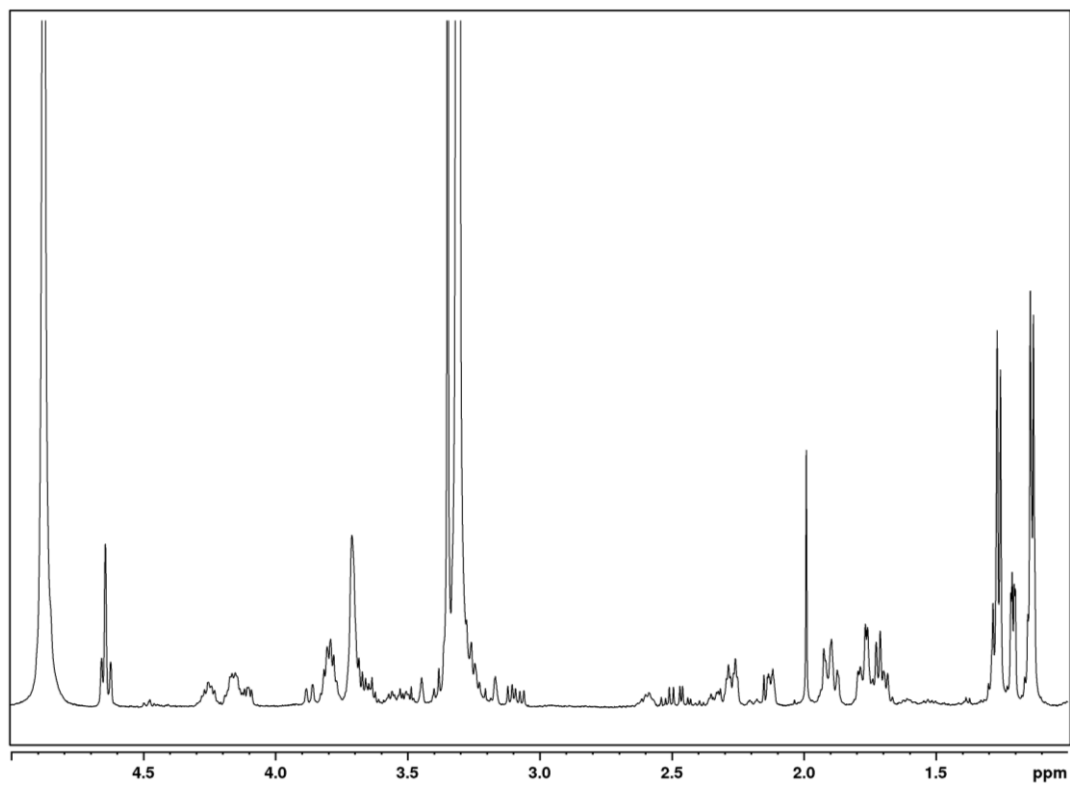


Figure S43: ^1H NMR spectrum of isolated 4GlcP-ascr#2.

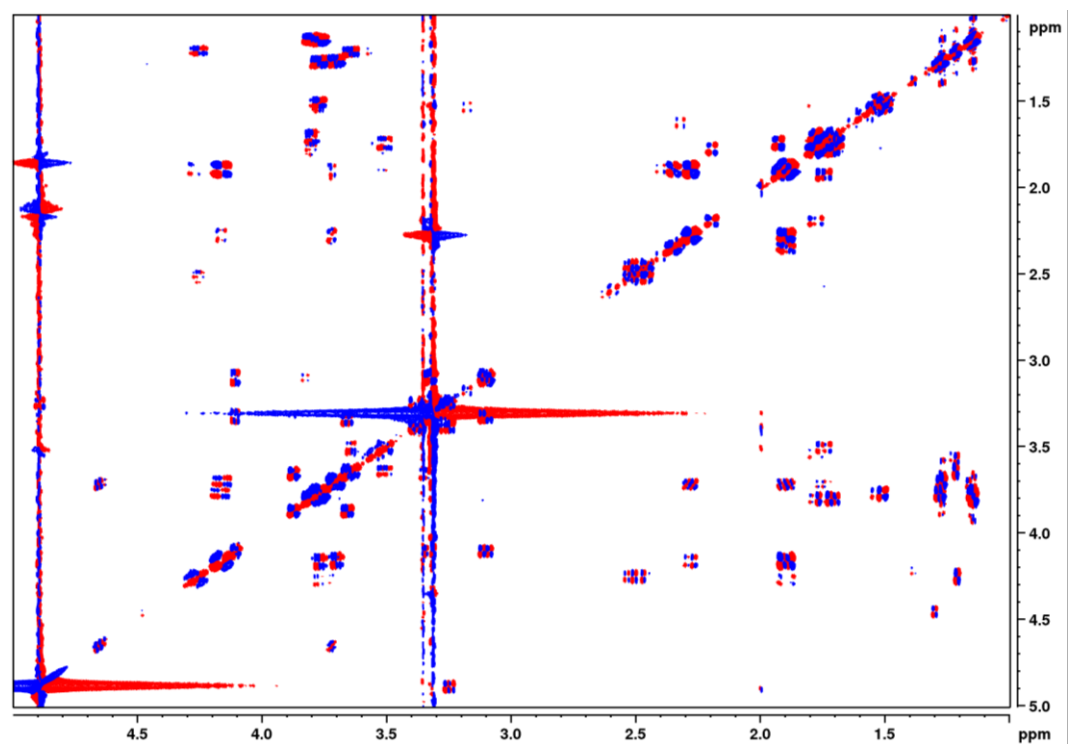


Figure S44: *dqf*-COSY spectrum of isolated 4GlcP-ascr#2.

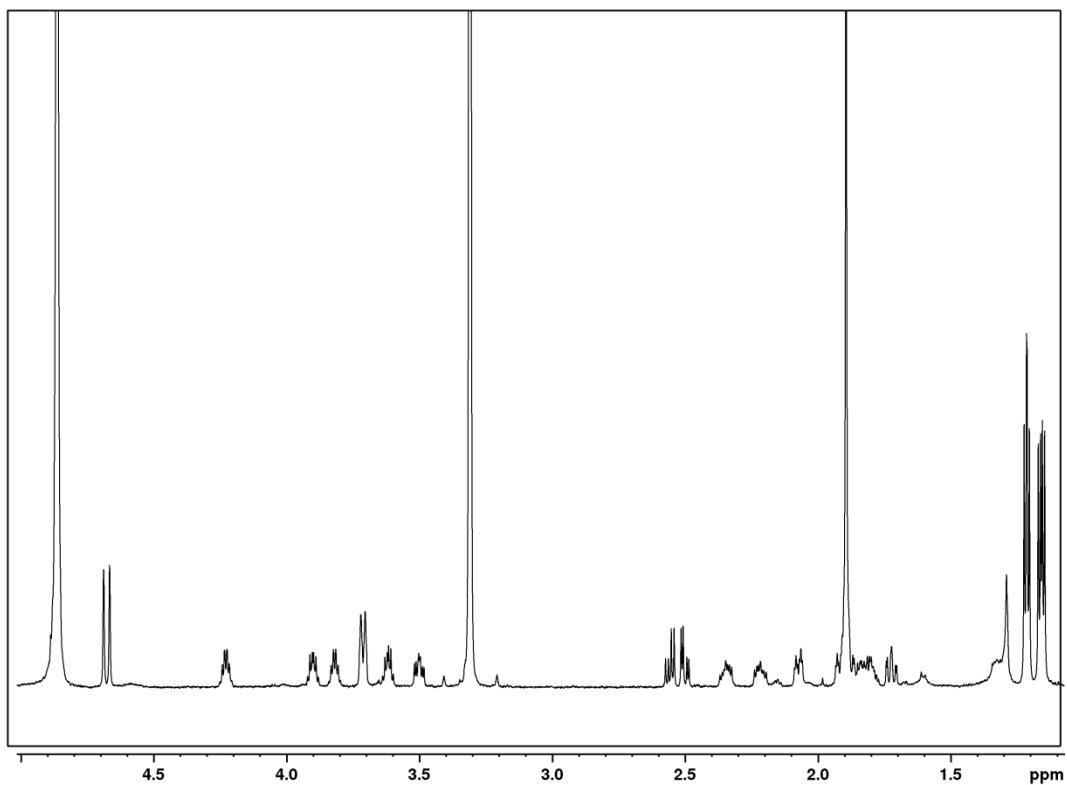


Figure S45: $^1\text{H-NMR}$ spectrum of isolated C4-C5.

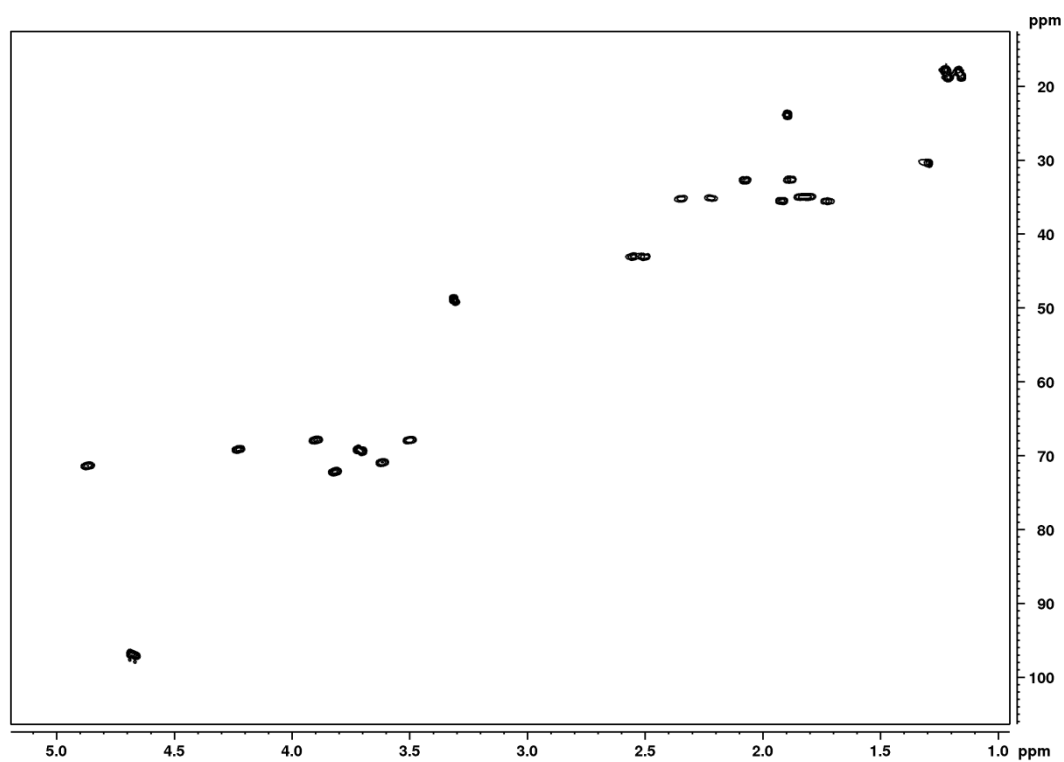


Figure S46: HSQC spectrum of isolated C4-C5.

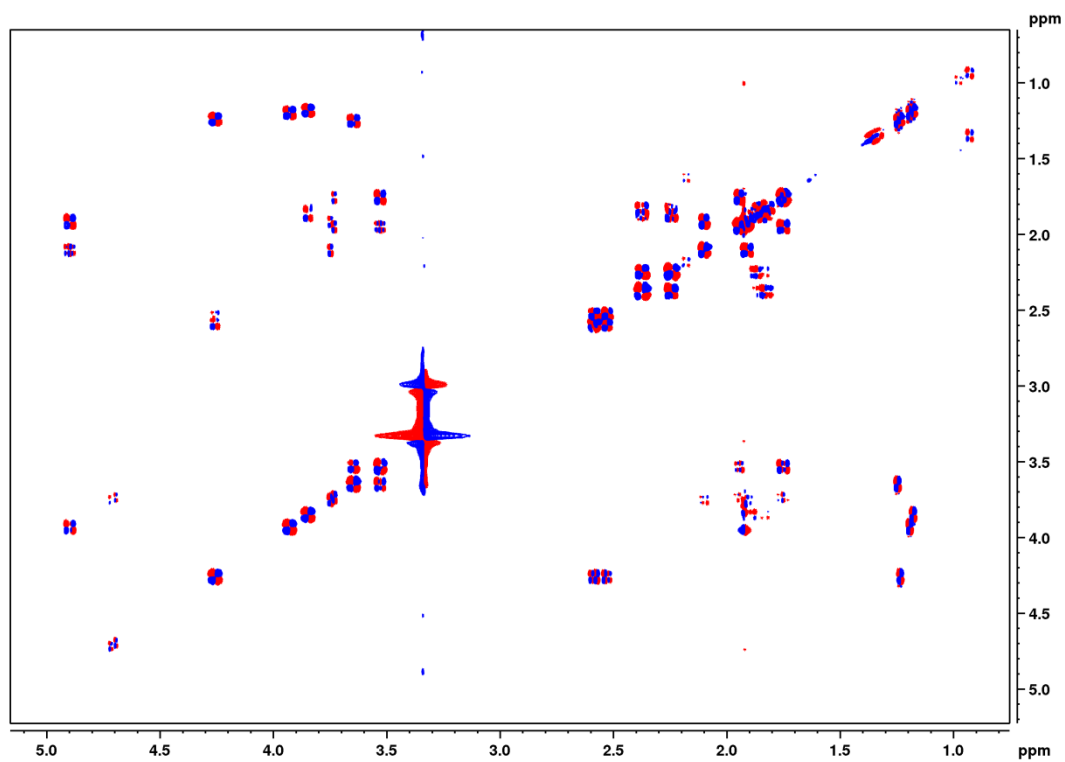


Figure S47: *dqf*-COSY spectrum of isolated C4-C5.

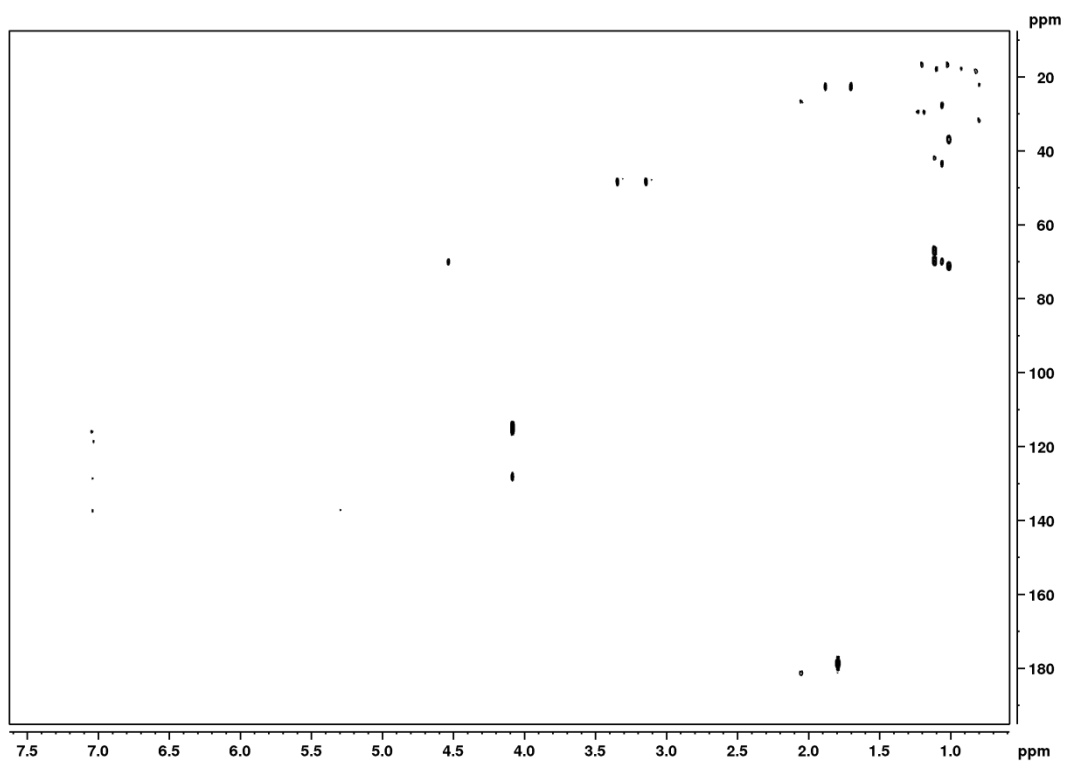
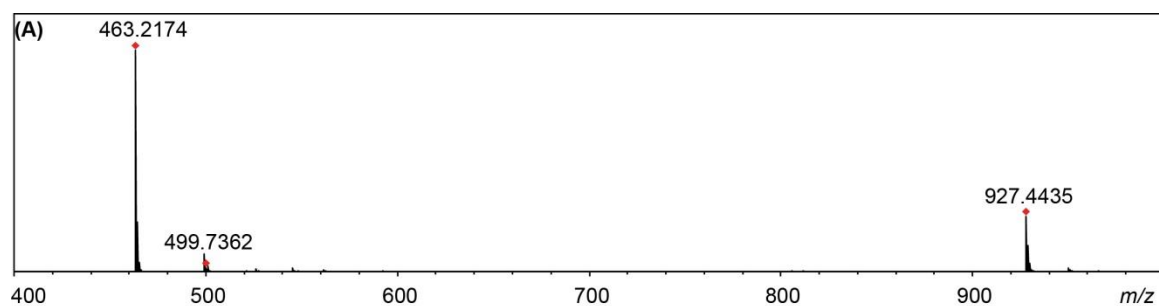
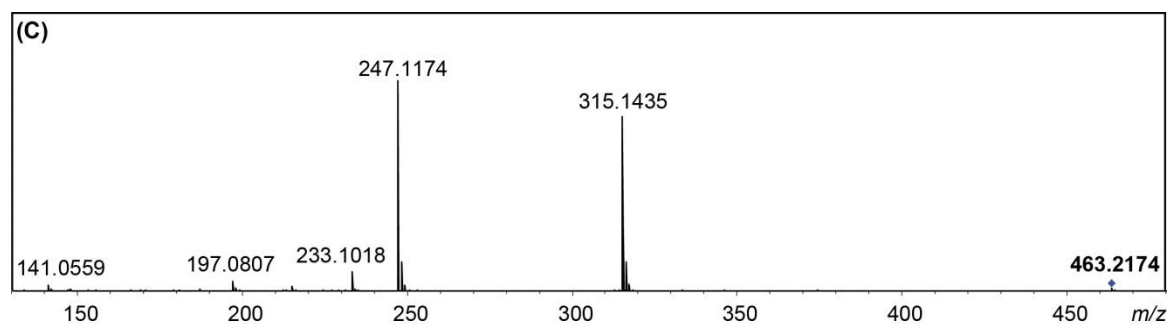


Figure S48: HMBC spectrum of isolated C4-C5.



(B)

Observed (m/z)	Calculated (m/z)	Error (ppm)	Ion Formula
463.2174	463.2185	2.3	$C_{21}H_{35}O_{11}^-$
499.1932	499.1915	-3.3	$C_{34}H_{27}O_{14}^-$
927.4435	927.4442	0.8	$C_{42}H_{71}O_{22}^-$



(D)

Observed (m/z)	Calculated (m/z)	Error (ppm)	Ion Formula
315.1449	315.1449	0	$C_{15}H_{23}O_7^-$
247.1195	247.1187	-3.2	$C_{11}H_{19}O_6^-$

Figure S49: Structure Characterization of C4-C5 by QTOF-HRMS analysis (A) and MS/MS fragmentation pattern (B) in negative ion mode.

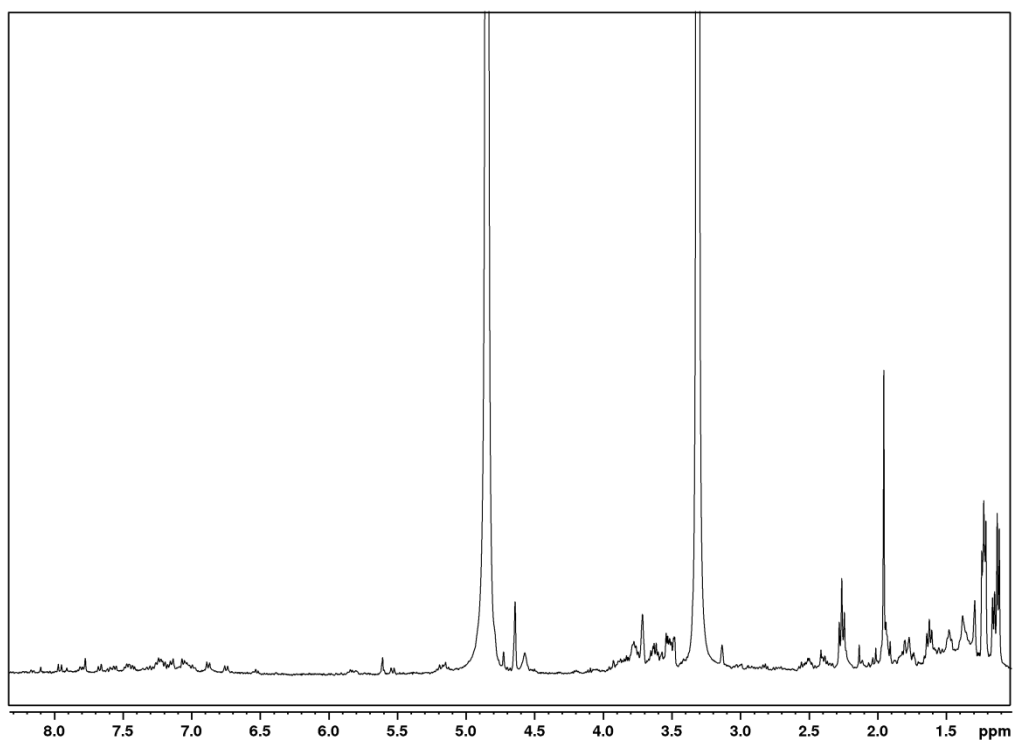


Figure S50: ^1H NMR spectrum of isolated C6-C5 from *C. nigrum*.

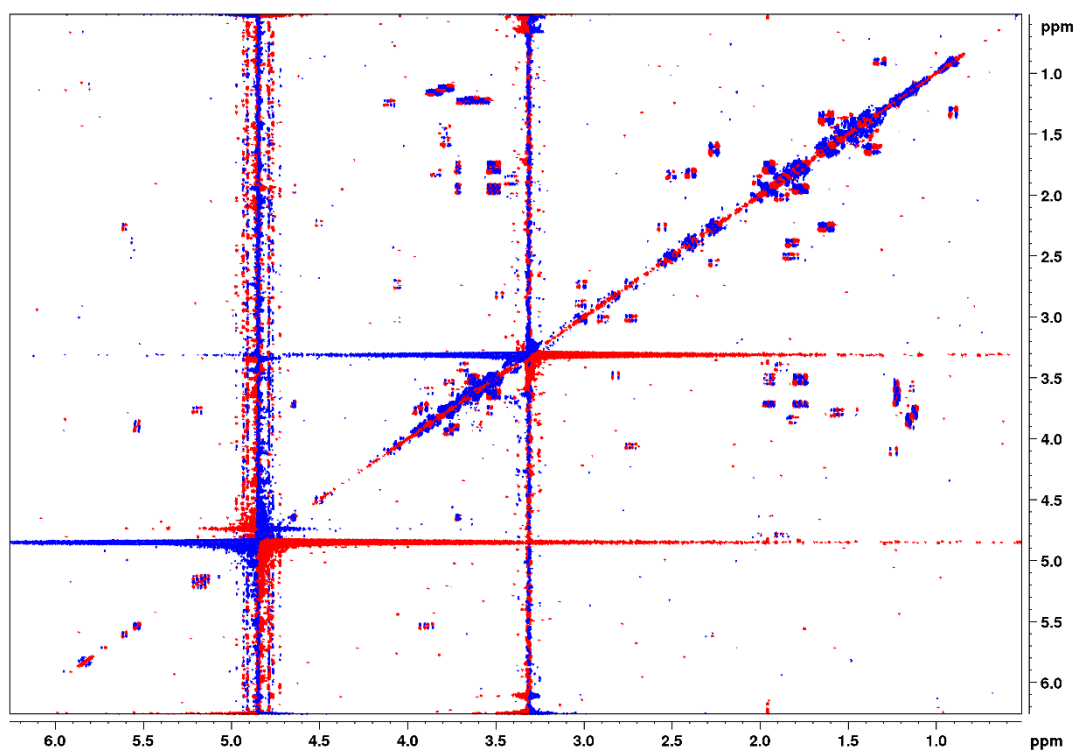
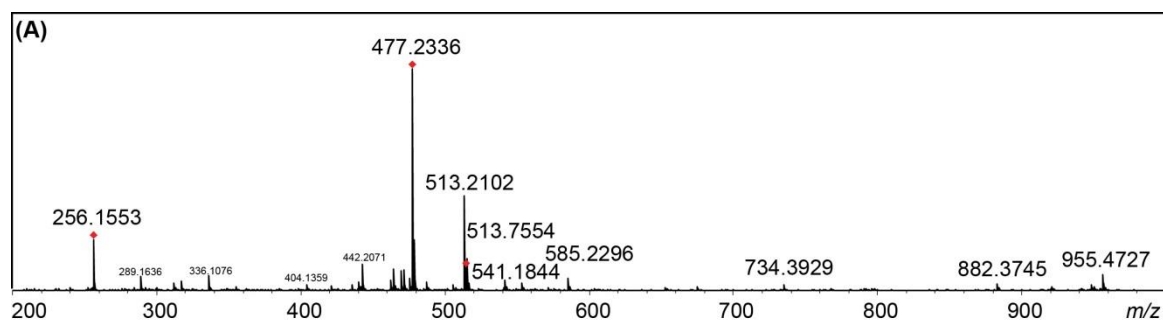
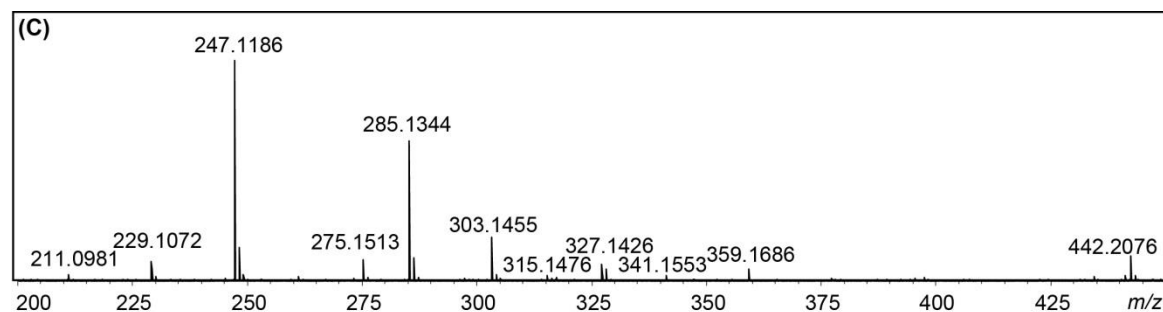


Figure S51: *dqf*-COSY spectrum of 2-position substituted C6-C5 from *C. nigrum*.



(B)

Observed (<i>m/z</i>)	Calculated (<i>m/z</i>)	Error (ppm)	Ion Formula
477.2336	477.2341	1.0	C ₂₂ H ₃₇ O ₁₁ ⁻
585.2296	585.2283	-2.3	C ₃₈ H ₃₃ O ₁₆ ⁻
955.4727	955.4755	2.9	C ₄₄ H ₇₅ O ₂₂ ⁻



(D)

Observed (<i>m/z</i>)	Calculated (<i>m/z</i>)	Error (ppm)	Ion Formula
477.2343	477.2341	-0.3	C ₂₂ H ₃₇ O ₁₁ ⁻
303.1455	303.1449	-1.8	C ₁₄ H ₂₃ O ₇ ⁻
285.1344	285.1344	-0.2	C ₁₄ H ₂₁ O ₆ ⁻
247.1186	247.1187	0.5	C ₁₁ H ₁₉ O ₆ ⁻

Figure S52: Structure Characterization of C6-C5 by QTOF-HRMS analysis (A) and MS/MS fragmentation pattern (B) in negative ion mode.

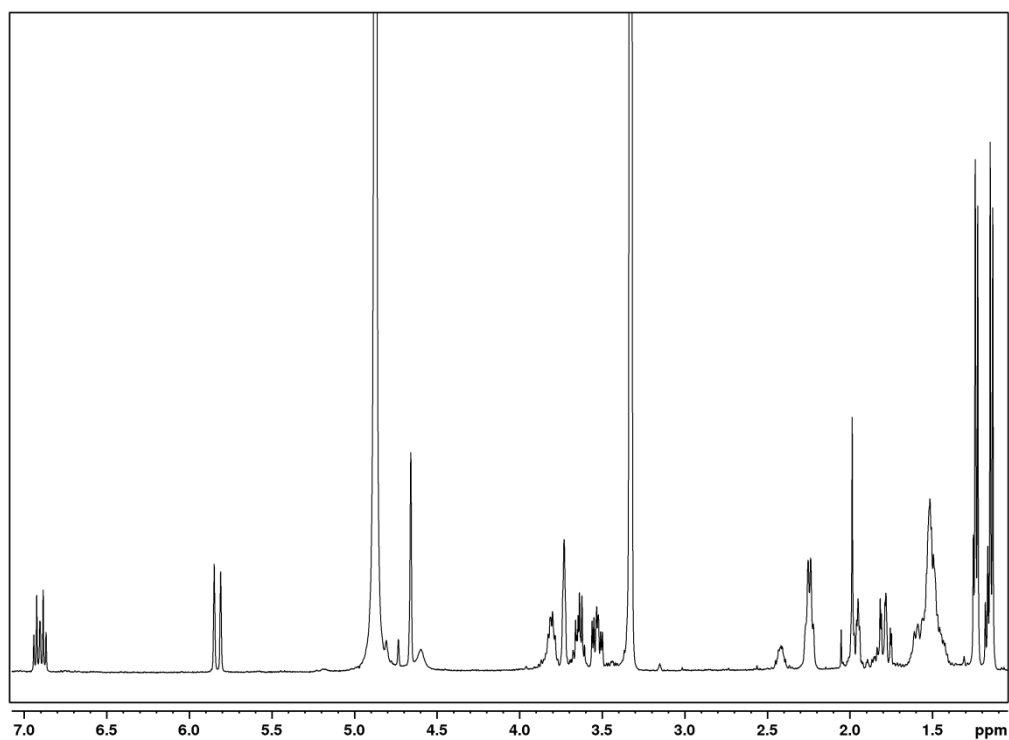


Figure S53: ^1H NMR spectrum of isolated C6-C6 from *C. nigoni*.

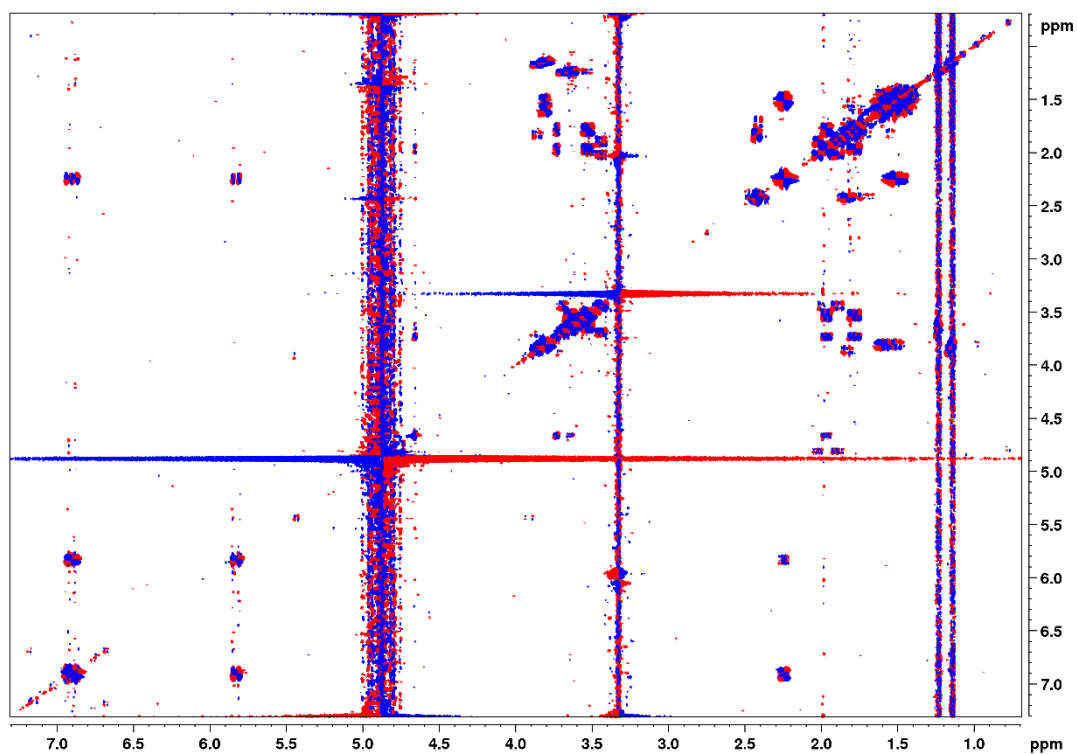
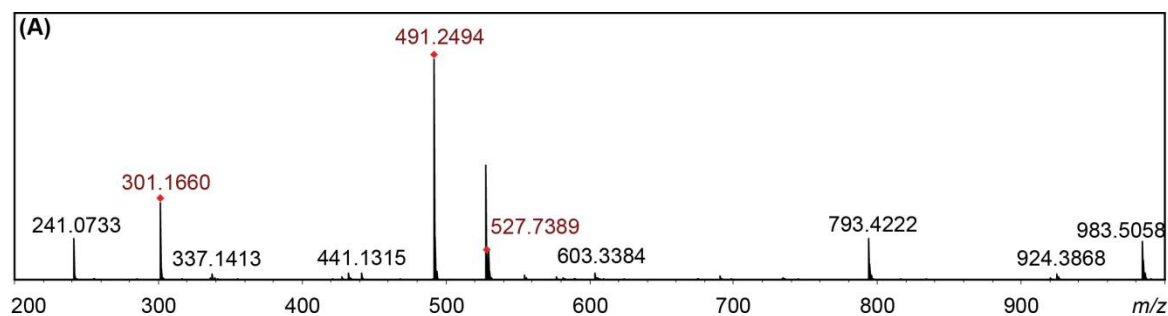
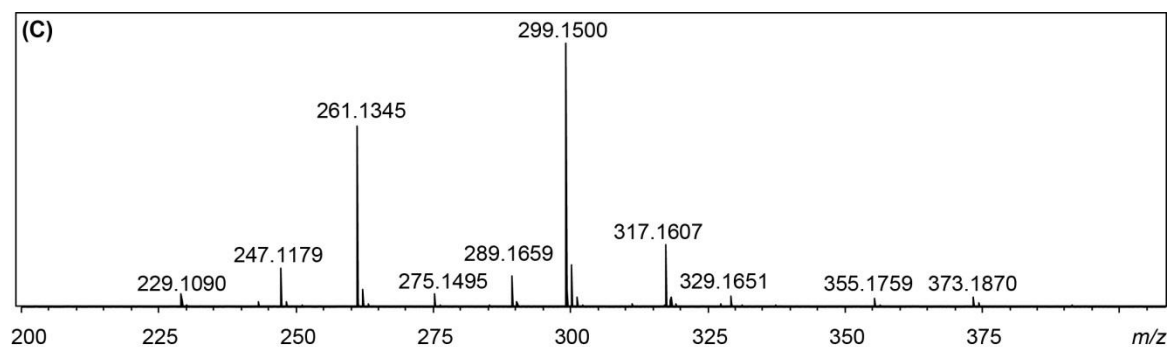


Figure S54: *dqf*-COSY spectrum of isolated 2-position substituted C6-C6 from *C. nigoni*.



(B)

Observed (<i>m/z</i>)	Calculated (<i>m/z</i>)	Error (ppm)	Ion Formula
491.2494	491.2498	0.8	C ₂₃ H ₃₉ O ₁₁ ⁻
527.2265	527.2287	4.1	C ₂₉ H ₃₅ O ₉ ⁻
793.4222	793.4227	0.7	C ₃₈ H ₆₅ O ₁₇ ⁻
983.5058	983.5068	1.1	C ₄₆ H ₇₉ O ₂₂ ⁻



(D)

Observed (<i>m/z</i>)	Calculated (<i>m/z</i>)	Error (ppm)	Ion Formula
491.2495	491.2498	0.6	C ₂₃ H ₃₉ O ₁₁ ⁻
317.1595	317.1606	3.3	C ₁₅ H ₂₅ O ₇ ⁻
299.1496	299.1500	1.2	C ₁₅ H ₂₃ O ₆ ⁻
261.1343	261.1344	0.3	C ₁₂ H ₂₁ O ₆ ⁻
247.1189	247.1187	-0.6	C ₁₁ H ₁₉ O ₆ ⁻

Figure S55: Structure Characterization of C6-C6 by QTOF-HRMS analysis (A) and MS/MS fragmentation pattern (B) in negative ion mode.

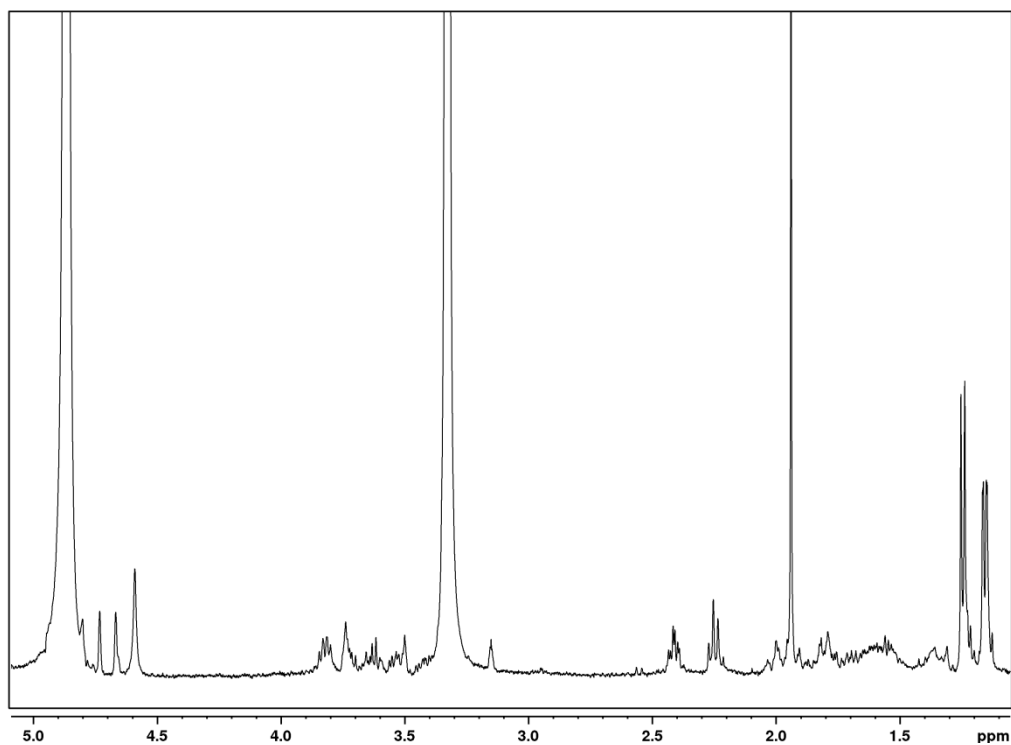


Figure S56: ^1H NMR spectrum of isolated C6-C7 from *C. nigrum*.

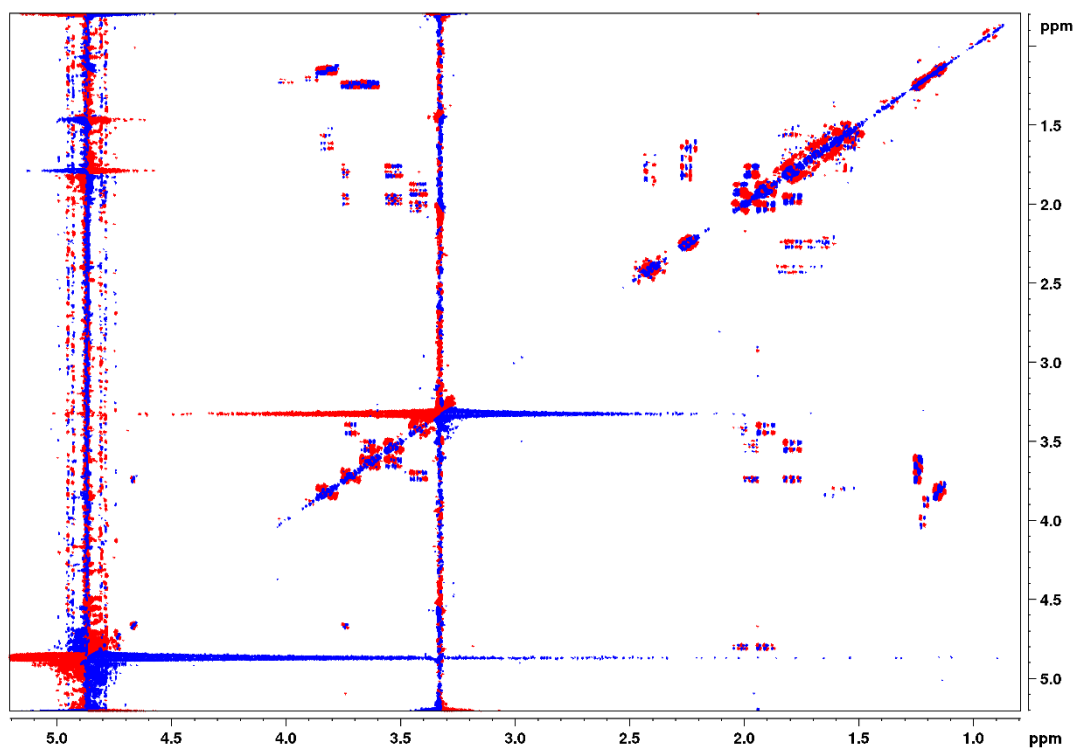
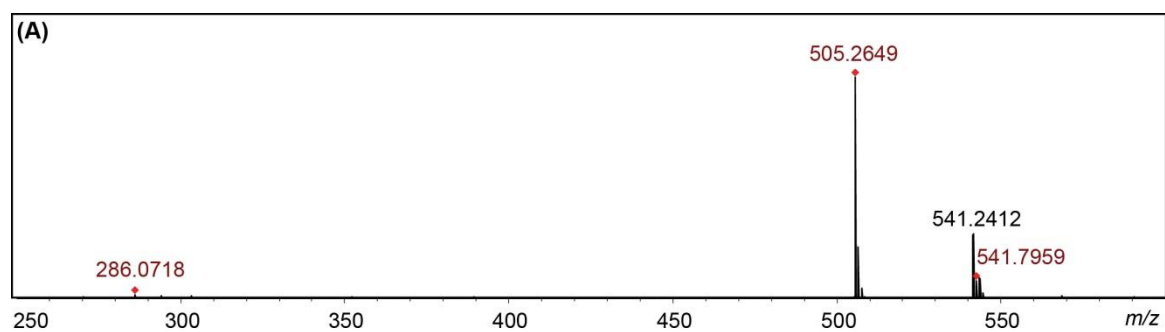
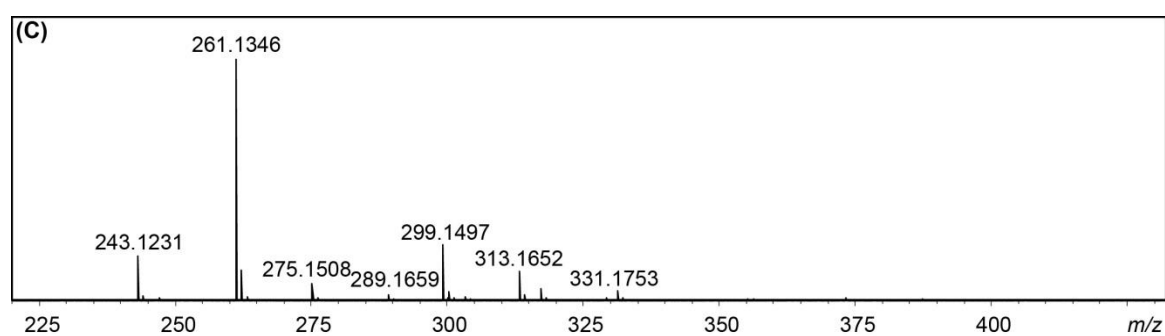


Figure S57: *dqf*-COSY spectrum of 2-position substituted C6-C7 from *C. nigrum*.



(B)

Observed (m/z)	Calculated (m/z)	Error (ppm)	Ion Formula
505.2649	505.2654	1.1	$C_{24}H_{41}O_{11}^-$
541.2412	541.2384	-5.1	$C_{37}H_{33}O_4^-$



(D)

Observed (m/z)	Calculated (m/z)	Error (ppm)	Ion Formula
299.1497	299.1500	0.9	$C_{15}H_{23}O_6^-$
261.1346	261.1344	-0.9	$C_{12}H_{21}O_6^-$

Figure S58: Structure Characterization of C6-C6 by QTOF-HRMS analysis (A) and MS/MS fragmentation pattern (B) in negative ion mode.

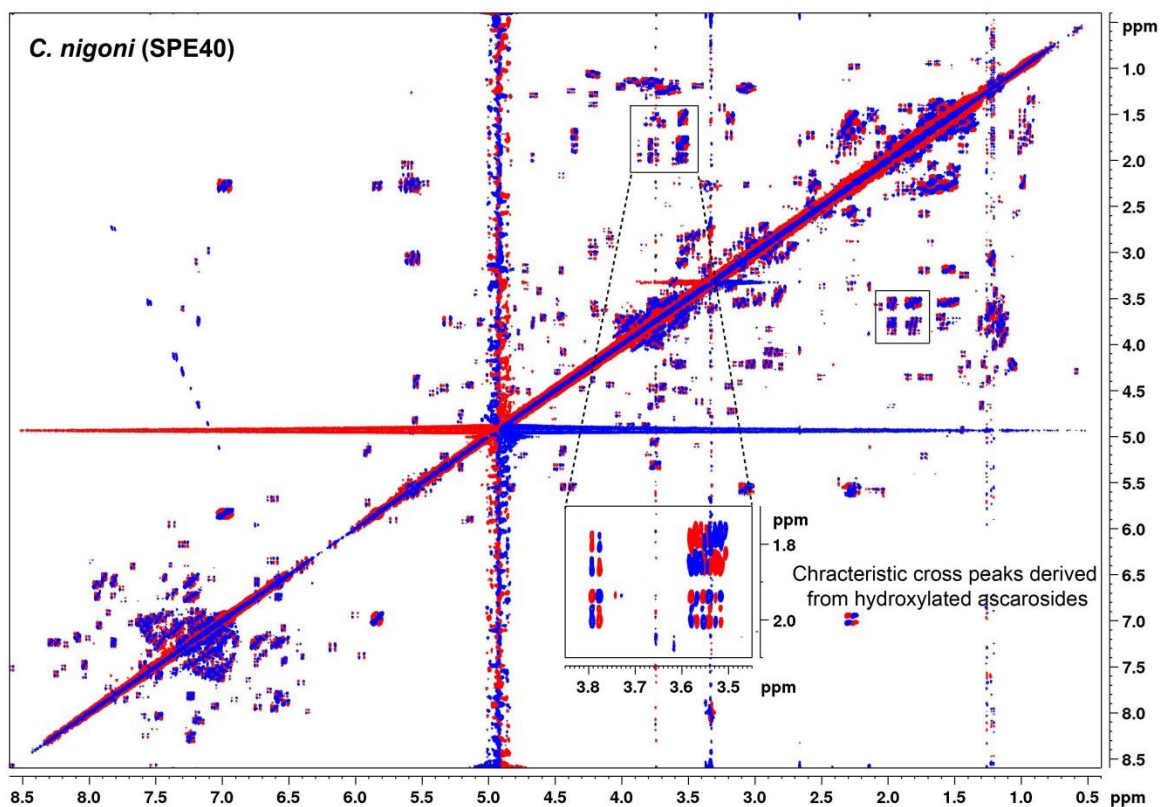


Figure S59: Hydroxylated ascarosides were enriched and detected in SPE40 fraction by *dqf*-COSY spectrum. Characteristic cross peaks (shown in enlarged section) derived from ascarlyose were detected by *dqf*-COSY spectrum.

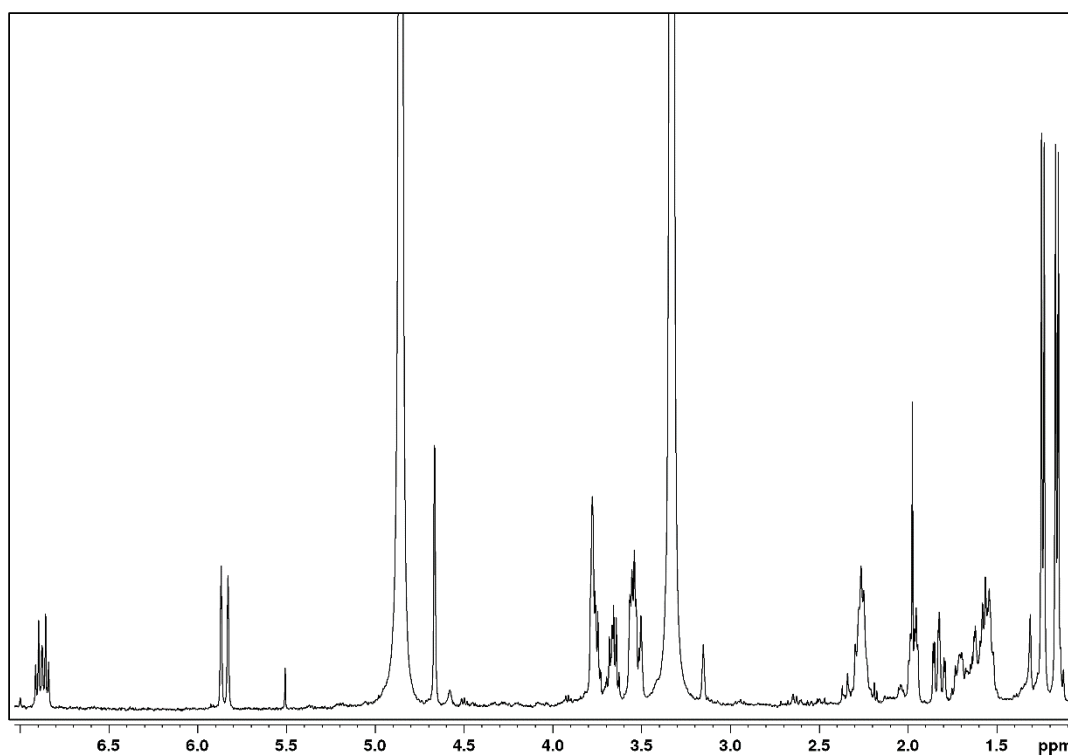


Figure S60: ^1H -NMR spectrum of isolated (ω -2)-*threo*-OH-ascr#3.

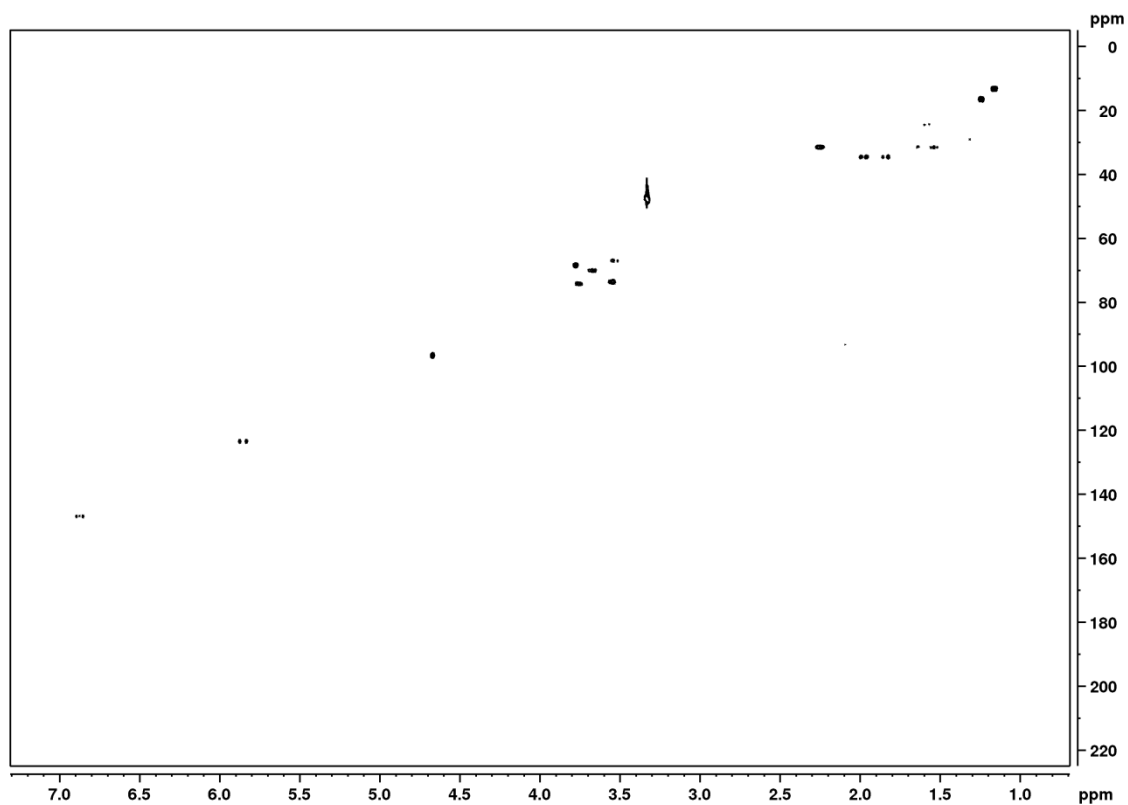


Figure S61: HSQC spectrum of isolated (ω -2)-*threo*-OH-ascr#3.

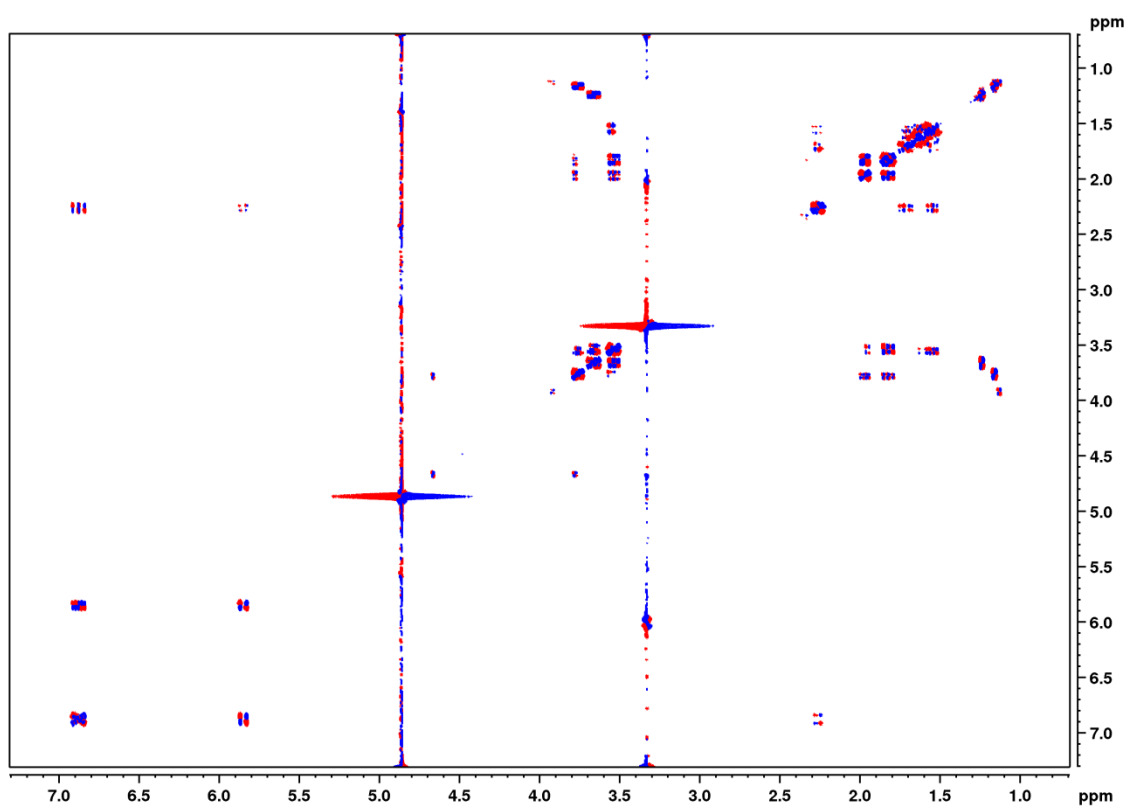
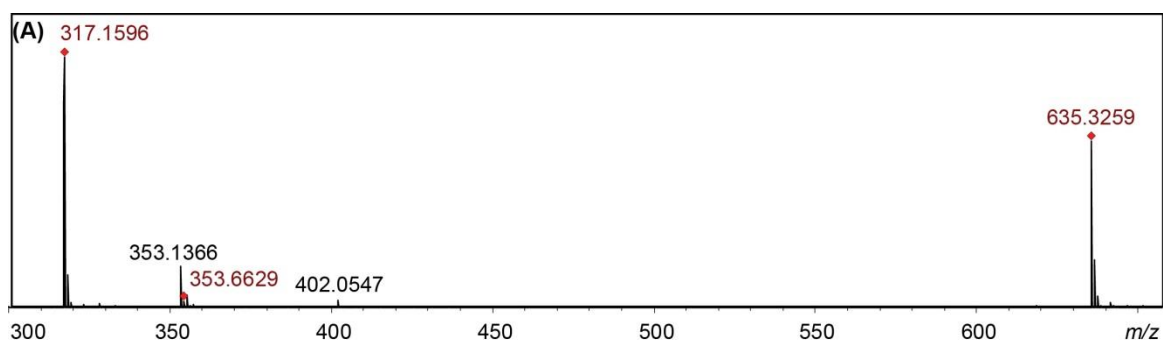
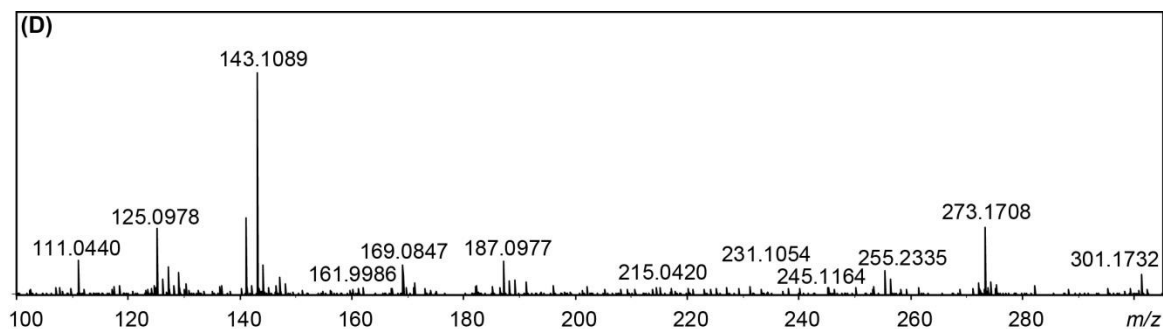
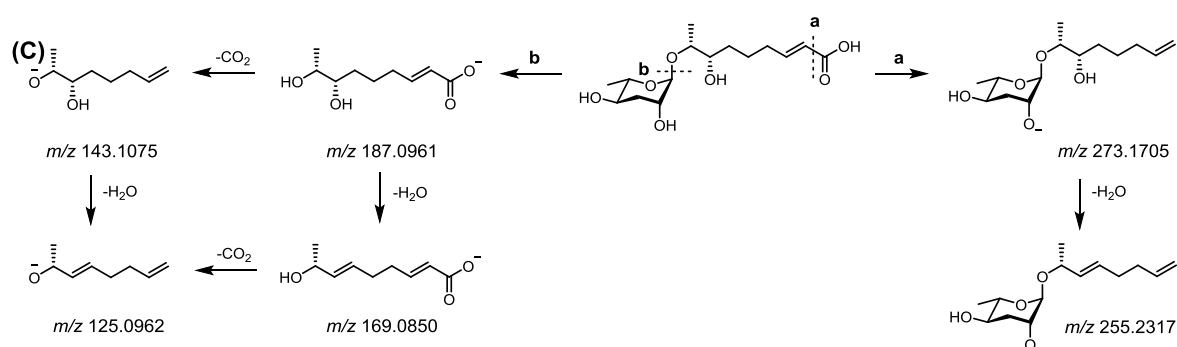


Figure S62: *dqf*-COSY spectrum of isolated (ω -2)-*threo*-OH-ascr#3.



(B)

Observed (m/z)	Calculated (m/z)	Error (ppm)	Ion Formula
317.1596	317.1606	3.2	$C_{15}H_{25}O_7^-$
635.3259	635.3284	4.0	$C_{30}H_{51}O_{14}^-$



(E)

Observed (m/z)	Calculated (m/z)	Error (ppm)	Ion Formula
273.1705	273.1707	-0.2	$C_{14}H_{25}O_5^-$
255.2317	255.2330	5.0	$C_{16}H_{31}O_2^-$
187.0961	187.0976	-0.7	$C_9H_{15}O_4^-$
169.0878	169.0870	-4.7	$C_9H_{13}O_3^-$

Figure S63: Structure Characterization of (ω -2)-*threo*-OH-*ascr*#3 by QTOF-HRMS analysis (A & B) and MS/MS fragmentation pattern (C, D & E) in negative ion mode.

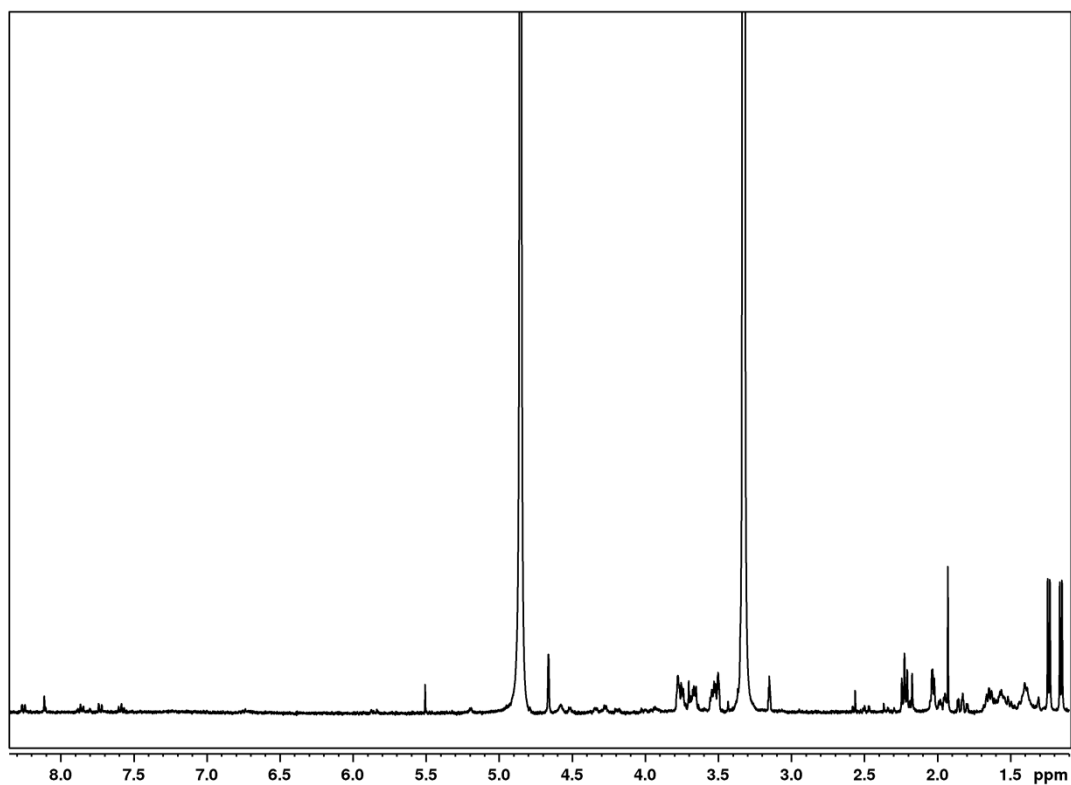


Figure S64: $^1\text{H-NMR}$ spectrum of isolated (ω -2)-*threo*-OH-ascr#10.

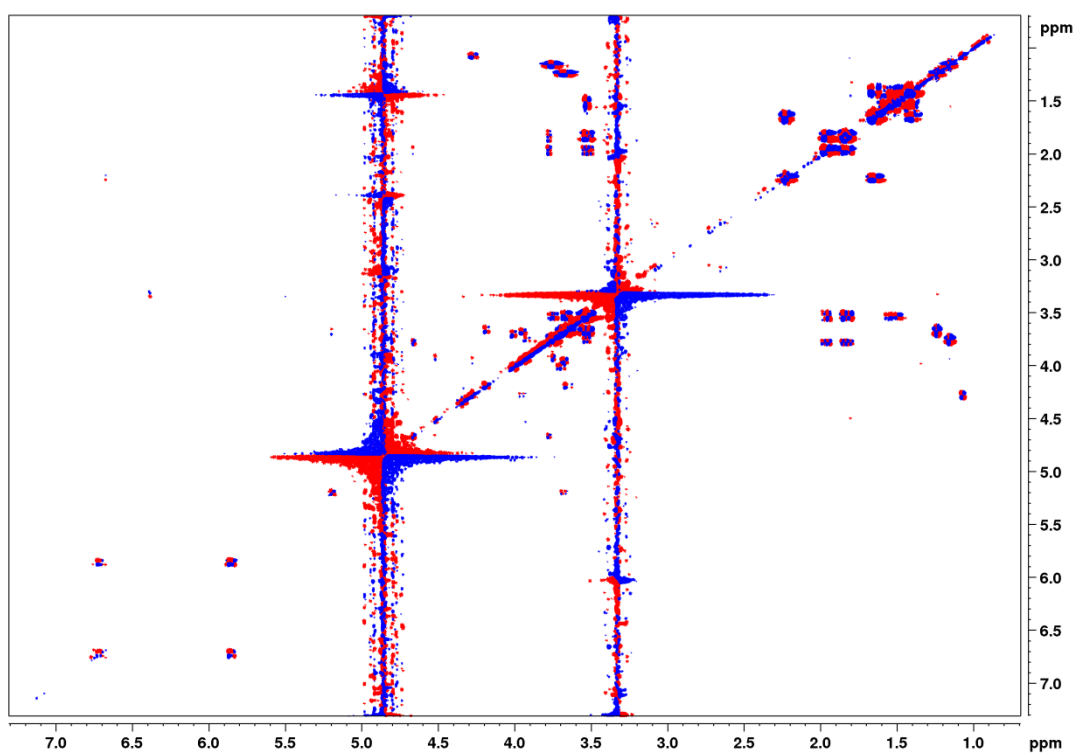
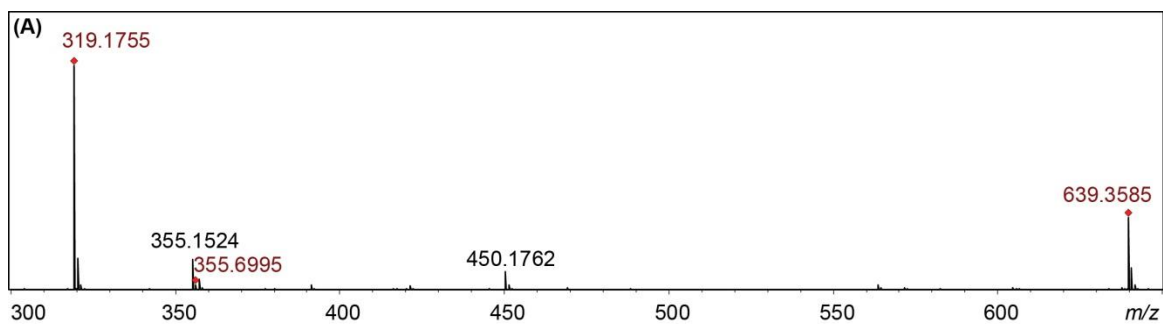
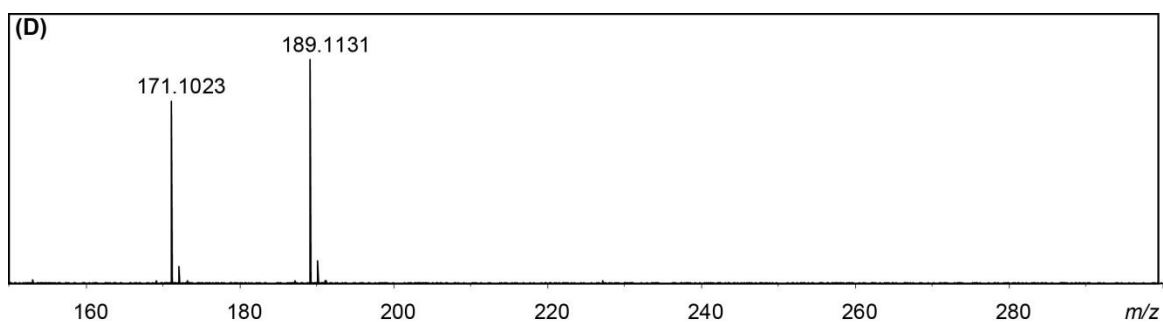
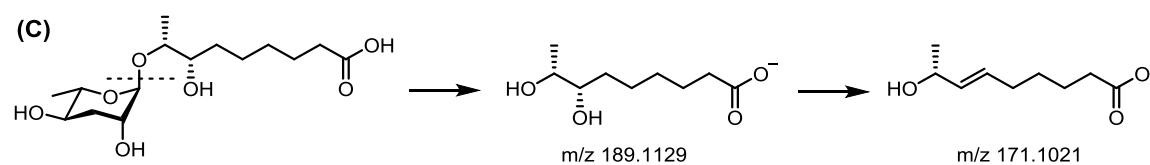


Figure S65: *dqf*-COSY spectrum of isolated (ω -2)-*threo*-OH-ascr#10.



(B)

Observed (m/z)	Calculated (m/z)	Error (ppm)	Ion Formula
319.1755	319.1762	2.3	$C_{15}H_{27}O_7^-$
639.3585	639.3597	2.0	$C_{30}H_{55}O_{14}^-$



(E)

Observed (m/z)	Calculated (m/z)	Error (ppm)	Ion Formula
189.1129	189.1132	1.8	$C_9H_{17}O_4^-$
171.1021	171.1027	3.0	$C_9H_{15}O_3^-$

Figure S66: Structure Characterization of (ω -2)-*threo*-OH-ascr#10 by QTOF-HRMS analysis (A & B) and MS/MS fragmentation pattern (C, D & E) in negative ion mode.

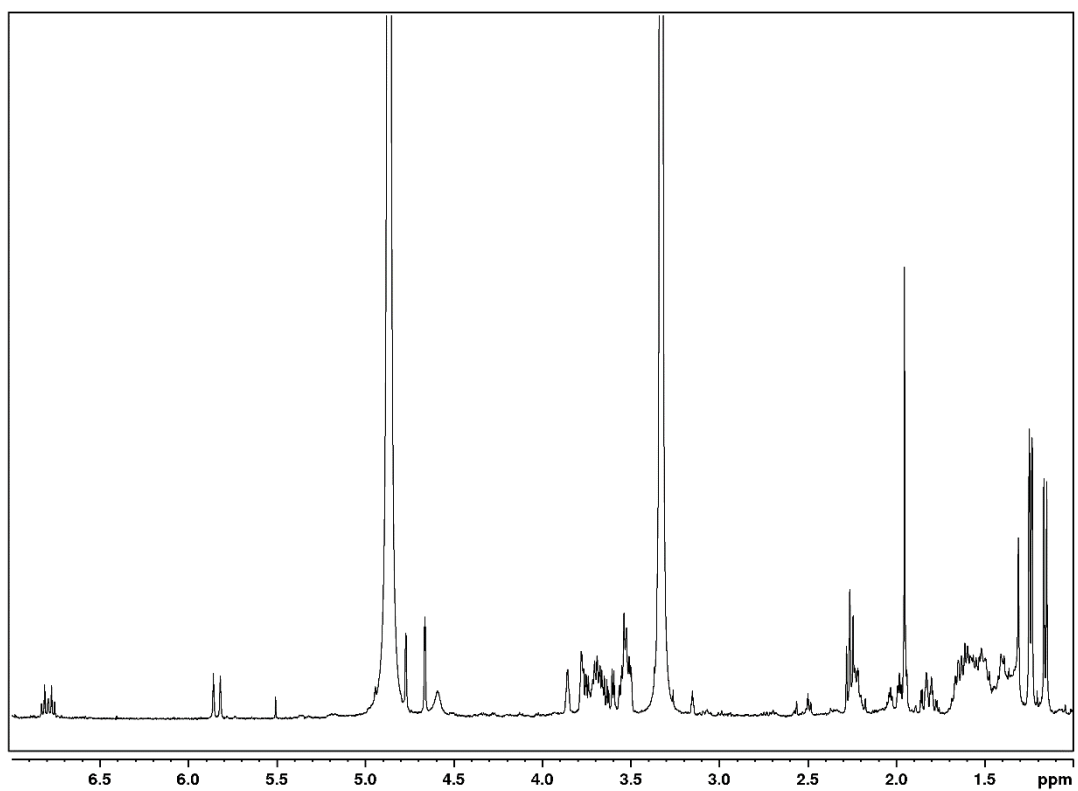


Figure S67: $^1\text{H-NMR}$ spectrum of isolated $(\omega)\text{-OH-ascr}\#3$.

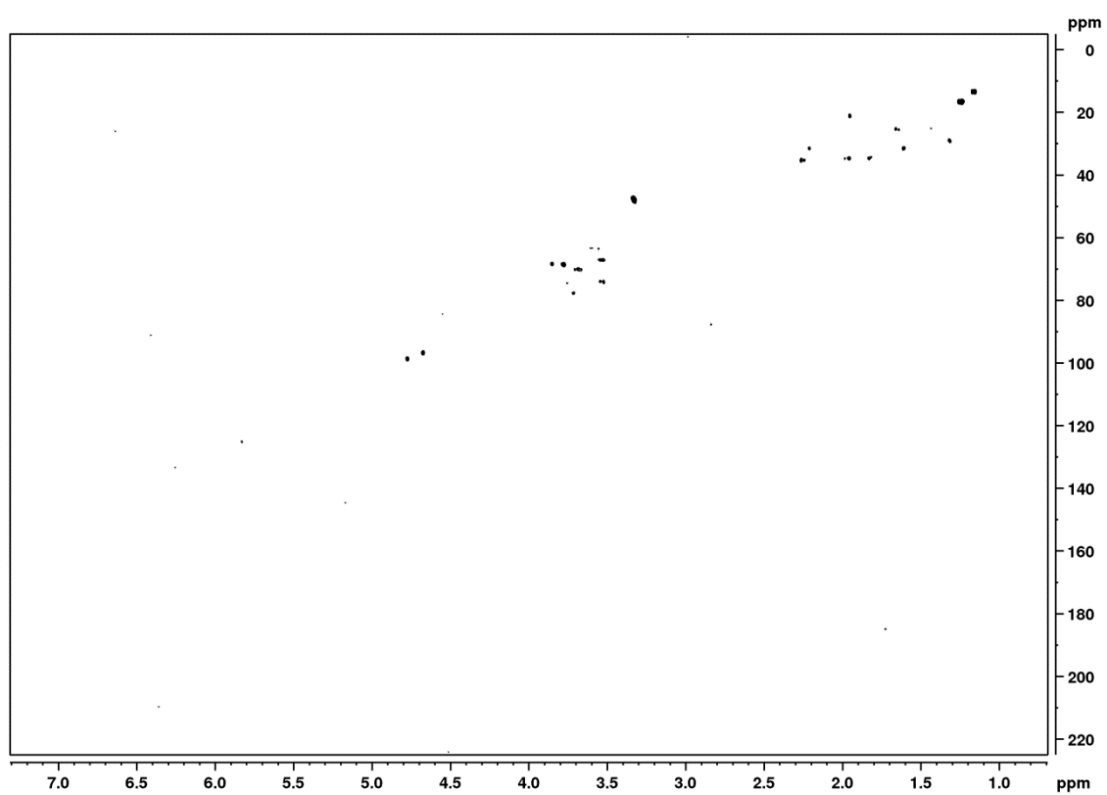


Figure S68: HSQC spectrum of isolated $(\omega)\text{-OH-ascr}\#3$.

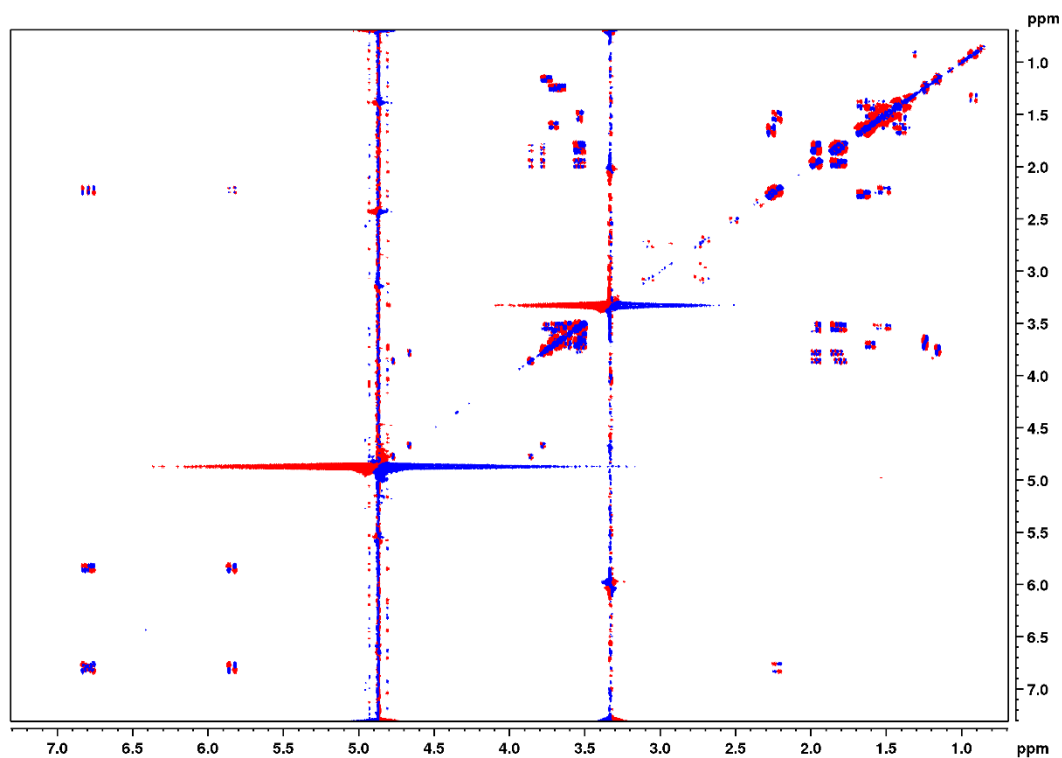
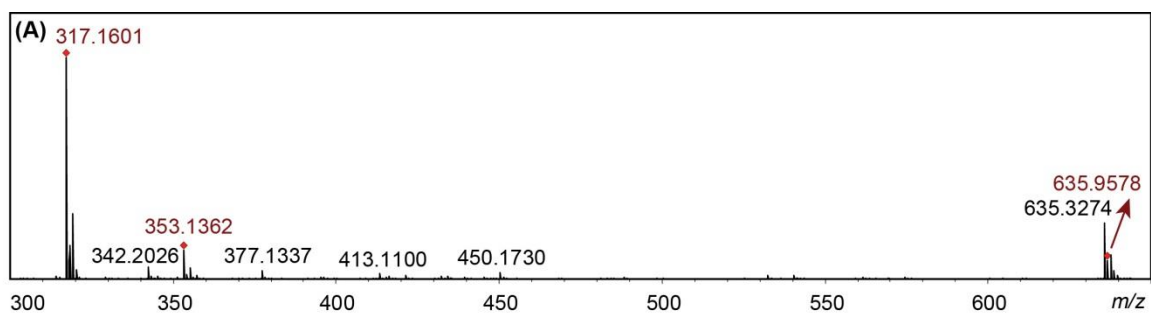


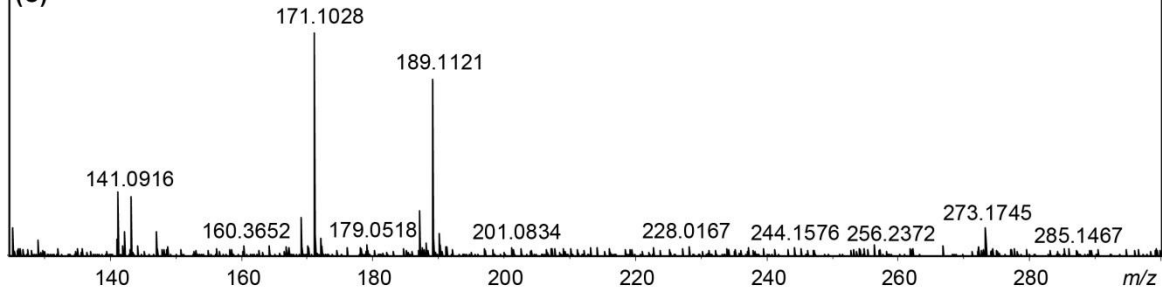
Figure S69: *dqf*-COSY spectrum of isolated (ω)-OH-ascr#3.



(B)

Observed (<i>m/z</i>)	Calculated (<i>m/z</i>)	Error (ppm)	Ion Formula
317.1601	317.1606	1.6	C ₁₅ H ₂₅ O ₇ ⁻

(C)



(D)

Observed (<i>m/z</i>)	Calculated (<i>m/z</i>)	Error (ppm)	Ion Formula
189.1120	189.1132	6.8	C ₉ H ₁₇ O ₄ ⁻
171.1027	171.1027	0.1	C ₉ H ₁₅ O ₃ ⁻
141.0915	141.0921	3.9	C ₈ H ₁₃ O ₂ ⁻

Figure S70: Structure characterization of (ω)-OH-ascr#3 by qTOF-HRMS analysis (A & B) and MS/MS fragmentation pattern (C & D).

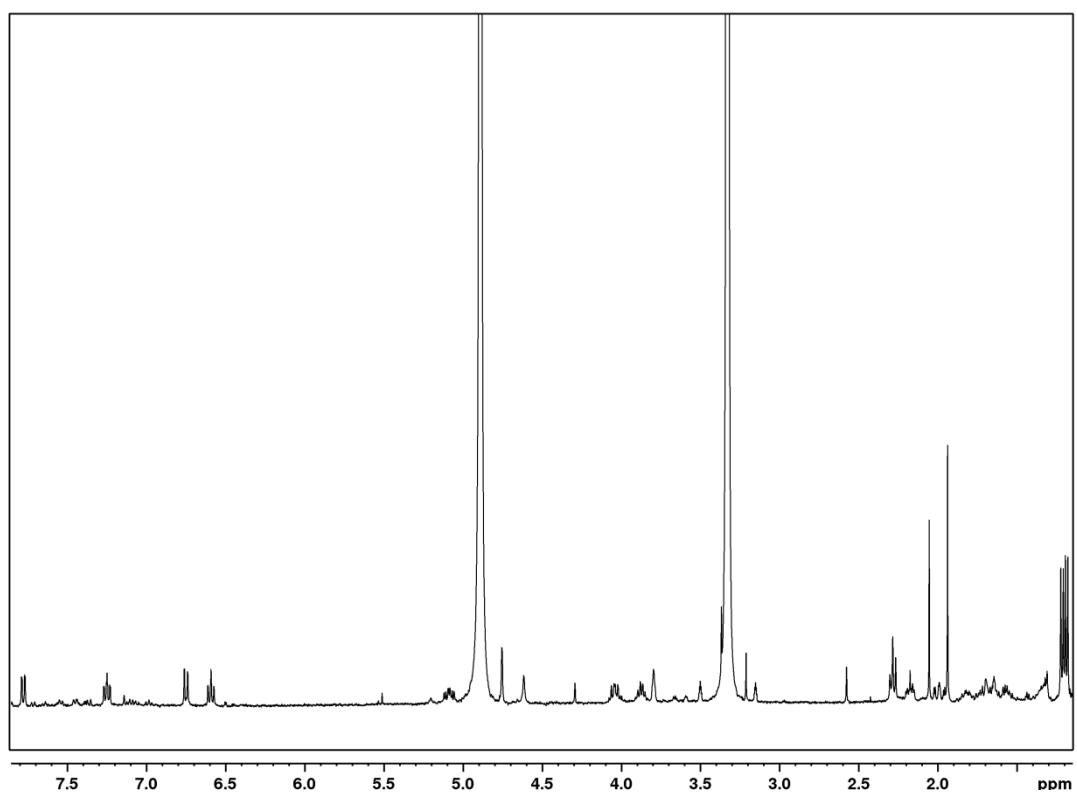


Figure S71: ¹H-NMR spectrum of isolated abas#12.

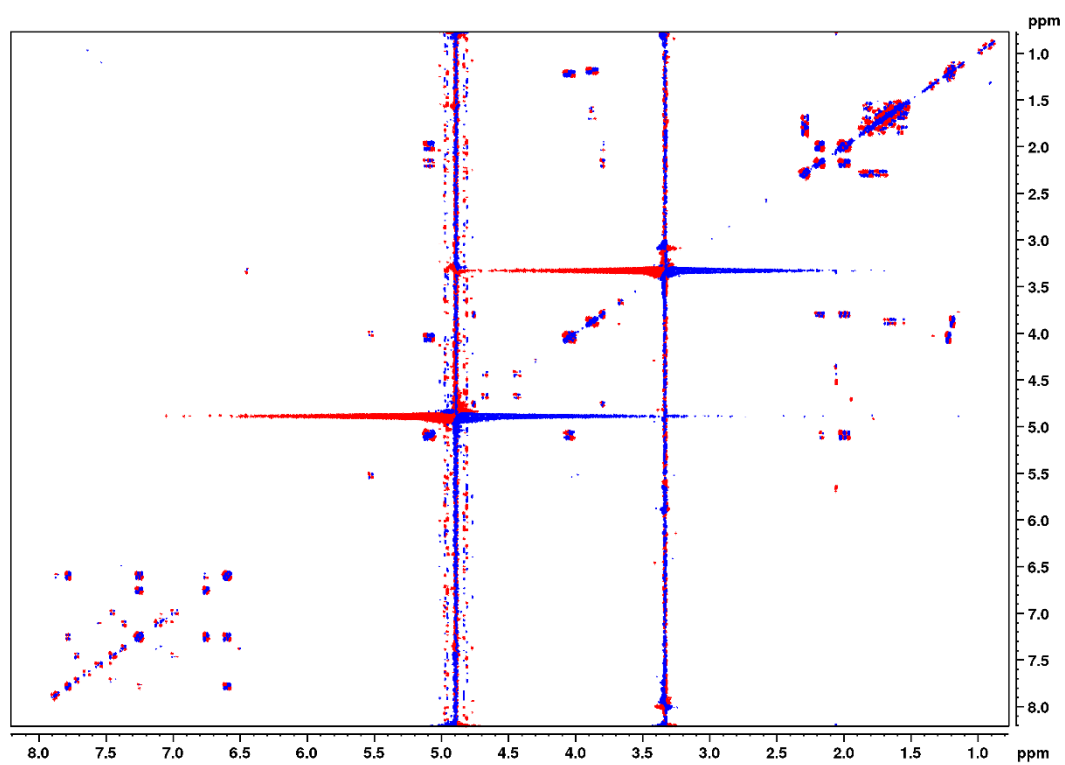


Figure S72: *dqf*-COSY spectrum of isolated abas#12.

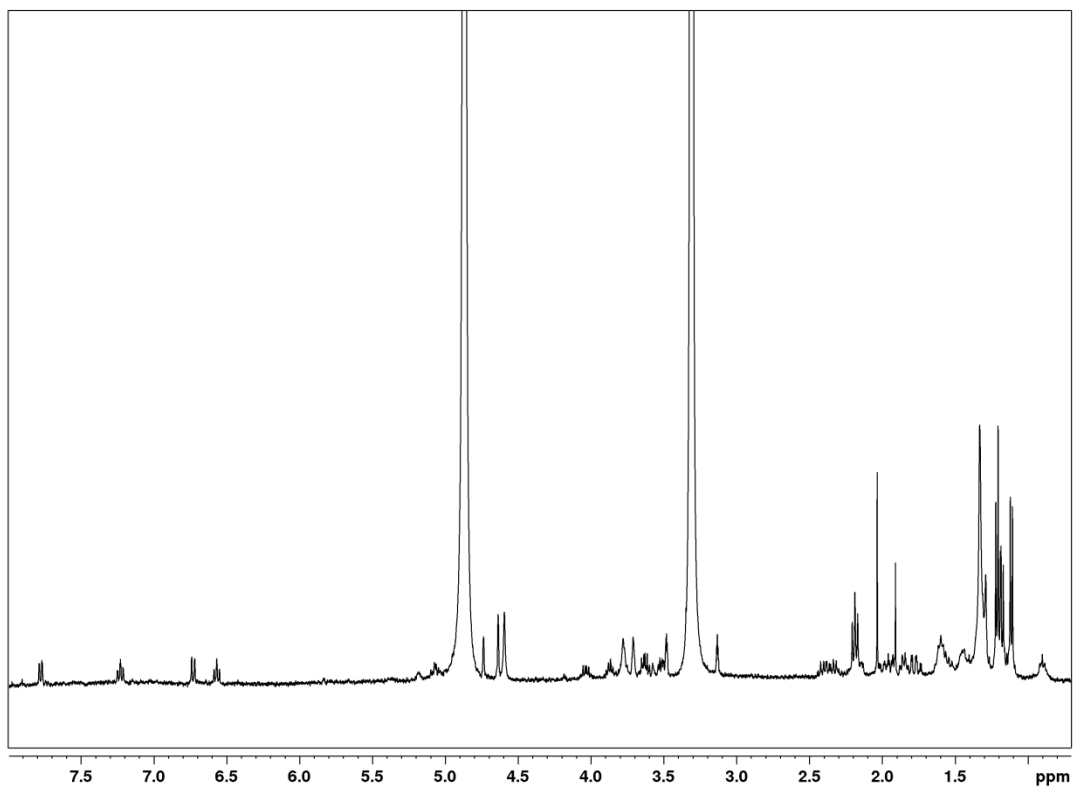


Figure S73: ^1H -NMR spectrum of isolated abas#9.

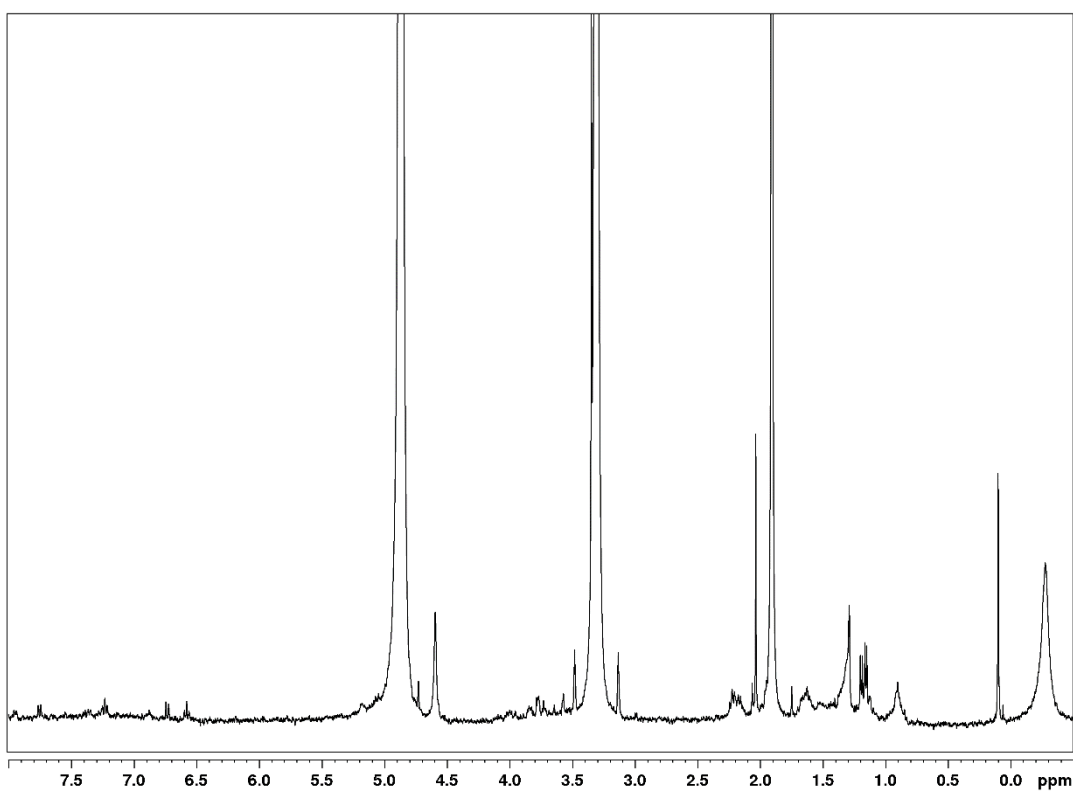


Figure S74: ^1H -NMR spectrum of isolated abas#1.

References

- [1] Andersen E. C., Gerke J. P., Shapiro J. A., Crissman J. R., Ghosh R., Bloom J. S. & Kruglyak L. (2012) Chromosome-scale selective sweeps shape *Caenorhabditis elegans* genomic diversity. **Nat. Genet.**, 44(3): 285-290.
- [2] Kiontke K. C., Félix M.-A., Ailion M., Rockman M. V., Braendle C., Pénigault J. B. & Fitch D. H. (2011) A phylogeny and molecular barcodes for *Caenorhabditis*, with numerous new species from rotting fruits. **BMC Evol. Biol.**, 11: 339.
- [3] Hodgkin J. & Doniach T. (1977) Natural variation and copulatory plug formation in *Caenorhabditis elegans*. **Genetics**, 146: 149-164.
- [4] Barrière A. & Félix M.-A. (2005) High local genetic diversity and low outcrossing rate in *Caenorhabditis elegans* natural populations. **Curr. Biol.**, 15(13): 1176-1184.
- [5] Barrière A. & Félix M.-A. (2007) Temporal dynamics and linkage disequilibrium in natural *Caenorhabditis elegans* populations. **Genetics**, 176(2): 999-1011.
- [6] The *C. elegans* Sequencing Consortium (1998) Genome sequence of the nematode *C. elegans*: a platform for investigating biology. **Science**, 282: 2012-2018.
- [7] Choe A., von Reuss S. H., Kogan D., Gasser R. B., Platzer E. G., Schroeder F. C. & Sternberg P. W. (2012) Ascaroside signaling is widely conserved among nematodes. **Curr. Biol.**, 22(9): 772-780.
- [8] von Reuss S. H. & Schroeder F. C. (2015) Combinatorial chemistry in nematodes: modular assembly of primary metabolism-derived building blocks. **Nat. Prod. Rep.**, 32(7): 994-1006.
- [9] Schroeder F. C. (2015) Modular assembly of primary metabolic building blocks: a chemical language in *C. elegans*. **Chem. Biol.**, 22(1): 7-16.
- [10] Golden J. W. & Riddle D. L. (1982) A pheromone influences larval development in the nematode *Caenorhabditis elegans*. **Science**, 218: 578-580.
- [11] Bartley J. P. (1996) Structure of the ascarosides from *Ascaris suum*. **J. Nat. Prod.**, 59: 921-926.
- [12] Jeong P.-Y., Jung M., Yim Y.-H., Kim H., Park M., Hong E., Lee W., Kim Y. H., Kim K. & Paik Y.-K. (2005) Chemical structure and biological activity of the *Caenorhabditis elegans* dauer-inducing pheromone. **Nature**, 433(7025): 541-545.
- [13] Butcher R. A., Fujita M., Schroeder F. C. & Clardy J. (2007) Small-molecule pheromones that control dauer development in *Caenorhabditis elegans*. **Nat. Chem. Biol.**, 3(7): 420-422.
- [14] Srinivasan J., Kaplan F., Ajredini R., Zachariah C., Alborn H. T., Teal P. E. A., Malik R. U., Edison A. S., Sternberg P. W. & Schroeder F. C. (2008) A blend of small molecules regulates both mating and development in *Caenorhabditis elegans*. **Nature**, 454(7208): 1115-1118.
- [15] Izrayelit Y., Srinivasan J., Campbell S. L., Jo Y., von Reuss S. H., Genoff M. C., Sternberg P. W. & Schroeder F. C. (2012) Targeted metabolomics reveals a male pheromone and sex-specific ascaroside biosynthesis in *Caenorhabditis elegans*. **ACS Chem. Biol.**, 7(8): 1321-1325.
- [16] Srinivasan J., von Reuss S. H., Bose N., Zaslaver A., Mahanti P., Ho M. C., O'Doherty O. G., Edison A. S., Sternberg P. W. & Schroeder F. C. (2012) A modular library of small molecule signals regulates social behaviors in *Caenorhabditis elegans*. **PLoS Biol.**, 10(1): e1001237.
- [17] Hollister K. A., Conner E. S., Zhang X., Spell M., Bernard G. M., Patel P., de Carvalho A. C. G. V., Butcher R. A. & Ragains J. R. (2013) Ascaroside activity in *Caenorhabditis elegans* is highly dependent on chemical structure. **Bioorg. Med. Chem.**, 21(18): 5754-5769.
- [18] Butcher R. A., Ragains J. R., Kim E. & Clardy J. (2008) A potent dauer pheromone

- component in *Caenorhabditis elegans* that acts synergistically with other components. **Proc. Natl. Acad. Sci. U S A**, 105(38): 14288-14292.
- [19] Butcher R. A., Ragains J. R. & Clardy J. (2009) An indole containing dauer pheromone component with unusual dauer inhibitory activity at higher concentrations. **Org. Lett.**, 11(14): 3100-3103.
- [20] Noguez J. H., Conner E. S., Zhou Y., Ciche T. A., Ragains J. R. & Butcher R. A. (2012) A novel ascaroside controls the parasitic life cycle of the entomopathogenic nematode *Heterorhabditis bacteriophora*. **ACS Chem. Biol.**, 7(6): 961-966.
- [21] Hsueh Y. P., Mahanti P., Schroeder F. C. & Sternberg P. W. (2013) Nematode-trapping fungi eavesdrop on nematode pheromones. **Curr. Biol.**, 23(1): 83-86.
- [22] Butcher R. A., Ragains J. R., Li W., Ruvkun G., Clardy J. & Mak H. Y. (2009) Biosynthesis of the *Caenorhabditis elegans* dauer pheromone. **Proc. Natl. Acad. Sci. U S A**, 106(6): 1875-1879.
- [23] von Reuss S. H., Bose N., Srinivasan J., Yim J. J., Judkins J. C., Sternberg P. W. & Schroeder F. C. (2012) Comparative metabolomics reveals biogenesis of ascarosides, a modular library of small-molecule signals in *C. elegans*. **J. Am. Chem. Soc.**, 134(3): 1817-1824.
- [24] Zhang X., Feng L., Chinta S., Singh P., Wang Y., Nunnery J. K. & Butcher R. A. (2015) Acyl-CoA oxidase complexes control the chemical message produced by *Caenorhabditis elegans*. **Proc. Natl. Acad. Sci. U S A**, 112(13): 3955-3960.
- [25] Macosko E. Z., Pokala N., Feinberg E. H., Chalasani S. H., Butcher R. A., Clardy J. & Bargmann C. I. (2009) A hub-and-spoke circuit drives pheromone attraction and social behaviour in *C. elegans*. **Nature**, 458(7242): 1171-1175.
- [26] Kim K., Sato K., Shibuya M., Zeiger D. M., Butcher R. A., Ragains J. R., Clardy J., Touhara K. & Sengupta P. (2009) Two chemoreceptors mediate developmental effects of dauer pheromone in *C. elegans*. **Science**, 326(5955): 994-998.
- [27] McGrath P. T., Xu Y., Ailion M., Garrison J. L., Butcher R. A. & Bargmann C. I. (2011) Parallel evolution of domesticated *Caenorhabditis* species targets pheromone receptor genes. **Nature**, 477(7364): 321-325.
- [28] Schroeder F. C., Gibson D. M., Churchill A. C. L., Sojikul P., Wursthorn E. J., Krasnoff S. B. & Clardy J. (2007) Differential analysis of 2D NMR spectra: new natural products from a pilot-scale fungal extract library. **Angew. Chem. Int. Ed. Engl.**, 46(6): 901-904.
- [29] Taggi A. E., Meinwald J. M. & Schroeder F. C. (2004) A new approach to natural products discovery exemplified by the identification of sulfated nucleosides in spider venom. **J. Am. Chem. Soc.**, 126: 10364-10369.
- [30] Gronquist M., Meinwald J., Eisner T. & Schroeder F. C. (2005) Exploring uncharted terrain in nature's structure space using capillary NMR spectroscopy: 13 steroids from 50 fireflies. **J. Am. Chem. Soc.**, 127: 10810-10811.
- [31] Pungalija C., Srinivasan J., Fox B. W., Malik R. U., Ludewig A. H., Sternberg P. W. & Schroeder F. C. (2009) A shortcut to identifying small molecule signals that regulate behavior and development in *Caenorhabditis elegans*. **Proc. Natl. Acad. Sci. U S A**, 106(19): 7708-7713.
- [32] Forseth R. R., Fox E. M., Chung D., Howlett B. J., Keller N. P. & Schroeder F. C. (2011) Identification of cryptic products of the gliotoxin gene cluster using NMR-based comparative metabolomics and a model for gliotoxin biosynthesis. **J. Am. Chem. Soc.**, 133(25): 9678-9681.
- [33] Schimming O., Challinor V. L., Tobias N. J., Adihou H., Grün P., Pöschel L., Richter C., Schwalbe H. & Bode H. B. (2015) Structure, biosynthesis, and occurrence of bacterial pyrrolizidine alkaloids. **Angew. Chem. Int. Ed. Engl.**, 54(43): 12702-12705.
- [34] Bose N., Ogawa A., von Reuss S. H., Yim J. J., Ragsdale E. J., Sommer R. J. & Schroeder F. C. (2012) Complex small molecule architectures regulate phenotypic plasticity in a nematode. **Angew. Chem. Int. Ed. Engl.**, 51: 12438-12443.

- [35] Choe A., Chuman T., von Reuss S. H., Dossey A. T., Yim J. J., Ajredini R., Kolawa A. A., Kaplan F., Alborn H. T., Teal P. E. A., Schroeder F. C., Sternberg P. W. & Edison A. S. (2012) Sex-specific mating pheromones in the nematode *Panagrellus redivivus*. **Proc. Natl. Acad. Sci. U S A**, 109(51): 20949-20954.
- [36] Dong C., Dolke F. & von Reuss S. H. (2016) Selective MS screening reveals a sex pheromone in *Caenorhabditis briggsae* and species-specificity in indole ascaroside signalling. **Org. Biomol. Chem.**, 14(30): 7217-7225.
- [37] Stiernagle T. (2006) Maintenance of *C. elegans*. In *WormBook*, ed. The *C. elegans* Research Community.
- [38] Hoye T. R., Jeffrey C. S. & Shao F. (2007) Mosher ester analysis for the determination of absolute configuration of stereogenic (chiral) carbinol carbons. **Nat. Protoc.**, 2(10): 2451-2458.
- [39] Maier R. M. & Soberón-Chávez G. (2000) *Pseudomonas aeruginosa* rhamnolipids: biosynthesis and potential applications. **Appl. Microbiol. Biotechnol.**, 54(5): 625-633.
- [40] Dey A., Jeon Y., Wang G. X. & Cutter A. D. (2012) Global population genetic structure of *Caenorhabditis remanei* reveals incipient speciation. **Genetics**, 191(4): 1257-1269.
- [41] Watts J. L. & Browse J. (2002) Genetic dissection of polyunsaturated fatty acid synthesis in *Caenorhabditis elegans*. **Proc. Natl. Acad. Sci. U S A**, 99(9): 5854-5859.
- [42] Brooks K. K., Liang B. & Watts J. L. (2009) The influence of bacterial diet on fat storage in *C. elegans*. **PLoS One**, 4(10): e7545.
- [43] Perez C. L. & Van Gilst M. R. (2008) A ¹³C isotope labeling strategy reveals the influence of insulin signaling on lipogenesis in *C. elegans*. **Cell Metab.**, 8(3): 266-274.
- [44] Grogan D. W. & Cronan Jr J. E. (1997) Cyclopropane ring formation in membrane lipids of bacteria. **Microbiol. Mol. Biol. Rev.**, 61(4): 429-441.
- [45] Chang Y.-Y. & Cronan Jr J. E. (1999) Membrane cyclopropane fatty acid content is a major factor in acid resistance of *Escherichia coli*. **Mol. Microbiol.**, 33(2): 249-259.
- [46] Stuart L. J., Buck J. P., Tremblay A. E. & Buist P. H. (2006) Configurational analysis of cyclopropyl fatty acids isolated from *Escherichia coli*. **Org. Lett.**, 8(1): 79-81.
- [47] Bruinsma J. J., Schneider D. L., Davis D. E. & Kornfeld K. (2008) Identification of mutations in *Caenorhabditis elegans* that cause resistance to high levels of dietary zinc and analysis using a genomewide map of single nucleotide polymorphisms scored by pyrosequencing. **Genetics**, 179(2): 811-828.
- [48] Davis D. E., Roh H. C., Deshmukh K., Bruinsma J. J., Schneider D. L., Guthrie J., Robertson J. D. & Kornfeld K. (2009) The cation diffusion facilitator gene *cdf-2* mediates zinc metabolism in *Caenorhabditis elegans*. **Genetics**, 182(4): 1015-1033.
- [49] Murphy J. T., Bruinsma J. J., Schneider D. L., Collier S., Guthrie J., Chinwalla A., Robertson J. D., Mardis E. R. & Kornfeld K. (2011) Histidine protects against zinc and nickel toxicity in *Caenorhabditis elegans*. **PLoS Genet.**, 7(3): e1002013.
- [50] Mehler A. H. & Tabor H. (1953) Deamination of histidine to form urocanic acid in liver. **J. Biol. Chem.**, 201: 775-784.
- [51] Kim H., Chin J., Choi H., Baek K., Lee T.-G., Park S. E., Wang W., Hahn D., Yang I., Lee J., Mun B., Ekins M., Nam S.-J. & Kang H. (2013) Phosphoiodynes A and B, unique phosphorus-containing iodinated polyacetylenes from a Korean sponge *Placospongia* sp. **Org. Lett.**, 15(1): 100-103.
- [52] Stupp G. S., von Reuss S. H., Izrayelit Y., Ajredini R., Schroeder F. C. & Edison A. E. (2013) Chemical detoxification of small molecules by *Caenorhabditis elegans*. **ACS Chem. Biol.**, 8(2): 309-313.
- [53] Yim J. J., Bose N., Meyer J. M., Sommer R. J. & Schroeder F. C. (2015) Nematode signaling molecules derived from multimodular assembly of primary metabolic

- building blocks. **Org. Lett.**, 17(7): 1648-1651.
- [54] Frézal L. & Félix M.-A. (2015) The natural history of model organism: *C. elegans* outside the petri dish. **eLife**, 4: e05849.
- [55] Zhang X., Li K., Jones R. A., Bruner S. D. & Butcher R. A. (2016) Structural characterization of acyl-CoA oxidases reveals a direct link between pheromone biosynthesis and metabolic state in *Caenorhabditis elegans*. **Proc. Natl. Acad. Sci. U S A**, (doi:10.1073/pnas.1608262113)
- [56] O'Brien R. V., Davis R. W., Khosla C. & Hillenmeyer M. E. (2014) Computational identification and analysis of orphan assembly-line polyketide synthases. **J. Antibiot.** (Tokyo), 67(1): 89-97.
- [57] Shou Q., Feng L., Long Y., Han J., Nunnery J. K., Powell D. H. & Butcher R. A. (2016) A hybrid polyketide-nonribosomal peptide in nematodes that promotes larval survival. **Nat. Chem. Biol.**, (doi:10.1038/nchembio.2144)
- [58] Manosalva P., Manohar M., von Reuss S. H., Chen S., Koch A., Kaplan F., Choe A., Micikas R. J., Wang X., Kogel K.-H., Sternberg P. W., Williamson V. M., Schroeder F. C. & Klessig D. F. (2015) Conserved nematode signalling molecules elicit plant defenses and pathogen resistance. **Nat. Commun.**, 6: 7795.
- [59] Mitkowski N. A. & Abawi G. S. (2003) Reproductive fitness on lettuce of populations of *Meloidogyne hapla* from New York state vegetable fields. **Nematology**, 5(1): 77-83.

Curriculum Vitae

Personal information

Name: Chuanfu Dong Birth: 13 July 1987
Nationality: Chinese E-mail: chuanfu.dong@tuebingen.mpg.de
Gender: Male Address: Niethammerstrasse 1, 72076, Tuebingen

Education

Max Planck Institute for Chemical Ecology & Friedrich-Schiller-University

December 2012-Present, Doctoral candidate in Chemistry

Thesis title: Small Molecule Signaling in Nematodes

Advisor: Prof. Dr. Stephan H. von Reuß

Kunming Institute of Botany, Chinese Academy of Sciences

September 2009-June 2012, Master of Science in Plant Natural Products

Thesis title: Chemical Constituents of *Illicium simonsii*

Advisor: Associate Prof. Yifen Wang

Jiangxi Agricultural University

September 2005-September 2009, Bachelor of Science in Chemical Engineering

Experience

Beijing Normal University

June 2012-November 2012 Research Assistant

Publications (* co-author)

5. Selective MS screening reveals a sex pheromone in *C. briggsae* and species specificity in indole ascaroside signaling
Dong C.*, Dolke F.* , von Reuß S. H.
Organic & Biomolecular Chemistry (2016), 14: 7217-7225. [Selected as Hot Article]
4. Chemical constituents of *Illicium burmanicum*
Wang J., Guan Z., Dong C., Gao L., Luo S., Wang Y.
Zhongguo Zhong Yao Za Zhi (2014), 39: 2526-2530. (Chinese)
3. Sesquiterpene and terpenoid-sesquiterpene: anti-AChE constituents from *Illicium simonsii*
Dong C.*, Liu L.* , Li X., Guan Z., Luo H., Wang Y.
Planta Medica (2013), 79: 338-347.

2. New monoterpene phenyl ethers from *Illicium micranthum*
Guan Z., Dong C., Gao L., Wang J., Wang Y.
Natural Products and Bioprospecting (2013), 3: 43-47.
1. Sesqueneolignans from the stem barks of *Illicium simonsii* and their anti-AChE activity
Dong C., Liu L., Luo H., Li X., Guan Y., Wang Y.
Natural Products and Bioprospecting (2012), 2: 133-137.

Presentation

Ascaroside Signals in Nematodes
Friedrich-Schiller-University, Jena, Germany, Dec 9th, 2014

Secondary Metabolites from *Illicium simonsii* and Nematode
Jiangxi Agricultural University, Nanchang, China, Jan 9th, 2014

Poster

Novel Phosphoryl Ascarosides from the *Caenorhabditis Elegans* Group
Dong C., Dolke F., Kulhlisch C., von Reuß S. H.
The Scientific Advisory Board Meeting, MPI for Chemical Ecology, May 2014

Novel Phosphoryl Ascarosides from the *Caenorhabditis Elegans* Group
Dong C., Dolke F., Kulhlisch C., von Reuß S.H.
Institute Symposium, MPI for Chemical Ecology, Jena, Sep 10th-11th, 2014

Course and Conference

1. MS Course (MAILDI Q Exactive Plus, Q Exactive XL, Ion Motility, IMPRS Course)
2. NMR Course (Theoretic and practical, IMPRS Course)
3. Expression and Purification of Protein (IMPRS Course)
4. Naturstofftreffen (Natural Products Research Symposium, 2013, 2014, 2015, 2016)

Honors

2008-2009 National Motivational Scholarship, Jiangxi Agricultural University
2006-2008 First Prize Scholarship, Jiangxi Agricultural University
2005-2006 Second Prize Scholarship, Jiangxi Agricultural University

Acknowledgments

The most important content in this thesis is my thanks to those people who provided lots of help and supports for me. Nothing will happen without their kindness and patience. Firstly, I would like to thank my supervisor Prof. Dr. Stephan H. von Reuß. If I recall the very first meeting with Stephan H. von Reuß is my arrival in Jena West Station in 28 December 2012, when I became his first PhD student. I can't believe that Stephan and Winnefeld Grit were waiting for a long time in such a heavy snow winter day. All the things were quickly done with his support and my PhD projects were smoothly stepping forwards because of Stephan's extensive supervisions and suggestions. I learned a lot about culturing nematodes and many analytical methods by working together with him in the lab. And most importantly, I learned enthusiasm and satisfaction from science, also, how to design experiments and deal with the results, and significantly benefited from these experience, I started to know the actual meanings of science. As a mentor, he discussed with me about every talk, poster and manuscript. I really enjoy talking and discussing with Stephan about science and everything. I am very lucky to have Prof. Dr. Stephan H. von Reuß to be my supervisor, and of course I learned and benefited too much from him. I am very grateful and thankful in my entire life for the supervisions, inputs, and his taking care of me in Germany by Prof. Dr. Stephan H. von Reuß.

I am also very lucky to have a great opportunity to work in the Department of Bioorganic Chemistry in Max Planck Institute for Chemical Ecology, where many biologists and chemists from different nations worked together friendly and this definitely allowed me to know many topics relating to chemical ecology. Technicians in the department are friendly and patient enough to solve the problems happened every day. Free discussions with Prof. Dr. Wilhelm Boland are always possible in his office. And, well equipped analytical instruments make my research proceed so well. The great advantage of working here is that I can always ask help from many other experts. For example, Michael Reichelt is such a kind and patient expert who helped to perform the selective screening experiment. Paetz Christian also helped to acquire NMR data in Biosynthesis/NMR research group, which allowed me to have much more information

about extreme low amount of ascarosides. As a doctoral candidate, my research and projects greatly benefited from the excellent scientific surroundings, what I need to do is just focusing on science. I am very grateful to the current and past group members for their help in science and normal life. I still remember that Dr. Huijuan Guo showed me around the city, directed me to the supermarket and helped to contact doctor in the hospital.

It is also a great chance for me to thank many excellent collaborator researchers. One of them is doctoral candidate Franziska Dolke (Max Planck Institute for Chemical Ecology) who worked on organic synthesis to support characterization of those newly discovered ascarosides. It would be my great honor to work tightly with such an excellent organic chemist. I am also very grateful to Prof. Dr. Jagan Srinivasan (Worcester Polytechnic Institute) for biological activities tests of hydroxylated ascarosides. And chemical analysis could not be performed without authentic standards of ascarosides kindly provided by Prof. Dr. F. C. Schroeder (Cornell University). All nematodes strains were provided by *Caenorhabditis* Genetics Center (CGC), which is funded by NIH Office of Research Infrastructure Programs (P40OD010440).

I would also like to thank the special committee members including Prof. Dr. Stephan H. von Reuß, Prof. Dr. Wilhelm Boland, Prof. Dr. Georg Pohnert, Prof. Dr. Jonathan Gershenzon, Prof. Dr. Hans-Dieter Arndt and Prof. Dr. Ivan Vilotijević for their efforts and inputs for manuscript revision.

All these things will not happen without the great support and encourage from my family members, including Mon, Dad, Sister, Brother and many others. Thanks to my parents and Jingyuan Chen for their patience, encourage, love and accompany. All of these make me move forwards to pursue what I really want. It is my great honor to have them always standing with me no matter what happened. Here, I would also like to thank many friends around here and China. The great experience here is that I can even play table tennis with so many Chinese friends. It is so nice to have them around here for those many accompany.

Thanks to Chemisch-Geowissenschaftliche Fakultät and Prof. Dr. Georg Pohnert in Friedrich-Schiller-University for accepting me as doctoral candidate and their help as well

as supports. Finally, great thanks for funding my PhD research by Max Planck Society and Max Planck Institute for Chemical Ecology.

Eigenständigkeitserklärung

Declaration of authorship / Selbständigkeitserklärung

Ich erkläre, dass ich die vorliegende Arbeit selbständig und unter Verwendung der angegebenen Hilfsmittel, persönlichen Mitteilungen und Quellen angefertigt habe.

I certify that the work presented here is, to the best of my knowledge and belief, original and the result of my own investigations, except as acknowledged, and has not been submitted, either in part or whole, for a degree at this or any other university.

Chuanfu Dong

Jena, 19.04.2017